Low-Slip Force Friction Connections for Early Phase Energy Dissipation in Steel Structures

by

Patrick Stephen Koch

A thesis submitted to the Graduate Faculty of
Auburn University
in partial fulfillment of the
requirements for the Degree of
Master of Science

Auburn, Alabama
December 12, 2015

Keywords: friction, damping, seismic, steel, structures

Approved by

Justin D. Marshall, Chair, Associate Professor of Civil Engineering
James S. Davidson, Gottlieb Professor of Civil Engineering
Robert W. Barnes, Associate Professor of Civil Engineering

Abstract

Previous research suggests adding early phase energy dissipation to structural steel systems can improve seismic performance. This can be achieved with a Low-slip Force Friction (LSFF) damper designed to activate prior to yielding of the seismic force resisting system. A friction device included in the simple gravity frame connections of a steel structure provides an economical mechanism for inducing early phase energy dissipation. This simple device can be installed in any steel structure as part of a conventional seismic-force resisting system, a performance-based seismic protective system, or the seismic rehabilitation of an existing structure. This connection will improve performance for structures during short return period earthquakes when few other lateral force resisting elements dissipate energy. The device will remain active during large events improving the response of buildings which have already demonstrated reliable performance for design and maximum considered events. This thesis will show the effects of early phase friction energy dissipation through nonlinear dynamic analysis of three and nine story structures designed with Special Moment Resisting Frames (SMRF) and Buckling-Restrained Brace (BRB) frames. A suite of earthquakes scaled to the hazard spectrum at four return-periods is used for the dynamic analyses. The comparison between baseline code-designed BRB and moment frames to those with early phase dissipation includes drift, acceleration, and ductility related metrics. Variations of friction device configurations are investigated including number, distribution, and slip force. This research provides the foundation to understanding a LSFF system and how steel structures can be

designed to provide more resilient, sustainable, and reliable infrastructure over a wide range of return periods without a significant construction or engineering cost increase.

Acknowledgments

First, I would like to thank Dr. Marshall. He has given me many opportunities to gain knowledge and experience throughout my college education. His guidance and expertise has made this work possible. This research had many difficulties, but Dr. Marshall remained a fount of solutions and encouragement. I would also like to acknowledge my appreciation of the structures faculty group. I have learned a great deal in my graduate studies, and I am grateful to those that have taught it to me.

I would like to thank the other students who have contributed their efforts to this project. Andrew Long, Christopher Kerner, and Weverton Marques Da Silva have all performed quality work, and I hope they, like myself, have learned from this research. I appreciate the contributions of the American Institute of Steel Construction in funding this research. I would also like to express my appreciation to my fellow graduate students whose advice and friendship has made my experience at Auburn a successful and enjoyable one.

Table of Contents

List of Tables

List of Illustrations

Chapter 1. Introduction

Engineers and researchers seek to develop resilient, economical, and sustainable structures. Designs for structures are predominantly controlled by statistical combinations of gravity loads and lateral loads. Gravity loads are vertical forces caused by the weight of the structure itself and the objects within it. Lateral loads are most commonly caused by environmental phenomena. Lateral loads are less predictable and can impart large amounts of energy into a structure. Some of this energy is dissipated by nonstructural elements. But, with infrequent and large magnitude lateral loads like earthquakes, structural elements are relied upon to absorb this energy through permanent deformation. Particularly in high seismic regions, additional energy dissipative methods are added to structural systems to safely resist lateral demands.

1.1 Purpose

Current seismic design utilizes deliberate inelastic mechanisms to provide life safety and collapse prevention during a design earthquake. However, frequent smaller scale earthquakes can cause enough damage to the lateral resisting system to require expensive repairs. An effort is being made to develop structural designs that meet higher performance objectives for multiple levels of seismic excitation. Passive multi-phased systems are utilized to reduce damage during more frequent events and transition into objectives like life safety for larger magnitude earthquakes. This research explores providing such a system with the addition of Low-Slip Force Friction (LSFF) devices in parallel with traditional lateral force resisting systems.

LSFF damping is an economical way to introduce energy dissipation that effectively reduces damage from moderate into extreme ground shaking. This damping will activate prior to significant yielding of lateral force resisting elements. Resulting in improved performance for earthquakes with shorter return periods while meeting or exceeding the requirements of the design earthquake. The addition of early phase energy dissipation through low-slip force friction devices can create more resilient, sustainable, and reliable infrastructure over a wide range of seismic hazards.

1.2 Scope

The work of this thesis began with the selection of a reliable friction damping device. Based on a catalogue of available literature and proprietary designs, the slotted bolted friction damper was selected as an appropriate and economical source of friction damping. A behavior model of slotted bolted friction dampers was synthesized from previous studies performed on such devices with adjustments to achieve a low activation force for early phase damping. An effort was then made to incorporate these friction devices into full three dimensional structural models. It was decided that these dampers should work in parallel with the existing lateral force resisting system. A scheme to include the dampers in the gravity frame connections was developed to achieve this.

After this early phase of the research, work began to create three dimensional mathematical models of steel structures in a structural analysis program. Two layouts of structures were chosen: a three story and a nine story. These steel frame structures were designed according to current codes and standards. A buckling restrained brace frame and a special moment resisting frame were utilized to assess the connections benefits with different lateral force resisting systems. Due to the objective to evaluate the effects of early phase energy dissipation, the detailed behaviors of various

elements were incorporated into the models. This included many lateral force resisting elements as well as the contribution of the gravity frame connections to the lateral system.

In order to measure the benefits of the connections for seismic applications, numerous inelastic models were developed for the structural elements within the models. A suite of ground motions was selected and imposed upon the models for analysis purposes. These ground motions were scaled to several seismic hazard levels in order to evaluate the effects of early phase energy dissipation through various hazard return periods.

The novelty of the LSFF connection and the detail of the structural models made selecting optimal parameters for the devices difficult. Designing and implementing these connections to provide the most benefit to the structural model required a parametric study. Variations of models were made with different combinations of friction device slip forces and number of devices. The performance of each permutation was compared to the others and to baseline models at different levels of ground shaking. The large number of elements in the three dimensional models, the number of models created with friction device permutations, the number of ground motions analyzed, and the various levels of ground motion scaling generated a large volume of raw data. A sizeable effort was made in collecting and processing the output of the structural analyses. The work done for this thesis concluded with the development and discussion of results of the parametric study and LSFF connection performance.

1.3 Organization of Thesis

This thesis is organized to convey the process of investigating background literature, developing mathematical models, and analyzing the performance of structures with LSFF connections.

Chapter 2 provides a review of literature pertaining to the structural elements composing the LSFF connection.

Chapter 3 describes the development of three dimensional structural models. The design methods, selected sizes, and modeled inelastic properties of structural elements are detailed. The selected ground motions and time history analysis methods are presented.

Chapter 4 discusses a parametric study of structures with LSFF connections. The varied parameters and resulting distinct models are outlined. A comparison of the models is presented and discussed.

Chapter 5 summarizes the efforts and findings of the thesis. Conclusions and recommendations for future research are offered.

Chapter 2. Literature Review

2.1 Introduction

Structural steel designs consist of both a gravity load and lateral load resisting system. These two systems are typically designed separately. The gravity load system is often idealized as consisting of pinned connections with negligible participation in the resistance of lateral loads. However, the gravity frame can offer considerable lateral stiffness. Gravity frame columns are continuous through the height of the structure. This forces them to take load when the structure displaces laterally. The lateral participation of the gravity frame is even greater when the rotational stiffness of gravity frame connections is considered. A common gravity frame connection is the shear tab connection. The lateral load system is primarily designed to resist the effects of wind and seismic activity on the structure. Lateral load resistance often relies on energy dissipative mechanisms to withstand large loads. Friction damping, provided by devices like the slotted bolted friction damper, is an effective source of energy dissipation in structures. The behavior of shear tab connections and use of slotted bolted friction dampers are key elements of the LSFF connection and provide a background for this thesis.

2.2 Shear Tab Connections

The most common steel gravity frame connection in North America is the single plate or Shear Tab Connection (STC) (Astaneh-Asl, Liu, & McMullin, 2002). This connection consists of a plate or “shear tab” fillet welded to a column or girder and bolted to the web of a beam or girder. The

design of these connections is meant to provide shear strength to support the beams and ensure the occurrence of ductile failure modes before the fracture of welds and bolts (Astaneh-Asl, Liu, & McMullin, 2002). Several examples of STCs are shown in Figure 2-1.

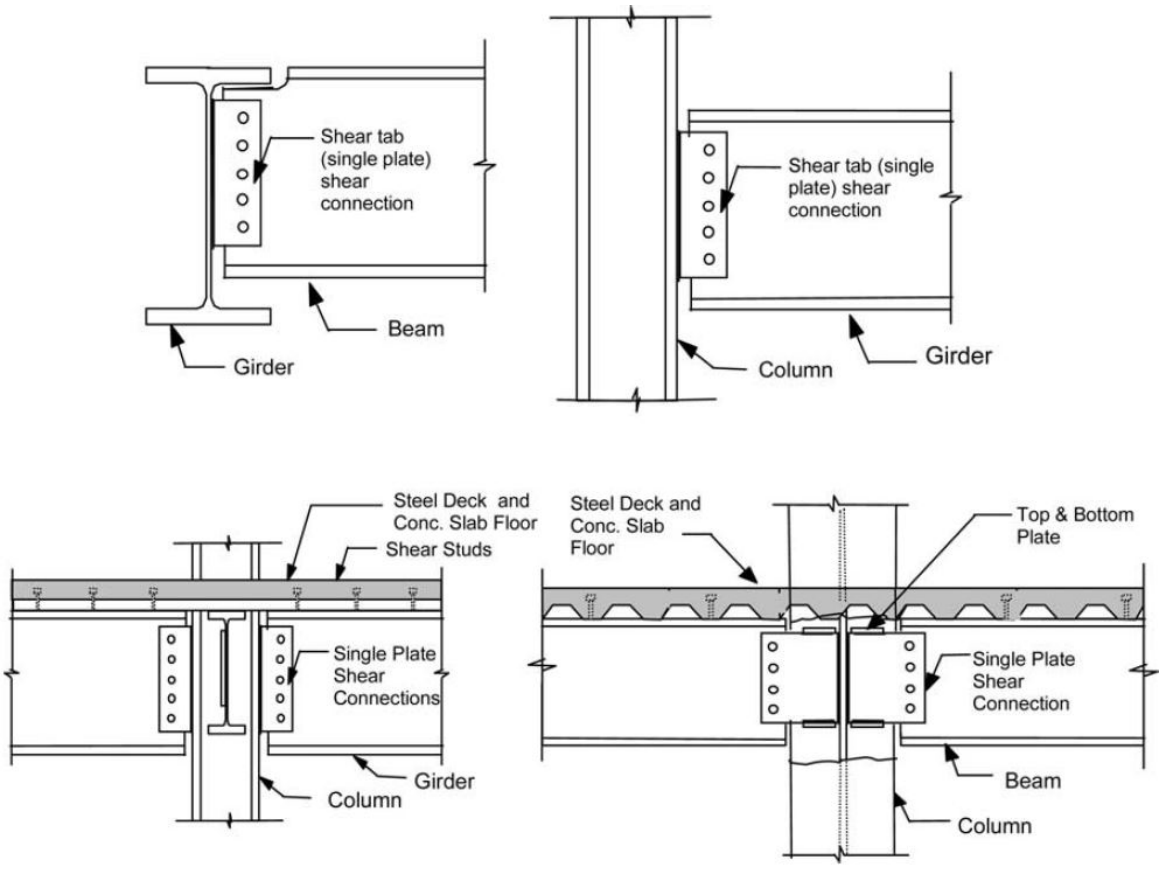

Figure 2-1. Single Plate Shear Tab Connections (Astaneh-Asl, Liu, & McMullin, 2002)

The AISC Steel Construction Manual Part 10 Design of Simple Shear Connections provides design requirements for single plate connections. These connections must meet Load and Resistance Factor Design (LRFD) strength requirements for the bolts, plate, and weld as well as various dimensional requirements (AISC, 2011). Satisfaction of Part 10 of the Steel Construction Manual is considered to provide sufficient rotation for seismic demands according to AISC 341-10 Seismic Provisions for Structural Steel Buildings Section D3 on Deformation Compatibility of Non-SFRS Members and Connections (2010). AISC 341-10 allows the connections to reach these

rotational demands through inelastic deformation provided this does not cause instabilities (2010). ASCE 7-10 Minimum Design Loads for Buildings and Other Structures Section 12.12.5 on Deformation Compatibility requires structural components that are not part of the Seismic Force Resisting System (SFRS) to be able to resist the combined effects of gravity loads and loads induced by the design story drifts (2010). AISC 340-10 identifies the load produced by drift on these connections as horizontal forces caused by column inclination (2010).

Gravity frame beams are often considered simply supported with STCs modeled merely as moment releases (Crocker & Chambers, 2004). As such, the shear connections must allow the beams to reach their rotational demands, and they are assumed to do so with little resistance (Astaneh-Asl, Liu, & McMullin, 2002). Gravity frames using STCs are typically ignored as contributors to the Lateral Force Resisting System (LFRS) because of this simply supported assumption (Crocker & Chambers, 2004). However, these connections have been shown to have significant rotational stiffness and resistance to lateral load (Liu & Astaneh-Asl, 2000).

Lateral displacement of a structure places demands on its STCs beyond those of the gravity loading. Predicting the lateral performance of these connections is important in predicting the seismic performance of the structures containing them (Crocker & Chambers, 2004). In cyclic testing, the behavior of STCs begins with slipping of the connection's bolts followed by ductile mechanisms leading to failure of the connection (Liu & Astaneh-Asl, 2000). Typically, the first of these mechanisms is yielding of the shear tab followed by bearing of the bolt holes and out-of-plane warping of the plate and beam web (Liu & Astaneh-Asl, 2000). Limit states observed in STCs include: yielding of the shear tab, fracture of the shear tab, bearing failure of the bolt holes, bolt fracture, and fracture of the weld (Liu & Astaneh-Asl, 2000). Figure 2-2 shows the progression of slip, yielding, and fracture of a STC.

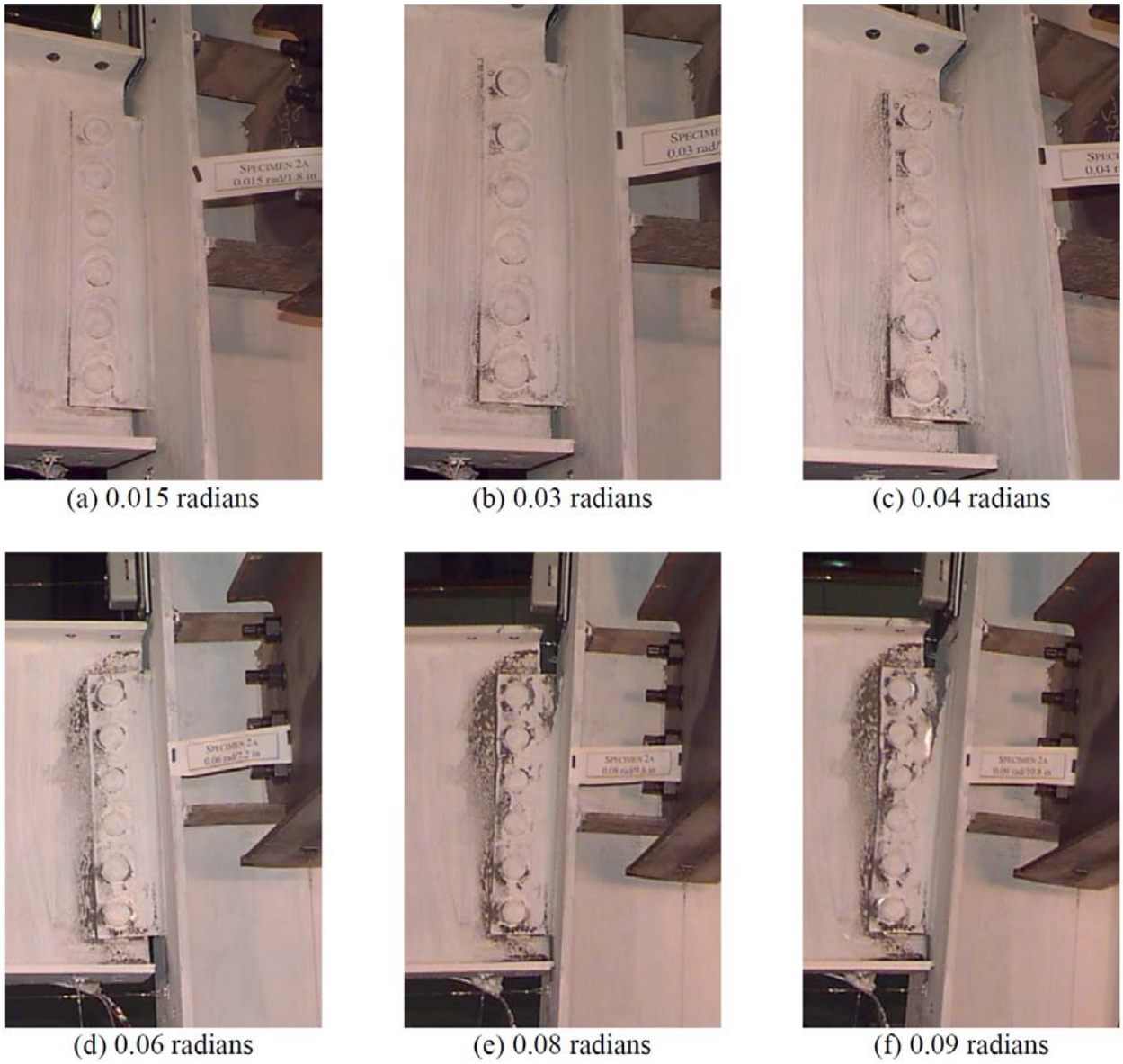

Figure 2-2. STC Failure Progression (Liu & Astaneh-Asl, 2000)

The maximum capacity of STCs is a function of the connection's neutral axis location (Crocker & Chambers, 2004). When the beam flange bears on the column at large rotations, the neutral axis moves to this point of contact (Crocker & Chambers, 2004). This dramatically increases the stiffness of the connection, causes yielding in column panel zones, and leads to

fracture of the shear tab (Liu & Astaneh-Asl, 2000). A STC with the bottom flange of the beam bearing against the column is shown in Figure 2-2 (e) and Figure 2-3.

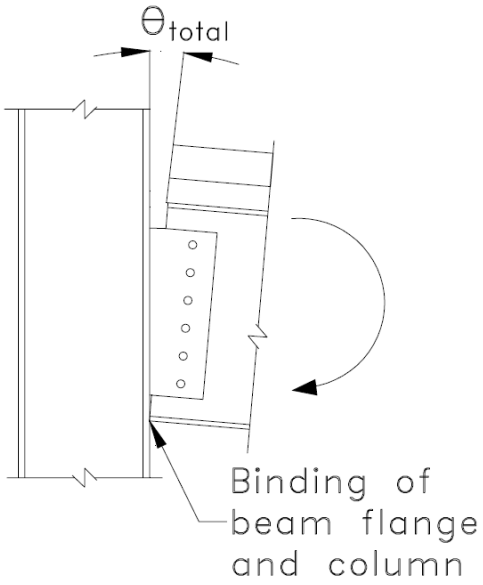

Figure 2-3. STC Rotation (Liu & Astaneh-Asl, 2000)

Some STCs are designed with angles fixing the bottom of the beams to the columns. STCs with these supplemental seat angels have significantly higher rotational stiffness and put heavy demands on columns (Liu & Astaneh-Asl, 2000). STCs strengthened with seat angles have been shown to induce yielding in column panel zones, followed by yielding in the seat angles, and then fracture of the angels and connection plate (Liu & Astaneh-Asl, 2000). Fig 2-4 shows a failed STC with a seat angle.

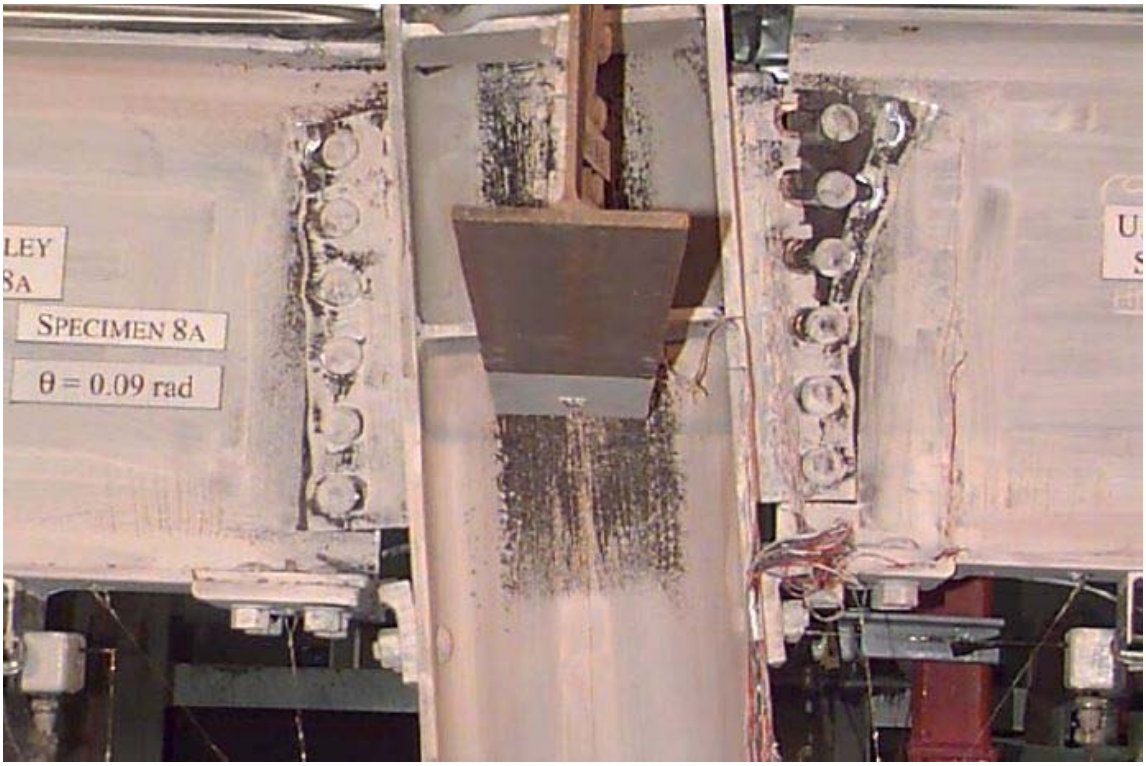

Figure 2-4. STC with Seat Angel Failure (Liu & Astaneh-Asl, 2000)

Steel gravity frames often support concrete floor slabs. Shear studs can be used to create composite action between the steel beams and the concrete slab. Laboratory testing has shown that the contribution of a composite concrete floor slab can roughly double the capacity of a STC (Liu & Astaneh-Asl, 2000). This benefit is lost after the slab surrounding the column is crushed at around 4% drift (Liu & Astaneh-Asl, 2000). A failed floor slab above a STC can be seen in Figure 2-5. Following the failure of the slab, the connection then behaves as an equivalent bare-steel STC that does not have a composite slab (Liu & Astaneh-Asl, 2000).

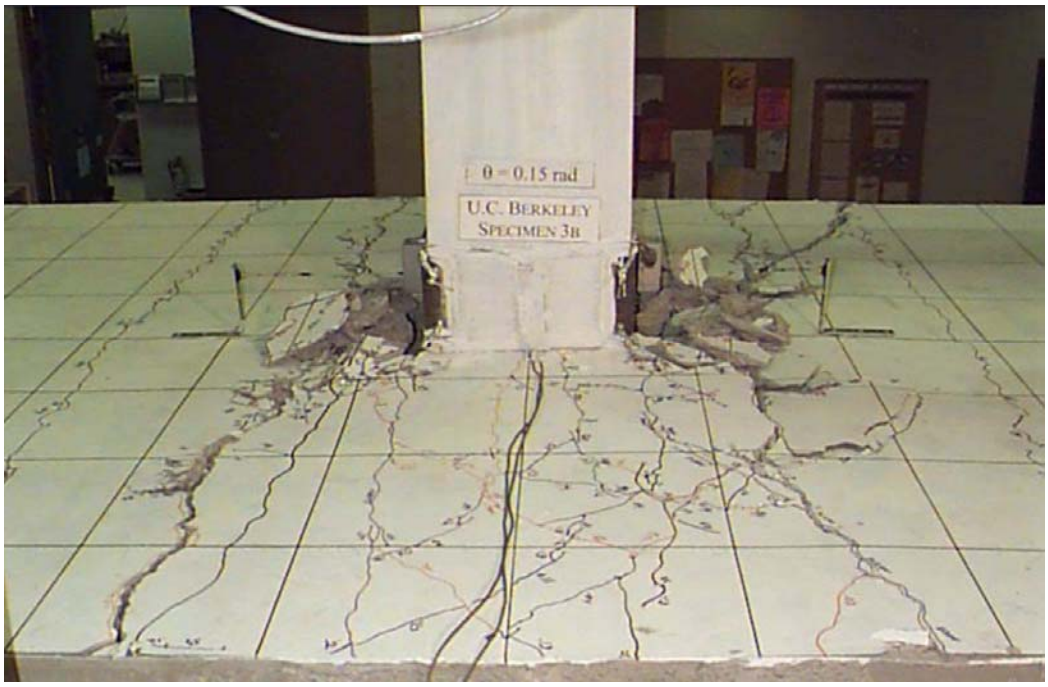

Figure 2-5. STC with Failed Concrete Slab (Liu & Astaneh-Asl, 2000)

Extensive laboratory testing of STCs was performed at the University of California at Berkley as part of Subtask 7.04 of Phase II of the SAC Steel Project. This research was performed to determine if STCs in the gravity frame could be relied upon to resist lateral loads (Liu & Astaneh-Asl, 2000). A variety of STCs were subjected to cyclic loading with simulated gravity loads (Liu & Astaneh-Asl, 2000). Models for STC moment capacity and rotation were developed from this research. Figure 2-6 outlines the general behavior of the model presented in the SAC Steel Project Report.

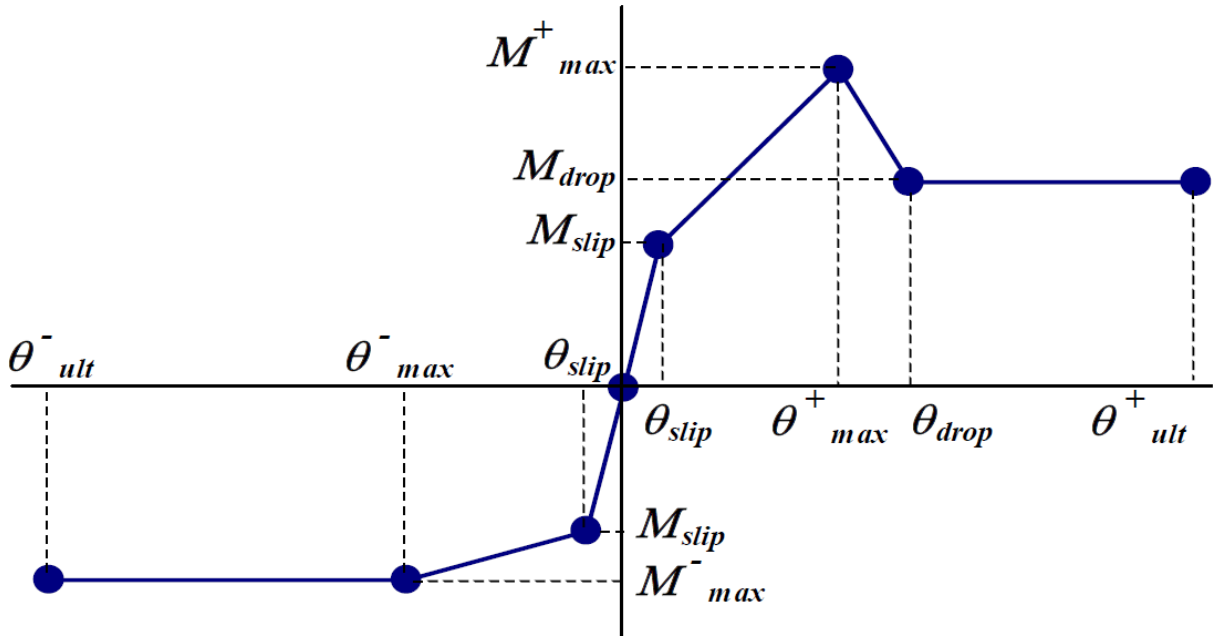

Figure 2-6. STC Moment-Rotation Model (Liu & Astaneh-Asl, 2000)

The initial stiffness of the connection is established by determining the moment and rotation required to overcome the static friction restraining the connection (Liu & Astaneh-Asl, 2000). This friction is caused by the bolt tension, and the moment required to overcome it is referred to as the "slip moment" (M_{slip}). Figure 2-2 (a) shows a STC that has just slipped. Calculated estimates of the slip moment begin with identifying the frictional force of one bolt. This assumes the minimum bolt tension defined in Section J3 of AISC 360-10 Specification for Structural Steel Buildings and the coefficient of static friction for a class A faying surface also given in AISC 360-10. An estimate of the slip moment (M^*_{slip}) is then calculated from the resultant force couple needed to overcome the static friction of each bolt. This is illustrated in Figure 2-7. The SAC experiments found these estimates to differ from experimental data by a consistent amount (Liu & Astaneh-Asl, 2000). An adjust factor was developed and with it an accurate estimate of the slip moment can be made (Liu & Astaneh-Asl, 2000). The slip rotation is determined empirically from the SAC experiments.

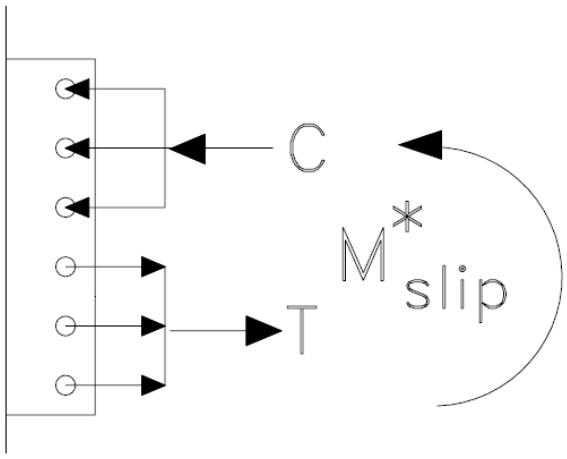

Figure 2-7. STC Slip Moment (Liu & Astaneh-Asl, 2000)

The connection's static friction is not present for multiple cycles of STC deformation (Liu & Astaneh-Asl, 2000). Once the STC slips, its stiffness decreases. The reduced resistance of subsequent cycles comes from kinetic friction in the connection. Therefore, it may be more appropriate to use the secant stiffness model (Liu & Astaneh-Asl, 2000). The secant stiffness model neglects the slip behavior. The secant stiffness is established by the maximum positive and negative moment capacity and corresponding rotation of the connection. This stiffness is roughly half of the initial stiffness based on the slipping of the connection (Liu & Astaneh-Asl, 2000). Figure 2-8 outlines the behavior of a STC showing the secant stiffness for positive moment. Though it is not depicted, the secant stiffness would also apply to negative moment-rotation relationship as well.

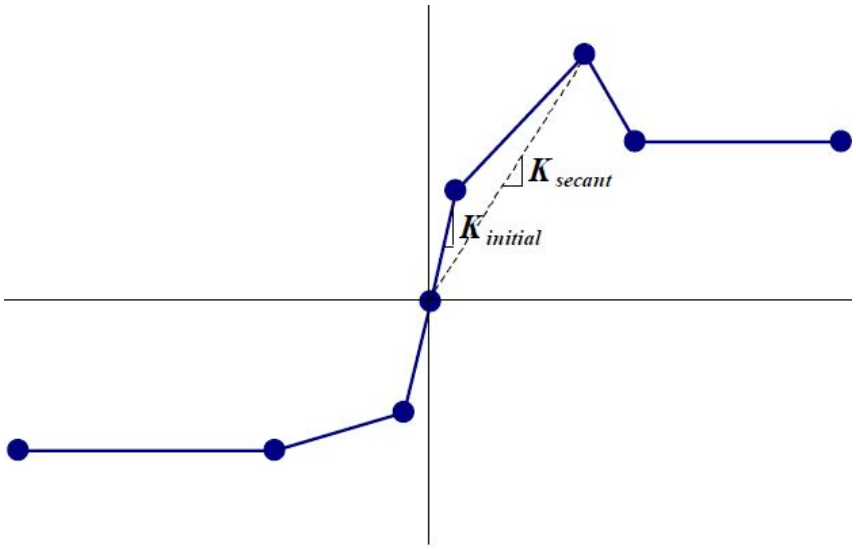

Figure 2-8. STC Secant Stiffness (Liu & Astaneh-Asl, 2000)

Design equations for calculating the maximum moment capacity of STCs have been developed and verified through cyclic testing as part of the SAC Steel Project. The rotation at which the maximum capacity first occurs is defined empirically. The ultimate rotation (θ_{ult}) is defined as the rotation at which the beam flange bears against the column. This is purely a function of the connection geometry.

The drop in the positive moment-rotation relationship of Figure 2-6 signifies the failure of the concrete slab. The rotation at which the slab is no longer effective (θ_{drop}) is an empirical value. The slab is considered only to participate when bending of the connection puts the concrete in compression. Thus, the negative portion of the STC moment-ration curve has no drop in capacity. The positive moment-rotation relationship mirrors this portion of the curve for bare-steel STCs and STCs with composite slabs following the failure of the concrete. The SAC moment-rotation models were developed as a basis for incorporating the behavior of simple connections in structures subjected to lateral loadings (Liu & Astaneh-Asl, 2000).

2.3 Slotted Bolted Friction Dampers

The Slotted Bolted Friction Damper (SBFD) is a commonly used device for dissipating energy. The device is a simple and inexpensive design that can be installed in many arrangements throughout a structure. A typical configuration for a slotted bolted friction device is shown in Figure 2-9. Generally, these devices are composed of three steel plates separated by two "shims" of a selected friction material with high strength bolts clamping all five layers together. Spring washers are used to retain bolt tension during loading cycles. The center plate contains slotted holes allowing it to move relative to the rest of the device. Friction is generated as the slotted plate slides past the shims above and below it. A detailed depiction of assembled SBFD is shown in Figure 2-10.

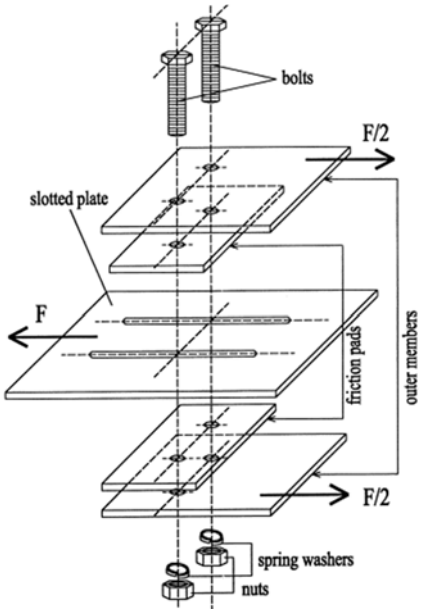

Figure 2-9. Typical SBFD Configuration (Balendra, Yu, & Lee, 2001)

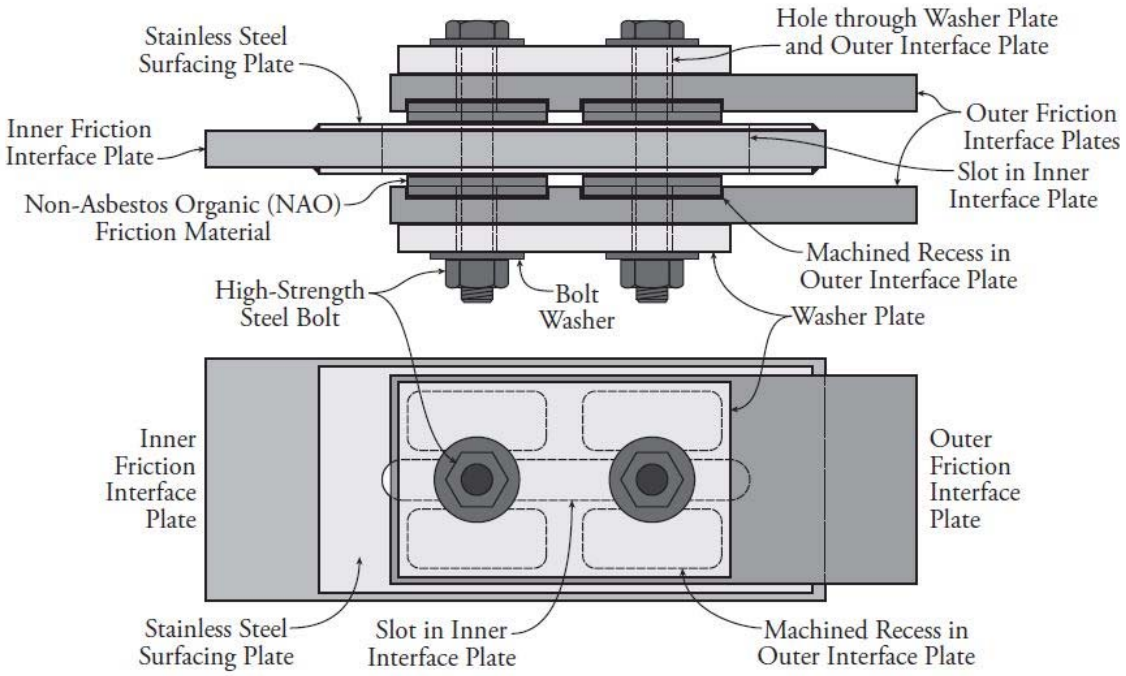

Figure 2-10. Slotted Bolted Friction Damper (Erochko, 2013)

Friction dampers resist motion as kinetic energy is converted into thermal energy by the abrasion of one surface against another. Friction dampers are assumed to behave according to the Coulomb friction model (Erochko, 2013). The Coulomb friction model is an empirical description of dry friction behavior (Bhavikatti & Rajashekarappa, 1998). It assumes that only a small portion of the friction surfaces are in atomically close contact thus the friction force is independent of the contact area (Bhavikatti & Rajashekarappa, 1998). The model assumes the friction force is linearly proportional to the normal force compressing the two friction surfaces together (Bhavikatti & Rajashekarappa, 1998). A coefficient of friction is an empirical multiplier that equates the normal force to the frictional force. A coefficient of friction is unique to the two contacting surfaces as well as the mode of friction. This classic model describes friction in two modes: static and kinetic (Bhavikatti & Rajashekarappa, 1998). Static friction can occur when friction surfaces are stationary relative to one another (Bhavikatti & Rajashekarappa, 1998). Kinetic friction occurs

when friction surfaces are in relative motion (Bhavikatti & Rajashekarappa, 1998). Friction is a more complicated physical interaction, but the Coulomb model is a simple and adequately accurate approximation of friction damper behavior (Bhavikatti & Rajashekarappa, 1998).

The SBFD is activated by axial deformation. A minimum of two bolts are needed to assure the device deforms in a straight line. As the device is loaded, there is an initial elastic stiffness (Golondrino, et al., 2013). The axial load on the device builds until the static friction force in the damper is overcome and the friction surfaces begin to slide past one another. The load at which this occurs is called the slip force. After the SBFD slips, there is a constant force of kinetic friction resisting the deformation of the device. This resistance is referred to as the sliding force. The SBFD behaves similarly under tensile or compressive loads. Figure 2-11 shows the SBFD sliding mechanics.

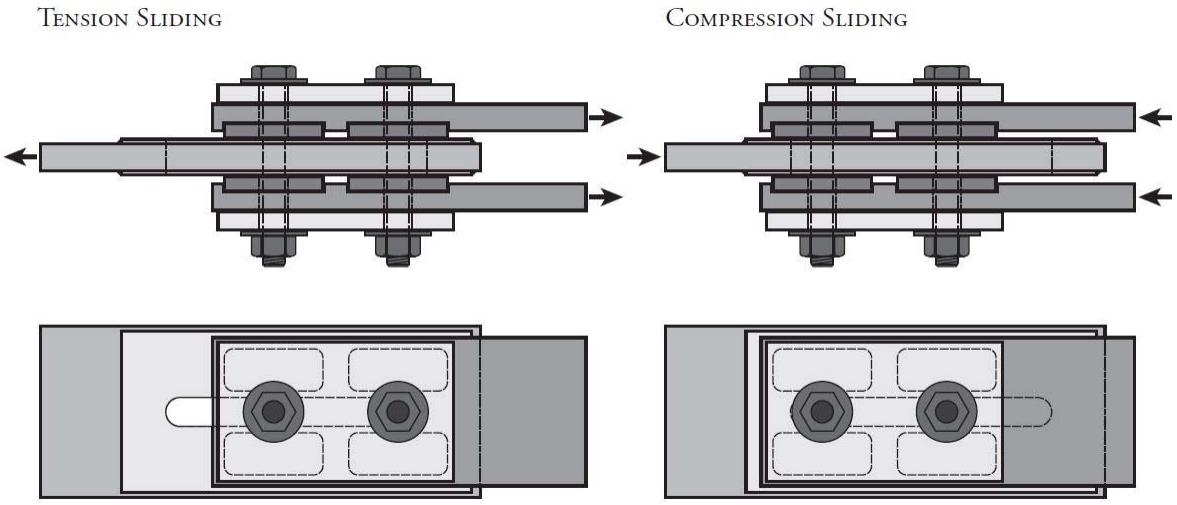

Figure 2-11. SBFD Mechanics (Erochko, 2013)

The friction force is a function of the normal force provided by the tension in the bolts and the friction coefficient for the sliding surfaces (Golondrino, et al., 2013). This relationship is described for a SBFD by Equation 2-1. In this equation, F_f represents the sliding force, μ_e is the effective coefficient of friction, n is the number of bolts, η is the number of friction planes, and T

is the bolt tension. The sliding force is set by adjusting the bolt tension. The other variables have been shown to remain reasonably constant (Golondrino, et al., 2013).

$$F_f = \mu_e * n * \eta * T \qquad \textbf{Equation (2-1)}$$

Energy is dissipated in moving the SBFD as a constant force must be exerted through the sliding distance. The energy required to deform the device can be shown in a plot of the applied force versus the resulting deformation. This plot is called a hysteresis. The behavior of the system is dependent upon the device's current state or history (Naeim, 2001). When a compressive force is applied to a SBFD, there is an elastic stiffness until the slip force is reached and large deformation occurs without requiring additional force. When this load is reversed, there is a delay in the large deformation as the device deforms elastically once again until the applied tension reaches the slip force (Naeim, 2001). Figure 2-12 shows the hysteresis of a SBFD. The area enclosed by the hysteresis loop represents the energy dissipated.

This hysteretic behavior of SBFDs changes for different friction shim materials (Golondrino, et al., 2012). Common materials used in SBFDs include: aluminum, brass, mild steel, and Non-Asbestos Organic (NAO) friction composites (Golondrino, et al., 2013). Hystereses of SBFDs using different metals as friction shims can be seen in Figure 2-13. Figure 2-12 shows the hysteresis of a SBFD using an NAO friction material. A friction device with a constant and repeatable slip force is desirable for design and reliable performance. These characteristics are evident in a stable hysteresis.

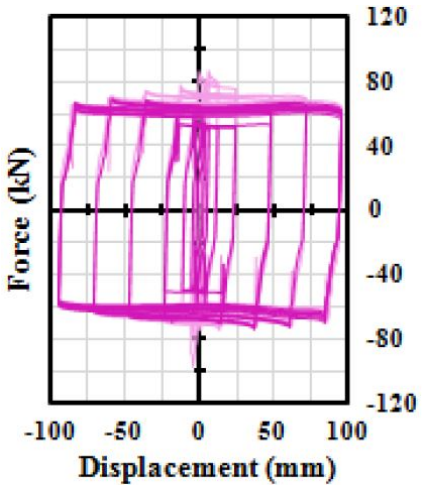

Figure 2-12. SBFD Hysteresis for NAO Friction Shims (Golondrino, et al., 2013)

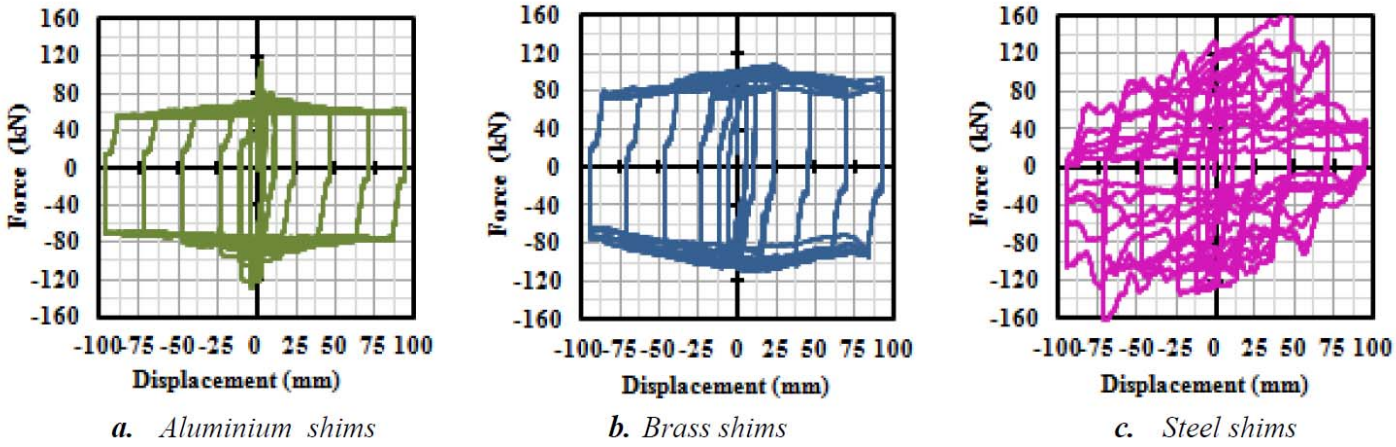

Figure 2-13. SBFD Hystereses for Different Metallic Shims (Golondrino, et al., 2012)

Certain metallic friction surfaces exhibit irregular hysteretic behavior like the mild steel to mild steel contact shown in Figure 2-13 (c). This is caused by particles that wear off of one surface and interfere with the friction contact (Khoo, et al., 2012). These wear particles can have an adhesive effect, and their physical presence between the two sliding surface can create more physical damage (Khoo, et al., 2012). The adhesive effect of these particles creates a "stick-slip" behavior resulting in erratic spikes in the sliding force (Khoo, et al., 2012). An upper and lower

bound design approach should be used for the friction coefficient to deal with uncertainty in the slip force (Erochko, 2013).

SBFDs with brass and aluminum shims have moderately stable hystereses, but still suffer some surface wear effects (Golondrino, et al., 2012). Ensuring a difference in hardness between the friction surfaces results in a more stable sliding performance and less wear (Khoo, et al., 2012). This allows the softer material to conform to the harder material and absorb wear particles (Khoo, et al., 2012). SBFDs with NAO composite shims provide a more stable hysteretic behavior than metallic friction surfaces (Golondrino, et al., 2013). This is visible when comparing the smooth hysteresis loops of a SBFD with NAO composite shims in Figure 2-12 to the sporadic hystereses of SBFDs with metallic shims in Figure 2-13. The components of a SBFD with NAO composite shims can be seen in Figure 2-14. The NAO material is bonded to machined recesses in the outer plates of the SBFD with epoxy (Erochko, 2013). A detailed depiction of a similar device is shown in Figure 2-10.

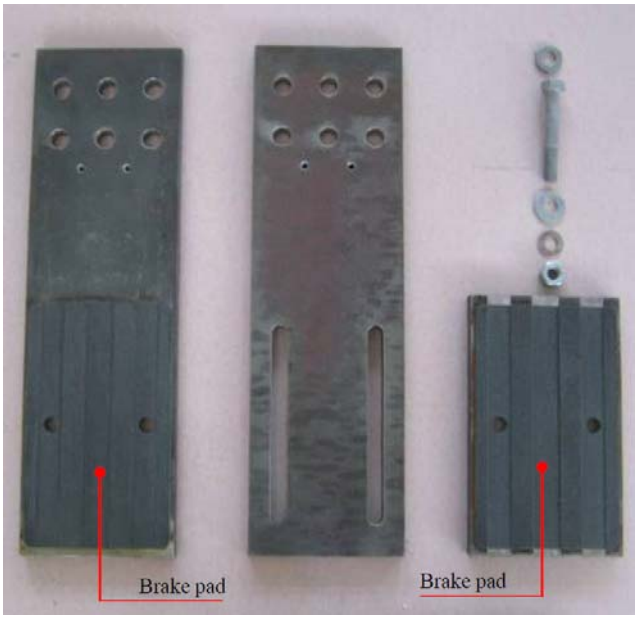

Figure 2-14. NAO Composite SBFD (Golondrino, et al., 2013)

NAO composite shims produce a constant friction force through the sliding length once a "steady wear" state is reached (Golondrino, et al., 2013). A steady wear state occurs when the wear resistant segments of the heterogeneous NAO composite carry the bolt load and the softer filler material has been worn and receded (Golondrino, et al., 2013). Wear continues after the steady state is reached, but the damage to the friction surfaces and adverse effects on friction behavior are considerably less than devices with metallic shims (Golondrino, et al., 2013). The stable and repeatable behavior of NAO composite friction pads and steel has led this to become a popular combination in friction applications (Erochko, 2013). However, the long term performance of SBFDs with NAO composite shims is not well documented. Issues with creep of the NAO material may lead to bolt relaxation and a reduced slip force (Erochko, 2013).

SBFDs have been used in a variety of structural applications. A prestressed concrete rocking wall with SBFDs is shown in Figure 2-15. These devices are commonly installed in beam-column connections of moment resisting frames and brace connections of braced frames (Golondrino, et al., 2013). Figure 2-16 depicts a beam-column joint with a SBFD. In this connection, the FDs can be activated by lateral displacement of the column as well as in-plane rotation at the end of the beam.

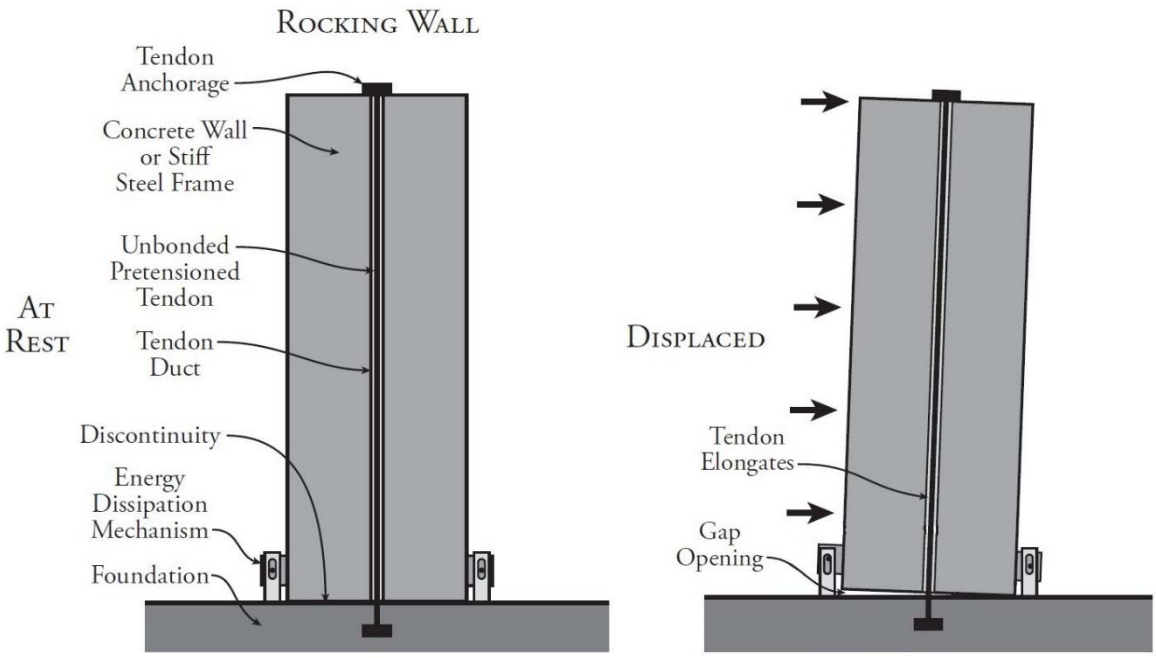

Figure 2-15. Rocking Wall with SBFD (Erochko, 2013)

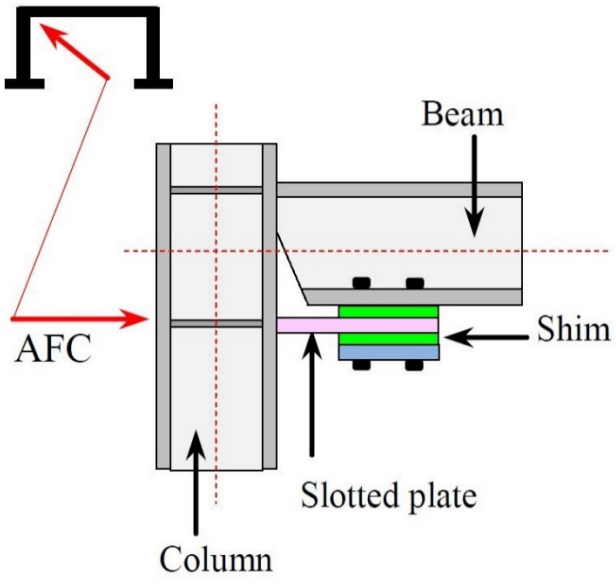

Figure 2-16. Beam-Column Connection with SBFD (Golondrino, et al., 2013)

The Sliding Hinge Joint (SHJ) is a moment resisting frame connection currently in use that contains bottom flange SBFDs (Khoo, et al., 2012). The SHJ utilizes NAO composite and stainless steel sliding surfaces (Khoo, et al., 2012). While the SHJ does not have a self-centering mechanism, residual drifts of structures with bottom flange friction devices are typically less than

structures that rely on beam hinging in the moment resisting frame (Khoo, et al., 2012). Figure 2-17 shows an illustration of a moment resisting frame with SBFDs at beam-column joints and self-centering post-tensioned strands. The magnified subfigure demonstrates the mechanics of the friction devices activating as the frame displaces laterally.

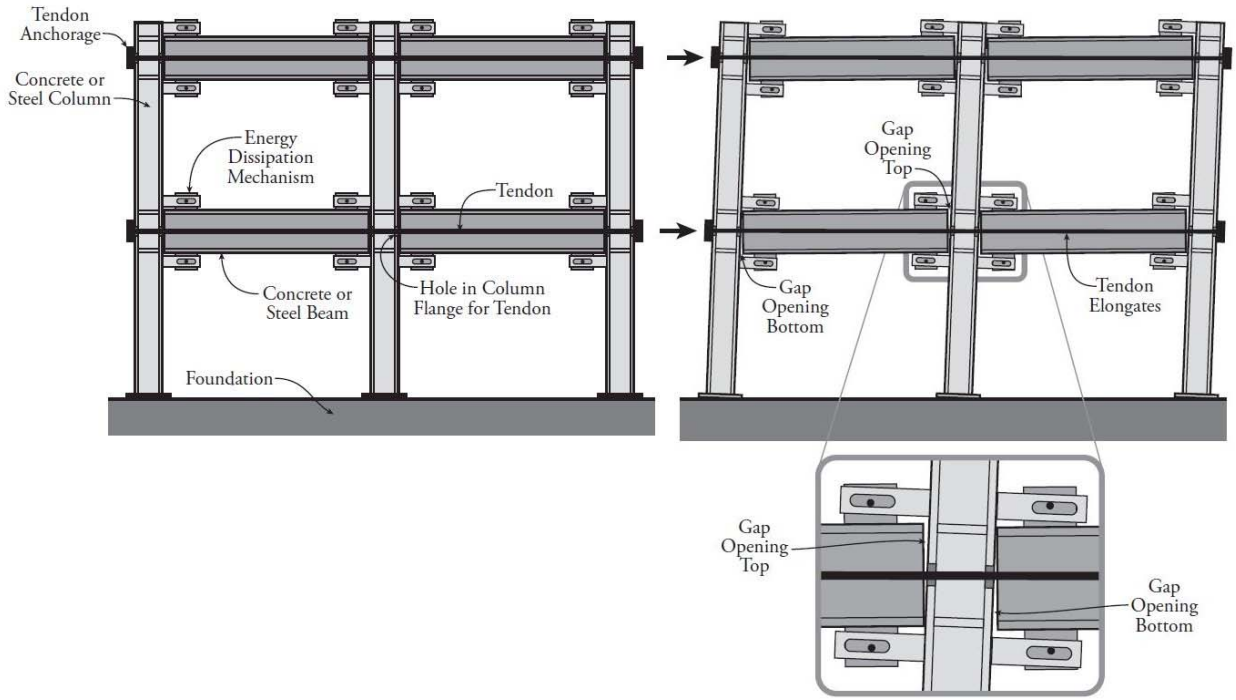

Figure 2-17. Self Centering Moment Frame with SBFD (Erochko, 2013)

SBFDs are also employed in braces. A typical use of a SBFD can be seen in Figure 2-18. Here, an SBFD has been incorporated into one of the brace connection. The Self-Centering Energy Dissipative (SCED) brace is a brace design with an internal friction damper. The SCED brace has internal pretensioned tendons that provide a self-centering mechanism (Erochko, 2013). Figure 2-19 shows an idealized SCED brace as it undergoes its full range of motion. The brace must first overcome the pretension force before the SBFD begins to take load and slip (Erochko, 2013). The flag-shaped hysteresis seen in Figure 2-19 is typical of self-centering devices with energy

dissipation (Erochko, 2013). The friction damping braces have been shown to decrease drifts while increasing accelerations when compared to conventionally braced structures (Erochko, 2013).

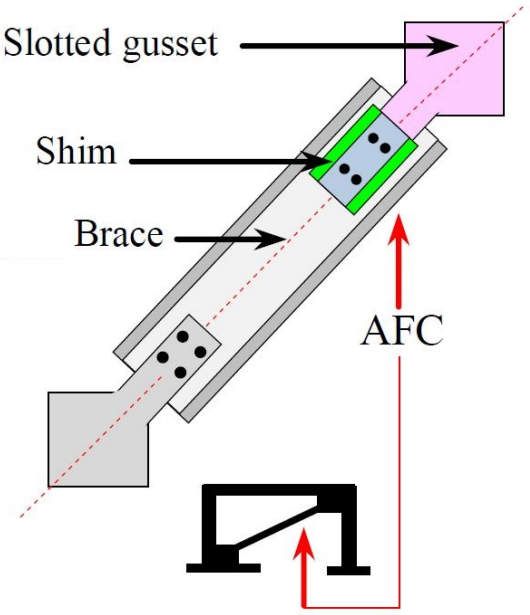

Figure 2-18. Brace with SBFD (Golondrino, et al., 2013)

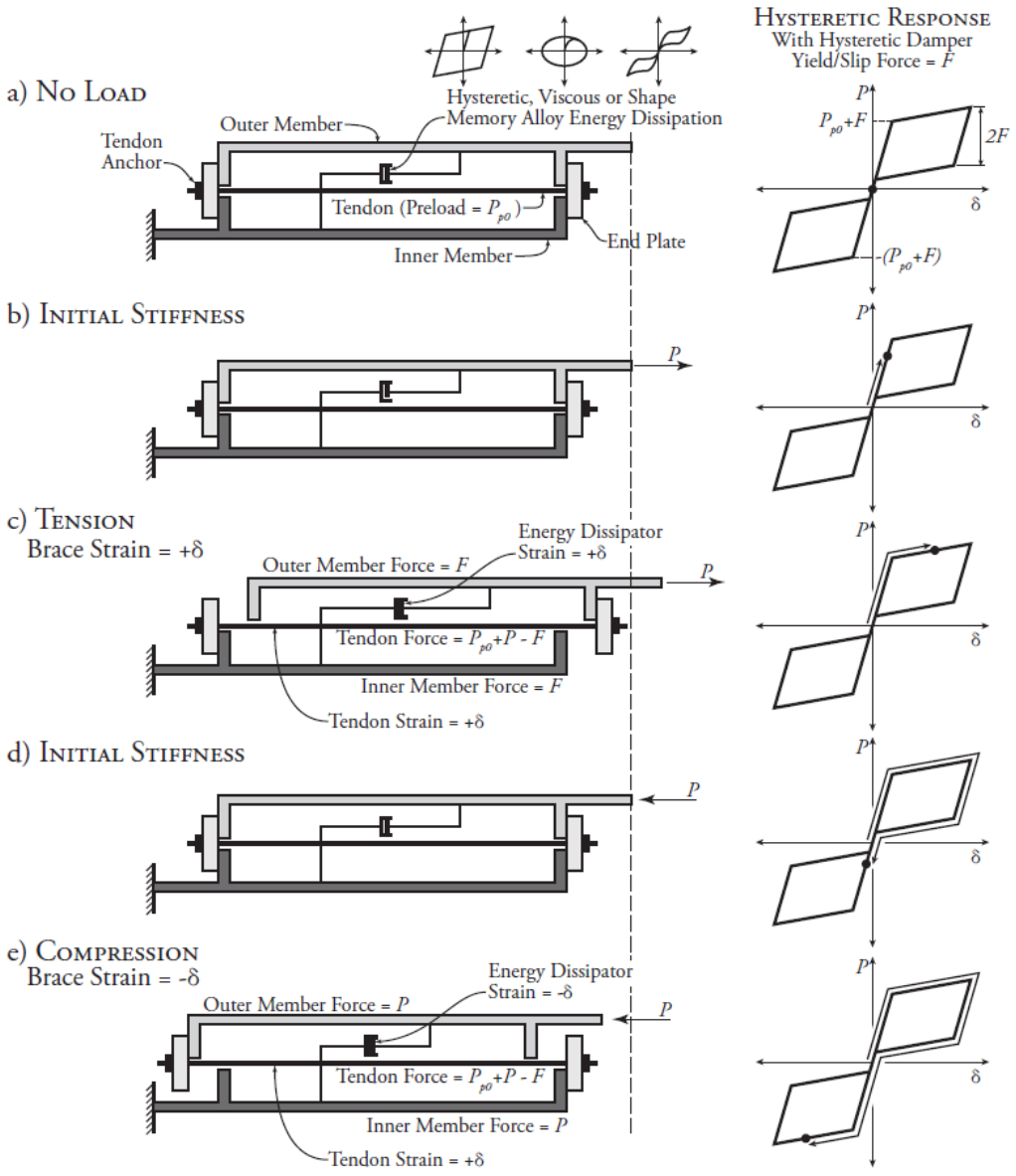

Figure 2-19. SCED Brace (Erochko, 2013)

2.4 Summary

This chapter was intended to provide a review of literature pertaining to shear tab gravity frame connections and slotted bolted friction devices in structural applications. The design, application, and performance of these structural elements are necessary in understanding the connections being analyzed in this thesis. The reviewed literature suggested slotted bolted friction dampers with NAO

composite shims provides a simple and reliable source of energy dissipation in a wide variety of structural applications. A scarce selection of literature was found on the effect the gravity frame has during lateral loading and how those effects should be accounted for in structural modeling.

Chapter 3. Building Design and 3D Inelastic Modeling

3.1 Introduction

In order to ascertain the effectiveness of early phase energy dissipation provided by LSFF connections, analysis was performed on three dimensional building models created in the SAP2000 structural analysis software. Two buildings, a three story and a nine story steel frame structure, were designed for this project using given requirements from the FEMA-355C SAC Model Building Project. Following the design of the buildings, several inelastic elements were designed and implemented in the models to capture the behavior of energy dissipating components. These buildings were then subjected to a suite of ground accelerations obtained from the Pacific Earthquake Engineering Research Center (PEER) Ground Motion Database in order to observe the seismic performance of a structural system with LSFF connections. The succeeding chapter covers the design process and detailed modeling of the test structures.

3.2 Design Inputs

SAC is a joint venture of the Structural Engineers Association of California, the Applied Technology Council, and California Universities for Research in Earthquake Engineering. The research venture was formed to address issues with steel moment frame structures after the 1994 Northridge earthquake. The Federal Emergency Management Agency (FEMA) provided most of the funding for the project. Several documents published by FEMA from the SAC Joint Venture were crucial to this research. The document FEMA 355C State of the Art Report on Systems

Performance of Steel Moment Frames Subject to Earthquake Ground Shaking was one of six state of the art reports of design and evaluation recommendations prepared by the SAC Joint Venture (FEMA, 2000 a). Appendix B of FEMA 355C details the SAC Model Buildings.

The SAC steel project commissioned three consulting firms to design typical steel moment frame office buildings in Los Angeles, Seattle, and Boston (FEMA, 2000 a). These buildings and their design criteria have also been used to create benchmark structures in other studies (Sabelli R. , 2001). The three story and nine story Seattle buildings were chosen to be modeled for this research. Figure 3-1 shows the original floor plan of these model buildings.

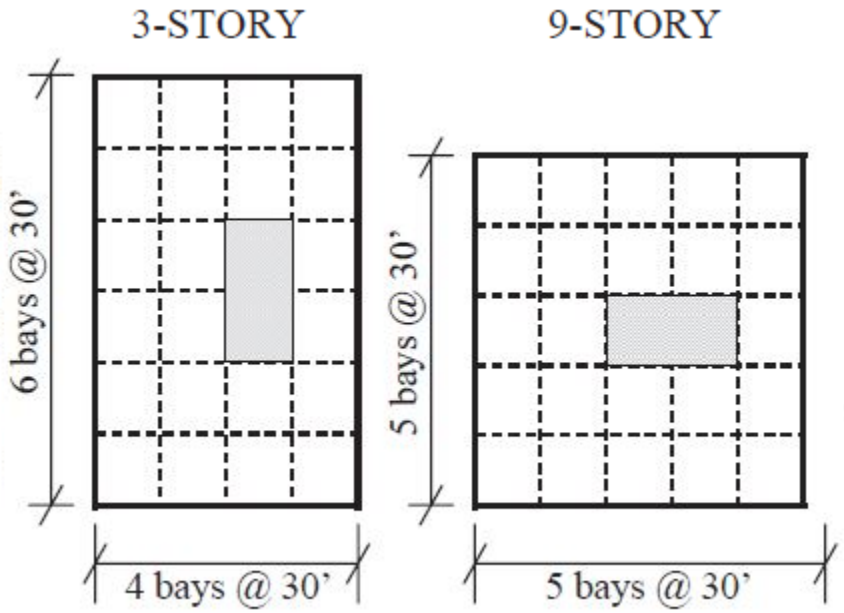

Figure 3-1. SAC Building Floor Plans (FEMA, 2000 a)

The structures were redesigned for this project to meet current code provisions. This process began with the program of requirements of the SAC buildings. One deviation from the SAC Model Building Project was the inclusion of buckling restrained braced frames in one direction. This modification was made to show the effects of the friction connections on two different Lateral

Force Resisting Systems (LFRS); a Special Moment Resisting Frame (SMRF) and a Buckling Restrained Braced Frame (BRBF).

3.3 Model Details

The structures analyzed in this research were designed utilizing the SAP2000 structural analysis software. Figure 3-2 and Figure 3-3 are displays of the full three dimensional building models from the SAP2000 software. Floor plans for these structures are shown in Figure 3-4. The X's indicate bays in which buckling restrained braces were added in a two story X configuration. Both buildings had 30 foot by 30 foot bays. The first story of the nine story structure had a story height of 18 feet while all other story heights were 13 feet. Each story of the three story structure was 13 feet. This geometry was given in the SAC Model Building Project. The direction running parallel to these braced frames is referred to throughout this document as the Braced Frame (BF) direction. The orthogonal direction is referred to the Moment Frame (MF) direction. The lateral force resisting system in this direction consists of SMRFs located at the perimeter on each side of the building.

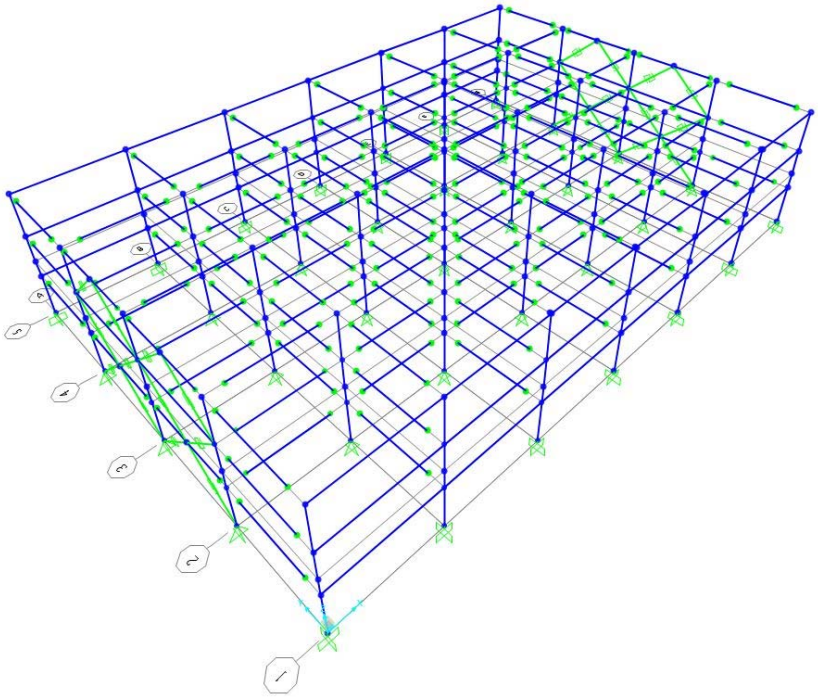

Figure 3-2. Three Story SAP2000 Model

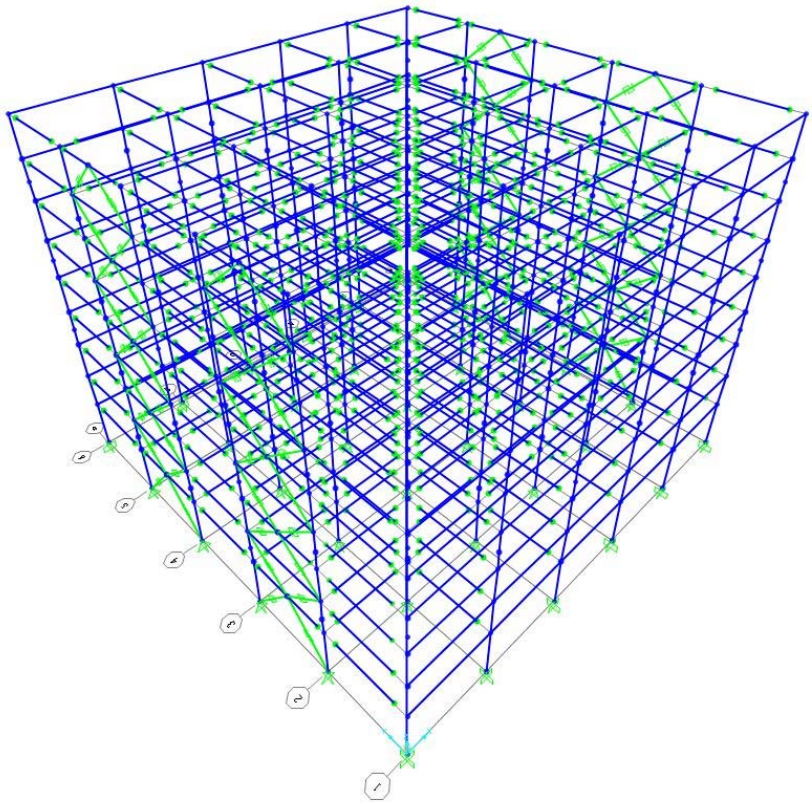

Figure 3-3. Nine Story SAP2000 Model

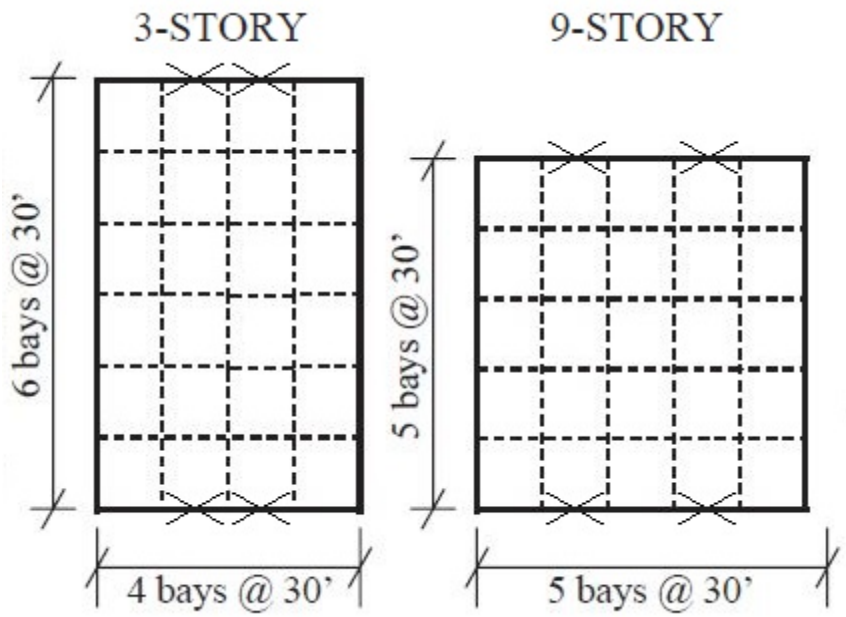

Figure 3-4. SAP2000 Model Floor Plans

The interior floor grid was formed by girders spanning between columns in the BF direction and beams framing into these girders in the MF direction. These girders were spaced at 30 feet and the beams at 7.5 feet. This orientation was chosen so that the beams in the SMRF took less of the floor load. In order to reduce the number of elements, gravity beams that did not frame into columns in the MF direction were not modeled, and the gravity load on girders in the BF direction was increased accordingly. The interiors of the structures were not designed as part of the LFRS. As such the interior frames are referred to as Gravity Frames (GF). Both of the GF flexural members were connected to columns with shear tab connections. During the initial design, these shear tab connections were modeled to allow these elements to freely rotate about their strong axis. Following the initial design, these shear tabs were modeled using multi-linear link elements. This is discussed further in Section 3.4.3.

3.3.1 Frame Element Releases and Joint Restraints

All the columns in the SAP2000 models were continuous through the height of the building. Column segments typically extended for two stories and were spliced six feet above the floor grid. The SMRF columns were fixed from rotation at the ground level. Figure 3-5 is a display of the three story SMRF in the SAP2000 software. GF columns were free to rotate at their base and oriented in the direction of the moment frame columns. The GF beams were allowed rotate at their ends. Figure 3-6 is a display of the three story BF direction GF in SAP2000. BRBF beams were fixed from rotating at ends where the BRBs framed into the connection and free to rotate elsewhere. This can be seen in Figure 3-7, which is a display of the three story BRBF from SAP2000.

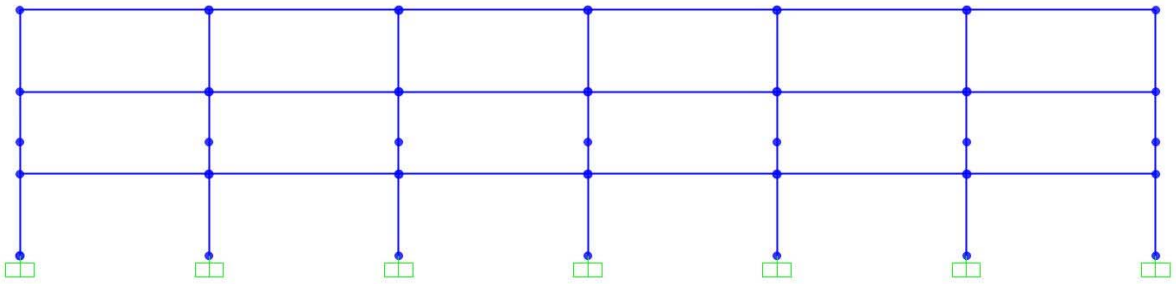

Figure 3-5. Three Story SAP2000 Model SMRF

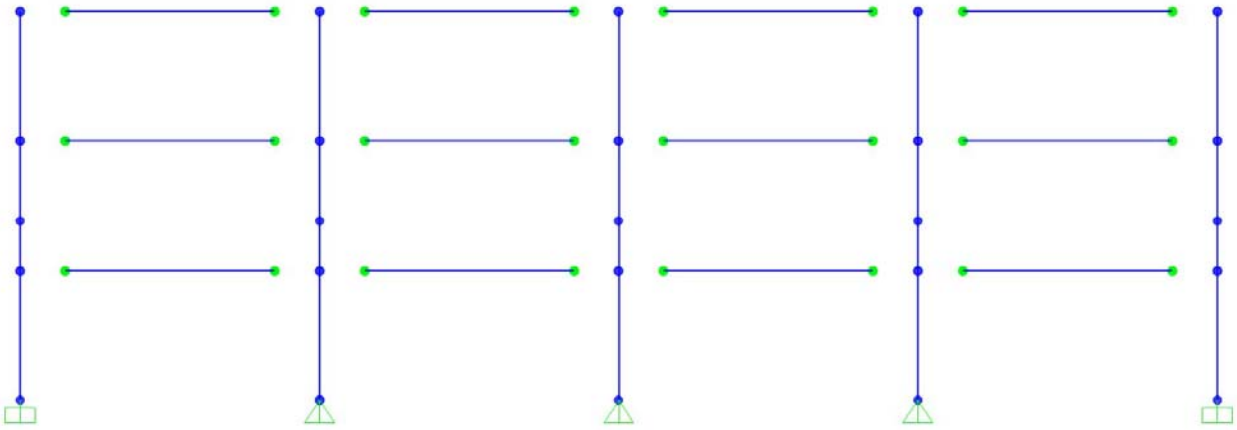

Figure 3-6. Three Story SAP2000 Model BF Direction GF

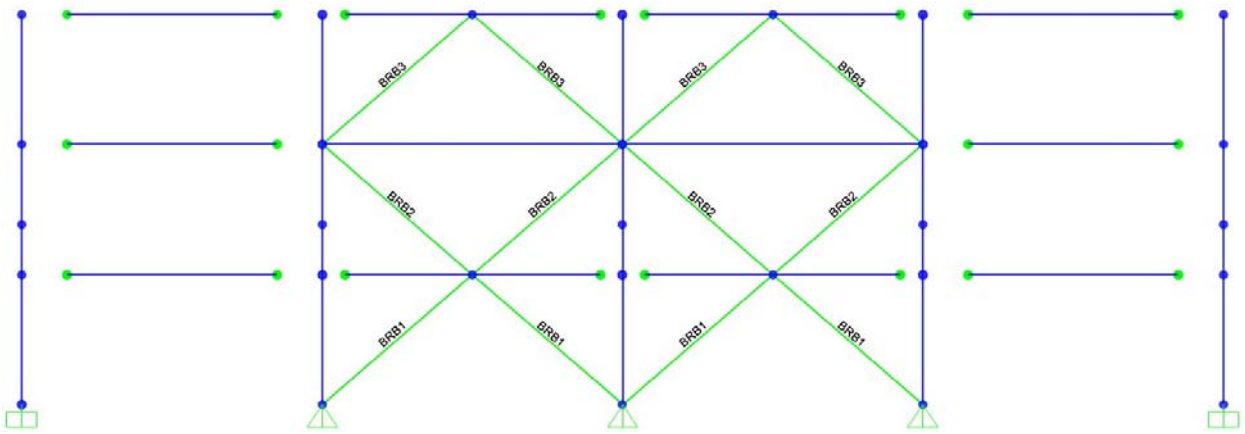

Figure 3-7. Three Story SAP2000 Model BRBF

3.3.2 Diaphragm Constraints and Joint Masses

The models' major grid points were located where column lines intersect floor planes. The joints at these locations were assigned a diaphragm constraint for each floor. A diaphragm constraint forces all the selected joints to displace as a planar diaphragm rigid against in-plane deformation. These joints cannot move relative to one another in plane as they are effectively connected by axially rigid link elements. This type of constraint does allow out of plane deformation. Figure 3-8 is a depiction of a diaphragm constraint taken form the SAP2000 reference manual. This joint constraint was created in the SAP2000 models to capture the effects of the concrete decking and its high in plane stiffness. A diaphragm constraint was chosen over shell or membrane elements to reduce the computational demands of the models during the dynamic analyses. A constraint reduces the size of the eigenvalue problem by reducing the horizontal degrees of freedom compared to other floor elements (Computers & Structures, Inc., 2014).

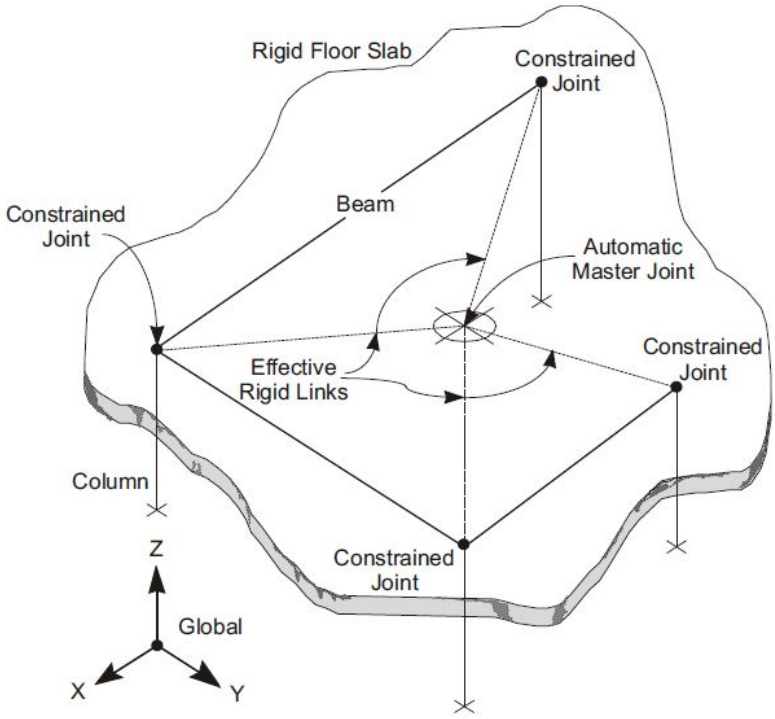

Figure 3-8. SAP2000 Diaphragm Constraint (Computers & Structures, Inc., 2014)

The floor joints located at major grid points were also assigned masses necessary for the seismic analysis. The seismic masses for each floor of the structures came directly from the SAC project and are given in Table 3-1. This table provides the total seismic mass for each floor. Portions of this mass were assigned to the floor joints according to each joint's tributary area.

Table 3-1. SAC Model Seismic Mass (FEMA, 2000 a)

3 Story Mass (kip-sec^2/ft)	
Roof	70.90
Floor 1-2	65.53

9 Story Mass (kip-sec^2/ft)	
Roof	73.10
Floor 2-8	67.86
Floor 1	69.04

3.4 Gravity Frame

The interiors of structures designed for this research consisted of steel W-Shapes and simple connections using shear tabs. GF columns and beams can be seen in Figure 3-9 and Figure 3-11. Figure 3-10 and Figure 3-12 show GF columns connecting to GF girders. The green dots represent end releases allowing the flexural members to freely rotate in the plane of the GF. The blue joints between floors represent column splices.

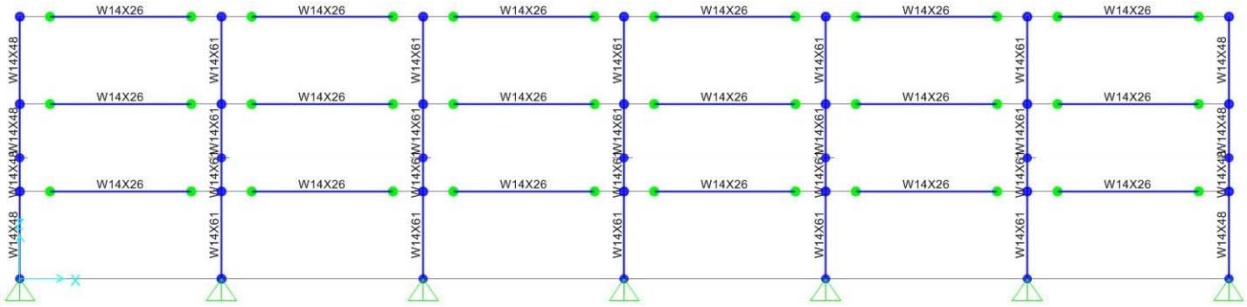

Figure 3-9. Three Story GF (MF Direction)

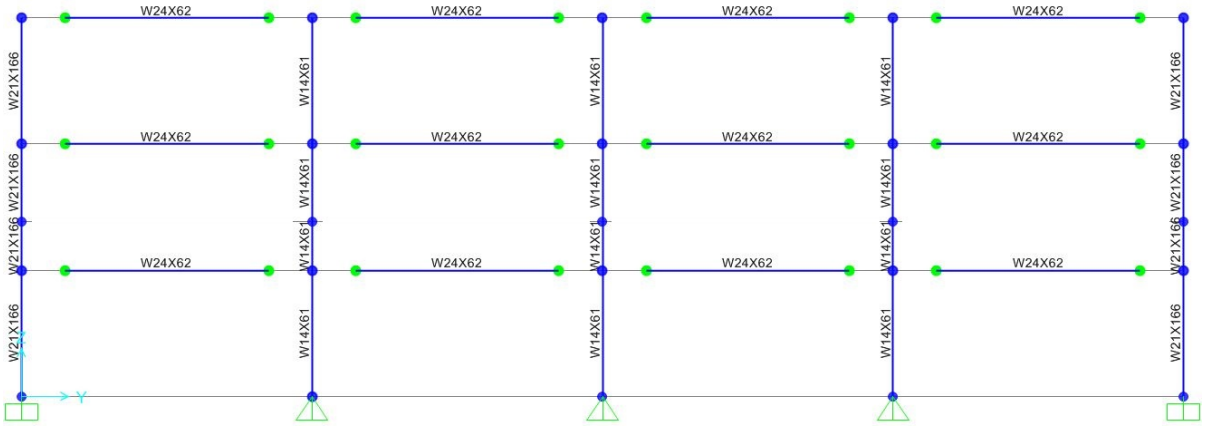

Figure 3-10. Three Story GF (BF Direction)

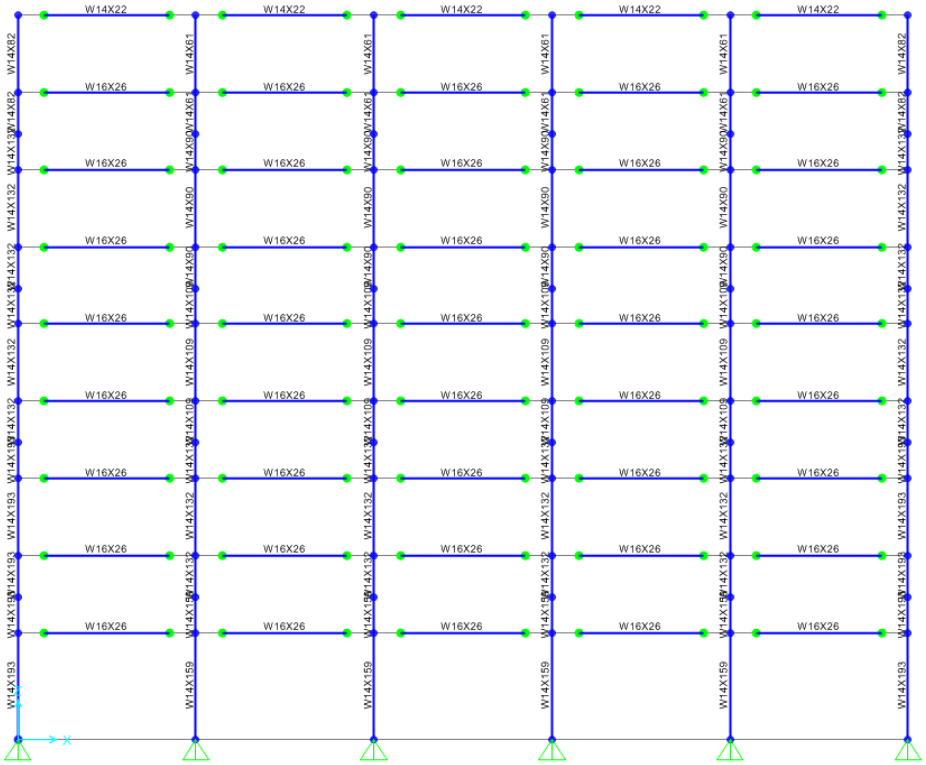

Figure 3-11. Nine Story GF (MF Direction)

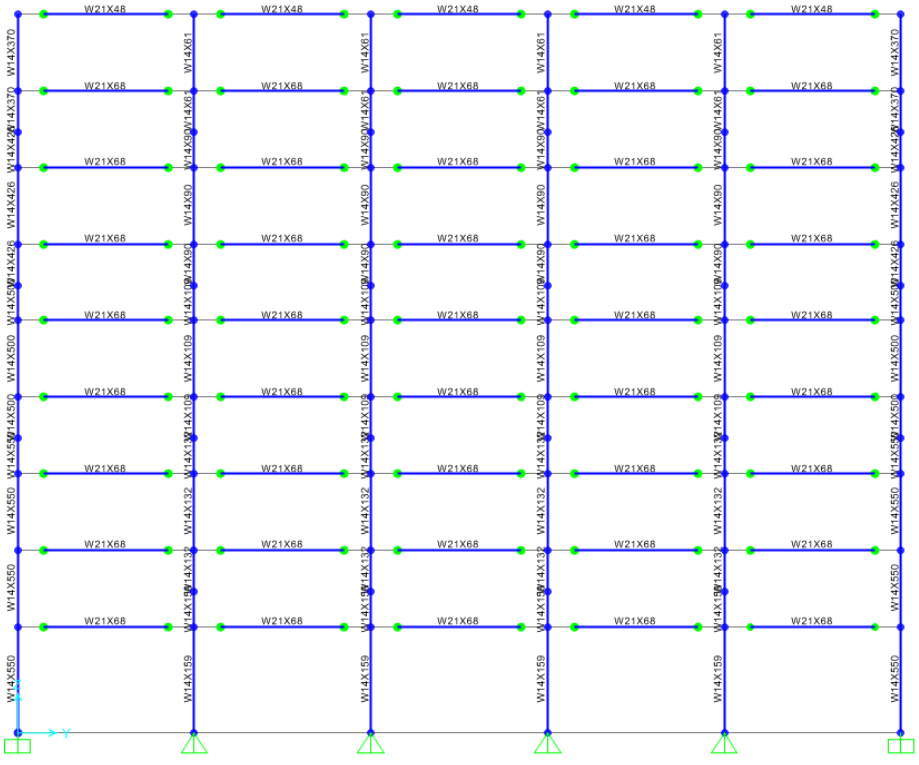

Figure 3-12. Nine Story GF (BF Direction)

3.4.1 Loads

All flexural members in these models were assigned linearly distributed gravity loads. Determining these gravity loads began with information provided by the SAC Model Building Project. SAC specified super imposed dead loads included metal decking with concrete fill, mechanical and electrical equipment, partitions, and exterior cladding with a roof parapet (FEMA, 2000 a). Given this information, ASCE/SEI 7-10 Minimum Design Loads for Buildings and Other Structures was used to determine floor loads. Appendix C Chapter C3 gave the weights of super imposed dead load elements listed in the SAC project. Provisions in Chapter 4 were used to determine reduced design area live loads. Snow loads were selected using Chapter 7 (ASCE/SEI, 2010). In addition to vertical loads, both wind and seismic design loads were applied to the structures. These lateral loads will be discussed further in Section 3.5.1.

3.4.2 Design

The Gravity Frame members in these models were designed using a Load and Resistance Factor Design specified in ANSI/AISC 360-10 Specification for Structural Steel Buildings. The flooring system was design with a one-way layout. In this load path, area floor loads were first resisted by beams spaced at 7.5 feet in the MF direction, then girders spaced at 30 feet in the BF direction, and finally by the columns. Loads were applied to floor beams in the SAP2000 models according to tributary areas. Loads on beams that were not modeled were applied directly to girders.

GF columns were modeled as continuous throughout the height of the structure. This caused the interior columns, which were not intended as part of the LFRS, to take some lateral load. Because of this, interior columns were oriented in the same direction as SMRF columns to resist the higher moment in that direction. These GF columns were designed to resist this increased demand.

Applied loads were factored and combined according to ASCE7-10 Section 2.3.2 load combinations (ASCE/SEI, 2010). The demands for which the structures were design came from demand envelopes in the SAP2000 structural analysis software. These envelopes displayed the maximum moments, shears, and axial loads throughout the length of members from all of the ASCE7 load combinations. Sufficient capacities were then determined using applicable sections of AISC 360-10. Table 3-2 lists the steel members that form the gravity frame.

Table 3-2. GF Member Sizes

3 Story GF Members	
Girders	W24x62
Beams	W14x26
Columns	W14x61

9 Story GF Members	
Girders (Roof)	W21x48
Girders (Floor 1-8)	W21x68
Beams (Roof)	W14x22
Beams (Floor 1-8)	W16x26
Columns (Floor 8-9)	W14x61
Columns (Floor 6-7)	W14x90
Columns (Floor 4-5)	W14x109
Columns (Floor 2-3)	W14x132
Columns (Floor 1)	W14x159

Design of the structures for stability was performed according to Chapter C of AISC 360-10. Initial imperfections were accounted for by applying notional loads prescribed in section C2.2. Stiffness reductions were applied according to section C2.3 (ANSI/AISC, 2010). Second-order structural analysis was performed in SAP2000. Controlling deflections will be discussed in Section 3.5.2 and Section 3.6.1 on LFRS design.

3.4.3 Inelastic Modeling

Following the design of the of GF members, the computer models were altered to include the stiffness and inelasticity of the shear tab connections. The chosen moment-rotation model for the STCs was taken from the SAC joint venture report, *Cyclic Tests on Simple Connections, Including Effects of the Slab*. The bare-steel moment rotation model was chosen to simplify the building

models and discount the effects of a slab, which may degrade throughout the duration of a seismic event. Similarly, the secant stiffness was used to neglect the initial stiffness and the slip behavior, which may degrade throughout an earthquake (Liu & Astaneh-Asl, 2000).

The STCs were modeled in the SAP2000 software with user defined link elements. These elements allow for independent plasticity properties to be specified in each degree of freedom. For the STCs, link elements with zero length were created connecting flexural members to columns. These links have hysteretic behavior models assigned to the rotational degree of freedom in-plane with the GF. All other degrees of freedom were made rigid. Four of these connections can be seen in Figure 3-13. The green brackets are the STC link elements.

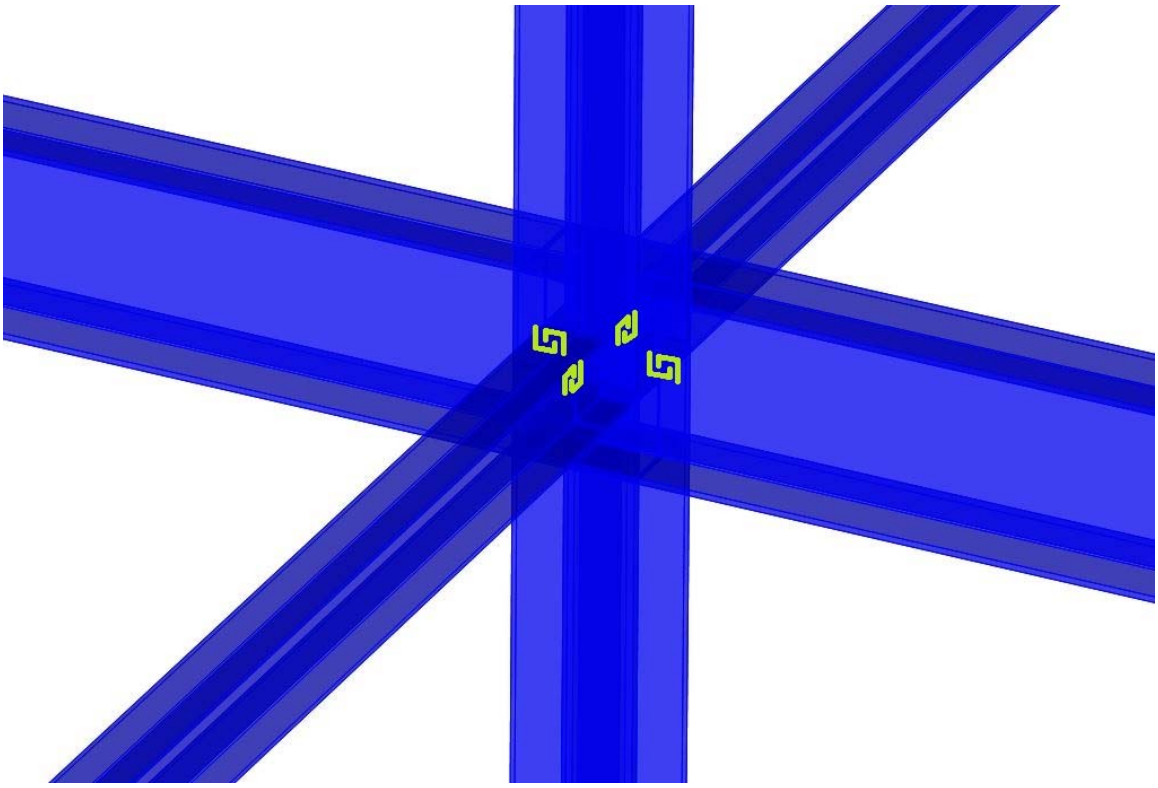

Figure 3-13. SAP2000 STCs

The STC link elements were assigned multi-linear kinematic plasticity properties. The kinematic plasticity model is the default hysteretic model for all metallic materials in the SAP2000

program. It is the recommended model for ductile behavior, and can dissipate a significant amount of energy (Computers & Structures, Inc., 2014). This property model is suitable for STCs which have been proven to have considerable moment capacity and ductile behavior through large rotations (Liu & Astaneh-Asl, 2000).

The multilinear kinematic plasticity model follows a force-deformation relationship based on a user-defined multi-linear curve (Computers & Structures, Inc., 2014). This curve, referred to as a backbone curve, delineates the behavior under monotonic loading. A hysteretic model based on kinematic hardening is used when loading is reversed (Computers & Structures, Inc., 2014). This behavior is illustrated in Figure 3-14.

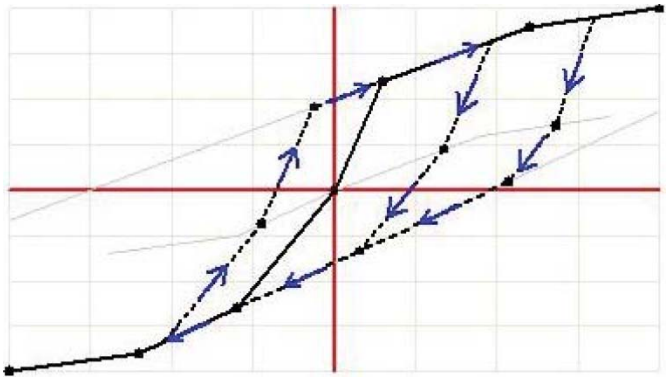

Figure 3-14. Multi-linear Kinematic Plasticity Model (Computers & Structures, Inc., 2014)

The general shape of the backbone curve of the STC link elements is shown in Figure 3-15. This behavioral model was assigned in the rotational degree of freedom in the plane of the frame containing the STC. All other degrees of freedom were fixed from movement. The values used for this backbone curve are based on Figure 2-6. Since both the added resistance of the composite slab and the static friction are not present for multiple cycles, a bare-steel STC model was used with an initial secant stiffness. The STC element behaves elastically following the secant stiffness until reaching a yield moment (M_y) corresponding to a ductile, bearing failure of the shear tab. This is the most common failure observed in cyclic testing of STCs (Liu & Astaneh-Asl, 2000).

Following the bearing failure, the STC elements deform plastically up to an ultimate rotation (Liu & Astaneh-Asl, 2000). A slight post-yield stiffness was added as recommended by the SAP2000 reference manual. The final point of the backbone curve corresponds to the maximum rotation possible where the beam flange contacts the column, see Figure 2-3. SAP2000 extrapolates the last two points on the curve to an infinite deformation (Computers & Structures, Inc., 2014). So, the STC elements were manually verified to not exceed the ultimate rotation.

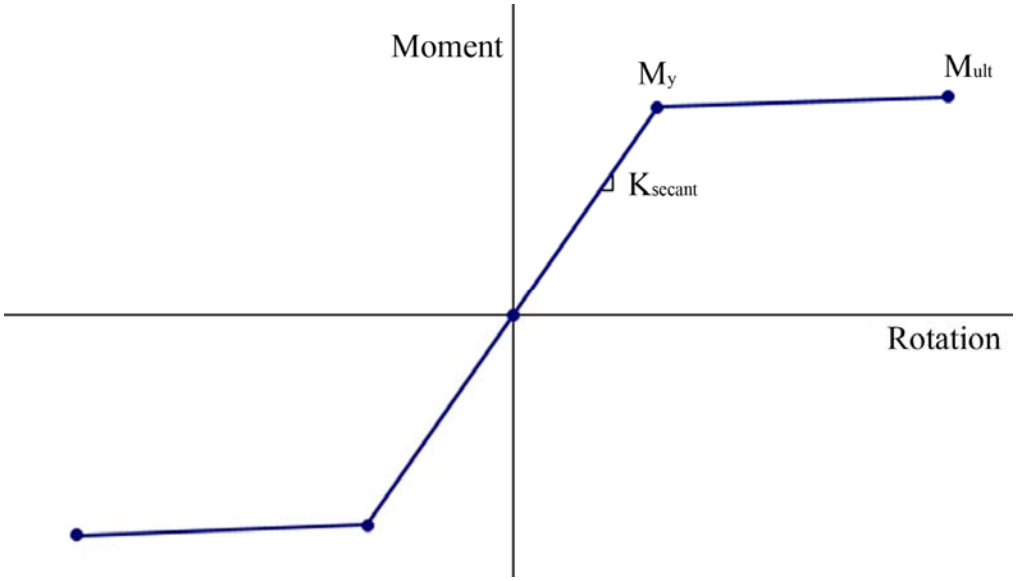

Figure 3-15. STC Backbone Curve

As previously mentioned, the gravity columns were continuous and did resist some of the lateral loads. GF flexural members were initially modeled with moment releases at each end, but with the addition of the STC link elements these connections became partially rigid. This change caused the GF flexural members to resist some of the lateral loads for which they were not initially designed. Some GF beams were resized because of this. The modeling of the GF was finalized with the addition of friction dampers. This is discussed in Section 3.7.

3.5 Special Moment Resisting Frame

The lateral force resisting system of structures designed for this research consisted of steel special moment resisting frames in one direction. These SMRFs can be seen in Figure 3-16 and Figure 3-17. The large color coded dots show the location of inelastic hinges assigned to the beams. The small blue joints in between floors represent column splices. All members were continuous, and columns were fixed at their bases.

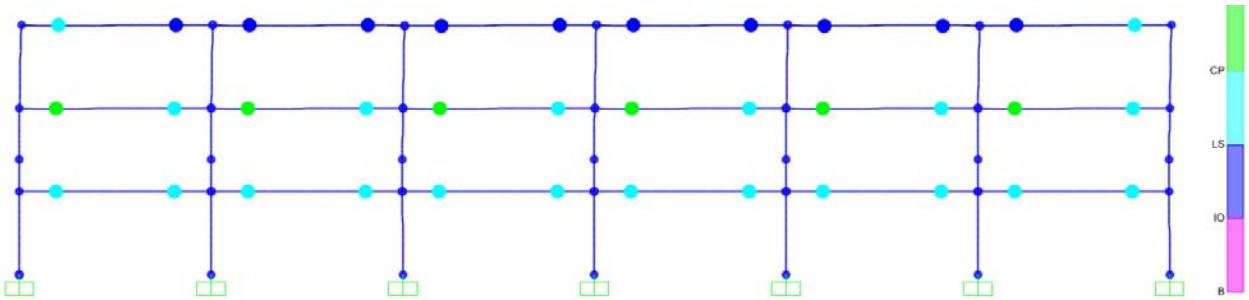

Figure 3-16. Three Story SMRF

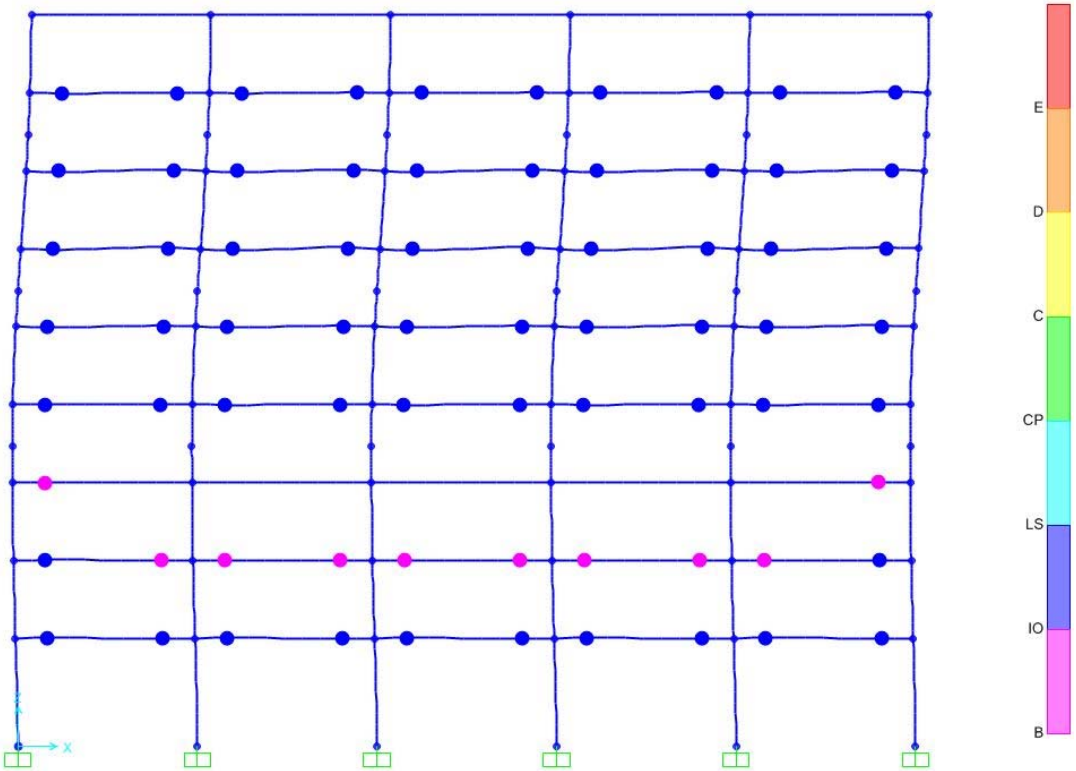

Figure 3-17. Nine Story SMRF

3.5.1 Loads

Linearly distributed gravity loads were assigned to the beams of the SMRF. These loads were discussed previously in Section 3.4.1. In addition to gravity loads, lateral wind and earthquake loads were assigned to LFRS flexural members. ASCE 7-10 was used to determine these lateral loads.

Chapter 11 and Chapter 12 of ASCE 7-10 give requirements for seismic design. The seismic loads were determined using an Equivalent Lateral Force (ELF) procedure described in Section 12.8. The structures were designed for the acceleration parameters of downtown Seattle, Washington; one of the three SAC Model Building design locations. The structures were designed for Site Class D as recommended by ASCE 7-10 when no geotechnical data is available (ASCE/SEI, 2010). Seismic weight was determined from masses listed in the SAC Model Building information of FEMA 355C. These masses are given in Table 3-1. A response modification factor of 8, an overstrength factor of 3, and a deflection amplification factor of 5.5 were used for the steel special moment frame. Story shears are the summation of seismic forces above the story considered (ASCE/SEI, 2010). These seismic forces were calculated from the ELF procedure. Distributed laterally applied loads were derived from the story forces and assigned to each floor of the structures with thirty percent of the load applied in the orthogonal BF direction as specified in Section 12.5.3a of ASCE 7-10. Torsional moments were applied to the structures according to Section 12.8.4 of the ELF procedure. Nonlinear static analyses were run on the structures using the seismic load combinations of Section 12.4.2.3. Deflections were determined from reduced EFL loads calculated using the SAP2000 model period with no upper limit as permitted by Section 12.8.6.2. These deflections were checked, according to Section 12.8.4, against the Allowable Story Drifts of Table 12.12-1 (ASCE/SEI, 2010). As with the rest of the structure, P-Delta Effects were modeled according to Chapter C of AISC 360-10.

Wind loads were calculated according to Chapter 26 and the Directional Procedure of Chapter 27 in ASCE 7-10. An Exposure Category of D was assumed, and design wind pressures were calculated using Equation 27.4-1 (ASCE/SEI, 2010). Laterally applied, distributed wind loads were determined from these pressures and assigned to each floor. Due to the large seismic loads, wind load combinations had no effect on the design of the LFRS.

3.5.2 Design and Modeling

The special moment resisting frame members in these models were designed according to ANSI/AISC 341-10 Seismic Provisions for Structural Steel Buildings, AISC 360-10, and ASCE 7-10. MF Members were initially sized to meet demands from ASCE 7-10 load combinations. Capacities were designed using AISC 360-10 to satisfy moment, shear, and axial loads obtained from the SAP2000 structural analysis.

MF members were then designed to meet the drift requirements in Section 12.12 of ASCE 7-10. Design story drifts were computed using Section 12.8.6 of the ELF procedure. Deflections from reduced ELF loads in a SAP2000 elastic analysis were increased proportional to the deflection amplification factor and importance factor. MF members were then increased in size until design story drifts were less than the allowable story drifts of Table 12.12-1 (ASCE/SEI, 2010).

MF members were designed to meet the specifications of AISC 341. Section E3 specifies the design of special moment resisting frames. These requirements are meant to provide inelastic deformation in beams and limited yielding of column panel zones before yielding occurs in columns. MF members were selected to meet the requirements of Section E3 predominantly the strong column, weak beam moment ratio of Equation E3-1 (ANSI/AISC, 2010).

Panel zones, the areas where beams frame into columns, often undergo shear yielding. The deformation of these regions has a significant effect on moment frame flexibility. Including both the elastic and inelastic response of panel zones in structural models is significant in seismic design and analysis (Charney & Marshall, 2006). For this research, panel zone behavior was included in the building models with rotational link elements at beam-column joints. These link elements were implemented using the Scissors model. The Scissors model simulates panel zone deformation with a rotational spring representing the shear deformation of the panel zone area and column flanges (Charney & Marshall, 2006). Figure 3-18 shows the configuration of the Scissors model.

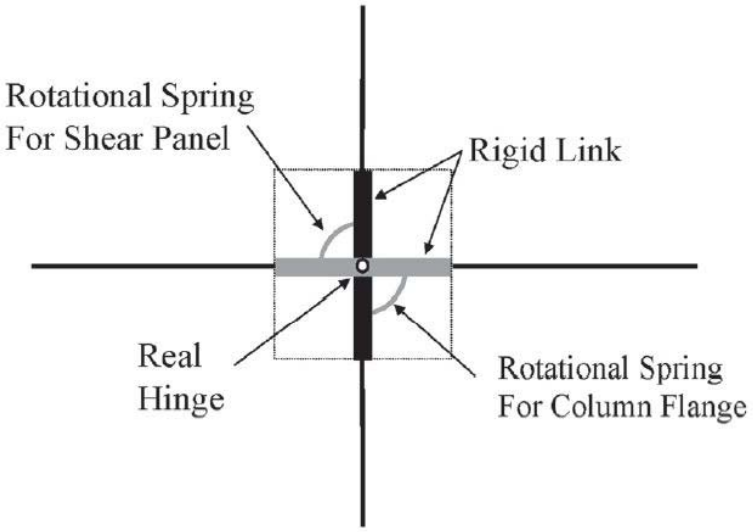

Figure 3-18. Panel Zone Scissors Model (Charney & Marshall, 2006)

The panel zone link elements were assigned multi-linear kinematic plasticity properties. The backbone curve used for these link elements came from the moment-rotation relationship detailed by the Scissors model. Figure 3-19 shows the moment-rotation relationship used in the Scissors model. The three part total curve was calculated at each joint based on beam and column geometry. This three part curve was used as the positive and negative moment-rotation relationship for the link element backbone curves.

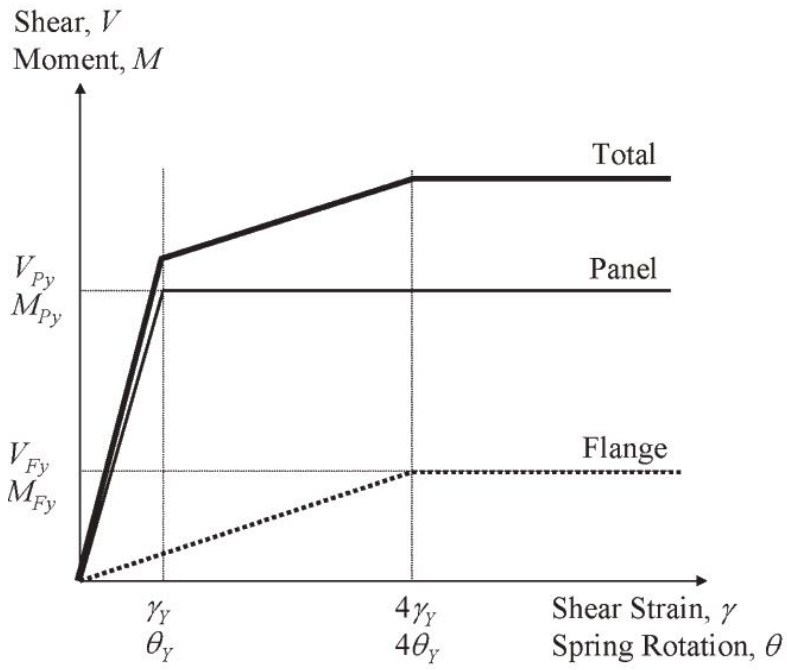

Figure 3-19. Scissors Model Moment-Rotation Relationship (Charney & Marshall, 2006)

Inelasticity was modeled in MF beams using SAP2000 plastic frame hinges. Frame hinges represent concentrated post-yield behavior. The general backbone curve used for hinge elements can be seen in Figure 3-20. The elastic deformation from point A to B occurs in the frame element, not the hinge. Inelastic deformation of the hinge occurs in the region between point B and point C. Acceptance criteria for performance based design were defined by ranges of rotation in this region. These criteria are: Immediate Occupancy, Life Safety, and Collapse Prevention. The stiffness in this region is caused by strain hardening. Point C is the ultimate strength of the hinge. Strength loss occurs for deformation beyond point C. Point D defines the residual strength. Point E represents total failure of the hinge.

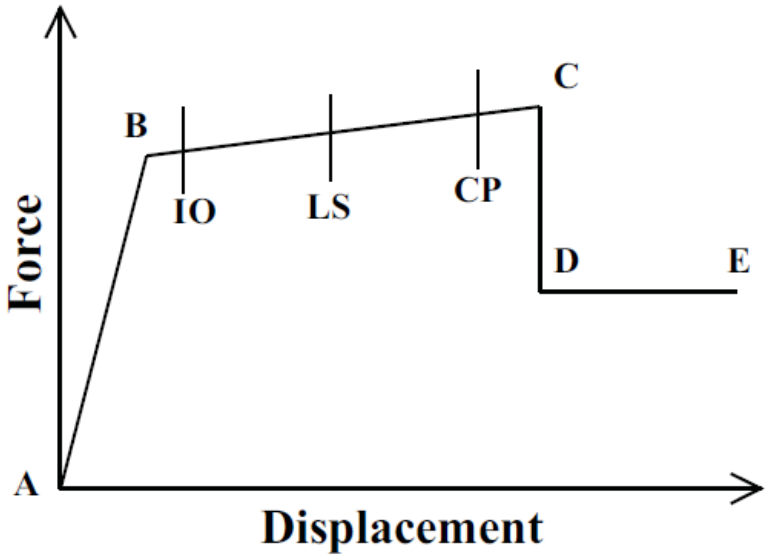

Figure 3-20. SAP2000 Hinge Backbone Curve (Computers & Structures, Inc., 2014)

MF beam hinge properties and performance level acceptance criteria were based on Chapter 5 of FEMA-356 Prestandard and Commentary for the Seismic Rehabilitation of Structures. The values of the hinge backbone curve were calculated using the material and section properties of the beams. Section 5.5.2 on Fully Restrained Moment Frames provided guidance for determining stiffness, strength, and strain hardening values for moment frame members. The beam flexure section of Table 5-6 of FEMA-356 lists recommended values for residual strength and acceptance criteria for different performance levels. This table is presented below in Table 3-3. The rotations in this table are normalized to the yield deformation (θ_y) (FEMA, 2000 b).

Table 3-3. Steel Beam Flexural Acceptance Criteria for Nonlinear Procedures (FEMA, 2000 b)

	Modeling Parameters			Acceptance Criteria				
	Plastic Rotation Angle, Radians		Residual Strength Ratio	Plastic Rotation Angle, Radians				
					Primary		Secondary	
Component/Action	a	b	c	IO	LS	CP	LS	CP
Beams—flexure								
a. $\frac{b_f}{2t_f} \le \frac{52}{\sqrt{F_{ye}}}$ and $\frac{h}{t_w} \le \frac{418}{\sqrt{F_{ye}}}$	$9\theta_y$	$11\theta_y$	0.6	$1\theta_y$	$6\theta_y$	$8\theta_y$	$9\theta_y$	$11\theta_y$
b. $\frac{b_f}{2t_f} \ge \frac{65}{\sqrt{F_{ye}}}$ or $\frac{h}{t_w} \ge \frac{640}{\sqrt{F_{ye}}}$	$4\theta_y$	$6\theta_y$	0.2	$0.25\theta_y$	$2\theta_y$	$3\theta_y$	$3\theta_y$	$4\theta_y$
c. Other	Linear interpolation between the values on lines a and b for both flange slenderness (first term) and web slenderness (second term) shall be performed, and the lowest resulting value shall be used							

Moment frame member sizes were controlled by ELF deflection limits. Deflections were taken from SAP2000 models with beam and panel zone inelasticities and reduced ELF seismic loads. Table 3-4 lists the steel members that form the special moment resisting frame.

Table 3-4. MF Member Sizes

3 Story MF Members	
Beams	W21x93
Columns	W21x166

9 Story MF Members	
Beams (Floor 8-9)	W21x68
Beams (Floor 6-7)	W24x76
Beams (Floor 4-5)	W30x116
Beams (Floor 1-3)	W33x130
Columns (Floor 8-9)	W14x370
Columns (Floor 6-7)	W14x426
Columns (Floor 4-5)	W14x500
Columns (Floor 1-3)	W14x550

3.6 Buckling Restrained Braced Frame

The lateral force resisting system of structures designed for this research consisted of steel buckling restrained braced frames in one direction. A BRB is a brace with a steel core encased in a steel tube with a concrete fill (Calado, et al., 2007). Figure 3-21 shows the configuration of a typical BRB. The encasement and fill prevent global flexural buckling of the brace, and force a higher buckling mode (Calado, et al., 2007). BRBs dissipate energy through stable tension-compression yield cycles without the stiffness degradation and strength deterioration exhibited in conventional braces (Calado, et al., 2007).

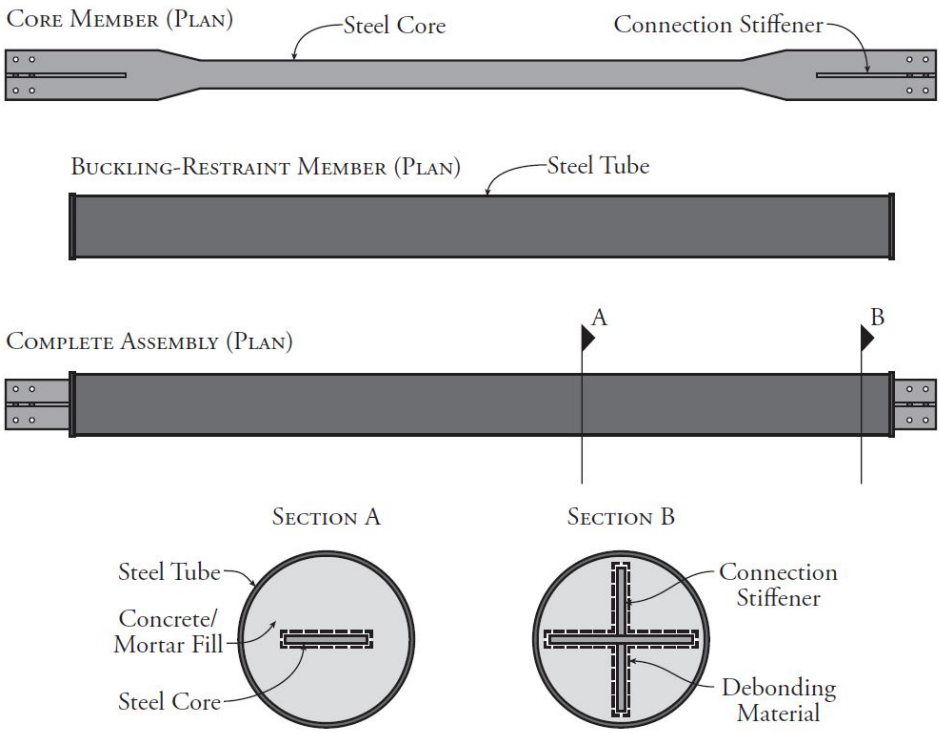

Figure 3-21. Buckling Restrained Brace Assembly (Erochko, 2013)

The BRBs for the SAP2000 structures were arranged in a two story X configuration. Figure 3-22 shows a two story X configuration of BRBs. The SAP2000 models each contained two

BRBFs. Each frame was designed to have two bays of braces. The SAP2000 BRBFs can be seen in Figure 3-7 and Figure 3-23 with the BRB link elements shown in green.

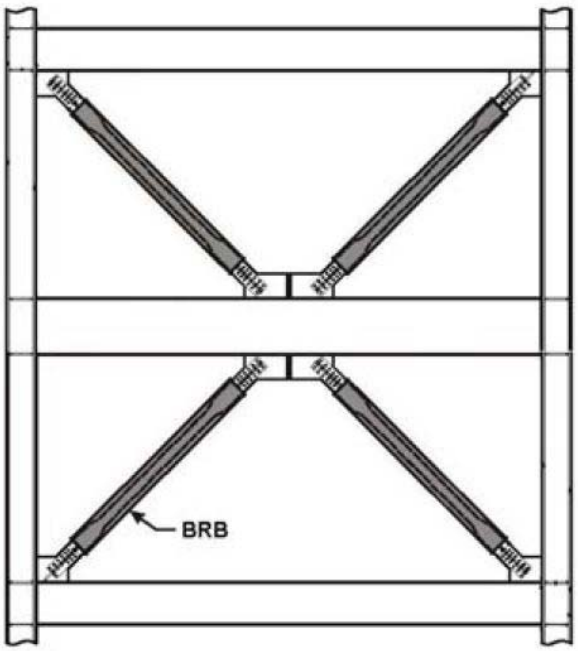

Figure 3-22. BRB Two Story X Configuration (Calado, et al., 2007)

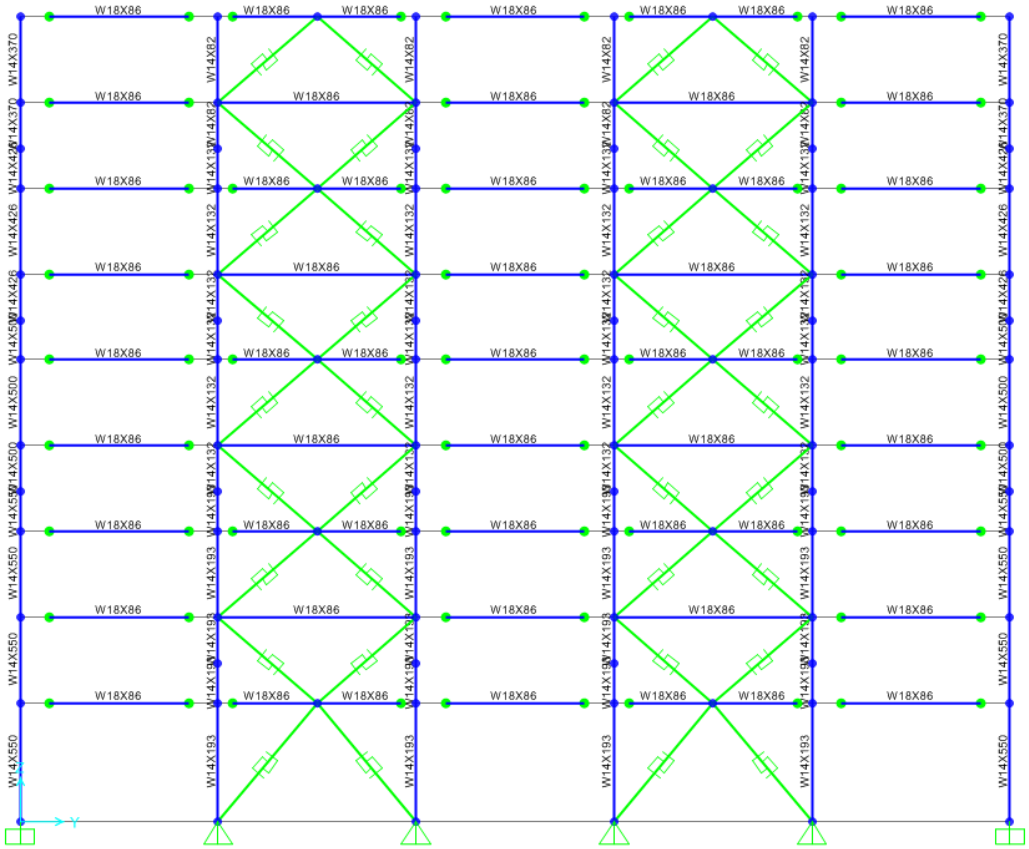

Figure 3-23. Nine Story SAP2000 Model BRBF

3.6.1 Design

Linearly distributed gravity loads were assigned to the beams of the BRBF. These loads were discussed previously in Section 3.4.1. In addition to gravity loads, ASCE 7-10 wind and earthquake loads were applied to the models. A response modification factor of 8, an overstrength factor of 2.5, and a deflection amplification factor of 5 were used for the BRBFs (ASCE/SEI, 2010). Lateral load determination is discussed in detail for the SMRF in Section 3.5.1. BRBF loads were determined using the same procedures. The calculated story shears were greater for each structure's BRBF largely because of the higher stiffness of the BRBFs.

The BRBs were designed according to Section 8.6.3 of FEMA 450 NEHRP Recommended Provisions for Seismic Regulations for New Buildings and Other Structures. The structures have

eight braces on each floor. Consequently, the steel core of each BRB was sized to resist 1/8 of the story shear. The beams and columns of the BRBFs were selected using AISC 360-10 to satisfy the demands of the SAP2000 structural analysis. Finally, the deflections of the BRBFs were checked in accordance with Section 12.12 of ASCE 7-10.

Table 3-5. BRBF Member Sizes

3 Story BRBF Members	
Girders	W21x44
Columns	W14x48

9 Story BRBF Members	
Girders	W18x86
Columns (Floor 8-9)	W14x82
Columns (Floor 4-7)	W14x132
Columns (Floor 1-3)	W14x193

3.6.2 Modeling

Buckling restrained braces were implemented in the SAP2000 models using multilinear kinematic link elements. The general backbone curve of the BRB link elements is shown in Figure 3-24. This behavioral model was assigned to the axial degree of freedom. The BRB element was allowed to freely deform in the other degrees of freedom. The axial yield strength was calculated from the size of the steel core. The elastic stiffness of the BRB link element was calculated based on the deformation of the steel core in series with the more rigid end zones of the brace. The link element was given a tensile post-yield stiffness to account for strain hardening. The transverse confinement increases compressive strength beyond the brace's tensile strength due to Poisson's effect (Calado, et al., 2007). Reflecting this, the compressive post-yield stiffness was made 7% higher than the tensile post-yield stiffness.

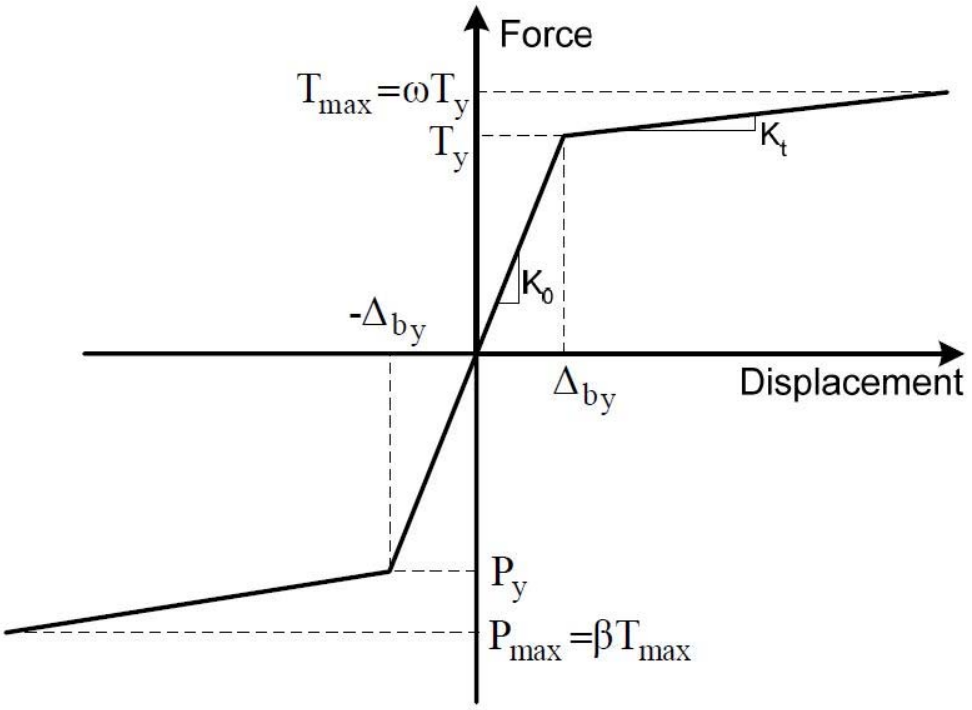

Figure 3-24. BRB Backbone Curve (Calado, et al., 2007)

3.7 Friction Damper

Additional energy dissipation was added to the gravity frame connections of the SAP2000 models using low-slip force friction dampers. These low-slip force dampers were designed to activate during ground accelerations before the other structural nonlinearities included in the models. The slip force of the friction dampers and their layout within the structures were variables evaluated in a parametric study. The effects of this early phase energy dissipation and the specifics of the parametric study are discussed in detail in Section 4.2.

3.7.1 Configuration

A slotted bolted friction damper was selected to provide early phase energy dissipation for this research. The slotted bolted device was chosen for its low cost and simple fabrication. The friction damping of the devices was provided by a steel and non-asbestos organic friction material sliding

surface. The NAO material was used for its stable and repeatable hysteric behavior (Golondrino, et al., 2013). A schematic of a steel slotted bolted friction damper with NAO friction material can be seen in Figure 2-10.

Figure 3-25 shows a drawing of a friction damper in the LSFF connection. The arrangement of the friction devices in a SAP2000 model is shown Figure 3-26. The friction dampers were added as a supplemental connection between the flexural member and the column in the gravity frame. The FDs were made to rotate freely at each end. This would be possible by connecting the FD to the column with a clevis. The other end of the friction device would be connected to a stiff steel stub with a clevis. This steel stub would then be welded to the bottom of the GF beam.

In the SAP2000 representation of the LSFF connection, the rigid stub was not allowed to deform in any degree of freedom. This assured the stub remained at a right angle with the connected portion of the beam. The stub and shear tab elements were connected to one end of the beam frame element. The zero length shear tab element was then connected to a short frame element which connected to the column. This was done to address the fact that the STC is at the column face away from the column center line.

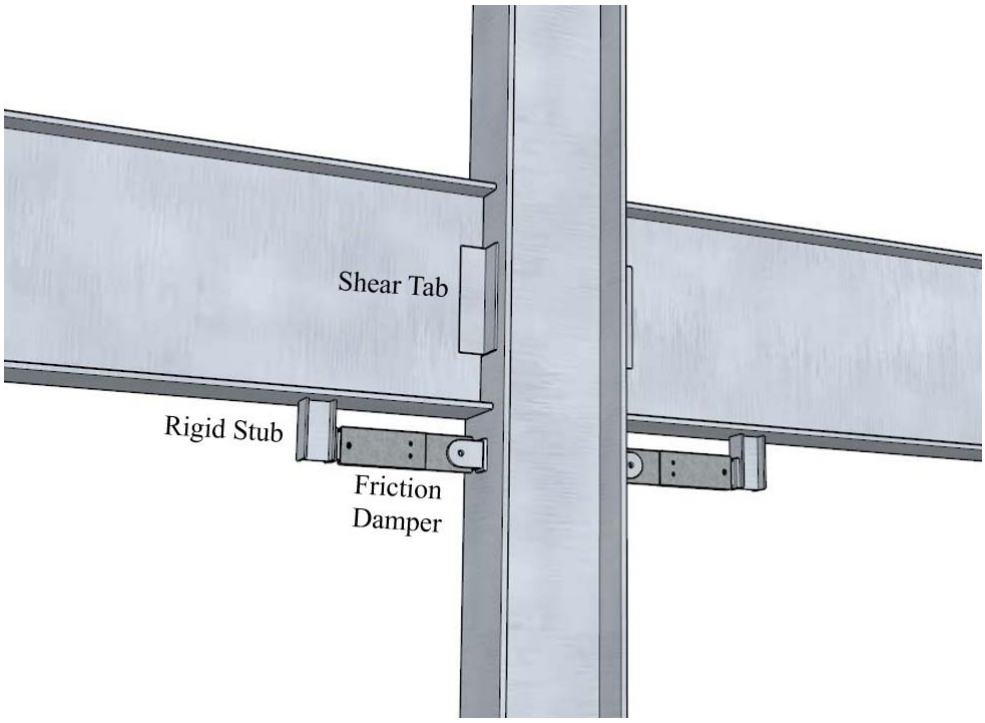

Figure 3-25. Low-Slip Force Friction Connection

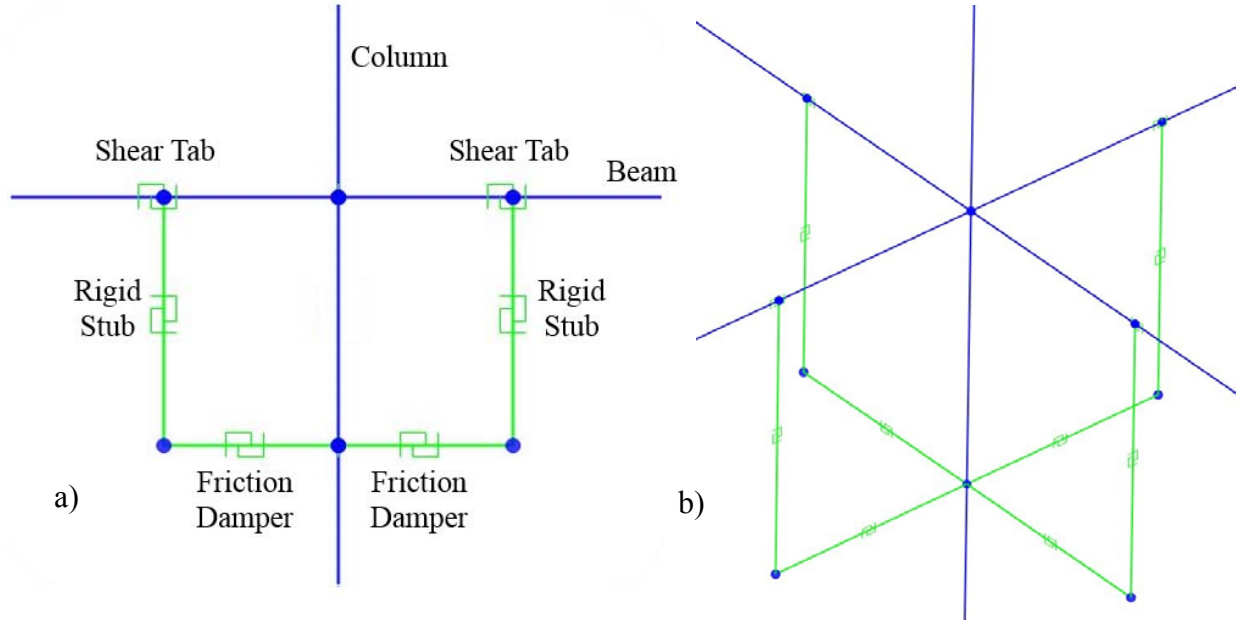

Figure 3-26. LSFF Connection in SAP2000 a) Planar view b) Isometric view

As part of a parametric study, several variations of both the three and nine story SAP2000 models were created. The slip force of the FDs was one of the varied parameters. Three different

slip forces of 7, 5, and 3 kips were selected. The other variable evaluated in the parametric study was the layout of FDs within the models. Three variations were selected with FDs at every GF beam-column connection, FDs at 60% of GF beam-column connections, and FDs at 30% of GF beam-column connections. The parametric study is discussed further in Section 4.2. In total, nine variations with FDs were created for each of the three and nine story SAP2000 models.

3.7.2 Inelastic Modeling

The friction dampers were modeled with multi-linear kinematic link elements. The FD link element backbone curve was developed from cyclic testing of slotted bolted friction dampers using NAO friction material. Figure 2-12 shows a hysteresis recorded during laboratory testing of a FD similar to those designed for this model. NAO FDs were found to have a high elastic stiffness. Several studies showed some changes in this stiffness before reaching the slipping force. However, for these link elements a constant elastic stiffness was approximated from FD test results. NAO FDs exhibit a constant friction force over the full sliding length with little degradation during multiple cycles (Golondrino, et al., 2013). A slight post slip stiffness was added to the FD link element backbone curve as recommended for the SAP2000 solver. Figure 3-27 shows the general shape of the FD link element backbone curve. This behavioral model was assigned in the axial degree with all others allowed to freely deform.

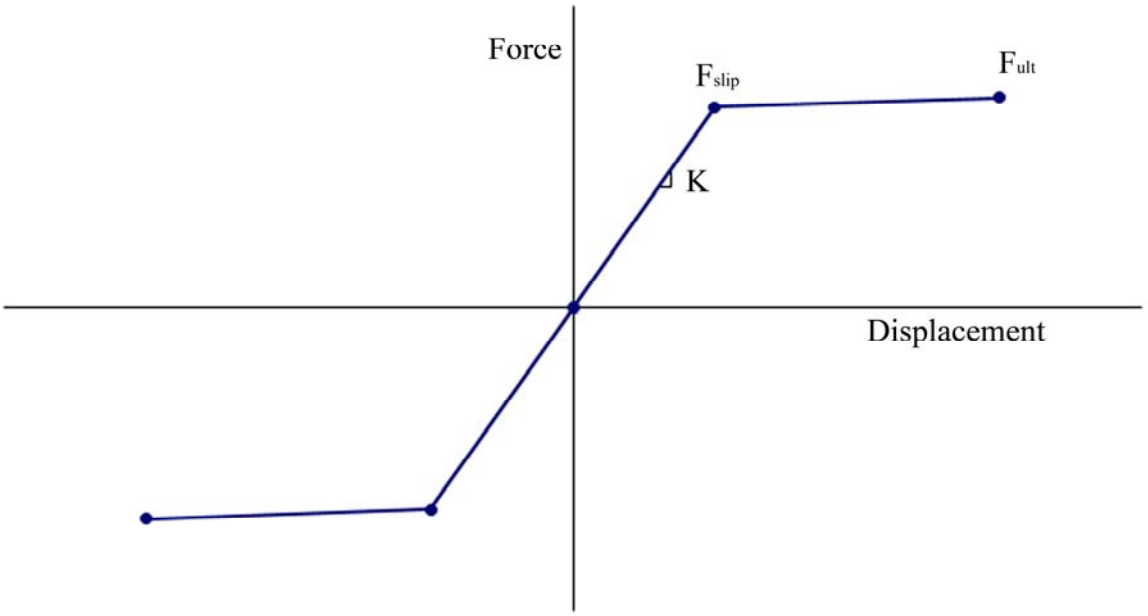

Figure 3-27. Friction Damper Backbone Curve

3.8 Ground Motions

The models created in SAP2000 were subjected to an ensemble of ground motions. These ground acceleration records were obtained from the ground motion database of Next Generation Attenuation Relationships (NGA) of the Pacific Earthquake Engineering Research Center (PEER). Each earthquake case run in SAP2000 contained two orthogonal ground motion records recorded simultaneously from the same site. These earthquake records were then scaled to the selected Seattle, Washington seismic hazard level. Four levels of earthquakes were used in the analysis of these models: a Maximum Credible Earthquake (MCE) with a 2% probability of exceedance in 50 years, a Design Basis Earthquake (DBE), and two Service Level Earthquakes (SLE). The DBE is scaled down to 67% of the MCE corresponding to a 10% probability of exceedance in 50 years. The first SLE was scaled down to 50% of the MCE event corresponding to a 20% probability of exceedance in 50 years. The second level of SLE was scaled down to 25% of the MCE

corresponding to a 50% probability of exceedance in 50 years. This information is summarized in Table 3-6.

Table 3-6. Ground Motion Suite

NGA#	Event	Year	Code	Time Step (s)	Scale Factors							
					3 Story				9 Story			
					MCE	DBE	SLE1	SLE2	MCE	DBE	SLE1	SLE2
77	San Fernando	1971	PUL	0.010	0.946	0.631	0.473	0.237	1.625	1.083	0.813	0.406
126	Gazli, USSR	1976	GAZ	0.005	1.353	0.902	0.677	0.338	1.665	1.110	0.833	0.416
143	Tabas, Iran	1978	TAB	0.020	1.022	0.681	0.511	0.256	0.939	0.626	0.470	0.235
184	Imperial Valley	1979	EDA	0.005	2.140	1.427	1.070	0.535	2.005	1.337	1.003	0.501
779	Loma Prieta	1989	LGP	0.005	1.283	0.855	0.642	0.321	1.318	0.879	0.659	0.330
825	Cape Mendocino	1992	CPM	0.020	1.197	0.798	0.599	0.299	1.516	1.011	0.758	0.379
1044	Northridge	1994	NWH	0.020	1.299	0.866	0.650	0.325	1.922	1.281	0.961	0.481
1048	Northridge	1994	STA	0.010	1.667	1.111	0.834	0.417	2.238	1.492	1.119	0.560
1120	Kobe, Japan	1995	TAK	0.010	0.945	0.630	0.473	0.236	1.311	0.874	0.656	0.328
1176	Kocaeli, Turkey	1999	YPT	0.005	2.290	1.527	1.145	0.573	1.960	1.307	0.980	0.490
1605	Duzce, Turkey	1999	DZC	0.005	1.748	1.165	0.874	0.437	1.173	0.782	0.587	0.293

The dynamic response of the structures was determined using a nonlinear direct-integration time-history analysis. A service load consisting of the unfactored dead load combined with 50% of the live load was applied to the structures while running the time-history analyses. These analyses included link element nonlinearities, plastic hinges assigned to frame elements, and P-delta effects discussed previously in this chapter (Computers & Structures, Inc., 2014). A nonlinear analysis requires an iterative solution where the stiffness, damping, and loading may change during the ground motion (Computers & Structures, Inc., 2014).

Direct integration is a step-by-step method that solves the full dynamic equilibrium equation without the simplification of modal superposition (Computers & Structures, Inc., 2014). Direct integration results are sensitive to time step size at larger time steps (Computers & Structures, Inc.,

2014). Sufficiently small input time steps were used for each ground motion. These are listed in seconds in Table 3-6. All analyses used an output time step of 0.02 seconds. The method used for solving the direct-integration time-history analyses was the Hilber-Hughes-Taylor (HTT) alpha method. This is the default and recommended integration method in the SAP2000 program (Computers & Structures, Inc., 2014). The parameter alpha was set at zero for these analyses. This value of alpha offers the highest accuracy and is equivalent to the Newmark method with gamma of 0.5 and beta of 0.25 (Computers & Structures, Inc., 2014). A Rayleigh damping matrix was assigned and computed by SAP2000 from specified fractions of critical damping at two different periods. These models used 2.5% of critical damping at the first fundamental period and the period corresponding to 95% or greater mass participation.

3.9 Summary

A three story and nine story structural steel building were designed for this research. Each building's lateral force resisting system consisted of a special moment resisting frame in one direction and a buckling restrained braced frame in the orthogonal direction. These buildings were represented as 3D models in the structural analysis software SAP2000. Multilinear inelastic elements were added to the models representing: shear tab connections in the gravity frame, plastic hinges in the moment resisting frame beams, buckling restrained braces, and friction dampers at gravity frame connections. The building models were then subjected to a suite of ground motions with varying return periods.

Chapter 4. Analytical Modeling and Results

4.1 Introduction

The purpose of this chapter is to present and discuss the results of the nonlinear time history analyses of the SAP2000 structural models. While the performance of all the LFRS elements were examined, an emphasis was placed on the energy dissipation of the LSFF connections. Variations of the structural models described in Chapter 3 were made to test combinations of LSFF connection properties. The model variants and reasoning behind their creation are discussed in Section 4.2. Following this, the results of this parametric study are presented. The chapter ends with an analysis of the effects of various LSFF devices on the performance of the SAP2000 models for an extensive range of earthquake hazards.

4.2 Parametric Study

The optimal use of early phase energy dissipation in the detailed three dimensional models was difficult to determine. Configuring the LSFF connections to provide the greatest benefit to lateral response required a parametric study. Permutations of the three and nine story structural models were made by varying the numbers and slip forces of the friction devices. The response of each variant was analyzed at different levels of ground excitation.

The first parameter explored was the slip force of the LSFF devices. Initially, five values were selected for the slip force. Devices with slip forces of nine kips and more remained inactive through many of the MCE level ground motions. A sensitivity study was then performed varying

the effective stiffness of the LSFF devices by ten percent. This had a negligible effect on the structural response, and the effective stiffness was not varied in further analyses. Following these initial tests, LSFF devices were selected for full parametric analysis with slip forces of seven, five, and three kips. These variations were labeled 1, 2, and 3 respectively.

The number of LSFF devices included in the models was chosen as a variable for the study. The first variant of both the three and nine story structures included LSFF devices at every gravity frame beam-column connection. This resulted in 76 devices at each floor of the three story model and 80 devices at each floor of the nine story model. Models with this layout were labeled A. Figure 4-1 shows the floor plan for the three and nine story structures with the A friction device layout. Each black dots represent a LSFF device. Each floor of the structure contains the same friction device layout. Targets were set at reducing the number of devices by one third and two thirds. From the results of the A models, devices with the least activity during the earthquakes were identified and removed. The three and nine story B models removed 32 devices at each floor from the A models. Figure 4-2 shows the floor plan for the three and nine story structures with the B friction device layout. The three story C model removed 52 devices at each floor from the A model, and the nine story removed 56. Figure 4-3 shows the floor plan for the three and nine story structures with the C friction device layout.

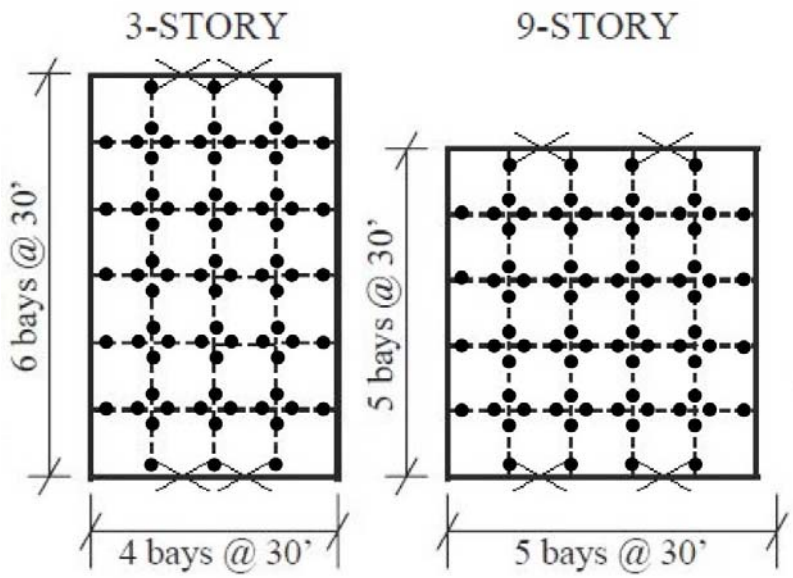

Figure 4-1. Friction Device Layout A

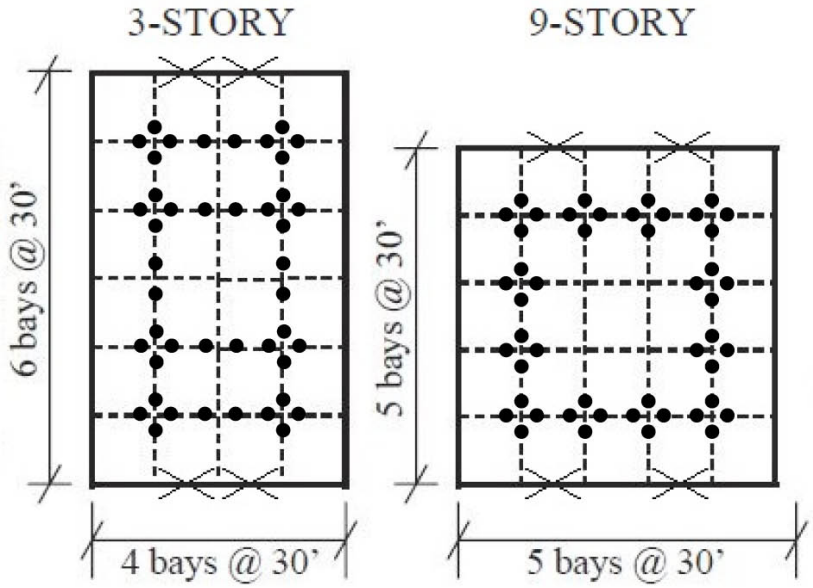

Figure 4-2. Friction Device Layout B

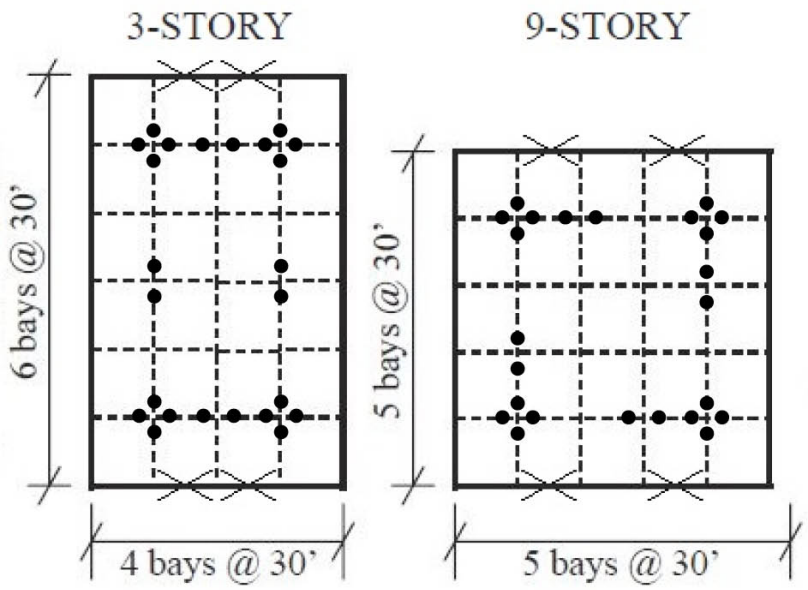

Figure 4-3. Friction Device Layout C

The parametric study included the evaluation of nine variations for each of the three and nine story structures containing LSFF devices. Accompanying the nine friction device models in the analysis were two baseline models. For each structure, a baseline model without friction devices and a baseline model without friction devices or shear tab elements were created. These models were labeled BLst and BL respectively. Beam-column connections in the BL model were free to rotate in plane with their respective frame.

As previously mentioned, four levels of ground shaking were applied to the structures. Each model variation was subjected to the MCE level earthquakes. Following the MCE analyses, the catalogue of models was reduced for the smaller scale ground motions. The A1 and C1 models were kept, because the seven kip slip force provided the most benefit at the MCE level. A three kip slip force model, A3, was also included. At the smaller scale ground motions, a three kip slip force device could generate better performance if a significant number of seven kip slip force devices were not activated. This made for a total of 22 models run through eleven ground motions at different levels of scaling.

4.3 Results and Discussion

The following results from the SAP2000 time history analyses show the effects of modeling the behavior of shear tab connections and LSFF devices. The hystereses of LFRS elements, shear tabs, and LSFF devices from two cases are included in this section to show the function of the elements during a ground motion. These hystereses were taken from the elements in the three story model that underwent the most deformation during any of the ground motions. The hystereses come from the BLst and A1 models to compare the performance of the elements with and without the presence of LSFF devices.

A series of graphs are presented illustrating the inter story drifts of each structure as a percent of the story height. These values reported are taken from the maximum drift that occurs during a ground motion and averaged over all eleven ground motions. The graphs report this data at every floor for the models described in Section 4.2. Each graph shows the drift of a selection of SAP2000 models at the same ground motion scaling in either the braced frame or moment frame direction. Corresponding graphs of the story accelerations are presented in Appendix A.

Eight tables following these graphs provide response data of various elements within the models. Each table presents data for the shear tab rotation, LSFF device displacement, story drift, story acceleration, and special moment frame beam plastic rotation or buckling restrained brace displacement. Similar to the graphs, these values were determined by averaging the maximum values that occur during the ground motions. Comparison of the information presented in these graphs and tables provides an assessment of the seismic performance of structures with LSFF devices.

4.3.1. Element Hystereses

Results for the moment frame hinges are shown in Figure 4-4. This graph shows only the plastic rotation of the hinges not the full rotation of the steel beams at the hinge locations. Comparing the baseline model to the A1 friction device model, the moment frame hinges do not exhibit any noticeable difference. Figure 4-5 and Figure 4-6 show the hystereses of shear tabs parallel to the moment frame and braced frame respectively. The MF shear tabs elements show some slight inelasticity. In the BF direction, there was no inelastic deformation. In both directions, the LSFF damping reduced the deformation.

The hysteric behavior of the buckling restrained braces is presented in Figure 4-7. There is nearly no change in the response of the BRB element between the A1 and BLst models. Figure 4-8 shows the hystereses of LSFF damping elements in the three story A1 model. Both seven kip friction devices were activated repeatedly during the ground motion. The BF direction device underwent greater displacements and dissipated a larger amount of energy.

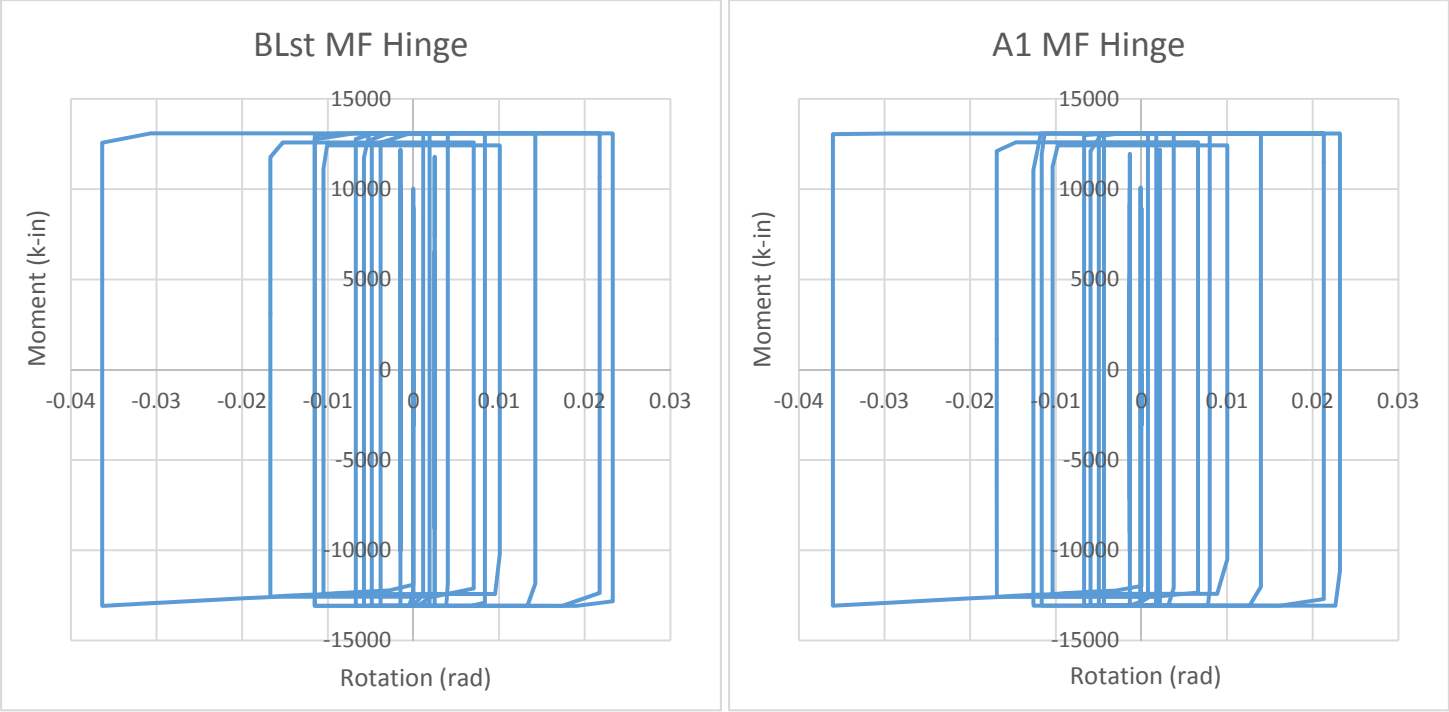

Figure 4-4. Three Story MCE MF Hinge Hysteresis

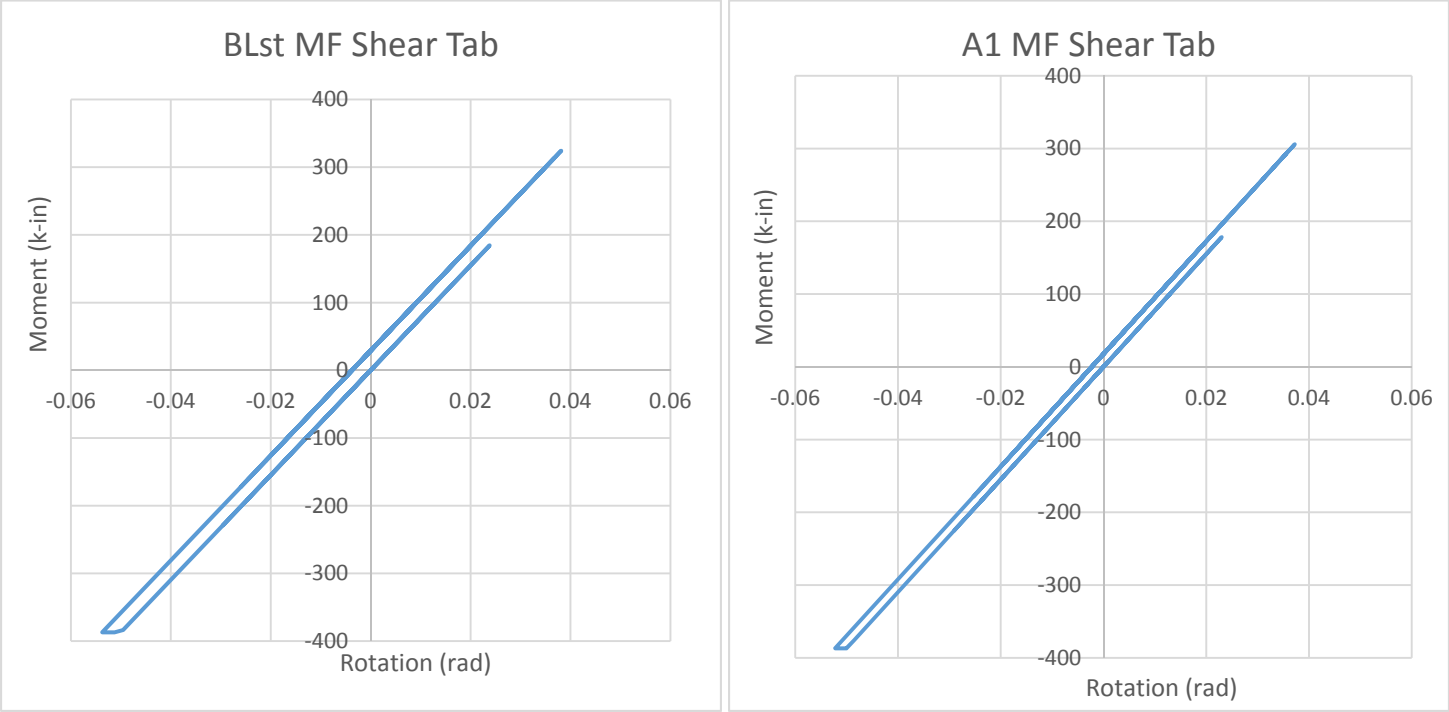

Figure 4-5. Three Story MCE MF Shear Tab Hysteresis

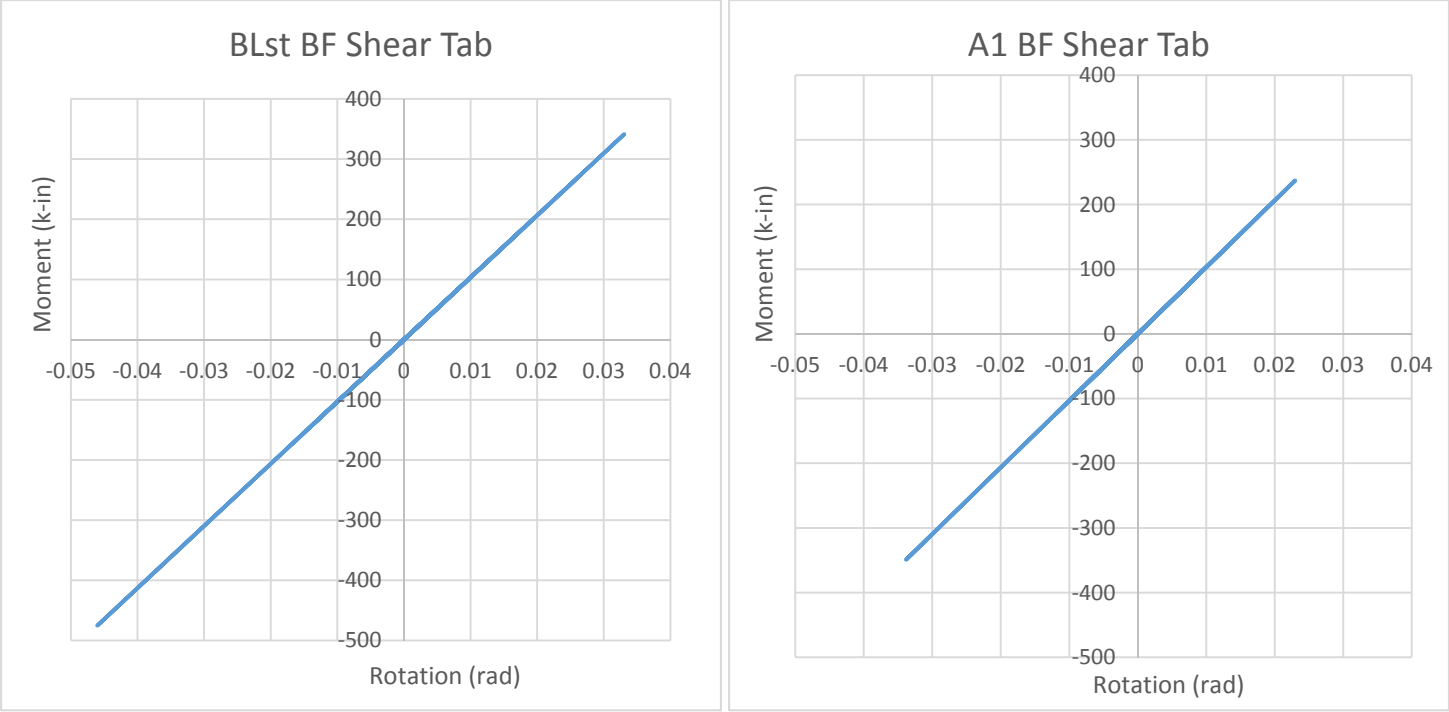

Figure 4-6. Three Story MCE BF Shear Tab Hysteresis

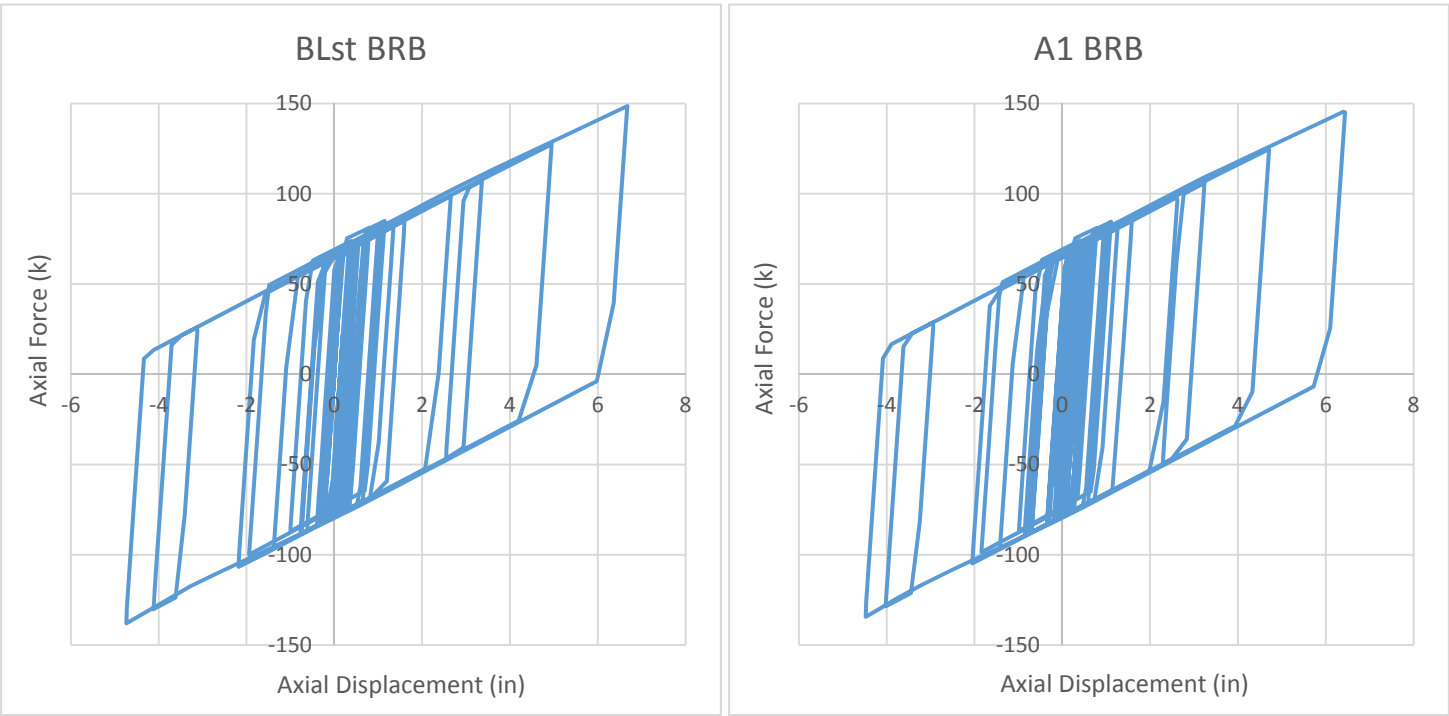

Figure 4-7. Three Story MCE BRB Hysteresis

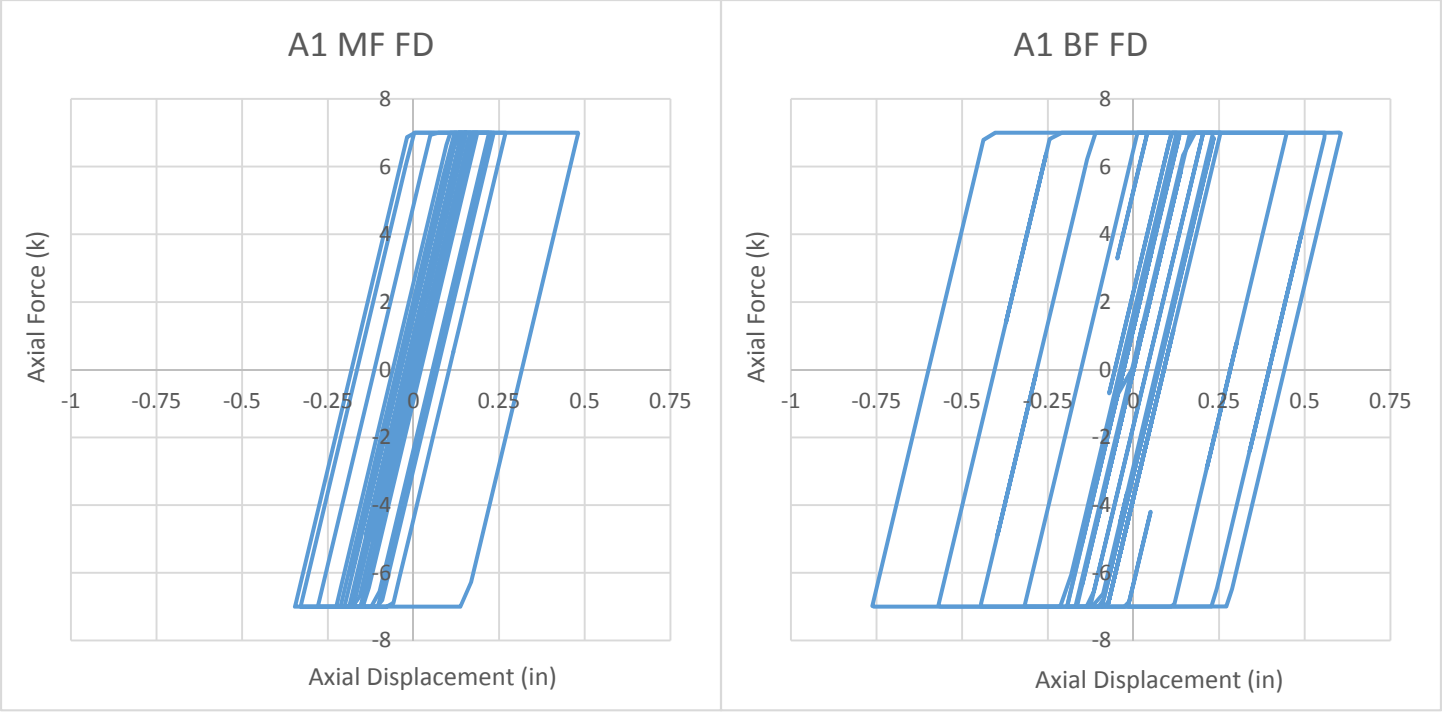

Figure 4-8. Three Story MCE LSSF Device Hysteresis

4.3.2. Story Drifts

Figure 4-9 through Figure 4-14 show the drift data for the three story maximum considered earthquake models in the special moment frame direction. Instead of depicting the drift of all nine MCE models on the same graph, each graph represents a group of MCE models with each model shown in two graphs. Though there is a noticeable difference in drift from the baseline models, all of the models with included shear tab elements vary little from one another. Table 4-1 shows the largest difference in drift from the baseline shear tab model occurs in the seven kip A layout (A1). However, this is only a 0.5% difference. The implementation of different LSFF devices did not have a significant impact on drift.

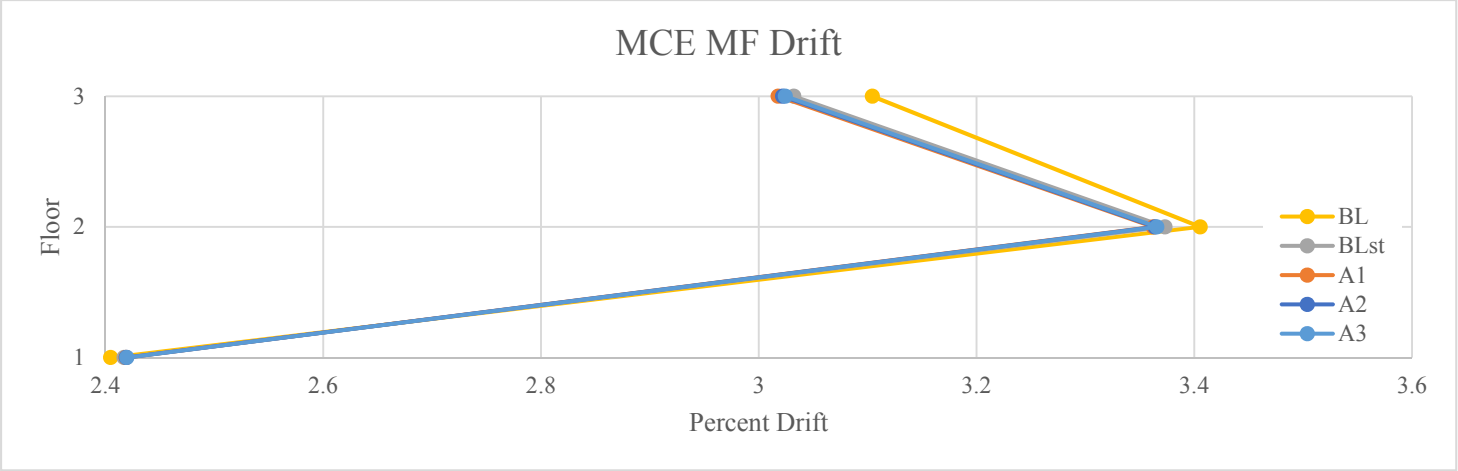

Figure 4-9. Three Story MCE MF Average Maximum Story Drift (A Layout)

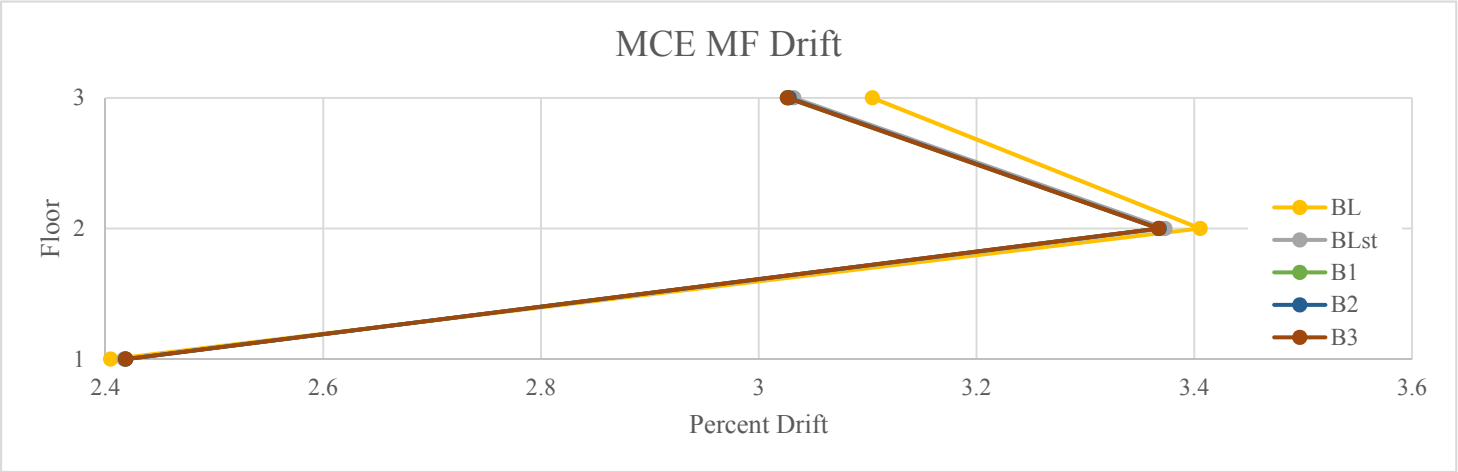

Figure 4-10. Three Story MCE MF Average Maximum Story Drift (B Layout)

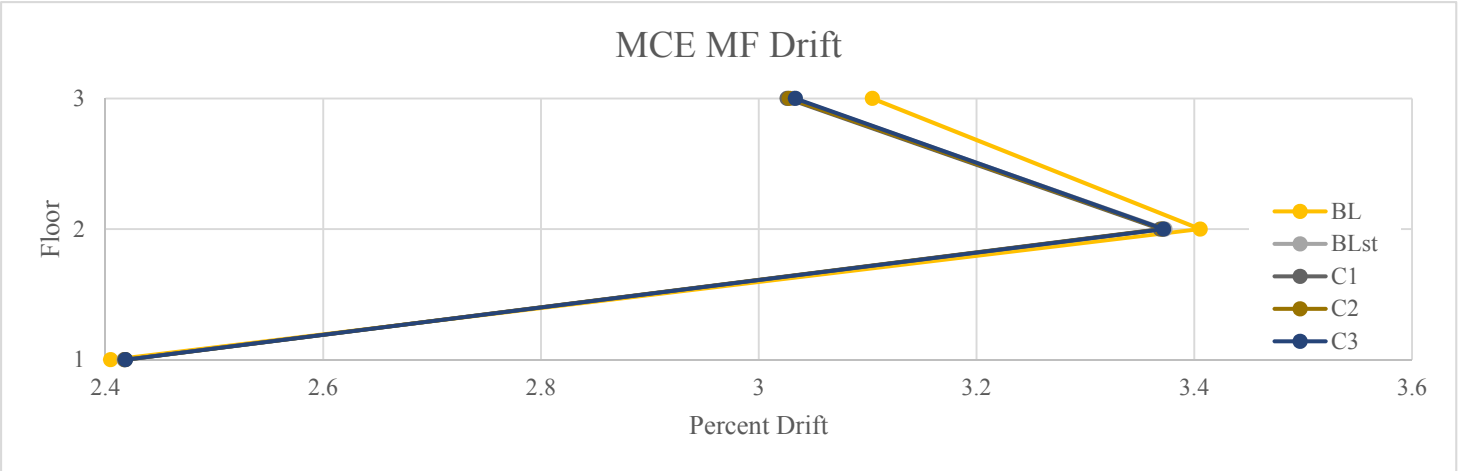

Figure 4-11. Three Story MCE MF Average Maximum Story Drift (C Layout)

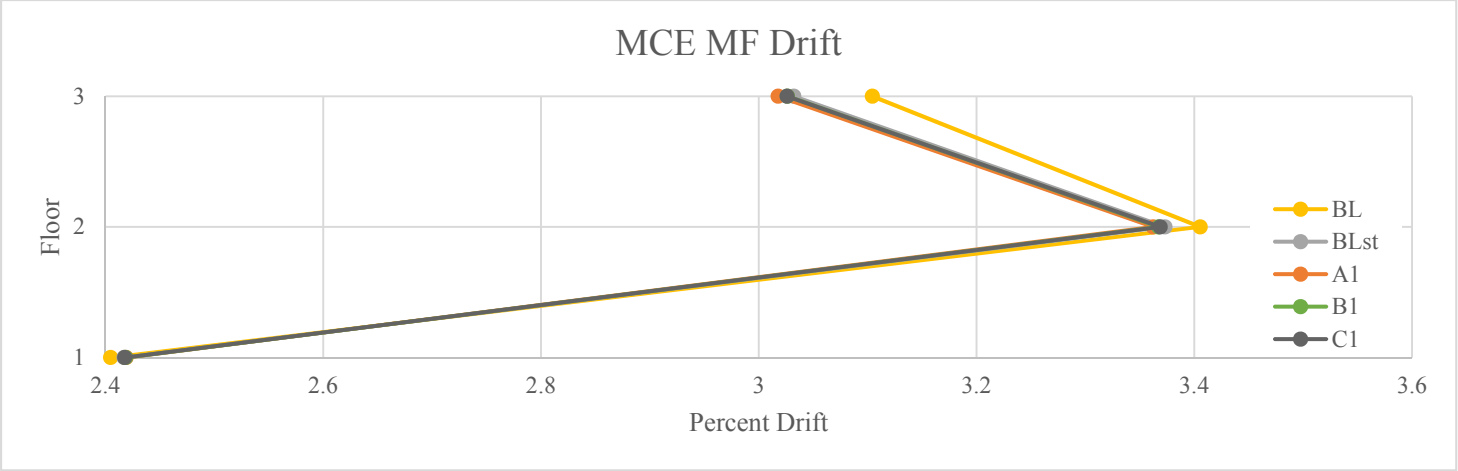

Figure 4-12. Three Story MCE MF Average Maximum Story Drift (7 kip Slip Force)

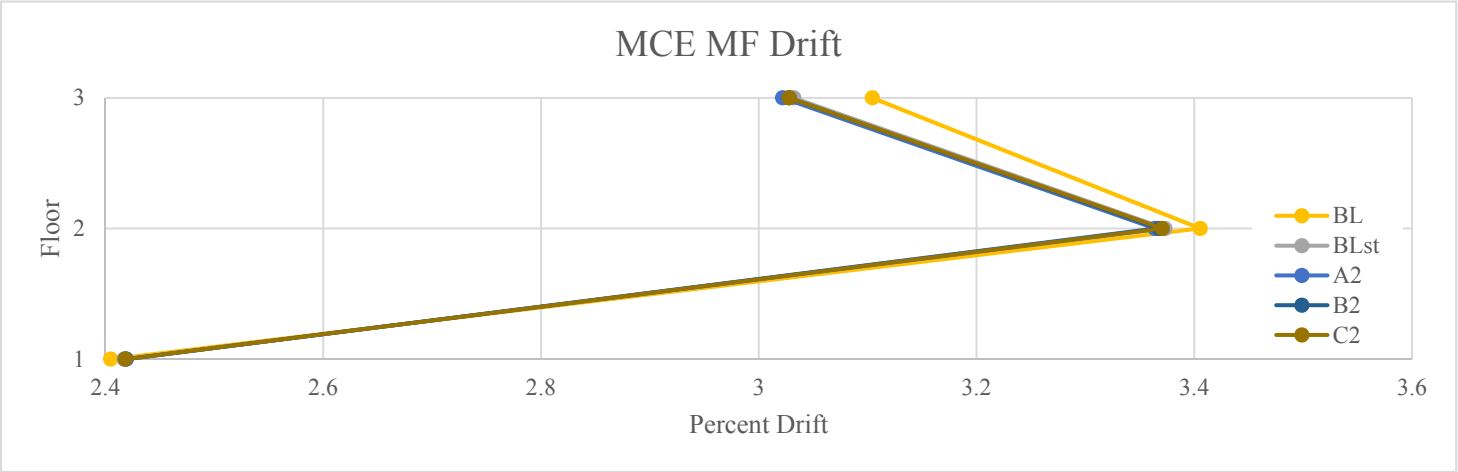

Figure 4-13. Three Story MCE MF Average Maximum Story Drift (5 kip Slip Force)

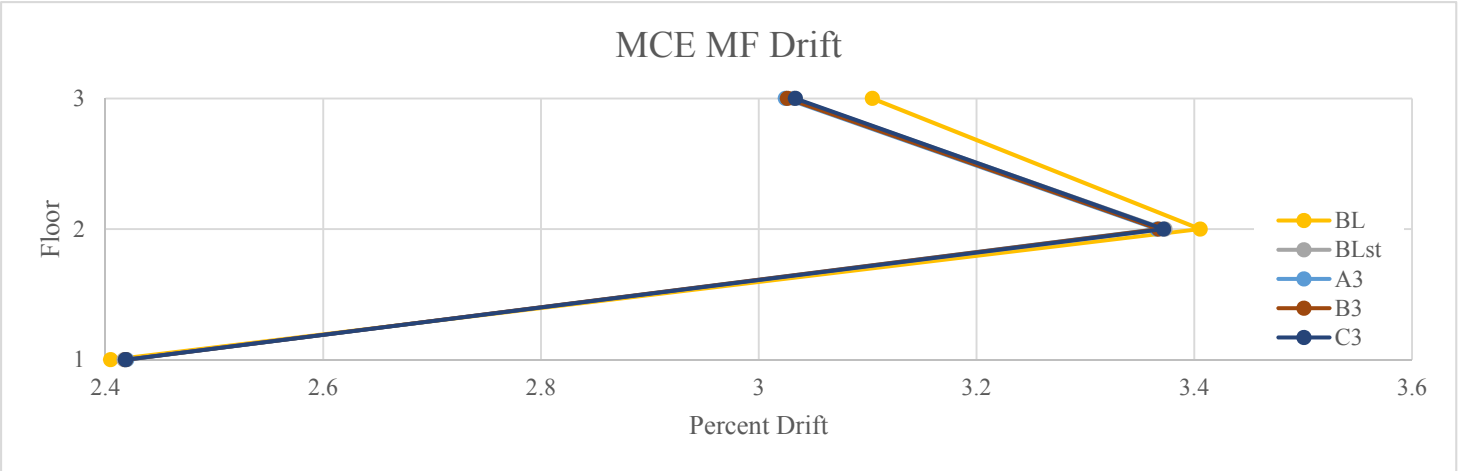

Figure 4-14. Three Story MCE MF Average Maximum Story Drift (3 kip Slip Force)

The effect of the early phase energy dissipation provided by LSFF devices was assessed at smaller scale ground motions. Figure 4-15 through Figure 4-17 below show the drift in the special moment frame direction of the design basis and service level earthquake models. These smaller scale ground motions produced less drift in all baseline and friction device models. Drifts, those of the second story in particular, decrease from MCE level models with similar rates to the decrease in ground motion scale. However, the percent difference in story drifts between models with and without LSFF damping was similar to those at the MCE level.

Figure 4-18 through Figure 4-23 show the drift data for the three story MCE models in the braced frame direction. LSFF devices added to the BF direction had only slightly different effects from those in the three story MF direction. At the roof level, the friction damping produced as much as 3.2% difference in drift from the model with shear tabs alone. This is reported in Table 4-3. While this is a greater difference than friction damping in the MF direction, it is still not a substantial impact on story drift. The reduction of roof level drift was accompanied by the redistribution of deformation to the first floor. At the first story, the BF drift increased slightly with the addition of shear tab elements and further with LSFF devices.

Figure 4-24 through Figure 4-26 show the percent story drift of DBE and SLE levels. LSFF devices in the BF direction showed slightly improved performance at the smaller scale ground motions compared to the MCE analysis. The negative effect of the dampers at the first floor was reduced, and other stories saw some reduction in drift. Nevertheless, LSFF devices incorporated into the braced frame lateral system had only a minor influence on story drift.

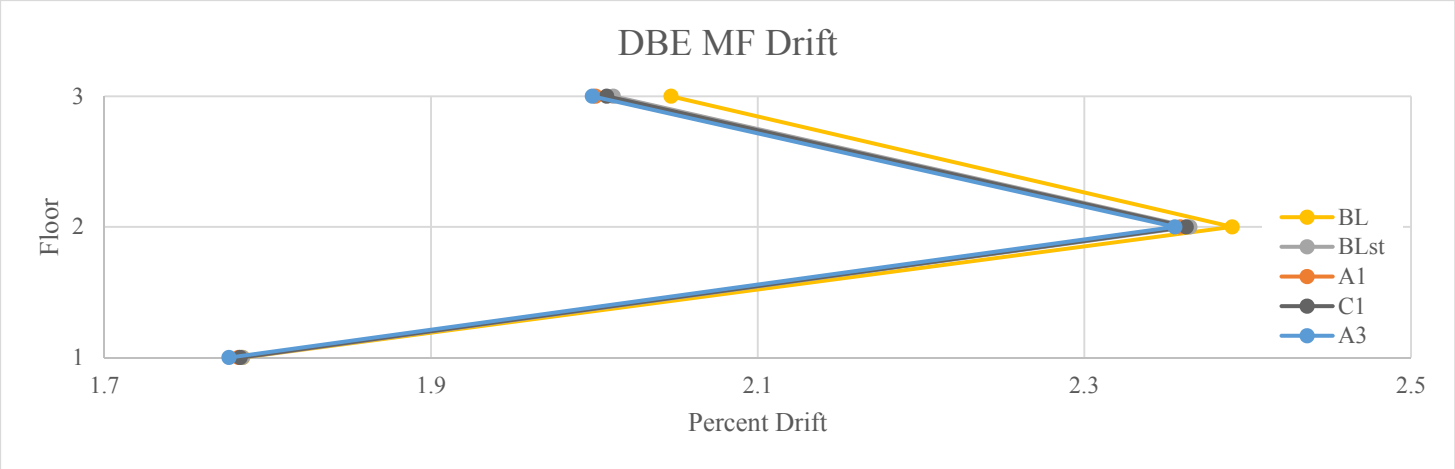

Figure 4-15. Three Story DBE MF Average Maximum Story Drift

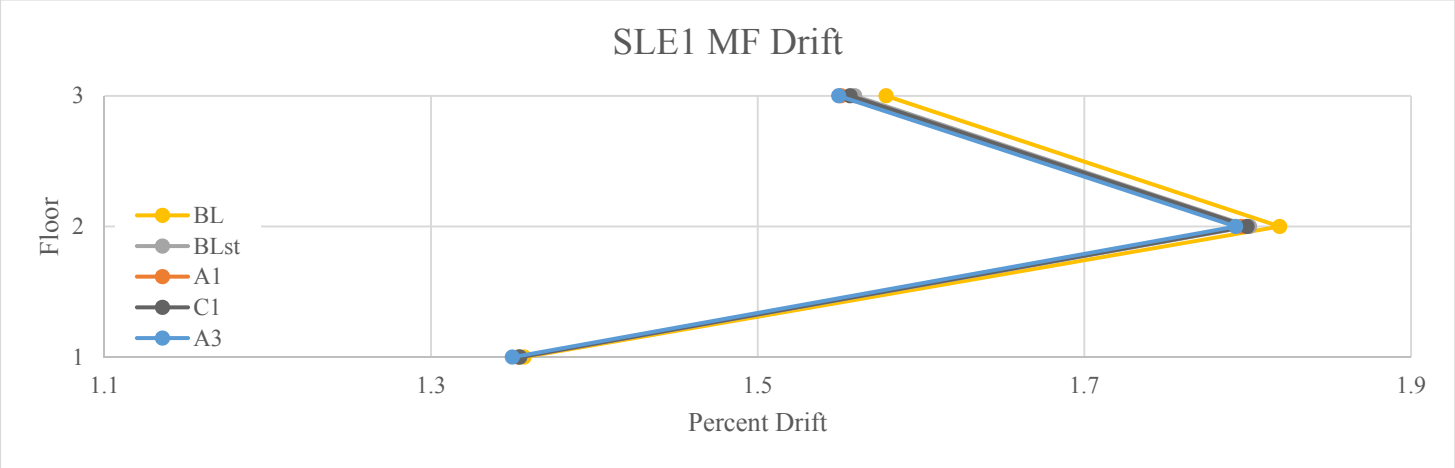

Figure 4-16. Three Story SLE1 MF Average Maximum Story Drift

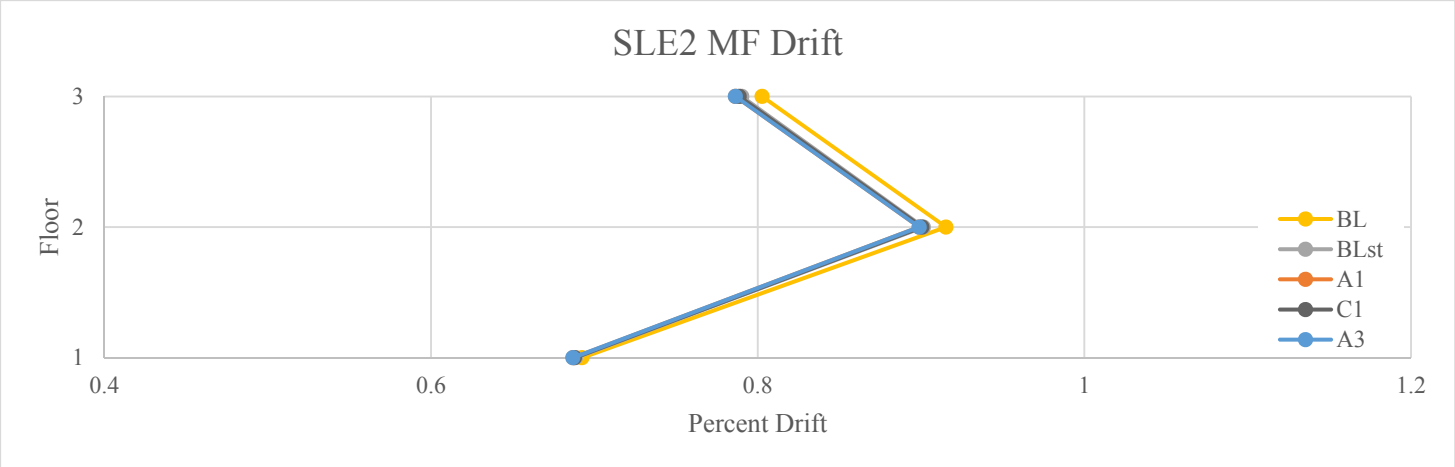

Figure 4-17. Three Story SLE2 MF Average Maximum Story Drift

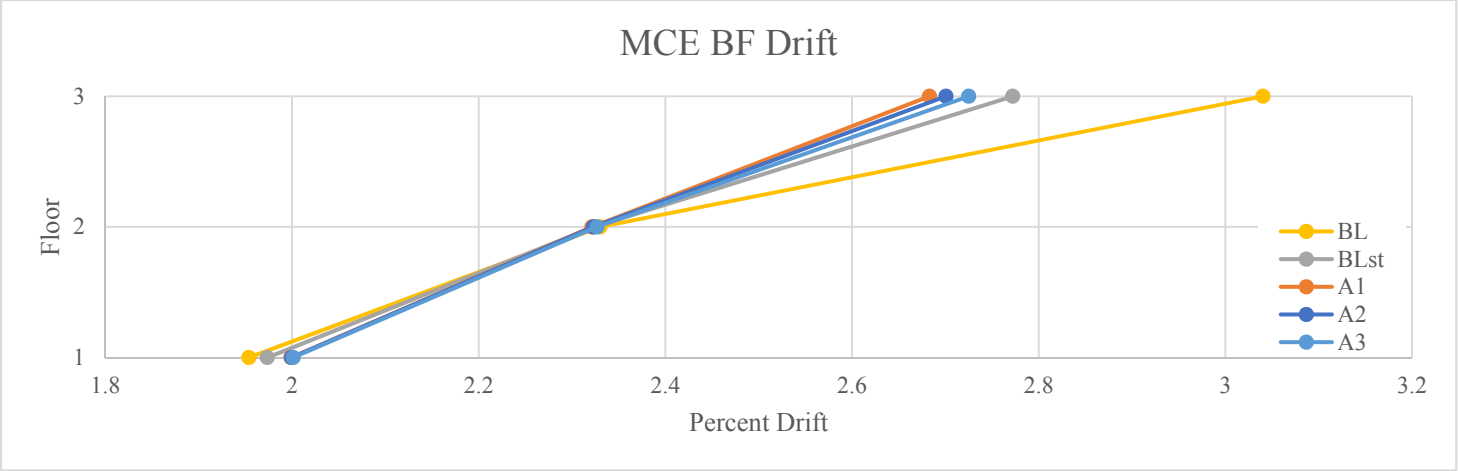

Figure 4-18. Three Story MCE BF Average Maximum Story Drift (A Layout)

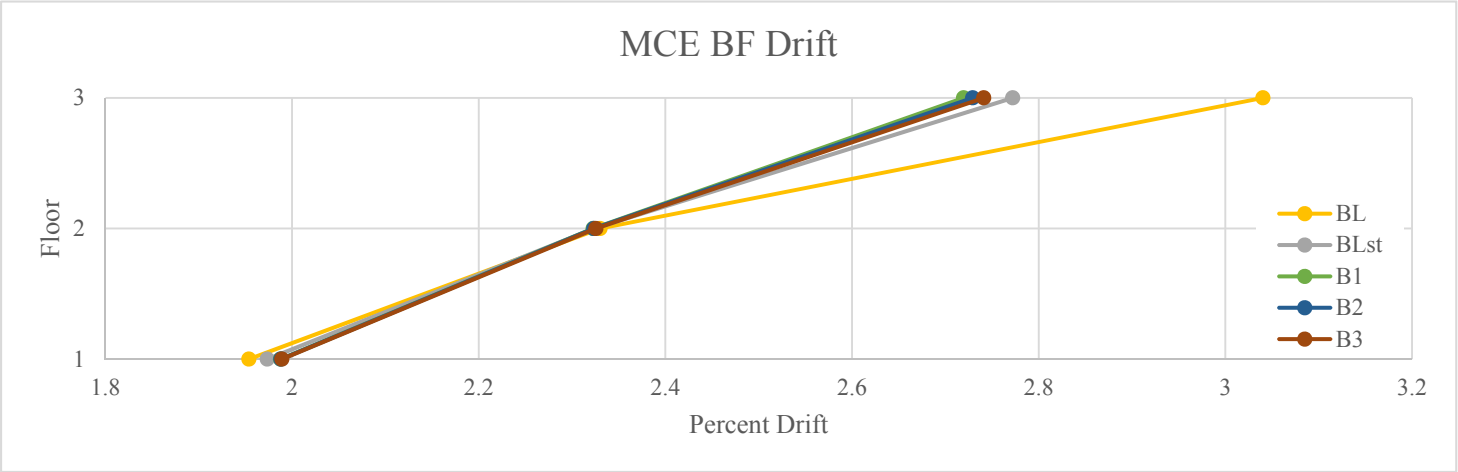

Figure 4-19. Three Story MCE BF Average Maximum Story Drift (B Layout)

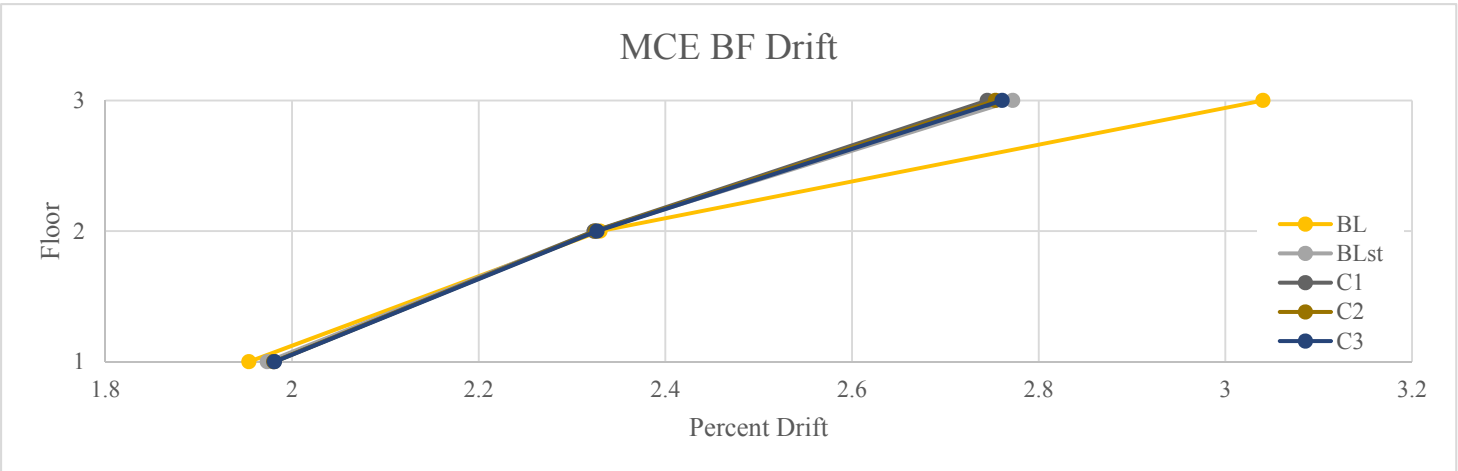

Figure 4-20. Three Story MCE BF Average Maximum Story Drift (C Layout)

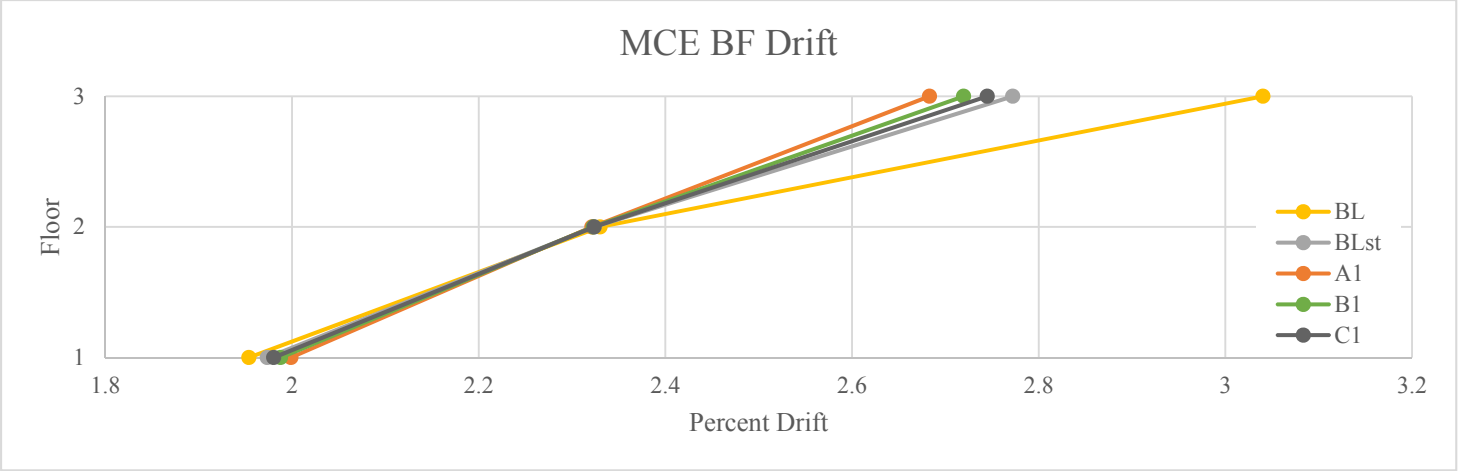

Figure 4-21. Three Story MCE BF Average Maximum Story Drift (7 kip Slip Force)

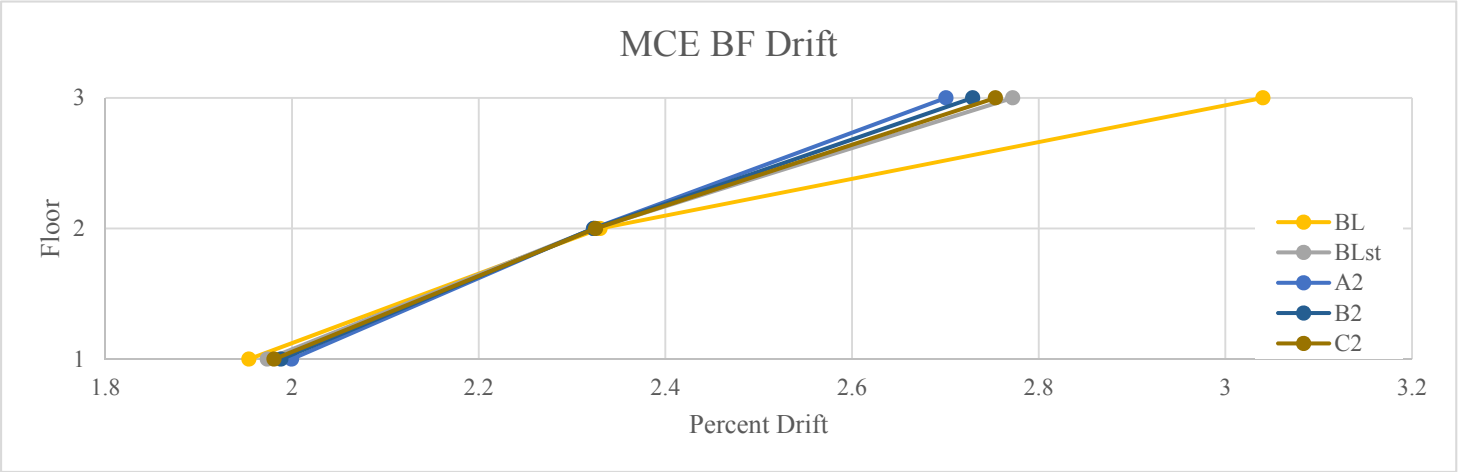

Figure 4-22. Three Story MCE BF Average Maximum Story Drift (5 kip Slip Force)

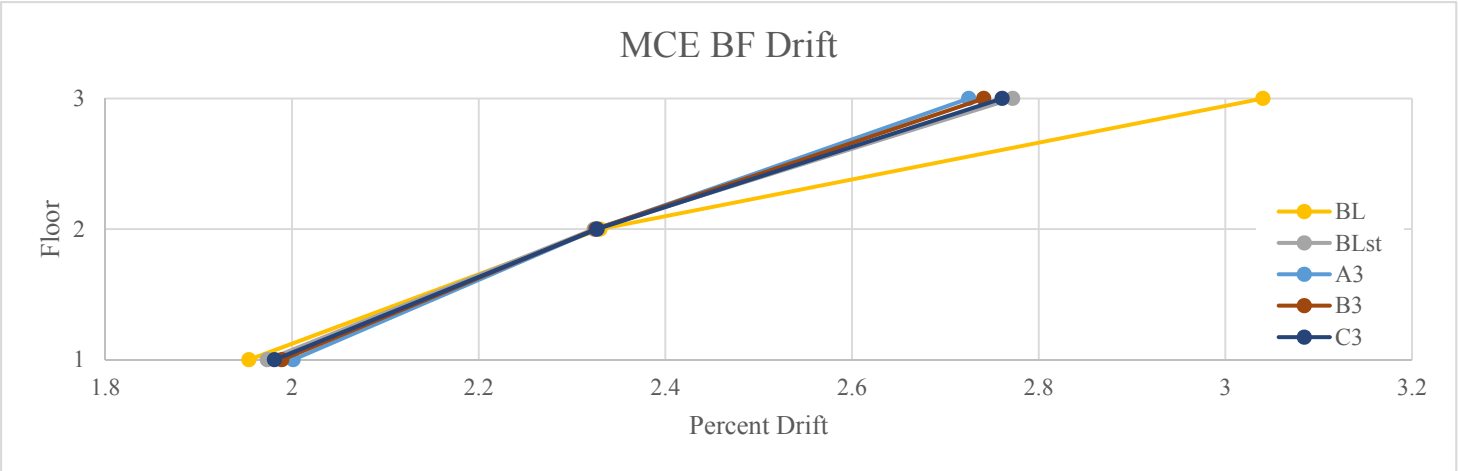

Figure 4-23. Three Story MCE BF Average Maximum Story Drift (3 kip Slip Force)

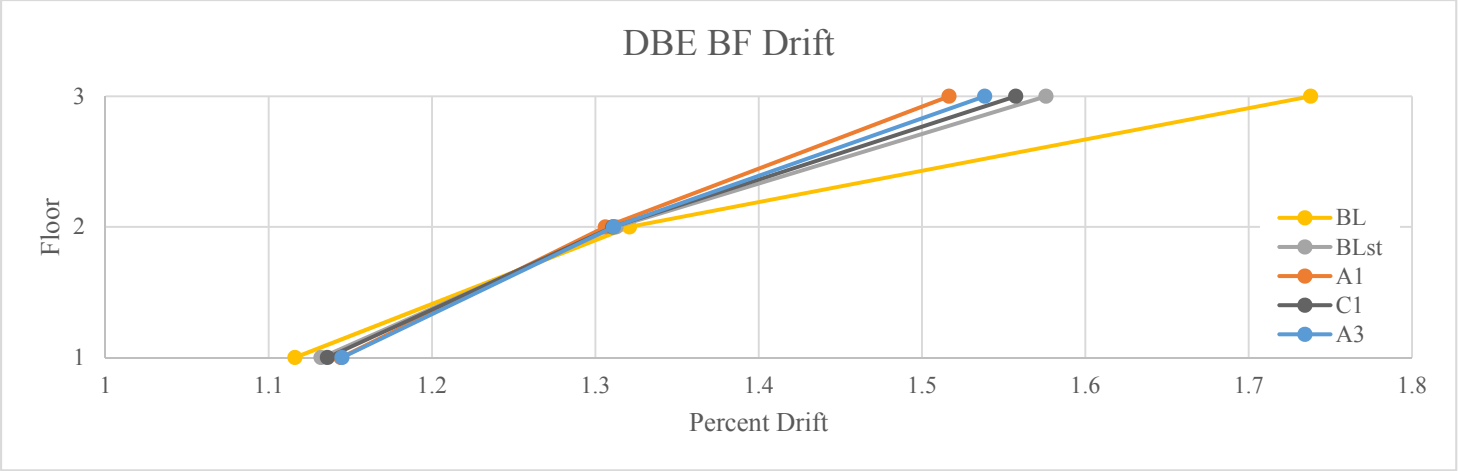

Figure 4-24. Three Story DBE BF Average Maximum Story Drift

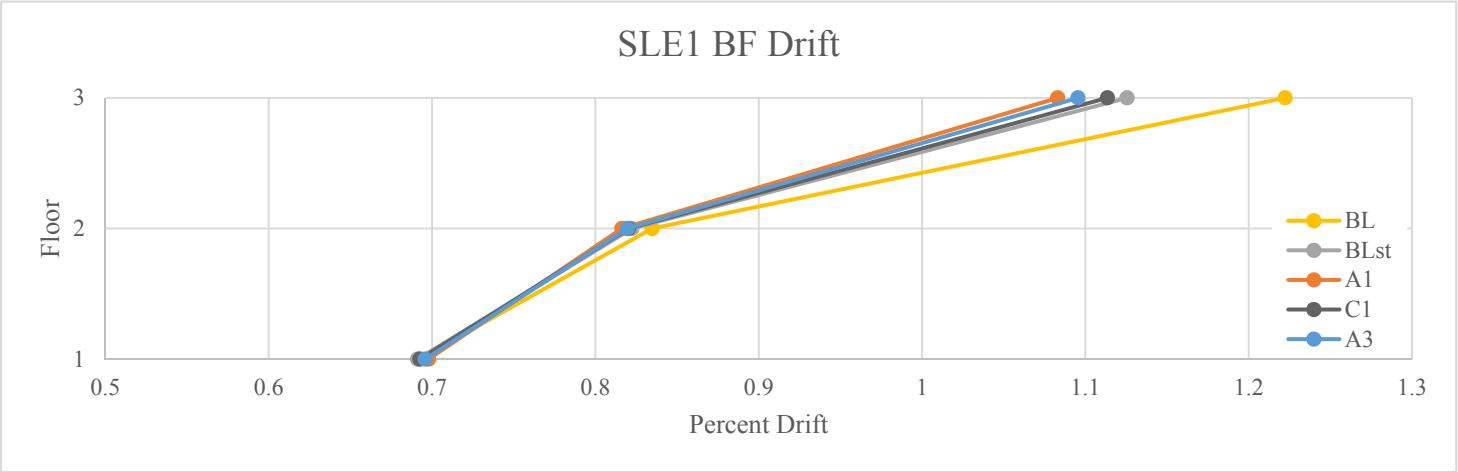

Figure 4-25. Three Story SLE1 BF Average Maximum Story Drift

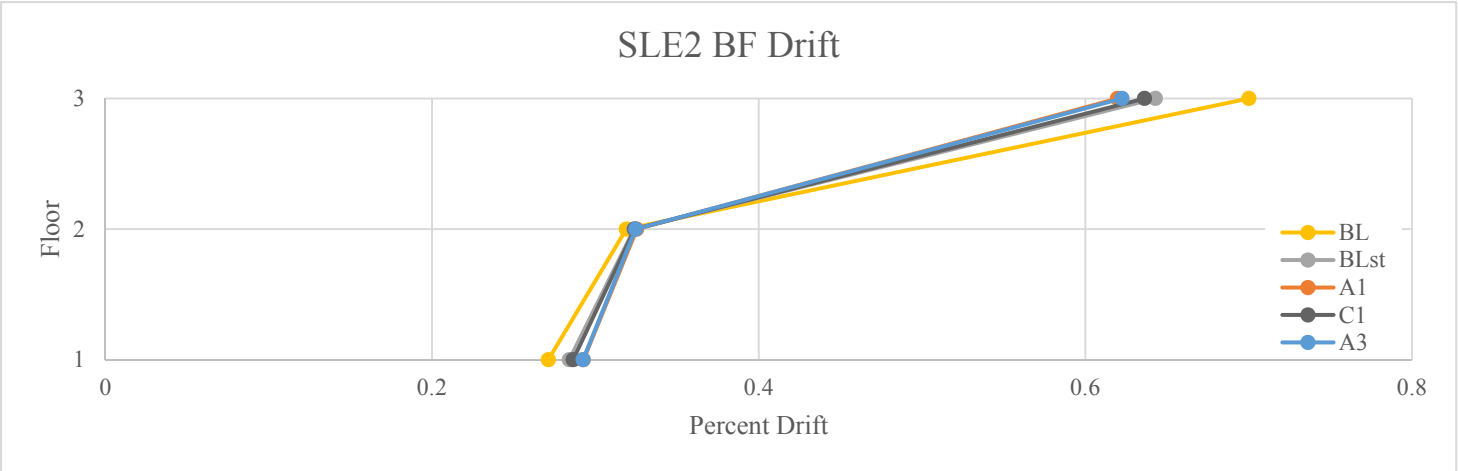

Figure 4-26. Three Story SLE2 BF Average Maximum Story Drift

Graphs showing the percent drift of the nine story SAP2000 models are presented below. Figure 4-27 through Figure 4-32 show the drift response in the MF direction of the MCE level models. The reduction in drift was slightly greater in the floors of the nine story MF than the three story. Figure 4-27 and Figure 4-30 show the A1 LSFF device generated the greatest reduction in drift. However, modeling the shear tab element behavior was again more effective than the further addition of friction devices in reducing story drifts. Figure 4-33 through Figure 4-35 show the drift in the MF direction of the nine story DBE and SLEs. The LSFF devices' improvement upon drift was less at these lower ground motions scales of the nine story moment frame.

Figure 4-36 through Figure 4-41 show story drift for the nine story MCE in the BF direction. The LSFF devices in the BF direction were less influential on drift than those in the MF. The drift of the baseline models was markedly closer to the BLst and friction device model drifts than in any other models. There was some small increase in drift at several floors with the addition of the shear tab elements. Unlike in the three story, this increased drift was reduced with added LSFF damping. Figure 4-42 through Figure 4-44 show the drift of the DBE and SLEs in the BF direction. The story drift reductions of the smaller scale ground motions differed only slightly from the MCE response.

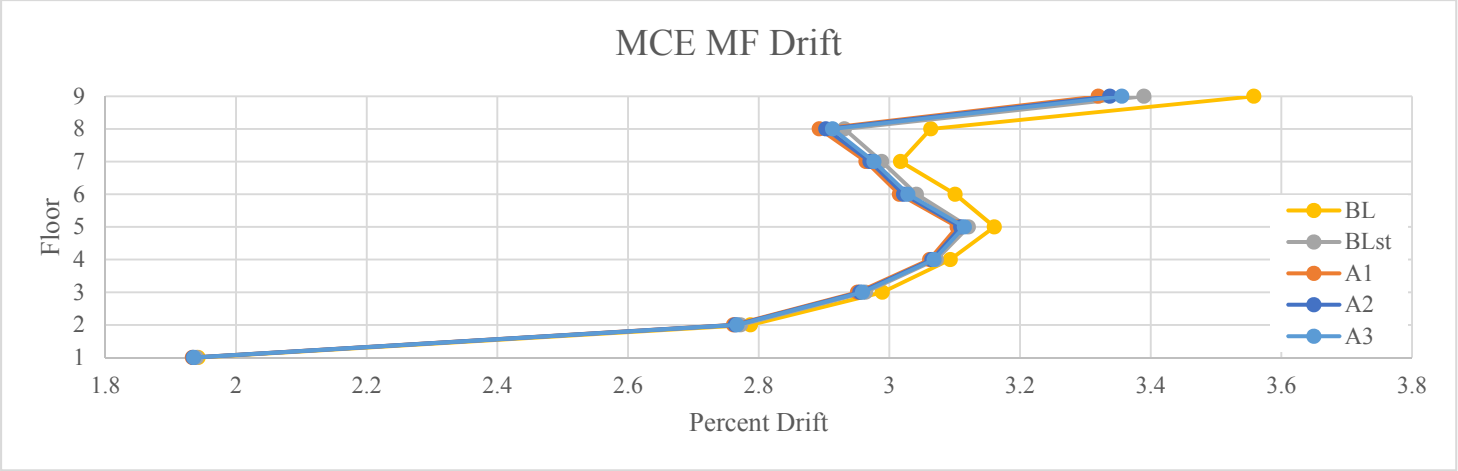

Figure 4-27. Nine Story MCE MF Average Maximum Story Drift (A Layout)

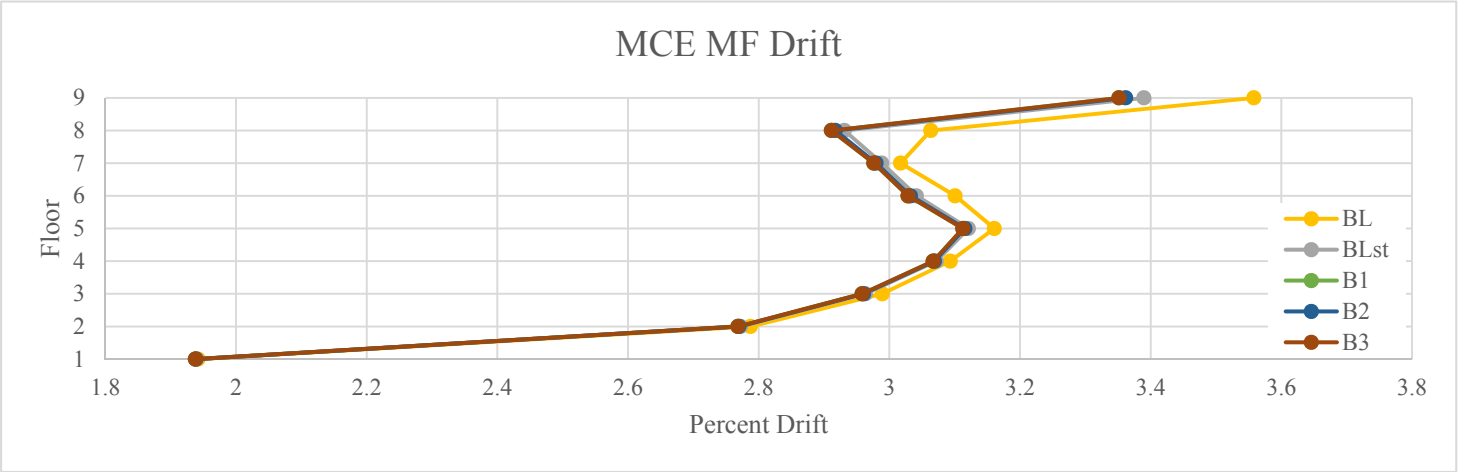

Figure 4-28. Nine Story MCE MF Average Maximum Story Drift (B Layout)

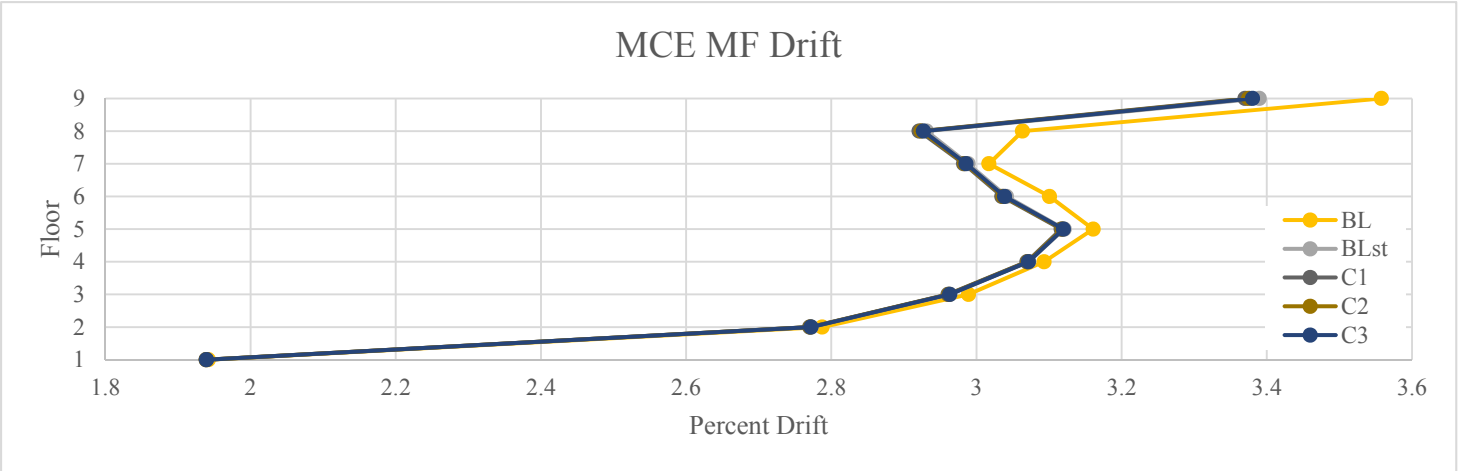

Figure 4-29. Nine Story MCE MF Average Maximum Story Drift (C Layout)

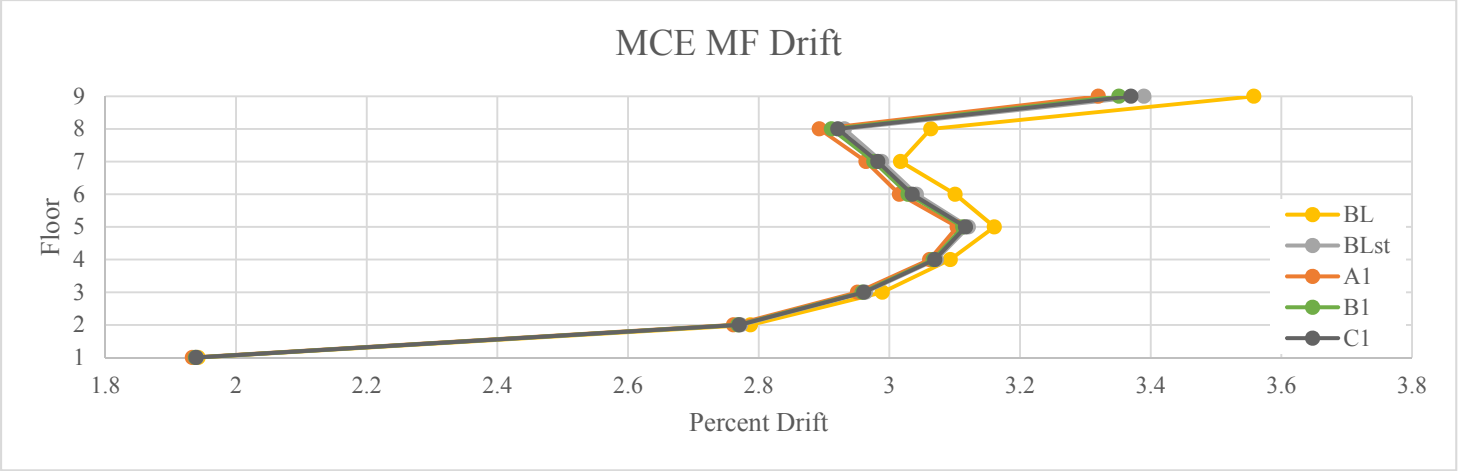

Figure 4-30. Nine Story MCE MF Average Maximum Story Drift (7 kip Slip Force)

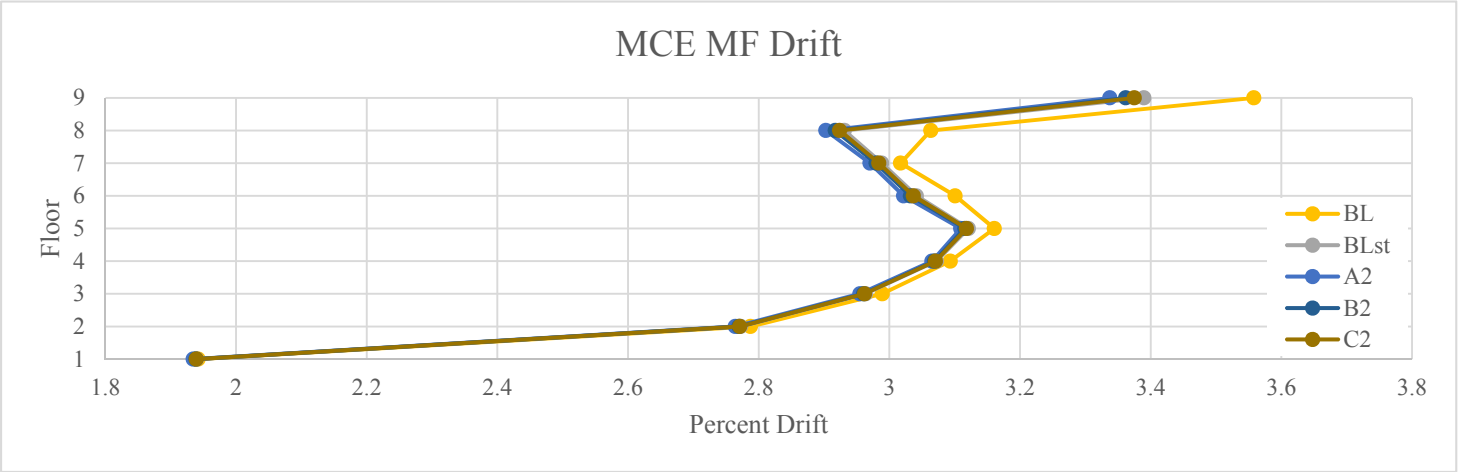

Figure 4-31. Nine Story MCE MF Average Maximum Story Drift (5 kip Slip Force)

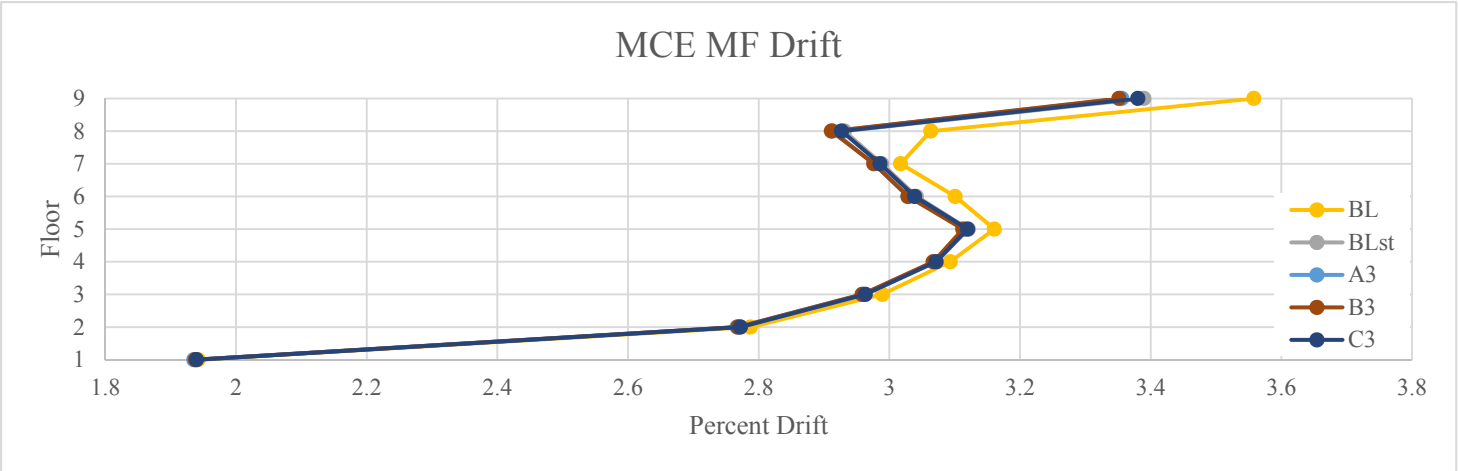

Figure 4-32. Nine Story MCE MF Average Maximum Story Drift (3 kip Slip Force)

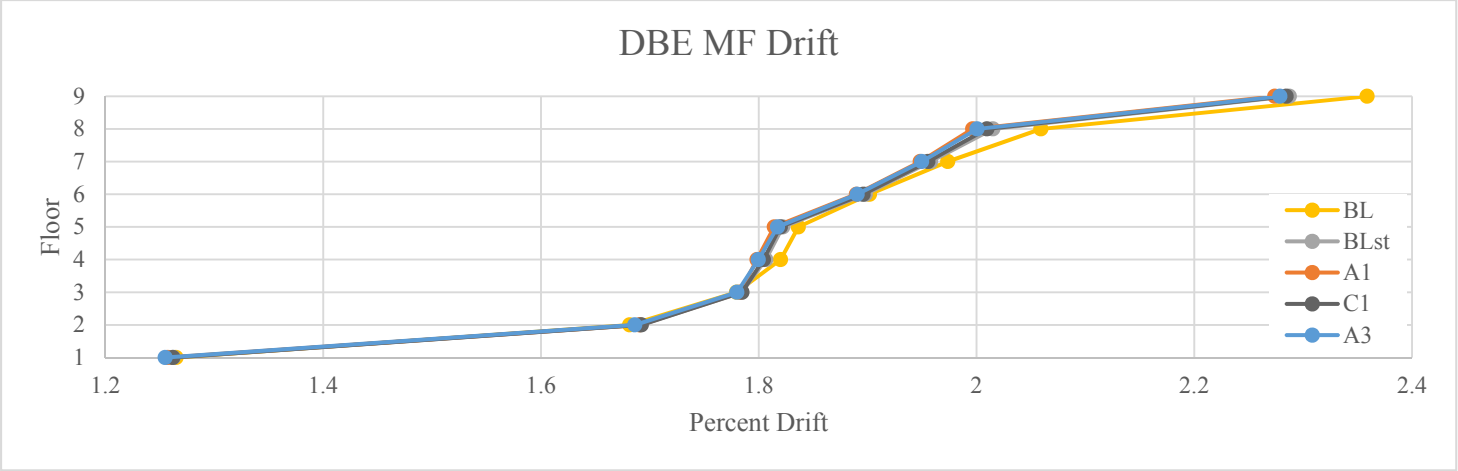

Figure 4-33. Nine Story DBE MF Average Maximum Story Drift

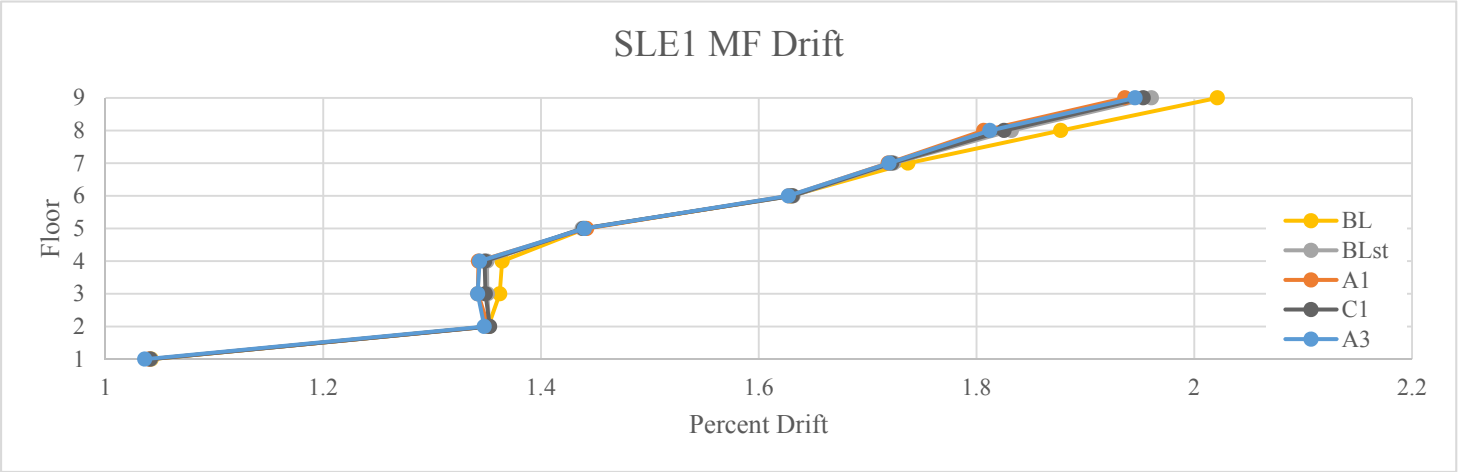

Figure 4-34. Nine Story SLE1 MF Average Maximum Story Drift

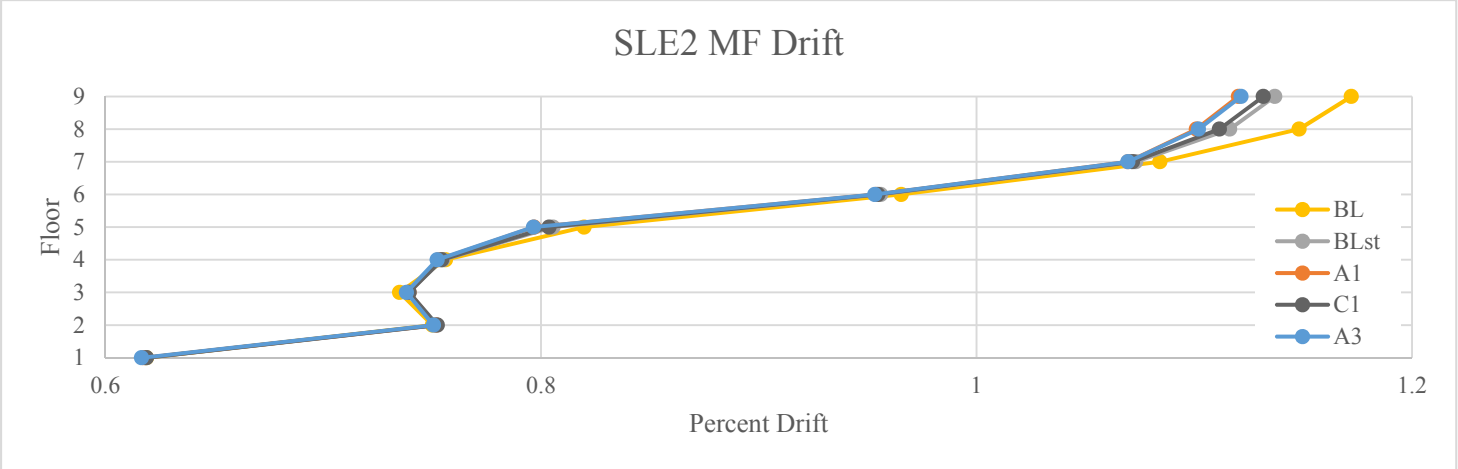

Figure 4-35. Nine Story SLE2 MF Average Maximum Story Drift

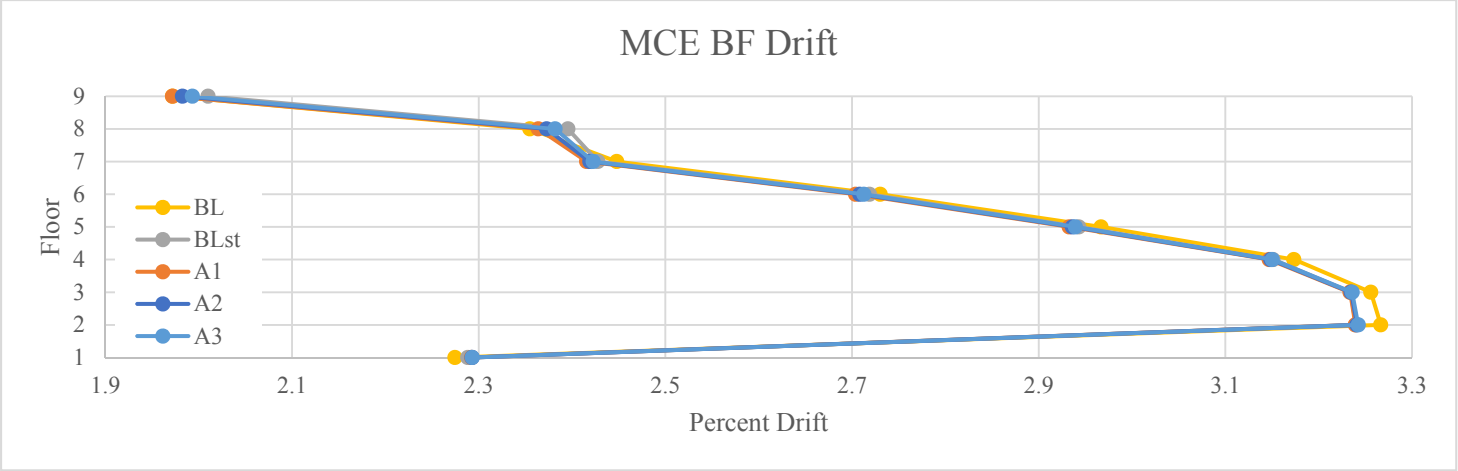

Figure 4-36. Nine Story MCE BF Average Maximum Story Drift (A Layout)

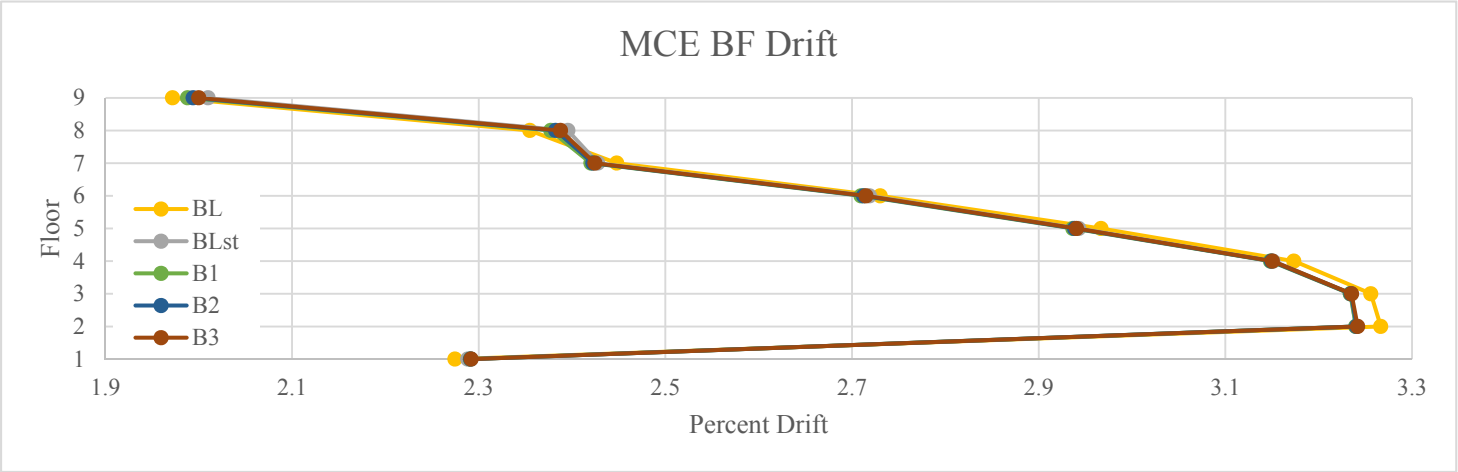

Figure 4-37. Nine Story MCE BF Average Maximum Story Drift (B Layout)

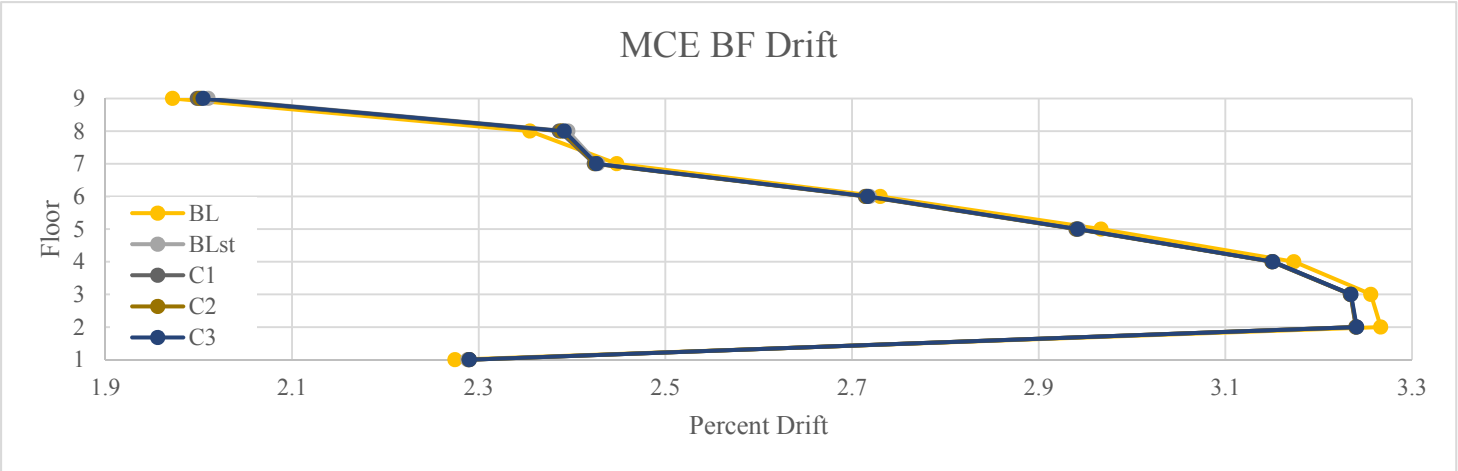

Figure 4-38. Nine Story MCE BF Average Maximum Story Drift (C Layout)

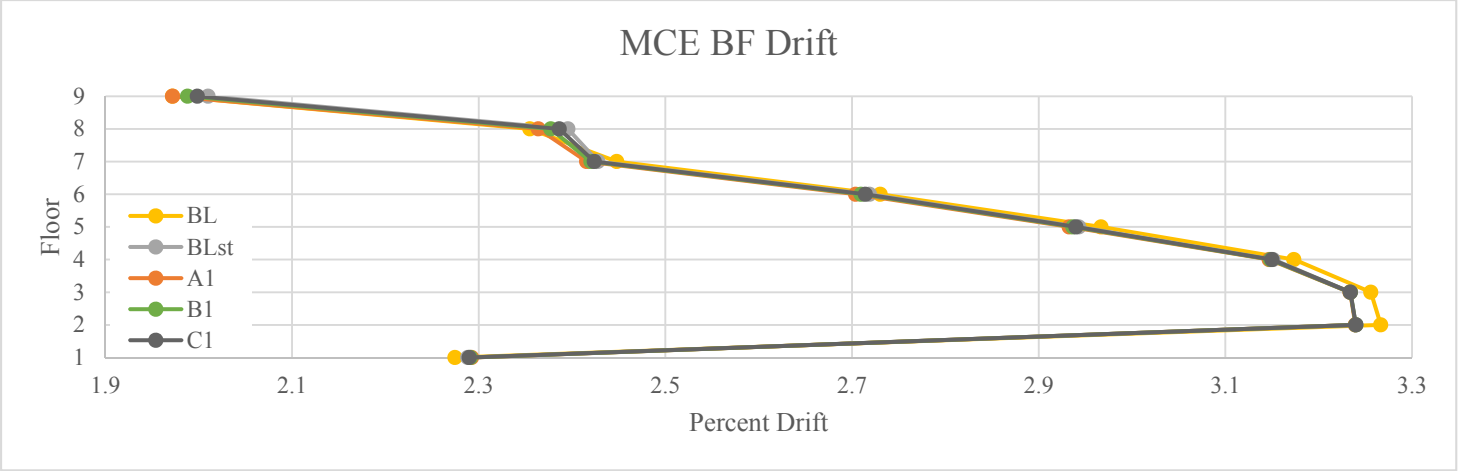

Figure 4-39. Nine Story MCE BF Average Maximum Story Drift (7 kip Slip Force)

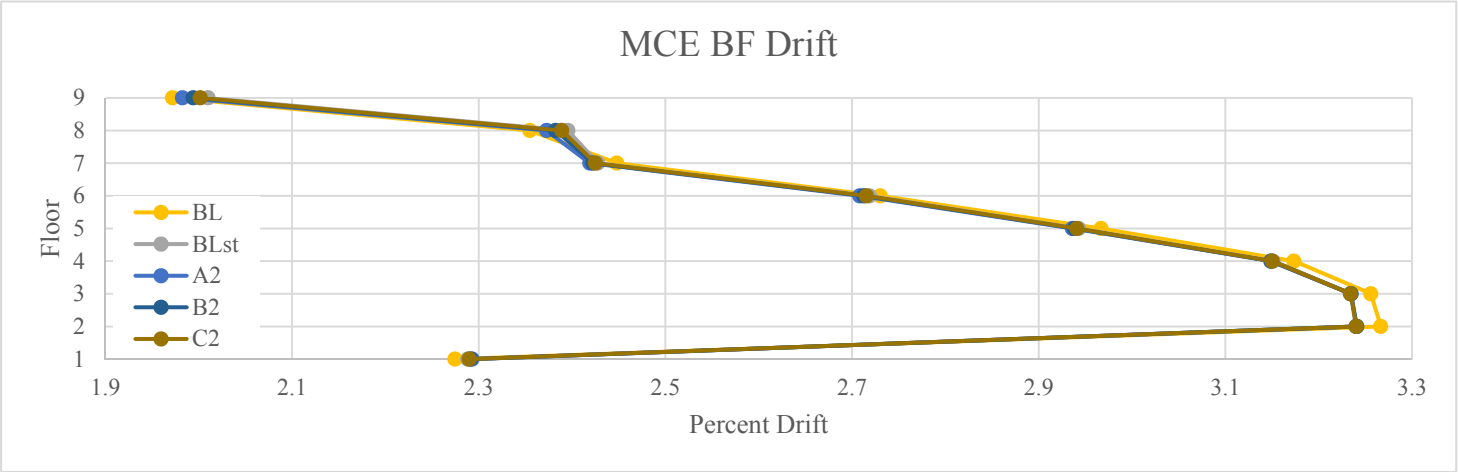

Figure 4-40. Nine Story MCE BF Average Maximum Story Drift (5 kip Slip Force)

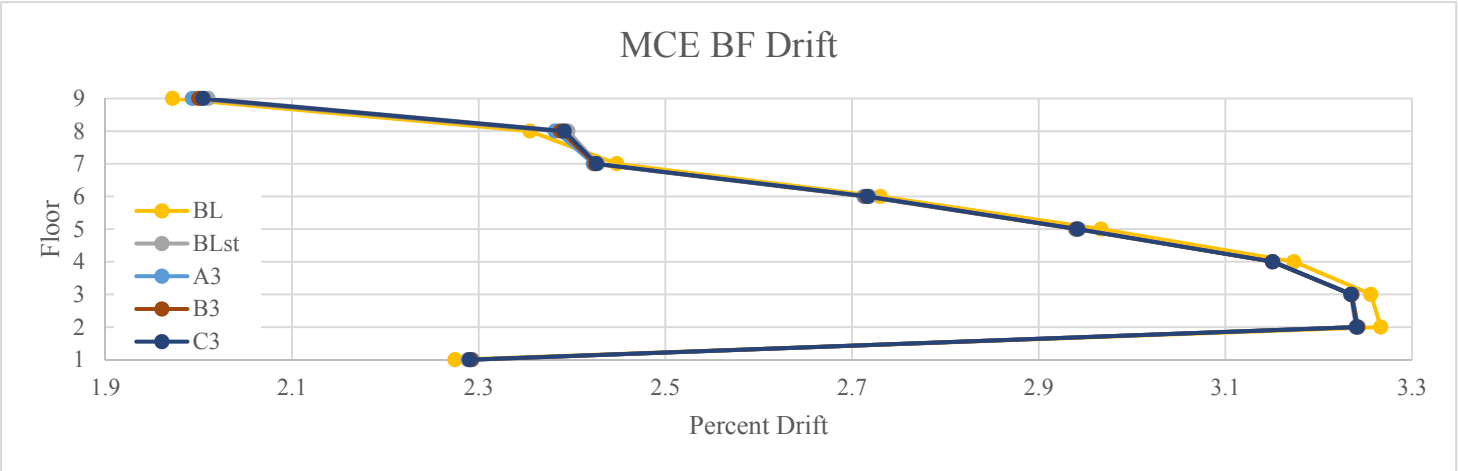

Figure 4-41. Nine Story MCE BF Average Maximum Story Drift (3 kip Slip Force)

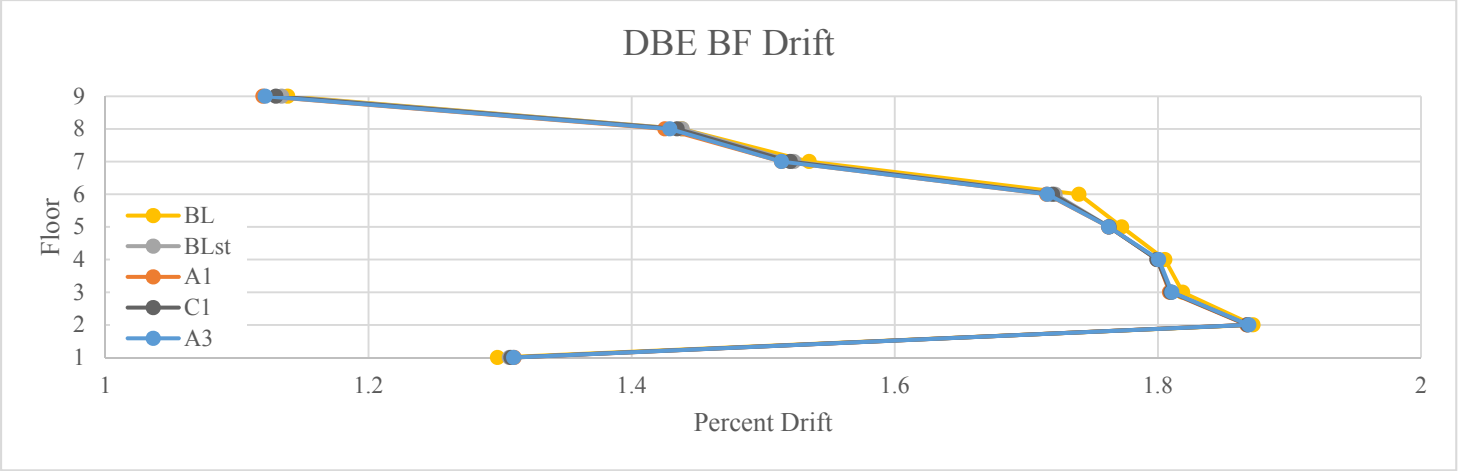

Figure 4-42. Nine Story DBE BF Average Maximum Story Drift

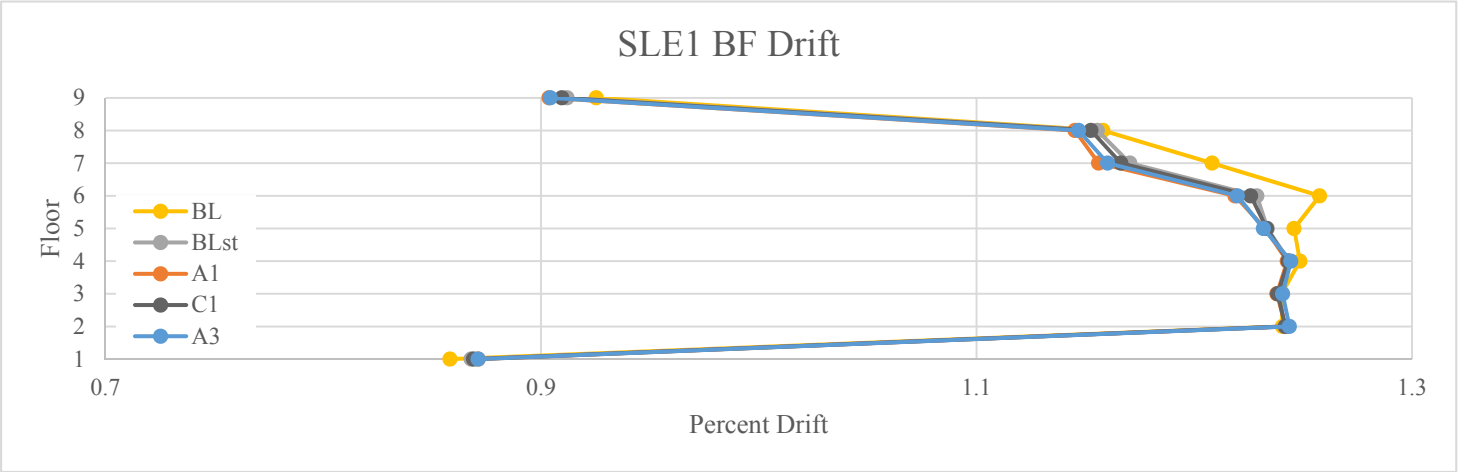

Figure 4-43. Nine Story SLE1 BF Average Maximum Story Drift

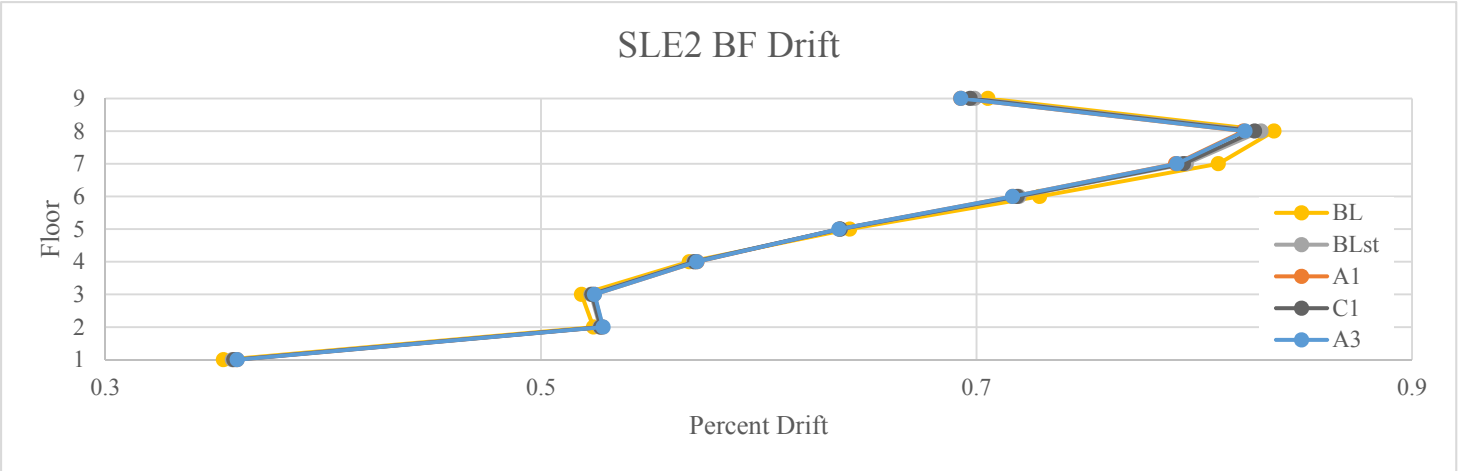

Figure 4-44. Nine Story SLE2 BF Average Maximum Story Drift

4.3.3. Response Tables

The response of several inelastic elements, story drift, and story acceleration in each model are compared in the following tables. Each column contains data for the shear tab rotation, LSFF device displacement, story drift, story acceleration, and special moment frame hinge plastic rotation or buckling restrained brace displacement. The plastic rotation of MF hinges and BRB axial displacement are presented to show the impact of the ground motion on the LFRS. The shear tab rotation shows the impact of the ground motion on the gravity frame.

The MF hinge plastic rotation is a measurement in radians of the rotation beyond yielding that occurs in the beams of the special moment resisting frame. This value is zero where hinges did not form. The friction device axial displacement is presented as a ratio of the maximum displacement to the slip displacement. Values less than one indicate that the LSFF devices did not activate. A higher number in this column doesn't necessarily mean more energy was dissipated as the slip forces may be different and this value does not show the number of cycles that the devices the device completed. Story displacement is presented as a percent of the story height, and story acceleration is presented in g units.

A column adjacent to each metric shows the percent difference between the corresponding model and the baseline model with shear tabs (BLst) for that metric. A negative value in this column indicates the friction damping increased this metric. This frequently occurred for the story accelerations. Appendix A contains tables showing the force as well as displacement data for elements in the SAP2000 analyses.

Table 4-1 lists the three story MF results for the MCE. Looking at the FD displacement, the LSFF devices were activated in every model. There was nearly no change in the story drift and acceleration with the addition of any of the LSFF devices, and only small differences between the baseline model with shear tabs and that without. The shear tab and moment frame hinge rotation

showed the largest improvement with the addition of friction damping. There was a small increase in shear tab rotation in models with the C friction device layout. This was likely due to increased stiffness in a few shear tab connections while others deformed more. In every metric, the A1 model generated the largest reduction in displacement.

Table 4-1. Three Story MCE MF Average Maximum Element Response

		MF Hinge Plastic Rotation		ST Rotation		FD Disp	Story Drift		Story Accl	
		rad	% Change	rad	% Change	Ratio	% Drift	% Change	g	% Change
Floor 3	**BL**	0.0320	N/A	N/A	N/A	N/A	3.10	N/A	1.385	N/A
	BLst	0.0275	N/A	0.0270	N/A	N/A	3.03	N/A	1.400	N/A
	A1	0.0266	3.3	0.0260	3.7	1.41	3.02	0.5	1.404	-0.3
	A2	0.0270	1.8	0.0262	2.9	2.00	3.02	0.3	1.404	-0.3
	A3	0.0272	1.1	0.0264	2.0	3.37	3.02	0.3	1.404	-0.3
	B1	0.0267	2.9	0.0269	0.5	1.41	3.03	0.2	1.401	-0.0
	B2	0.0270	1.8	0.0269	0.4	2.01	3.03	0.1	1.402	-0.1
	B3	0.0273	0.7	0.0269	0.4	3.38	3.03	0.1	1.402	-0.1
	C1	0.0269	2.2	0.0273	-1.3	1.39	3.03	0.2	1.401	-0.1
	C2	0.0272	1.1	0.0272	-0.9	1.99	3.03	0.1	1.403	-0.2
	C3	0.0274	0.4	0.0272	-0.7	3.37	3.03	0.0	1.403	-0.2
Floor 2	**BL**	0.0424	N/A	N/A	N/A	N/A	3.41	N/A	1.233	N/A
	BLst	0.0388	N/A	0.0314	N/A	N/A	3.37	N/A	1.250	N/A
	A1	0.0380	2.1	0.0306	2.5	1.69	3.36	0.3	1.252	-0.2
	A2	0.0384	1.0	0.0308	1.9	2.40	3.36	0.3	1.252	-0.2
	A3	0.0385	0.8	0.0310	1.3	4.02	3.37	0.2	1.252	-0.2
	B1	0.0381	1.8	0.0313	0.3	1.70	3.37	0.2	1.250	-0.1
	B2	0.0384	1.0	0.0313	0.4	2.40	3.37	0.2	1.251	-0.1
	B3	0.0386	0.5	0.0313	0.4	4.02	3.37	0.1	1.251	-0.1
	C1	0.0383	1.3	0.0317	-1.2	1.67	3.37	0.1	1.251	-0.1
	C2	0.0385	0.8	0.0316	-0.8	2.38	3.37	0.1	1.251	-0.1
	C3	0.0387	0.3	0.0315	-0.4	4.01	3.37	0.0	1.251	-0.1

Floor 1	**BL**	0.0343	N/A	N/A	N/A	N/A	2.40	N/A	1.317	N/A
	BLst	0.0330	N/A	0.0276	N/A	N/A	2.42	N/A	1.323	N/A
	A1	0.0327	0.9	0.0269	2.7	1.42	2.42	0.1	1.321	0.2
	A2	0.0328	0.6	0.0271	2.1	2.01	2.42	0.1	1.323	0.0
	A3	0.0329	0.3	0.0273	1.4	3.38	2.42	0.1	1.323	0.0
	B1	0.0327	0.9	0.0276	0.1	1.42	2.42	0.1	1.321	0.1
	B2	0.0328	0.6	0.0276	0.2	2.01	2.42	0.1	1.323	0.0
	B3	0.0329	0.3	0.0276	0.3	3.38	2.42	0.1	1.323	0.0
	C1	0.0328	0.6	0.0281	-1.5	1.40	2.42	0.0	1.324	0.0
	C2	0.0329	0.3	0.0279	-1.1	1.99	2.42	0.0	1.325	-0.1
	C3	0.0329	0.3	0.0278	-0.6	3.36	2.42	0.1	1.325	-0.2

Table 4-2 shows results from the SLE1 nonlinear time history analyses for the three story model MF direction. The friction devices were only activated in the A3 model. These smaller scale earthquakes were not able to cause the seven kip friction devices to slip. Models with LSFF devices showed negligible changes in story drift and acceleration. The energy dissipation of the A3 model produced the largest reduction in damage to the SMRF. Though at this service level, even the baseline models had only slight moment frame plastic hinging which was not entirely prevented with the friction damping.

Table 4-2. Three Story SLE1 MF Average Maximum Element Response

		MF Hinge Plastic Rotation		**ST Rotation**		**FD Disp**	**Story Drift**		**Story Accl**	
		rad	**% Change**	**rad**	**% Change**	**Ratio**	**% Drift**	**% Change**	**g**	**% Change**
Floor 3	**BL**	0.000	N/A	N/A	N/A	N/A	1.58	N/A	0.848	N/A
	BLst	0.000	N/A	0.0138	N/A	N/A	1.56	N/A	0.859	N/A
	A1	0.000	0.0	0.0131	4.9	0.71	1.55	0.5	0.861	-0.2
	C1	0.000	0.0	0.0140	-1.8	0.69	1.56	0.2	0.860	-0.1
	A3	0.000	0.0	0.0133	3.3	1.69	1.55	0.6	0.858	0.1
Floor 2	**BL**	0.0069	N/A	N/A	N/A	N/A	1.82	N/A	0.710	N/A
	BLst	0.0061	N/A	0.0165	N/A	N/A	1.80	N/A	0.716	N/A
	A1	0.0059	3.9	0.0158	3.7	0.87	1.80	0.3	0.717	-0.1
	C1	0.0060	1.3	0.0167	-1.7	0.86	1.80	0.1	0.717	-0.1
	A3	0.0058	4.5	0.0161	2.2	2.09	1.79	0.5	0.715	0.1

Floor 1	**BL**	0.0090	N/A	N/A	N/A	N/A	1.36	N/A	0.687	N/A
	BLst	0.0081	N/A	0.0152	N/A	N/A	1.35	N/A	0.692	N/A
	A1	0.0077	4.4	0.0146	3.8	0.77	1.35	0.1	0.693	-0.1
	C1	0.0080	1.5	0.0155	-2.1	0.75	1.35	0.0	0.692	0.0
	A3	0.0076	5.6	0.0148	2.6	1.83	1.35	0.3	0.692	0.0

Table 4-3 presents three story MCE results in the BF direction. The LSFF devices were activated in every model. At the top floor, LSFF damping reduced displacement demands in the BRBs, shear tabs, and story drift with only a slight increase in acceleration. However, the effects of the LSFF devices on the first floor of these models were inconsistent with the typical result of the friction damping. Displacements were increased and accelerations were reduced. This effect was minor, and may have been caused by the increase in stiffness at the upper levels of the structure.

Table 4-3. Three Story MCE BF Average Maximum Element Response

		BRB Disp		**ST Rotation**		**FD Disp**	**Story Drift**		**Story Accl**	
		Ratio	**% Change**	**rad**	**% Change**	**Ratio**	**% Drift**	**% Change**	**g**	**% Change**
Floor 3	**BL**	17.6	N/A	N/A	N/A	N/A	3.04	N/A	0.394	N/A
	BLst	16.1	N/A	0.0292	N/A	N/A	2.77	N/A	0.419	N/A
	A1	15.6	3.0	0.0277	5.2	2.34	2.68	3.2	0.423	-1.0
	A2	15.7	2.5	0.0280	4.1	3.32	2.70	2.6	0.424	-1.1
	A3	15.8	1.8	0.0284	2.7	5.60	2.73	1.7	0.424	-1.2
	B1	15.8	1.7	0.0287	1.7	1.83	2.72	1.9	0.421	-0.6
	B2	15.8	1.5	0.0288	1.5	2.65	2.73	1.6	0.421	-0.6
	B3	15.9	1.1	0.0289	1.1	4.54	2.74	1.1	0.422	-0.7
	C1	15.9	0.8	0.0290	0.7	1.86	2.74	1.0	0.420	-0.3
	C2	16.0	0.6	0.0291	0.5	2.68	2.75	0.7	0.420	-0.3
	C3	16.0	0.4	0.0291	0.3	4.58	2.76	0.4	0.420	-0.3

Floor 2	**BL**	13.1	N/A	N/A	N/A	N/A	2.33	N/A	0.702	N/A
	BLst	13.1	N/A	0.0245	N/A	N/A	2.32	N/A	0.707	N/A
	A1	13.1	0.1	0.0237	3.2	1.97	2.32	0.1	0.709	-0.2
	A2	13.1	0.4	0.0237	3.0	2.77	2.32	0.0	0.710	-0.4
	A3	13.1	0.4	0.0240	2.1	4.65	2.33	0.1	0.711	-0.6
	B1	13.1	0.0	0.0243	0.8	1.95	2.32	0.0	0.711	-0.5
	B2	13.1	0.2	0.0242	0.9	2.76	2.32	0.0	0.711	-0.5
	B3	13.1	0.3	0.0243	0.8	4.66	2.33	0.1	0.711	-0.6
	C1	13.1	0.0	0.0244	0.2	1.96	2.32	0.0	0.708	-0.2
	C2	13.1	0.0	0.0244	0.1	2.79	2.33	-0.1	0.709	-0.3
	C3	13.1	0.0	0.0245	0.1	4.69	2.33	-0.1	0.709	-0.3
Floor 1	**BL**	11.2	N/A	N/A	N/A	N/A	1.95	N/A	0.810	N/A
	BLst	11.3	N/A	0.0261	N/A	N/A	1.97	N/A	0.798	N/A
	A1	11.4	-1.1	0.0259	0.6	2.22	2.00	-1.3	0.797	0.1
	A2	11.4	-0.9	0.0260	0.5	3.12	2.00	-1.3	0.799	-0.2
	A3	11.3	0.3	0.0260	0.5	5.20	2.00	-1.4	0.800	-0.3
	B1	11.4	-0.6	0.0263	0.8	1.45	1.99	-0.7	0.798	0.0
	B2	11.4	-0.5	0.0262	0.5	2.07	1.99	-0.7	0.798	0.1
	B3	11.3	0.3	0.0261	0.2	3.53	1.99	-0.8	0.799	-0.1
	C1	11.3	0.3	0.0262	-0.6	1.44	1.98	-0.3	0.797	0.0
	C2	11.3	0.3	0.0262	-0.4	2.08	1.98	-0.4	0.798	0.0
	C3	11.3	0.1	0.0261	0.3	3.54	1.98	-0.4	0.798	0.1

Table 4-4 shows the BF direction results for the three story SLE1 analyses. At this service level, only the A3 LSFF devices were activated. Despite this, the A1 model had the greatest influence on response. The smaller scale ground motion saw slightly greater improvement with LSFF damping in the upper floor compared to the MCE analyses. Like the MCE, the first floor sustained greater displacements with LSFF devices.

Table 4-4. Three Story SLE1 BF Average Maximum Element Response

		BRB Disp		ST Rotation		FD Disp	Story Drift		Story Accl	
		Ratio	% Change	rad	% Change	Ratio	% Drift	% Change	g	% Change
Floor 3	BL	7.07	N/A	N/A	N/A	N/A	1.22	N/A	0.288	N/A
	BLst	6.52	N/A	0.0126	N/A	N/A	1.13	N/A	0.304	N/A
	A1	6.29	3.5	0.0116	7.6	0.98	1.08	3.8	0.311	-2.4
	C1	6.45	1.0	0.0125	0.6	0.74	1.11	1.1	0.306	-0.6
	A3	6.37	2.4	0.0120	4.3	2.37	1.10	2.7	0.308	-1.3
Floor 2	BL	4.85	N/A	N/A	N/A	N/A	0.83	N/A	0.504	N/A
	BLst	4.78	N/A	0.0096	N/A	N/A	0.82	N/A	0.506	N/A
	A1	4.75	0.6	0.0093	3.7	0.76	0.82	0.8	0.505	0.2
	C1	4.77	0.2	0.0097	-0.3	0.73	0.82	0.2	0.506	0.0
	A3	4.77	0.2	0.0094	2.4	1.81	0.82	0.3	0.505	0.1
Floor 1	BL	4.18	N/A	N/A	N/A	N/A	0.69	N/A	0.486	N/A
	BLst	4.18	N/A	0.0090	N/A	N/A	0.69	N/A	0.480	N/A
	A1	4.22	-0.8	0.0088	2.3	0.75	0.70	-1.0	0.479	0.2
	C1	4.19	-0.2	0.0090	0.7	0.48	0.69	0.2	0.479	0.1
	A3	4.21	-0.6	0.0089	1.2	2.37	0.70	-0.7	0.478	0.4

For the nine story SAP2000 models the output tables only display the odd numbered stories. This was done to condense the data being shown. The full output tables for the nine story models are shown in the Appendix A. The nine story MF results for the MCE analyses are listed in Table 4-5. The friction devices were activated in every model. The largest benefit of LSFF damping in these models is in reducing the rotational demands in the moment frame and gravity frame beams. The story drifts and accelerations were only minimally impacted by the addition of friction dampers.

Table 4-5. Nine Story MCE MF Average Maximum Element Response

		MF Hinge Plastic Rotation		ST Rotation		FD Disp	Story Drift		Story Accl	
		rad	% Change	rad	% Change	Ratio	% Drift	% Change	g	% Change
Floor 9	BL	0.0323	N/A	N/A	N/A	N/A	3.56	N/A	0.798	N/A
	BLst	0.0306	N/A	0.0323	N/A	N/A	3.39	N/A	0.809	N/A
	A1	0.0302	1.3	0.0308	4.5	1.67	3.32	2.1	0.812	-0.3
	A2	0.0302	1.3	0.0312	3.3	2.37	3.34	1.5	0.812	-0.4
	A3	0.0303	1.0	0.0316	2.1	4.00	3.36	1.0	0.813	-0.4
	B1	0.0304	0.7	0.0324	-0.5	1.62	3.35	1.1	0.811	-0.2
	B2	0.0304	0.7	0.0324	-0.3	2.31	3.36	0.8	0.811	-0.2
	B3	0.0305	0.3	0.0323	0.2	3.91	3.37	0.5	0.812	-0.3
	C1	0.0305	0.3	0.0326	-1.0	1.63	3.37	0.6	0.810	-0.1
	C2	0.0305	0.3	0.0325	-0.7	2.32	3.38	0.4	0.810	-0.1
	C3	0.0305	0.3	0.0324	-0.5	3.92	3.38	0.3	0.811	-0.1
Floor 7	BL	0.0257	N/A	N/A	N/A	N/A	3.02	N/A	0.775	N/A
	BLst	0.0245	N/A	0.0292	N/A	N/A	2.99	N/A	0.766	N/A
	A1	0.0239	2.4	0.0285	2.5	1.86	2.96	0.8	0.767	-0.1
	A2	0.0240	2.0	0.0287	1.6	2.63	2.97	0.6	0.768	-0.2
	A3	0.0241	1.6	0.0289	0.8	4.43	2.98	0.4	0.769	-0.3
	B1	0.0241	1.6	0.0291	0.2	1.69	2.98	0.4	0.767	-0.1
	B2	0.0242	1.2	0.0291	0.3	2.39	2.98	0.3	0.768	-0.1
	B3	0.0243	0.8	0.0291	0.4	4.03	2.98	0.2	0.768	-0.2
	C1	0.0243	0.8	0.0294	-0.8	1.69	2.98	0.2	0.767	-0.1
	C2	0.0244	0.4	0.0293	-0.6	2.40	2.98	0.1	0.767	-0.1
	C3	0.0244	0.4	0.0293	-0.3	4.04	2.99	0.1	0.767	-0.1
Floor 5	BL	0.0333	N/A	N/A	N/A	N/A	3.16	N/A	0.730	N/A
	BLst	0.0324	N/A	0.0306	N/A	N/A	3.12	N/A	0.738	N/A
	A1	0.0320	1.2	0.0299	2.2	1.93	3.10	0.5	0.741	-0.4
	A2	0.0321	0.9	0.0301	1.4	2.72	3.11	0.4	0.741	-0.4
	A3	0.0322	0.6	0.0304	0.7	4.57	3.11	0.2	0.741	-0.4
	B1	0.0322	0.6	0.0309	-1.0	1.79	3.11	0.3	0.740	-0.3
	B2	0.0323	0.3	0.0308	-0.7	2.52	3.12	0.2	0.740	-0.3
	B3	0.0323	0.3	0.0307	-0.4	4.24	3.12	0.1	0.740	-0.3
	C1	0.0323	0.3	0.0311	-1.7	1.79	3.12	0.1	0.739	-0.1
	C2	0.0323	0.3	0.0310	-1.3	2.53	3.12	0.1	0.739	-0.1
	C3	0.0323	0.3	0.0309	-1.0	4.25	3.12	0.0	0.739	-0.1

Floor 3	**BL**	0.0152	N/A	N/A	N/A	N/A	2.99	N/A	0.697	N/A
	BLst	0.0148	N/A	0.0296	N/A	N/A	2.96	N/A	0.705	N/A
	A1	0.0147	0.7	0.0291	1.6	1.86	2.95	0.4	0.710	-0.6
	A2	0.0147	0.7	0.0293	1.0	2.62	2.95	0.3	0.710	-0.7
	A3	0.0147	0.7	0.0295	0.4	4.39	2.96	0.2	0.710	-0.7
	B1	0.0148	0.0	0.0300	-1.5	1.73	2.96	0.2	0.707	-0.3
	B2	0.0148	0.0	0.0299	-1.1	2.44	2.96	0.1	0.708	-0.3
	B3	0.0148	0.0	0.0298	-0.7	4.10	2.96	0.0	0.708	-0.4
	C1	0.0148	0.0	0.0301	-1.8	1.73	2.96	0.1	0.706	-0.2
	C2	0.0148	0.0	0.0300	-1.4	2.44	2.96	0.1	0.706	-0.2
	C3	0.0148	0.0	0.0299	-1.1	4.10	2.96	0.0	0.707	-0.2
Floor 1	**BL**	0.0082	N/A	N/A	N/A	N/A	1.94	N/A	0.861	N/A
	BLst	0.0081	N/A	0.0234	N/A	N/A	1.94	N/A	0.858	N/A
	A1	0.0080	1.1	0.0229	2.1	1.44	1.93	0.3	0.859	-0.1
	A2	0.0080	1.0	0.0231	1.4	2.03	1.93	0.3	0.859	-0.2
	A3	0.0080	1.0	0.0233	0.6	3.41	1.94	0.2	0.860	-0.2
	B1	0.0080	0.5	0.0238	-1.7	1.34	1.94	0.1	0.859	-0.1
	B2	0.0080	0.4	0.0237	-1.3	1.89	1.94	0.1	0.859	-0.1
	B3	0.0080	0.4	0.0236	-0.8	3.17	1.94	0.0	0.859	-0.2
	C1	0.0080	0.2	0.0240	-2.2	1.34	1.94	0.0	0.858	-0.1
	C2	0.0080	0.2	0.0238	-1.7	1.89	1.94	0.0	0.859	-0.1
	C3	0.0080	0.2	0.0237	-1.3	3.17	1.94	0.0	0.859	-0.1

Results from the SLE1 analyses for the nine story model MF direction are shown in Table 4-6. There was little energy dissipation from friction dampers other than the three kip devices in model A3. Despite many of the friction dampers not activating, the A1 model seems to have had the greatest impact. Though, friction damping did not significantly impact any particular metric. The effects on response from the seven kip models are likely caused by the added stiffness the LSFF devices provide to gravity frame connections.

Table 4-6. Nine Story SLE1 MF Average Maximum Element Response

		MF Hinge Plastic Rotation		**ST Rotation**		**FD Disp**	**Story Drift**		**Story Accl**	
		rad	**% Change**	**rad**	**% Change**	**Ratio**	**% Drift**	**% Change**	**g**	**% Change**
Floor 9	**BL**	0.0092	N/A	N/A	N/A	N/A	2.02	N/A	0.628	N/A
	BLst	0.0085	N/A	0.0184	N/A	N/A	1.96	N/A	0.632	N/A
	A1	0.0084	1.8	0.0175	5.0	0.94	1.94	1.2	0.632	0.1
	C1	0.0085	0.8	0.0188	-1.8	0.91	1.95	0.4	0.632	0.0
	A3	0.0085	0.4	0.0179	3.0	2.26	1.95	0.8	0.631	0.1

Floor 7	**BL**	0.0098	N/A	N/A	N/A	N/A	1.74	N/A	0.497	N/A
	BLst	0.0096	N/A	0.0180	N/A	N/A	1.72	N/A	0.500	N/A
	A1	0.0094	2.1	0.0175	2.7	1.13	1.72	0.3	0.500	0.0
	C1	0.0095	0.8	0.0181	-0.9	1.02	1.72	0.1	0.500	0.0
	A3	0.0096	0.3	0.0178	1.1	2.69	1.72	0.2	0.499	0.1
Floor 5	**BL**	0.0018	N/A	N/A	N/A	N/A	1.44	N/A	0.454	N/A
	BLst	0.0024	N/A	0.0153	N/A	N/A	1.44	N/A	0.455	N/A
	A1	0.0025	-2.9	0.0149	2.6	0.96	1.44	0.3	0.455	0.1
	C1	0.0025	-2.8	0.0156	-1.8	0.87	1.44	0.1	0.455	0.0
	A3	0.0025	-3.1	0.0151	1.2	2.28	1.44	0.1	0.455	0.0
Floor 3	**BL**	0.000	N/A	N/A	N/A	N/A	1.36	N/A	0.465	N/A
	BLst	0.000	N/A	0.0133	N/A	N/A	1.35	N/A	0.469	N/A
	A1	0.000	0.0	0.0129	2.9	0.83	1.34	0.6	0.471	-0.6
	C1	0.000	0.0	0.0136	-2.1	0.76	1.35	0.1	0.469	-0.1
	A3	0.000	0.0	0.0131	1.7	1.98	1.34	0.7	0.471	-0.4
Floor 1	**BL**	0.000	N/A	N/A	N/A	N/A	1.04	N/A	0.484	N/A
	BLst	0.000	N/A	0.0121	N/A	N/A	1.04	N/A	0.483	N/A
	A1	0.000	0.0	0.0118	2.7	0.74	1.04	0.2	0.483	0.0
	C1	0.000	0.0	0.0125	-3.1	0.69	1.04	0.0	0.483	0.0
	A3	0.000	0.0	0.0119	1.8	1.76	1.04	0.5	0.483	0.0

Table 4-7 presents nine story MCE results for the BF direction. LSFF devices were activated in every model except at the top floor. Neither the addition of LSFF damping nor shear tab elements changed any of the response metrics significantly from the BL model. Table 4-8 shows the BF direction results for the nine story SLE1 analyses. At this smaller ground motion scaling the friction devices had even less impact than at the MCE level. The LSFF damping had little effect on the BF response, and at certain levels deformations increased and accelerations were reduced.

Table 4-7. Nine Story MCE BF Average Maximum Element Response

		BRB Disp		ST Rotation		FD Disp	Story Drift		Story Accl	
		Ratio	% Change	rad	% Change	Ratio	% Drift	% Change	g	% Change
Floor 9	BL	11.0	N/A	N/A	N/A	N/A	1.95	N/A	0.450	N/A
	BLst	11.4	N/A	0.0168	N/A	N/A	2.01	N/A	0.450	N/A
	A1	11.1	2.8	0.0162	3.3	0.87	1.97	1.9	0.463	-3.0
	A2	11.1	2.1	0.0163	2.5	1.23	1.98	1.4	0.463	-3.0
	A3	11.2	1.3	0.0165	1.6	2.06	1.99	0.8	0.463	-3.0
	B1	11.2	1.6	0.0166	0.9	0.69	1.99	1.1	0.462	-2.8
	B2	11.2	1.2	0.0166	0.7	0.99	1.99	0.8	0.462	-2.8
	B3	11.3	0.7	0.0167	0.5	1.68	2.00	0.5	0.462	-2.8
	C1	11.3	0.8	0.0167	0.4	0.69	2.00	0.6	0.461	-2.6
	C2	11.3	0.6	0.0167	0.3	0.99	2.00	0.4	0.461	-2.6
	C3	11.3	0.4	0.0167	0.3	1.68	2.00	0.3	0.461	-2.6
Floor 7	BL	13.2	N/A	N/A	N/A	N/A	2.45	N/A	0.597	N/A
	BLst	13.1	N/A	0.0247	N/A	N/A	2.43	N/A	0.597	N/A
	A1	13.1	0.6	0.0241	2.4	1.43	2.42	0.5	0.591	1.1
	A2	13.1	0.4	0.0242	2.0	2.02	2.42	0.4	0.591	1.0
	A3	13.1	0.2	0.0243	1.6	3.37	2.42	0.2	0.592	0.9
	B1	13.1	0.4	0.0244	1.2	1.38	2.42	0.3	0.591	1.1
	B2	13.1	0.3	0.0244	1.1	1.94	2.42	0.2	0.591	1.0
	B3	13.1	0.2	0.0244	1.1	3.25	2.42	0.1	0.592	1.0
	C1	13.1	0.2	0.0245	0.9	1.38	2.42	0.2	0.591	1.1
	C2	13.1	0.1	0.0244	0.9	1.95	2.43	0.1	0.591	1.0
	C3	13.1	0.1	0.0244	1.0	3.25	2.43	0.1	0.591	1.0
Floor 5	BL	16.2	N/A	N/A	N/A	N/A	2.97	N/A	0.579	N/A
	BLst	16.1	N/A	0.0290	N/A	N/A	2.94	N/A	0.579	N/A
	A1	16.0	0.4	0.0284	2.0	1.70	2.93	0.3	0.584	-0.9
	A2	16.0	0.3	0.0285	1.8	2.39	2.94	0.2	0.584	-0.9
	A3	16.0	0.2	0.0286	1.5	3.99	2.94	0.1	0.585	-0.9
	B1	16.0	0.3	0.0287	1.1	1.65	2.94	0.2	0.583	-0.6
	B2	16.0	0.2	0.0287	1.1	2.33	2.94	0.1	0.583	-0.6
	B3	16.0	0.1	0.0287	1.1	3.90	2.94	0.1	0.583	-0.6
	C1	16.0	0.1	0.0288	0.9	1.66	2.94	0.1	0.582	-0.4
	C2	16.0	0.1	0.0288	0.9	2.34	2.94	0.1	0.582	-0.4
	C3	16.1	0.1	0.0287	1.0	3.90	2.94	0.0	0.582	-0.4

Floor 3	**BL**	18.5	N/A	N/A	N/A	N/A	3.26	N/A	0.633	N/A
	BLst	18.3	N/A	0.0335	N/A	N/A	3.23	N/A	0.633	N/A
	A1	18.3	0.0	0.0329	1.5	1.96	3.23	0.0	0.632	0.1
	A2	18.3	0.0	0.0330	1.4	2.76	3.23	0.0	0.632	0.0
	A3	18.3	0.0	0.0330	1.2	4.60	3.24	0.1	0.633	0.0
	B1	18.3	0.0	0.0332	0.8	1.91	3.23	0.0	0.631	0.2
	B2	18.3	0.0	0.0332	0.9	2.68	3.23	0.0	0.631	0.2
	B3	18.3	0.0	0.0331	0.9	4.47	3.24	0.0	0.632	0.1
	C1	18.3	0.0	0.0332	0.8	1.91	3.23	0.0	0.631	0.3
	C2	18.3	0.0	0.0332	0.9	2.68	3.23	0.0	0.631	0.2
	C3	18.3	0.0	0.0331	0.9	4.47	3.23	0.0	0.631	0.2
Floor 1	**BL**	15.9	N/A	N/A	N/A	N/A	2.27	N/A	0.774	N/A
	BLst	16.0	N/A	0.0341	N/A	N/A	2.29	N/A	0.774	N/A
	A1	16.0	0.2	0.0336	1.5	2.01	2.29	0.2	0.777	-0.5
	A2	16.0	0.1	0.0337	1.4	2.83	2.29	0.2	0.778	-0.5
	A3	16.0	0.0	0.0337	1.3	4.70	2.29	0.2	0.778	-0.6
	B1	16.0	0.1	0.0338	0.8	1.67	2.29	0.1	0.777	-0.5
	B2	16.0	0.1	0.0338	0.9	2.35	2.29	0.1	0.778	-0.5
	B3	16.0	0.1	0.0338	1.0	3.92	2.29	0.2	0.778	-0.5
	C1	16.0	0.1	0.0338	0.8	1.67	2.29	0.1	0.778	-0.5
	C2	16.0	0.0	0.0338	0.9	2.35	2.29	0.1	0.778	-0.5
	C3	16.0	0.0	0.0338	1.0	3.92	2.29	0.1	0.778	-0.5

Table 4-8. Nine Story SLE1 BF Average Maximum Element Response

		BRB Disp		**ST Rotation**		**FD Disp**	**Story Drift**		**Story Accl**	
		Ratio	**% Change**	**rad**	**% Change**	**Ratio**	**% Drift**	**% Change**	**g**	**% Change**
Floor 9	**BL**	4.53	N/A	N/A	N/A	N/A	0.93	N/A	0.359	N/A
	BLst	4.58	N/A	0.0076	N/A	N/A	0.91	N/A	0.358	N/A
	A1	4.56	0.5	0.0074	2.3	0.40	0.90	0.9	0.359	-0.3
	C1	4.57	0.2	0.0076	0.0	0.31	0.91	0.3	0.359	-0.1
	A3	4.55	0.7	0.0074	2.2	0.92	0.90	0.8	0.359	-0.1
Floor 7	**BL**	5.74	N/A	N/A	N/A	N/A	1.21	N/A	0.420	N/A
	BLst	5.55	N/A	0.0119	N/A	N/A	1.17	N/A	0.422	N/A
	A1	5.47	1.3	0.0116	2.6	0.69	1.16	1.2	0.421	0.4
	C1	5.53	0.4	0.0118	0.7	0.66	1.17	0.4	0.422	0.1
	A3	5.49	1.0	0.0117	2.1	1.62	1.16	0.9	0.421	0.3

Floor 5	**BL**	6.25	N/A	N/A	N/A	N/A	1.25	N/A	0.421	N/A
	BLst	6.19	N/A	0.0129	N/A	N/A	1.23	N/A	0.419	N/A
	A1	6.18	0.2	0.0126	2.2	0.75	1.23	0.1	0.418	0.1
	C1	6.19	0.1	0.0128	0.6	0.72	1.23	0.0	0.419	0.0
	A3	6.17	0.2	0.0126	1.9	1.75	1.23	0.1	0.418	0.1
Floor 3	**BL**	6.59	N/A	N/A	N/A	N/A	1.24	N/A	0.420	N/A
	BLst	6.58	N/A	0.0129	N/A	N/A	1.24	N/A	0.421	N/A
	A1	6.58	0.1	0.0127	1.8	0.76	1.24	0.0	0.421	0.0
	C1	6.58	0.0	0.0129	0.5	0.73	1.24	0.0	0.421	0.0
	A3	6.60	-0.2	0.0128	1.3	1.77	1.24	0.2	0.421	0.0
Floor 1	**BL**	6.05	N/A	N/A	N/A	N/A	0.86	N/A	0.443	N/A
	BLst	6.11	N/A	0.0130	N/A	N/A	0.87	N/A	0.440	N/A
	A1	6.14	-0.3	0.0127	1.8	0.76	0.87	0.4	0.438	0.3
	C1	6.12	-0.1	0.0129	0.6	0.63	0.87	0.1	0.439	0.1
	A3	6.14	-0.4	0.0128	1.3	1.79	0.87	0.4	0.438	0.3

The addition of LSFF damping to these structures had minimal effects on response despite changing ground motion scaling and friction device properties. The responses of the friction device variations showed little difference. Though, the A1 models consistently exhibited the best performance. The three kip slip force devices performed better in several cases where the seven kip devices were not activated. The layout of the devices within the structure had a larger influence on response than the slip force.

The inclusion of shear tab elements had a greater effect on response than the addition of friction dampers. The shear tab elements generally remained elastic. Considering this and the influence of LSFF devices that were not activated, changes in response were largely caused by the added stiffness to the gravity frame. However, early phase energy dissipation did reduce deformations further. This is evident in service level cases where models with activated dampers performed better than those without.

The LSFF damping's influence on response was not as significant as expected. Each friction device variation showed only marginal improvements in response at every ground motion level. At the MCE and DBE levels, the LFRS dissipates a much larger amount of energy relative to the

provided LSFF damping. The minimal impact of these devices at the service level events is more surprising. It may be that the friction dampers do not provide sufficient energy dissipation to impact seismic response. It is possible that the friction device and shear tab link elements in the SAP2000 model do not accurately represent the behavior of the LSFF connections. The modeled behavior in SAP2000 is an approximation of the connection, and laboratory testing of the connection has been planned to validate the models. Test results may provide a more accurate connection behavior that could have a greater impact on response.

4.4 Summary

The effects of LSFF damping were assessed by comparing different deformation responses of 22 three dimensional SAP2000 models subjected to suites of ground motions. The friction devices reduced story drifts and plastic deformation of the inelastic elements in the models. However, these improvements were typically minor in the range of 0 to 4% difference from models without LSFF devices. In several cases, comparable improvements were observed in models with LSFF devices that did not activate during the ground motions. The difference between models with and those without shear tab elements, which rarely suffered inelastic deformation, showed the largest differences in response. This was due to the additional stiffness in the gravity frame connections. The early phase energy dissipation of the LSFF dampers produced marginal reductions in inelastic deformations for a variety of earthquake hazard levels.

Chapter 5. Conclusions

5.1 Summary

The purpose of this research was to explore the effects of early phase energy dissipation provided by low slip force friction damping for seismic applications in steel structures. This begins with a literature review exploring the behavior and applications of friction damping. Variations of slotted bolted friction dampers were reviewed along with schematics of different damper installations. The results of cyclic testing of such devices and the performance of different friction materials were presented.

A segment details the mathematical models created for this research. A three and a nine story structure were designed and modeled in the SAP2000 structural analysis software. Each model included a buckling restrained brace frame and a special moment frame as the two orthogonal LFRSs. Multi-linear plastic elements were incorporated into the three dimensional models to capture the inelastic deformations and hystereses of various structural components. Various friction device elements were added to create an array of structural models for a parametric study. These models were then subjected to a suite of eleven time history analyses. These analyses used ground motion records scaled to different seismic hazard levels representing the maximum considered earthquake, the design basis earthquake, and two smaller service level earthquakes.

A section is provided to outline and explain the parametric study. Following this, the response of the various SAP2000 models are presented and discussed. This analysis of results includes graphs comparing the global response of the structures and tables showing the difference in response of

specific elements within the models. These comparisons are made to identify the effects of low slip force friction damping at various levels of seismic activity.

5.2 Conclusions

The LSFF connection successfully dissipated energy. Shear tab elements deformed, but rarely yielded. The friction devices activated during the ground motions. In general, the LSFF devices improved the response of the global structure and specific elements within the structure. The friction damping reduced story drifts and plastic deformation of LFRS elements. Overall, the addition of LSFF damping had only marginally beneficial effects regardless of friction device properties, distribution, or the level of seismic hazard.

The greatest benefit of the friction damping was seen in the LFRS elements. In the three story models, the plastic rotation of the special moment frame hinges and the axial deformation of buckling restrained braces were reduced as much as 4% from the shear tab model without friction dampers. These results were somewhat better at the service level ground motions. The drawback of the LSFF damping was a minuscule increase in acceleration.

The variables changed in the parametric study produced little difference in the effects of the connections. The seven kip slip force devices exhibited the best performance and greatest energy dissipation. An exception to this was in some service level earthquakes were the seven kip devices were not activated. In these situations, the three kip force devices, which did activate, produced a greater reduction in deformations. The number of devices had greater influence on response than the slip force.

The addition of shear tab elements, which generally remained elastic, had the most pronounced effect on the structural response. The additional stiffness added by the shear tab and friction device elements had a greater impact than the energy dissipation of the friction devices.

The underperformance of the LSFF connection may be due to insufficient energy dissipation of the friction dampers. Dampers with a higher slip force may provide more energy dissipation if activate, but the seven kip slip force dampers were not always activated even at MCE levels.

The results of this research revealed the importance of accurately modeling the lateral contributions of the gravity frame system. However, the early phase energy dissipation provided by LSFF damping did not affect response as significantly as anticipated. These findings should not discourage the possible benefits of early phase energy dissipation nor asymmetrical friction damping. The following section proposes further research in these areas that could produce structures with greater seismic resilience.

5.3 Recommendations for Future Work

The underwhelming performance of the LSFF connection raises questions for further research. Early phase energy dissipation and asymmetrical friction devices at beam-column connections are concepts meriting investigative consideration. The development of the LSFF connection behavior in the mathematical models of this research relied on many assumptions. The following recommendations for future work are proposed to lessen these uncertainties and utilize the concepts of this research to develop structural systems with greater seismic resilience.

A major finding of this research is the impact the gravity framing system has on seismic response. The specific behavioral models used for the shear tab connections in this research may not accurately depict the cyclic deformations occurring throughout an earthquake. Future empirical testing would verify uncertainties in the hysteretic behavior. It is possible that a single rotational element will not be sufficient to capture behaviors like cracking of the concrete slab and other inelasticities that result from lateral movement of the gravity frame. Accurately depicting the lateral contribution of the gravity frame, typically ignored in steel LFRSs, is important and requires

further examination. More laboratory testing and extensive computer modeling are needed to develop standards for including the lateral impacts of the gravity frame system.

The LSFF connection behavior modeled in this research approximated the connections function taken from literature on shear tab connections and slotted bolted friction dampers. The combination of these elements in the connection may not function as assumed. The elastic stiffness and hysteretic behavior of the LSFF connection should be verified with empirical tests. Laboratory testing of the connection is currently planned at Auburn University. This experimentation should provide a more accurate behavioral model for the LSFF connection.

Early phase energy dissipation is a beneficial addition to a lateral system. Applications of early phase energy dissipative elements should be explored further. Adding these elements to conventional LFRSs to create multi-phase energy dissipation is a promising concept. Though the results of this research did not yield substantial improvements to seismic response, they can hopefully provide some benefit to future research in these areas and improve the safety of engineered structures.

References

AISC. (2011). *Steel Construction Manual.* Chicago, IL: American Institute of Steel Construction, Inc.

ANSI/AISC. (2010). *Seismic Provisions for Structural Steel Buildings.* Chicago, IL: American Institute of Steel Construction, Inc.

ANSI/AISC. (2010). *Specification for Structural Steel Buildings.* Chicago, IL: American Institute of Steel Construction, Inc.

Applied Technology Council. (2009). *Quantification of Building Seismic Performance Factors (FEMA P695).* Washington, D.C.: Federal Emergency Management Agency.

Applied Technology Council. (2012). *Seismic Performance Assessment of Buildings Volume 1 - Methodology.* Washington, D.C.: Federal Emergency Management Agency.

Applied Technology Council. (2012). *Seismic Performance Assessment of Buildings Volume 3 - Performance Assessment Calculation Tool (PACT).* Washington, D.C.: Federal Emergency Management Agency.

ASCE/SEI. (2010). *Minimum Design Loads for Buildings and Other Structures: ASCE Standard 7-10.* Reston, VA: ASCE Publications.

Astaneh-Asl, A., Liu, J., & McMullin, K. M. (2002). Behavior and Design of Single Plate Shear Connections. *Journal of Constructional Steel Research*, 1121-1141.

Balendra, T., Yu, C., & Lee, F. L. (2001). An Economical Structural System for Wind and Earthquake Loads. *Engineering Structures, 23*(5), 491-501.

Bertero, R. D., & Bertero, V. V. (2002). Performance-based seismic engineering: the need for a reliable. *Earthquake engineering and structural dynamics, 31*, 627-652. doi:10.1002/eqe.146

Bhavikatti, S. S., & Rajashekarappa, K. G. (1998). *Engineering Mechanics.* New Delhi: New Age International.

Calado, L., Proenca, J. M., Panao, A., Nsieri, E., Rutenbrg, A., & Levy, R. (2007). *Prohitech WP5, Innovative Materials and Techniques, Buckling-Restrained Braces.*

Charney, F. A., & Marshall, J. D. (2006). A Comparison of the Krawinkler and Scissors Models for Including Beam-Column Joint Deformations in the Analysis of Moment-Resisting Steel Frames. *Engineering Journal*, 31-48.

Computers & Structures, Inc. (2014). *CSI Analysis Reference Manual (For SAP2000, ETABS, SAFE, and CSiBridge).* Berkeley, California: Computers & Structures, Inc.

Crocker , J. P., & Chambers, J. J. (2004). Single Plate Shear Connection Response to Rotation Demands Imposed by Frames Undergoing Cyclic Lateral Displacements. *Journal of Structural Engineering*, 934-941.

Erochko, J. A. (2013). *Improvements to the Design and Use of Post-Tensioned Self-Centering Energy-Dissipative (SCED) Braces.* Toronto, Canada: University of Toronto.

FEMA. (2000 a). *FEMA 355-C State of the Art Report on Systems Performance of Steel Moment Frames Subjected to Earthquake Ground Shaking.* Washington, DC.

FEMA. (2000 b). *FEMA 356 Prestandard and Commentary for the Seismic Rehabilitation of Buildings.* Washington, DC.

FEMA. (2003). *FEMA 450 NEHRP Recommended Seismic Provisions for Seismic Regulations for New Buildings and Other Strucutres.* Washington D.C.: Federal Emergency Management Agency.

Ghobarah, A. (2001). Performance-based Design in Earthquake Engineering: State of Development. *Engineering Structures*(23), 878-884.

Golondrino, J. C., MacRae, G. A., Chase, J. G., Rodgers, G. W., Clifton, C. G., & . (2012). Behavior of Asymmetrical Friction Connections Using Different Shim Materials. *New Zealand Society for Earthquake Engineering.* Christchurch, New Zealand.

Golondrino, J. C., MacRae, G. A., Chase, J. G., Rodgers, G. W., Clifton, G. C., & . (2013). Application of Brake Pads on Asymmetrical Friction Connection (AFC). *New Zealand Society for Earthquake Engineering.* Wellington, New Zealand.

Grigorian, C. E., & Popov, E. P. (1994). *Energy Dissipation with Slotted Bolted Connections (Report UCB/EERC-94/02).* Berkeley, CA: Earthquake Engieering Research Center.

Khoo, H.-H., Clifton, C., Butterworth, J., MacRae, G., Ferguson, G., & . (2012). Influence of Steel Shim Hardness on the Sliding Hinge Joint Performance. *Journal of Construction Steel Research*, 119-129.

Liu, J., & Astaneh-Asl, A. (2000). *Cyclic Tests on Simple Connections Including Effects of the Slab.* Sacramento.

McCormick, J., Aburano, H., Ikenaga, M., Nakashima, M., , , ... (2008). Permissible Residual Deformation Levels for Building Structures Considering Both Safety and Human Elements. *World Conference on Earthquake Engineering.* Beijing, China.

Miranda, E., & Aslani, H. (2003). *Probabilistic Response Assessment for Building Specific Loss Estimation (PEER Report 2003/03).* Berkeley, CA: Pacific Earthquake Engineering Research Center.

Naeim, F. (2001). *The Seismic Design Handbook.* New York, NY: Springer.

NEESTIPS. (2009). *Network for Earthquake Engineering Simulation (NEES): Tools for isolation and protective systems (TIPS).* Retrieved from http://www.neng.usu.edu/cee/faculty/kryan/NEESTIPS/PBEE_study.html

Sabelli, R. (2001). *The 2000 NEHRP Professional Fellowship Report: Research on Improving the Design and Analysis of Earthquake-Resistant Steel-Braced Frames.* Washington D.C.: Federal Emergency Management Agency of the U.S. Department of Homeland Security.

Sabelli, R., Mahin, S., & Chang, C. (2009). Seismic Demands on Steel Braced Frame Buildings with Buckling Restrained Braces. *Engineering Structures, 25*, 655-66.

Appendix A. Gap Damper Design Drawings

Appendix A presents the results not included in Section 4.3. The new data provided includes graphs displaying story accelerations and tables listing force values and data for all of the stories of the nine story models.

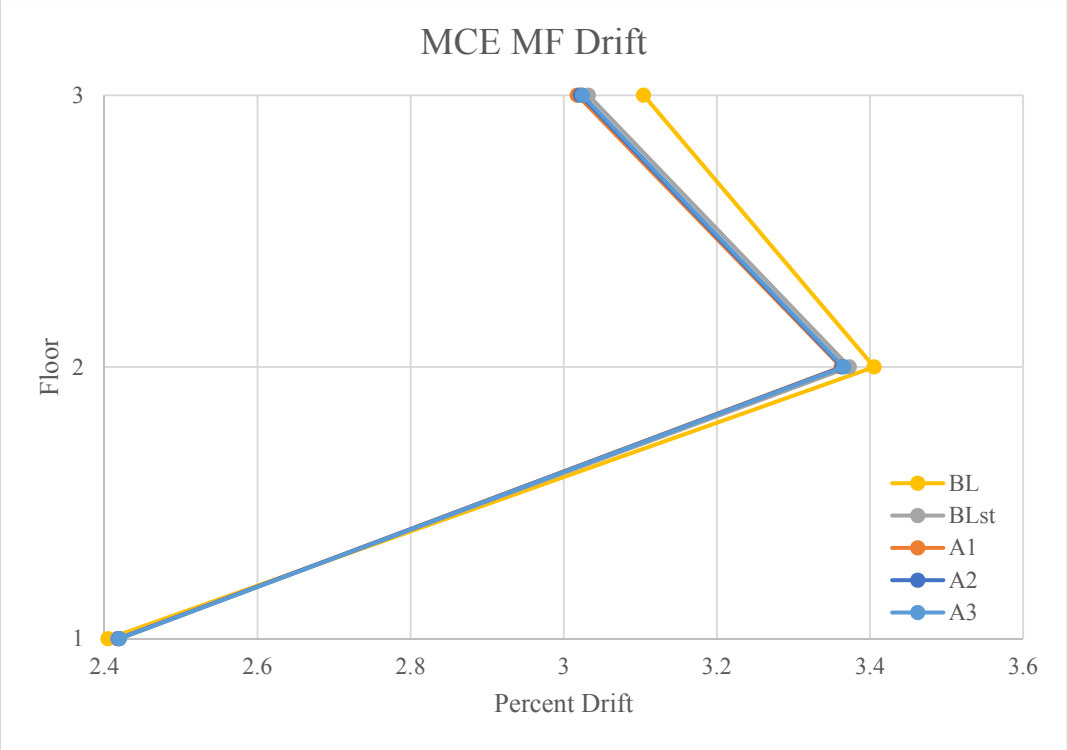

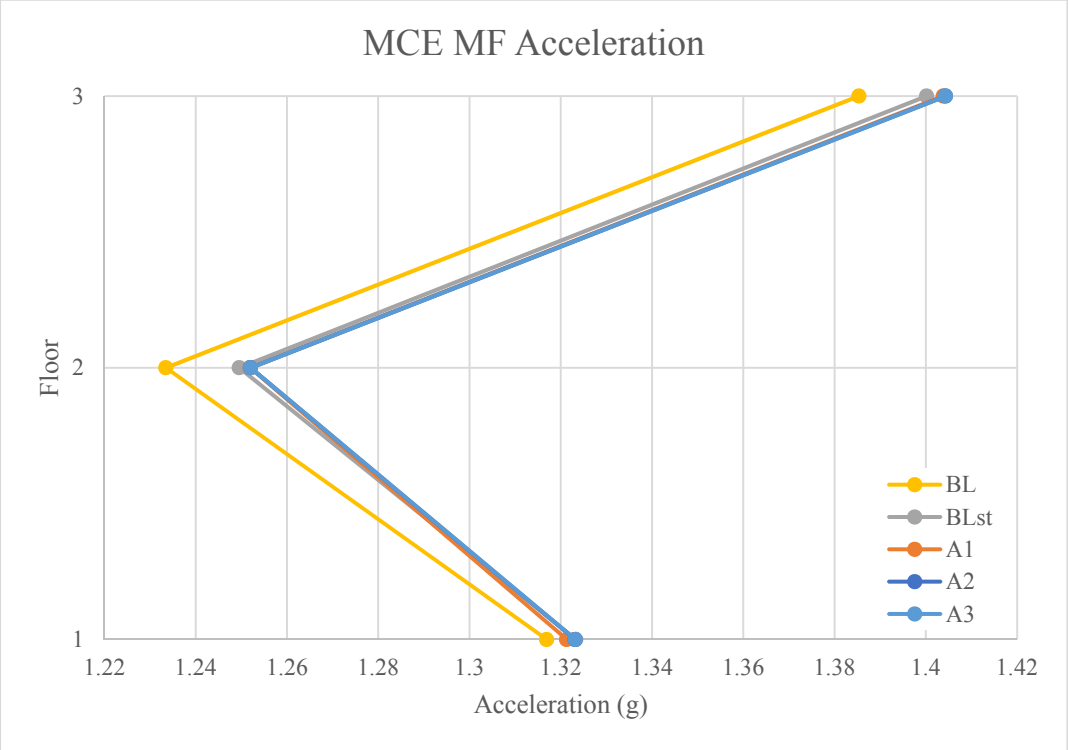

Figure A-1. Three Story MCE MF Average Maximum Global Response (A Layout)

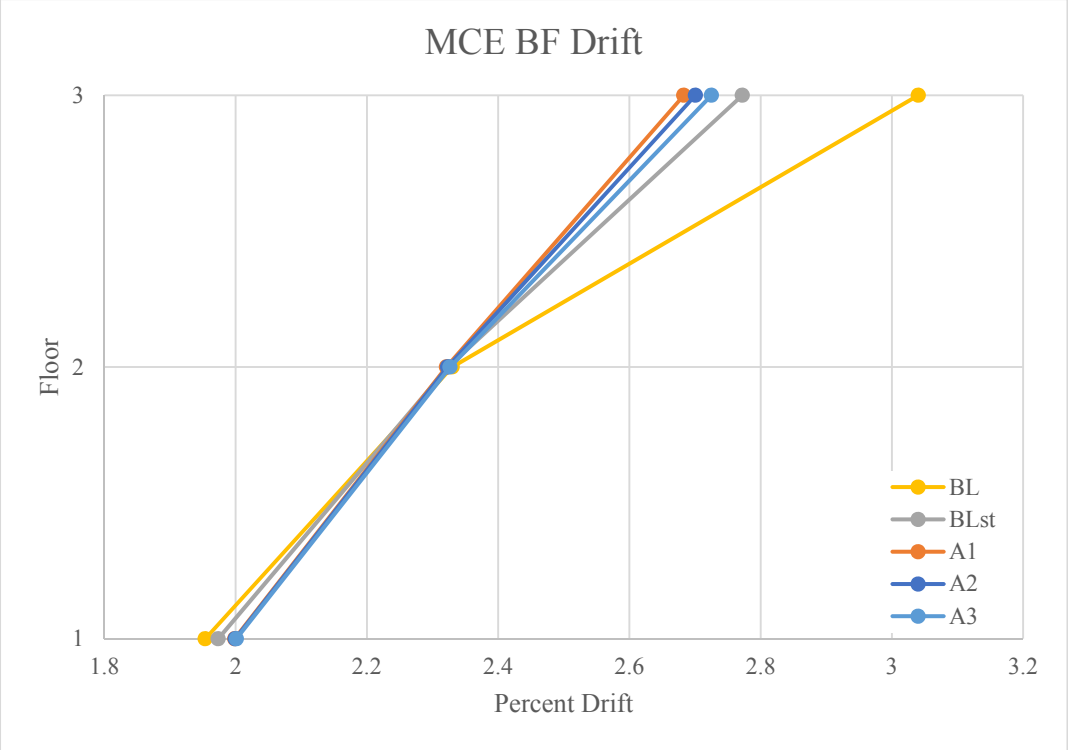

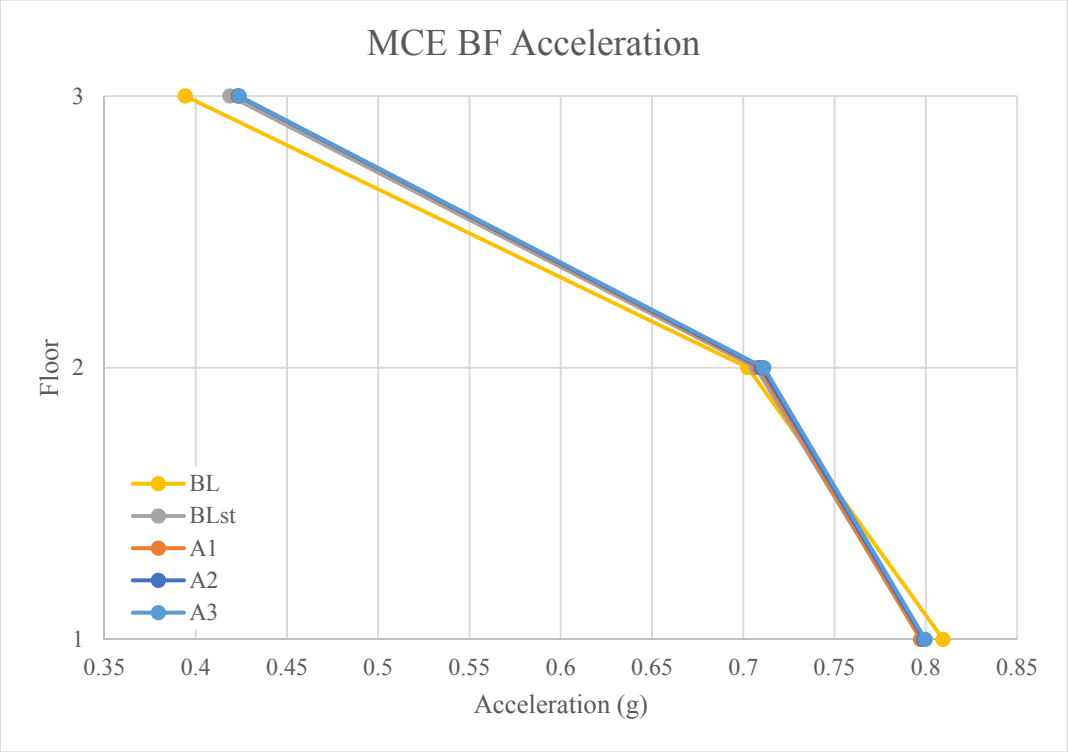

Figure A-2. Three Story MCE BF Average Maximum Global Response (A Layout)

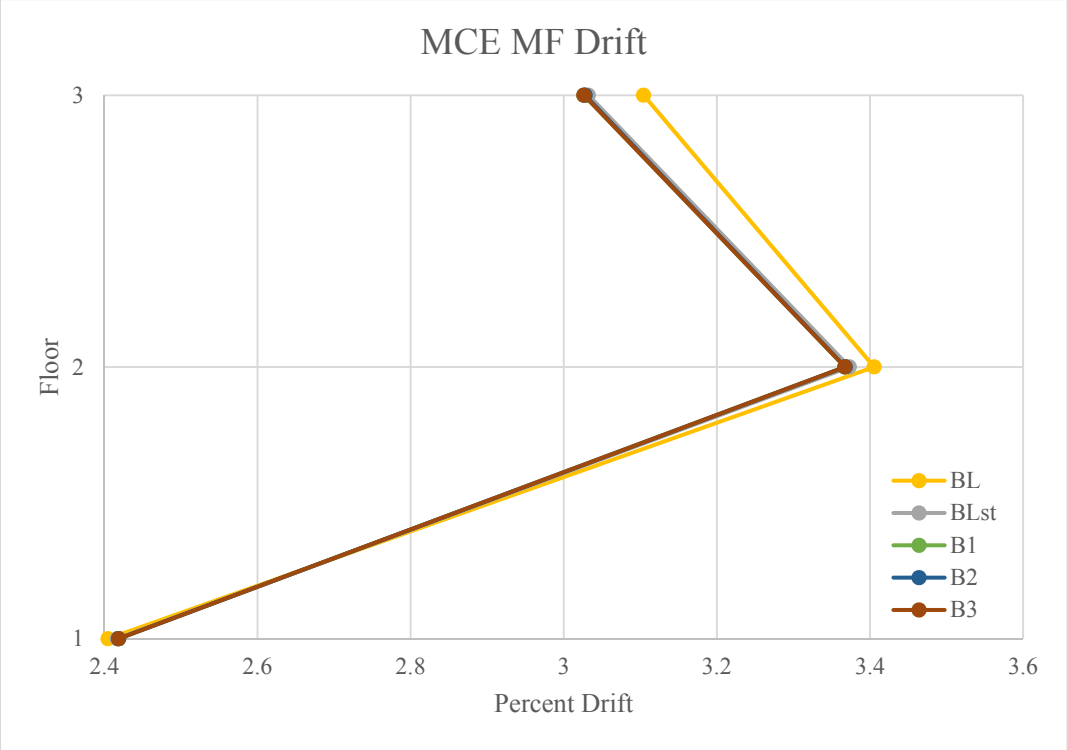

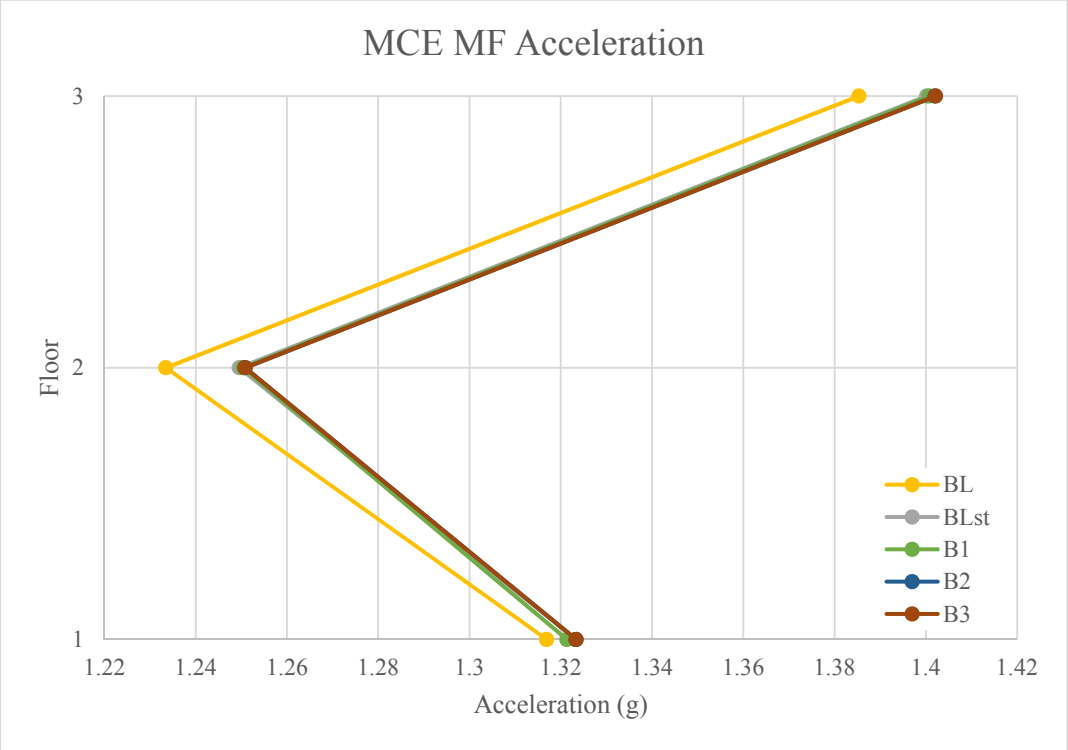

Figure A-3. Three Story MCE MF Average Maximum Global Response (B Layout)

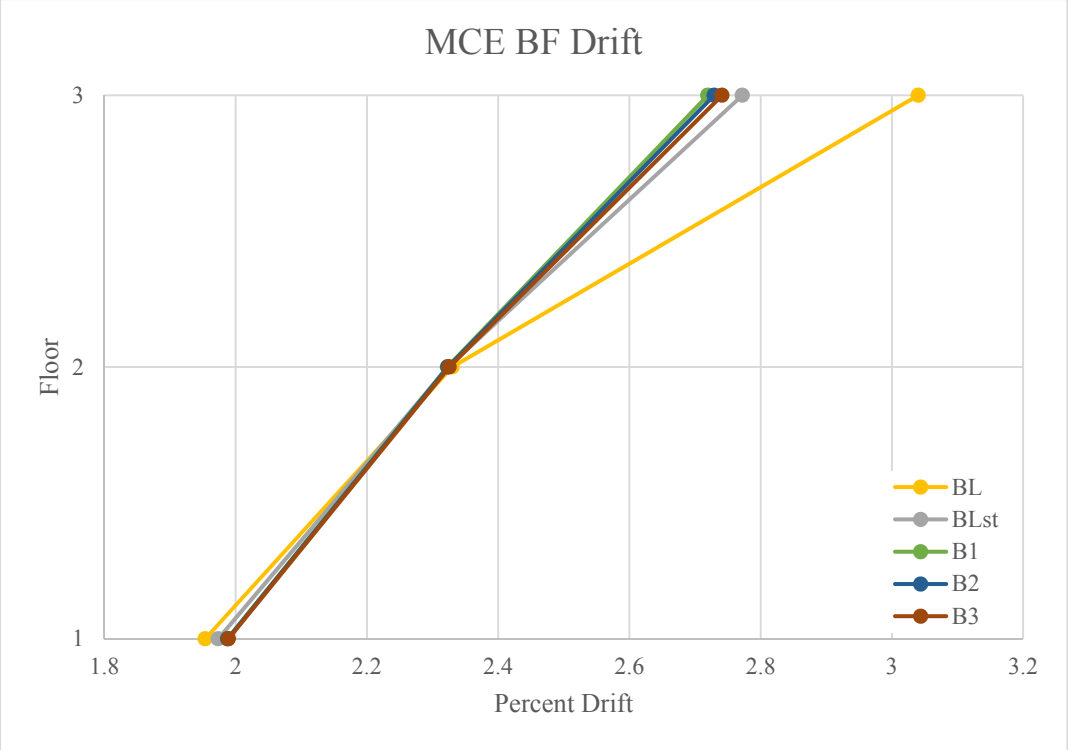

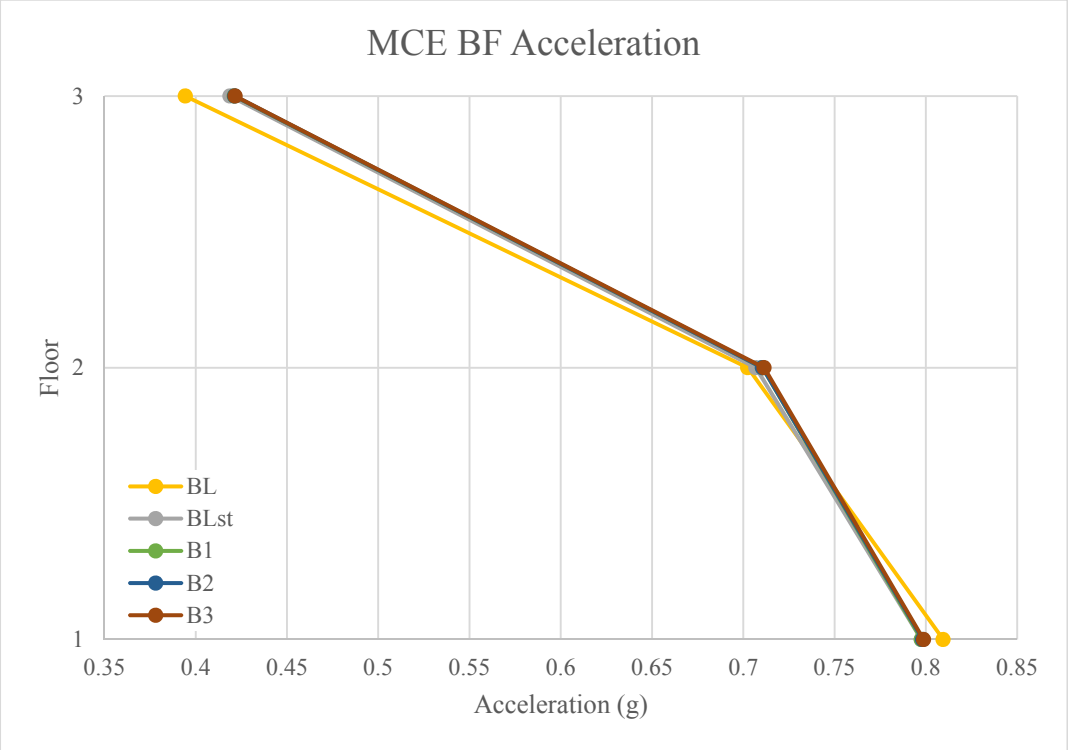

Figure A-4. Three Story MCE BF Average Maximum Global Response (B Layout)

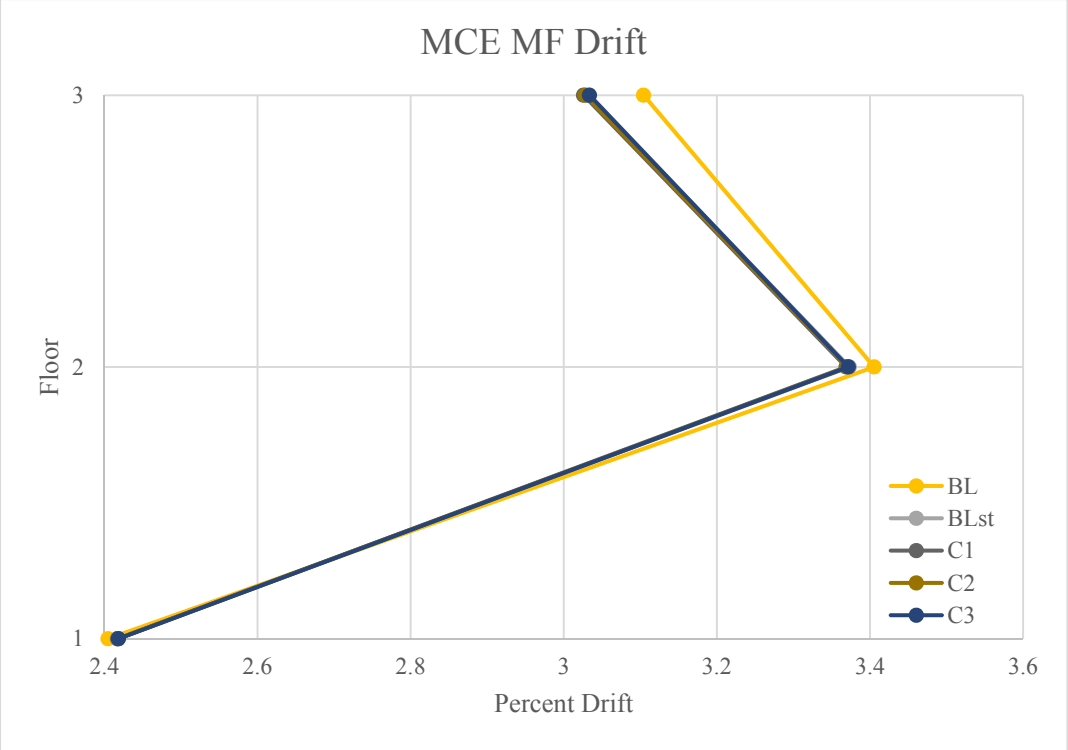

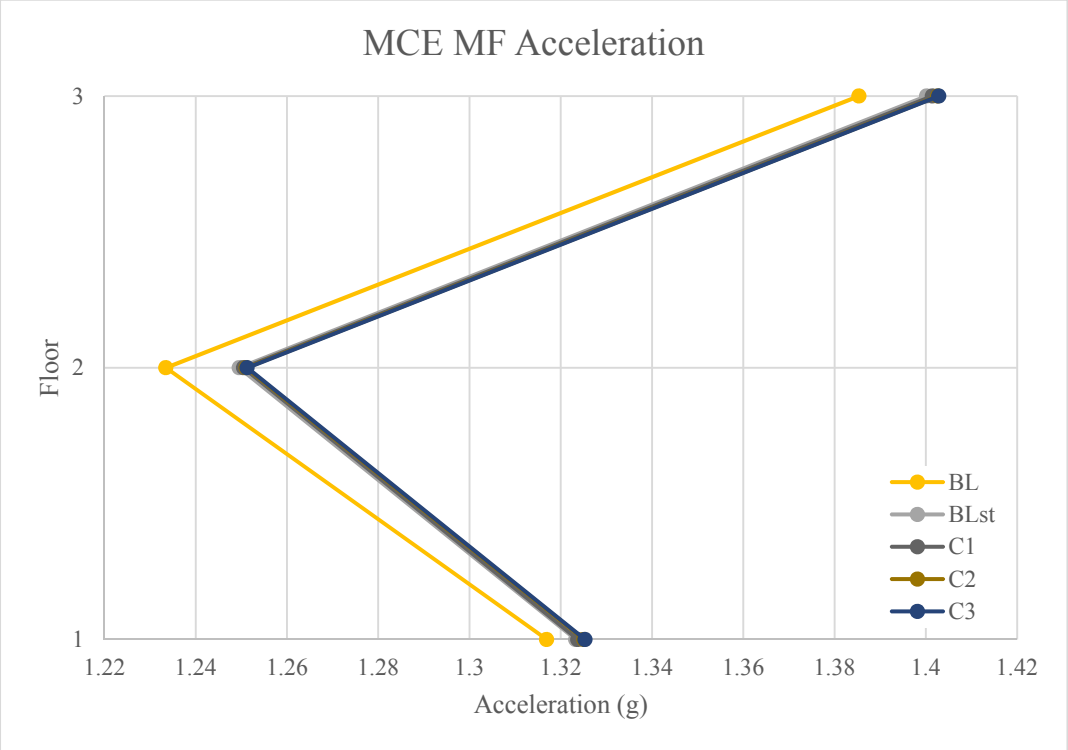

Figure A-5. Three Story MCE MF Average Maximum Global Response (C Layout)

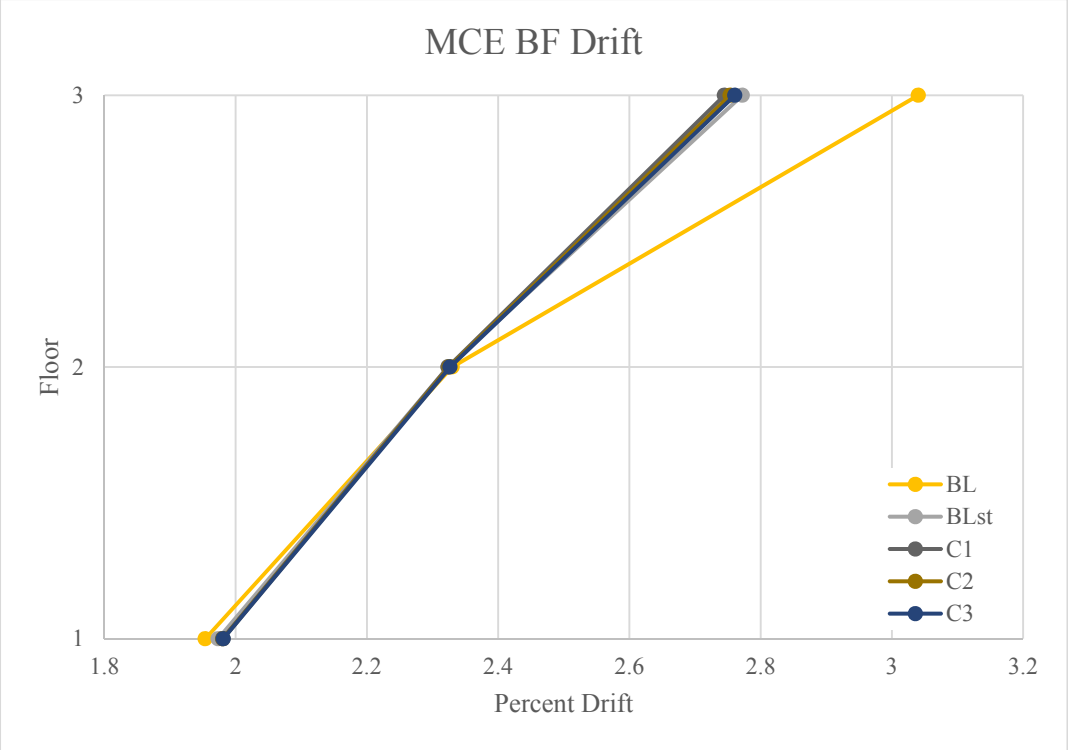

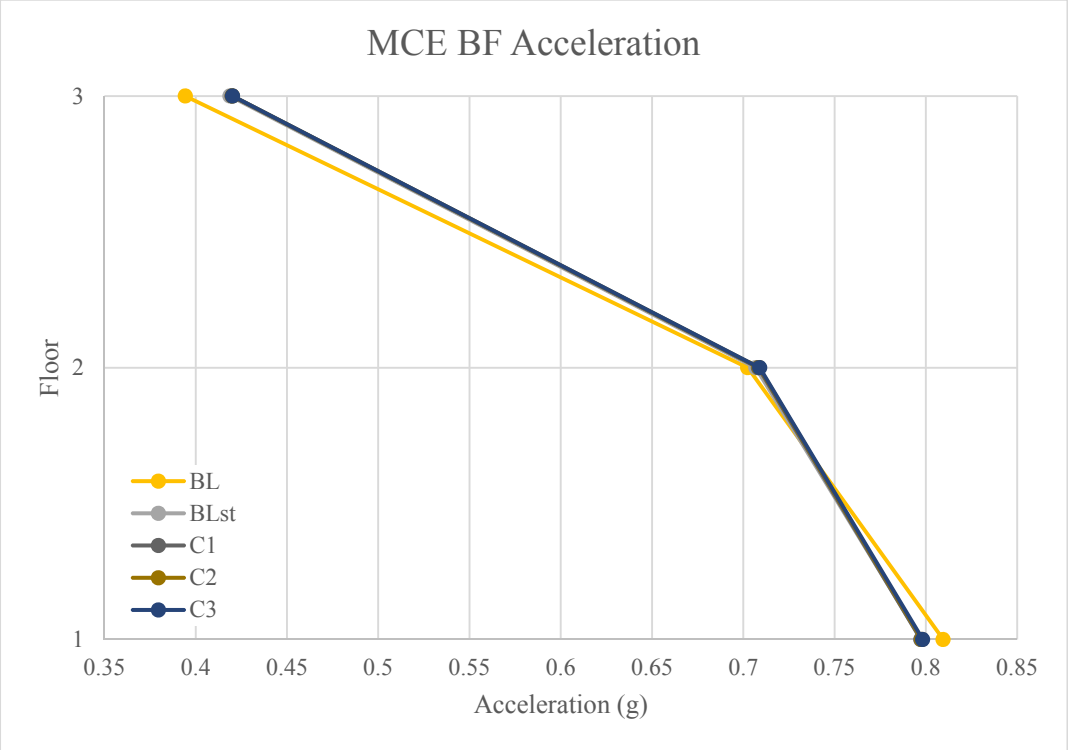

Figure A-6. Three Story MCE BF Average Maximum Global Response (C Layout)

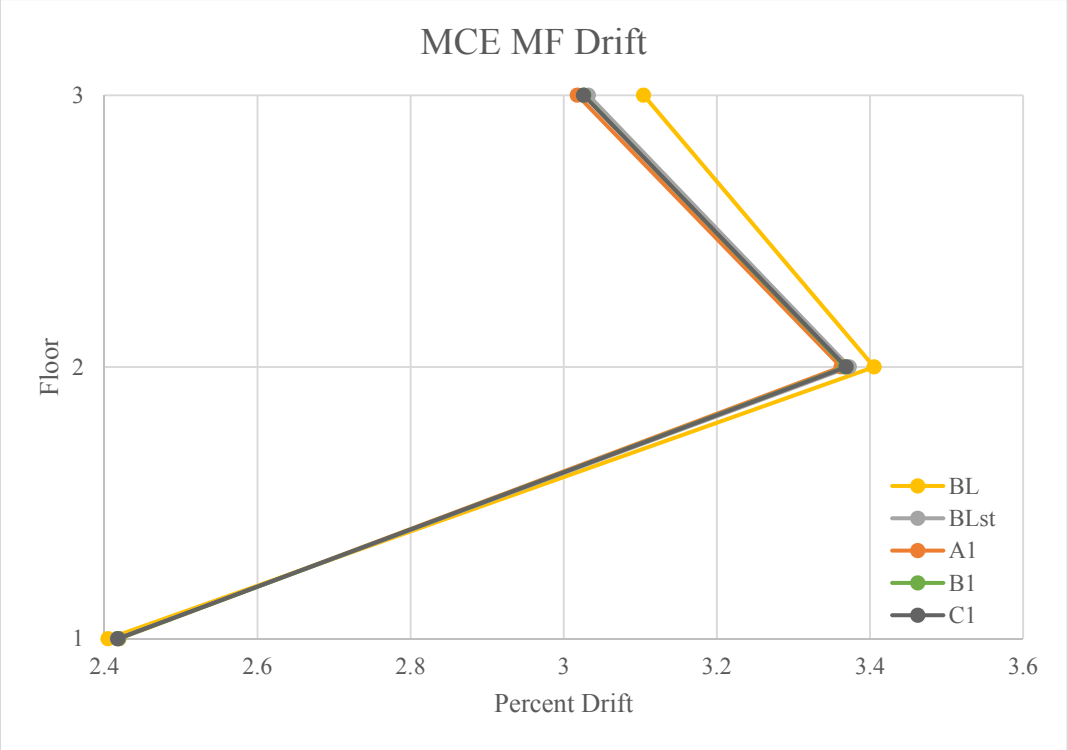

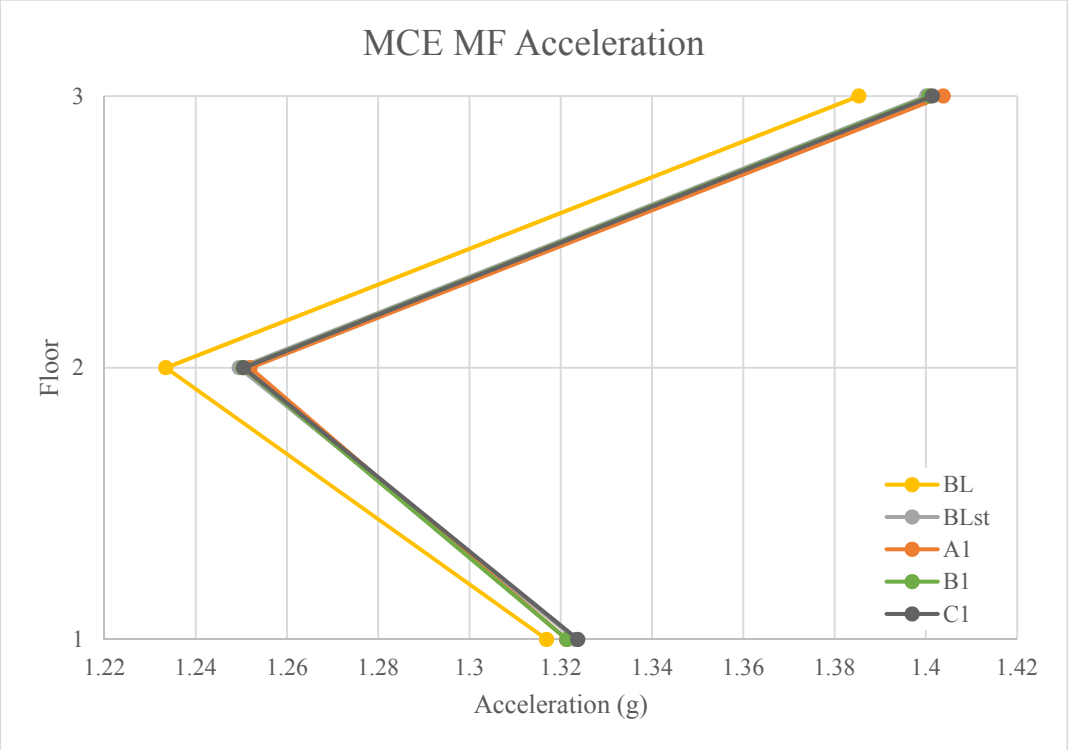

Figure A-7. Three Story MCE MF Average Maximum Global Response (7 kip Slip Force)

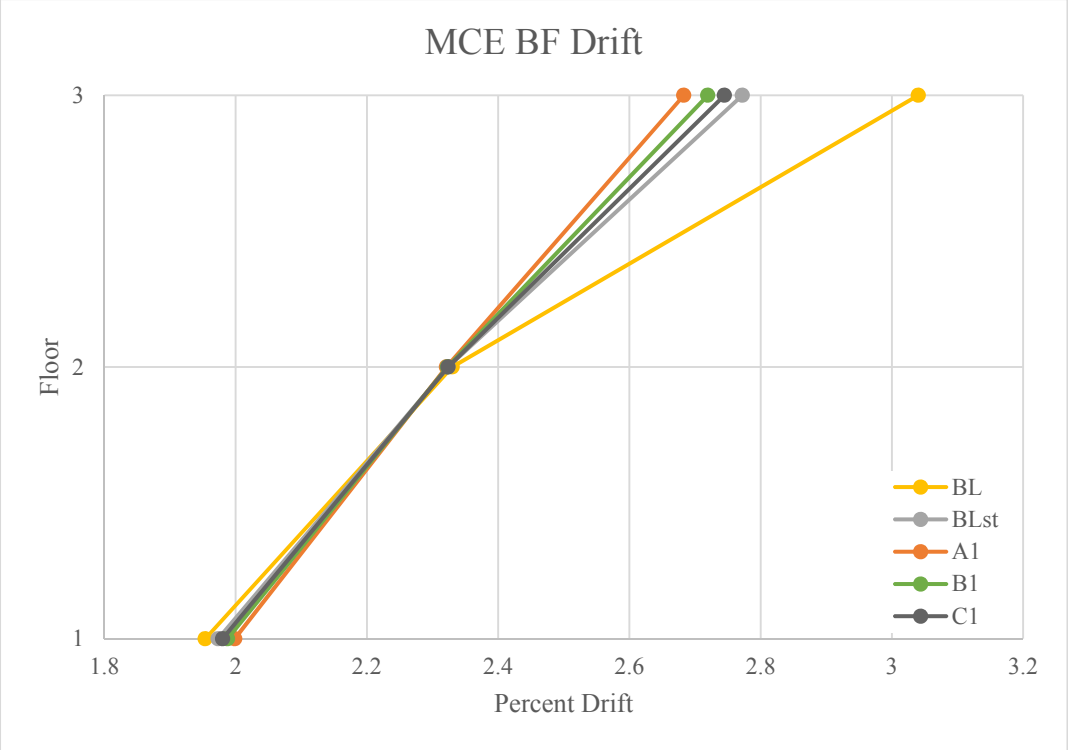

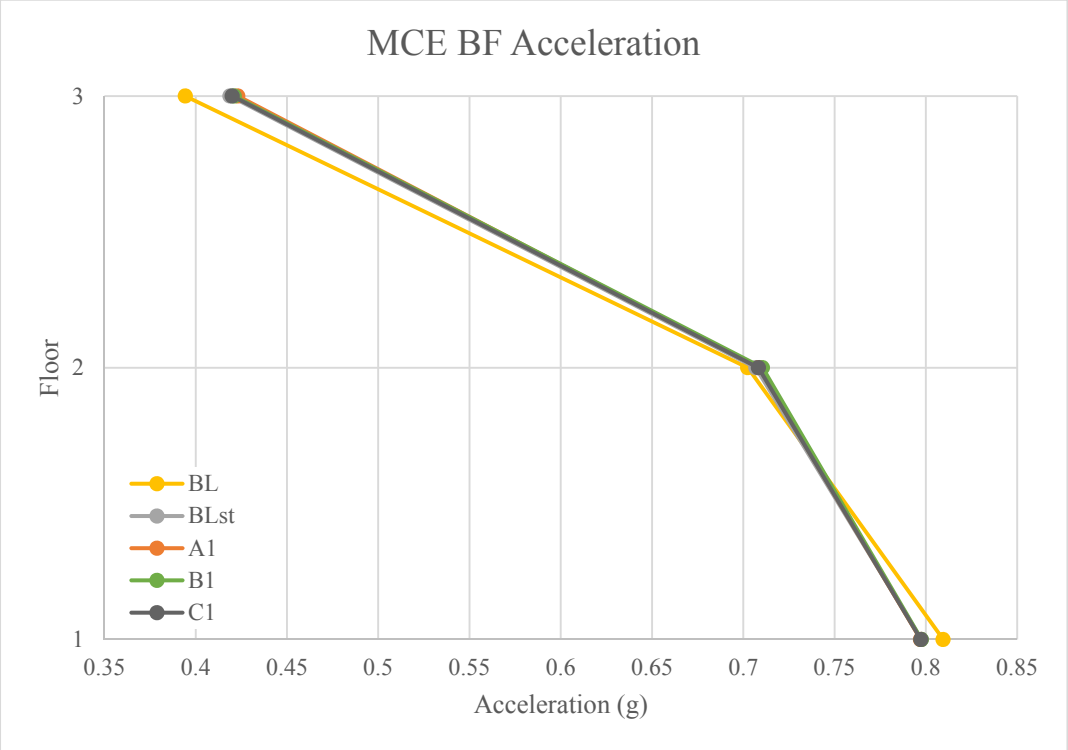

Figure A-8. Three Story MCE BF Average Maximum Global Response (7 kip Slip Force)

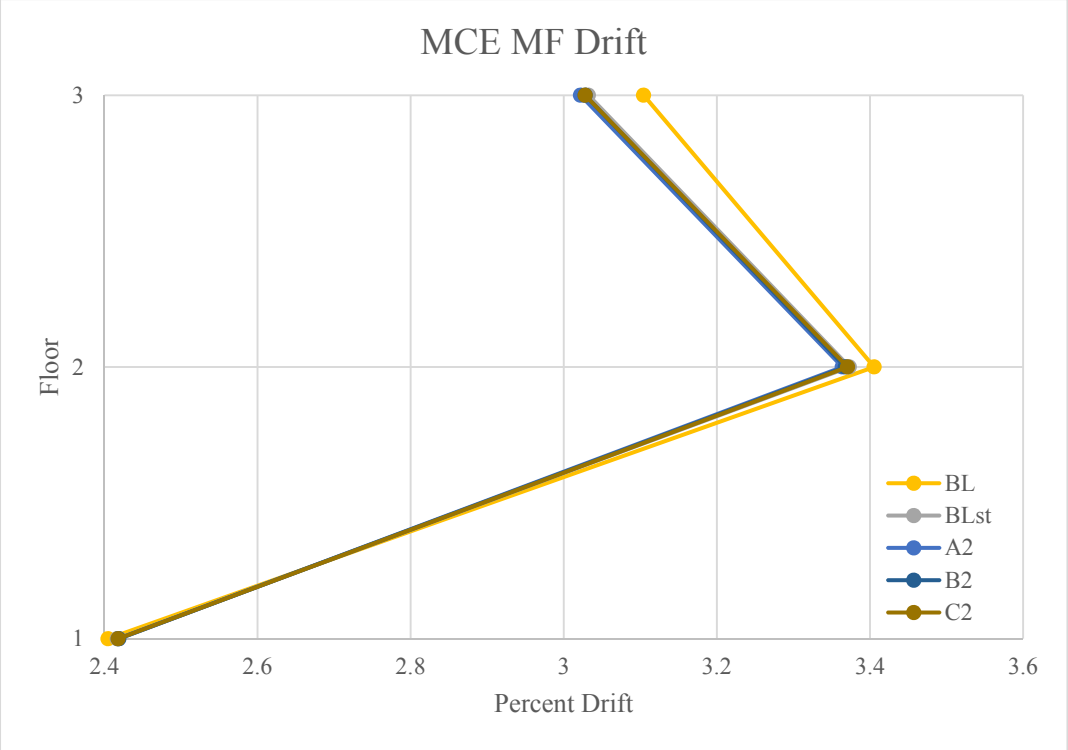

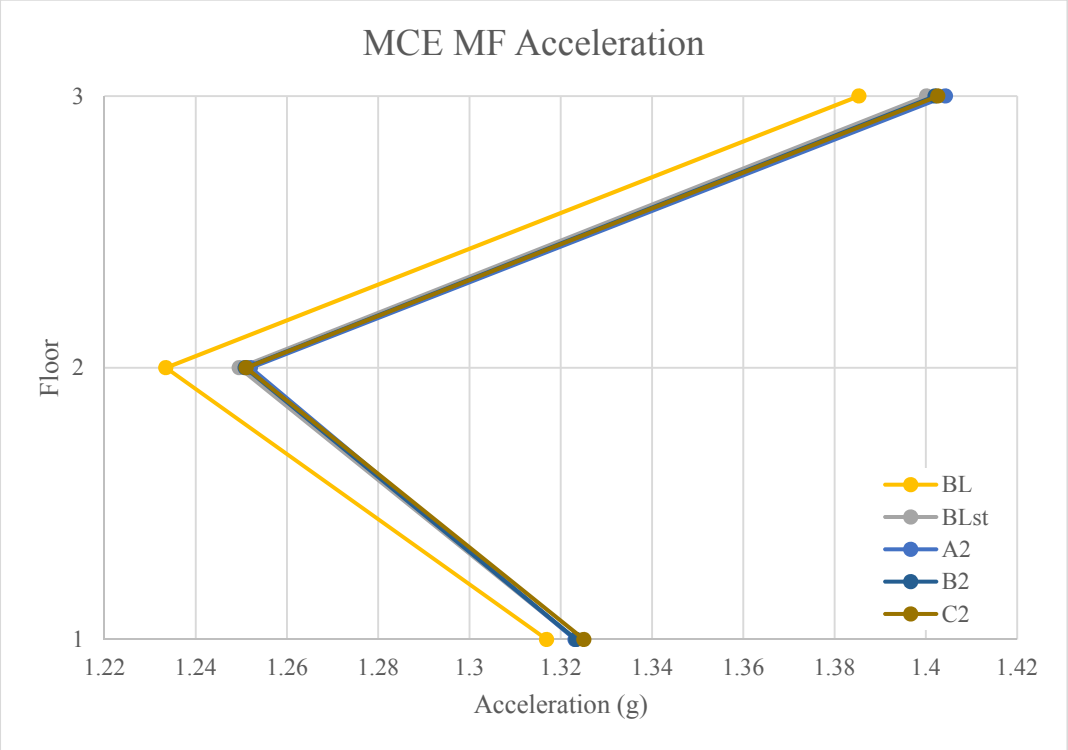

Figure A-9. Three Story MCE MF Average Maximum Global Response (5 kip Slip Force)

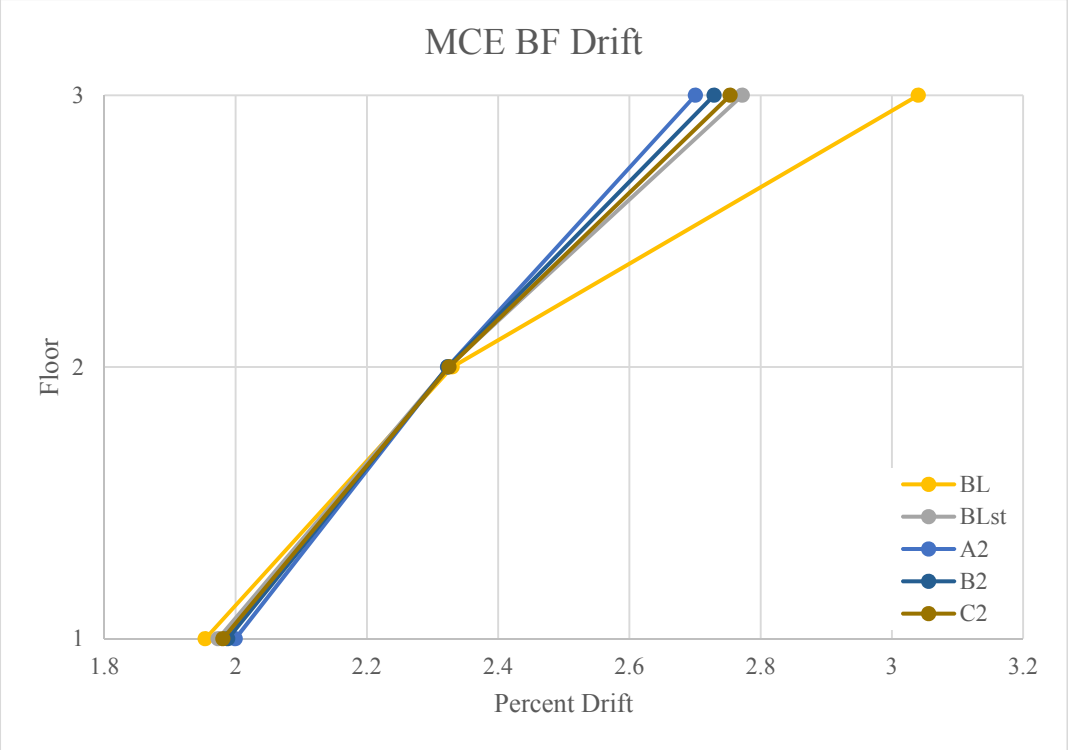

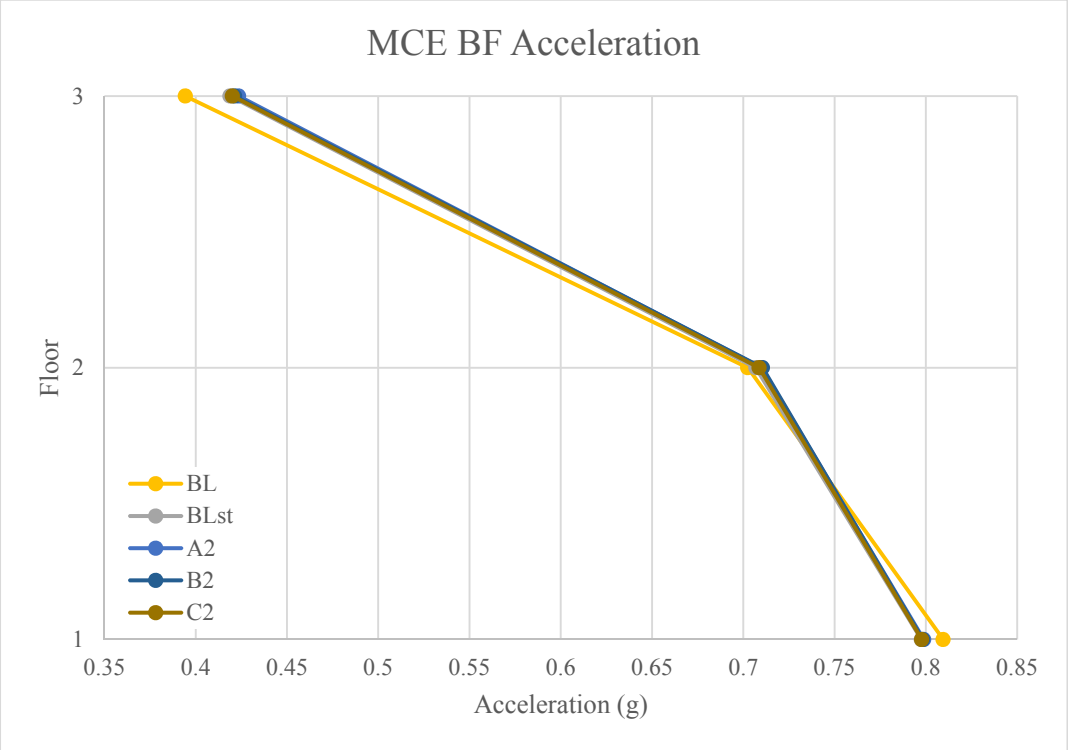

Figure A-10. Three Story MCE BF Average Maximum Global Response (5 kip Slip Force)

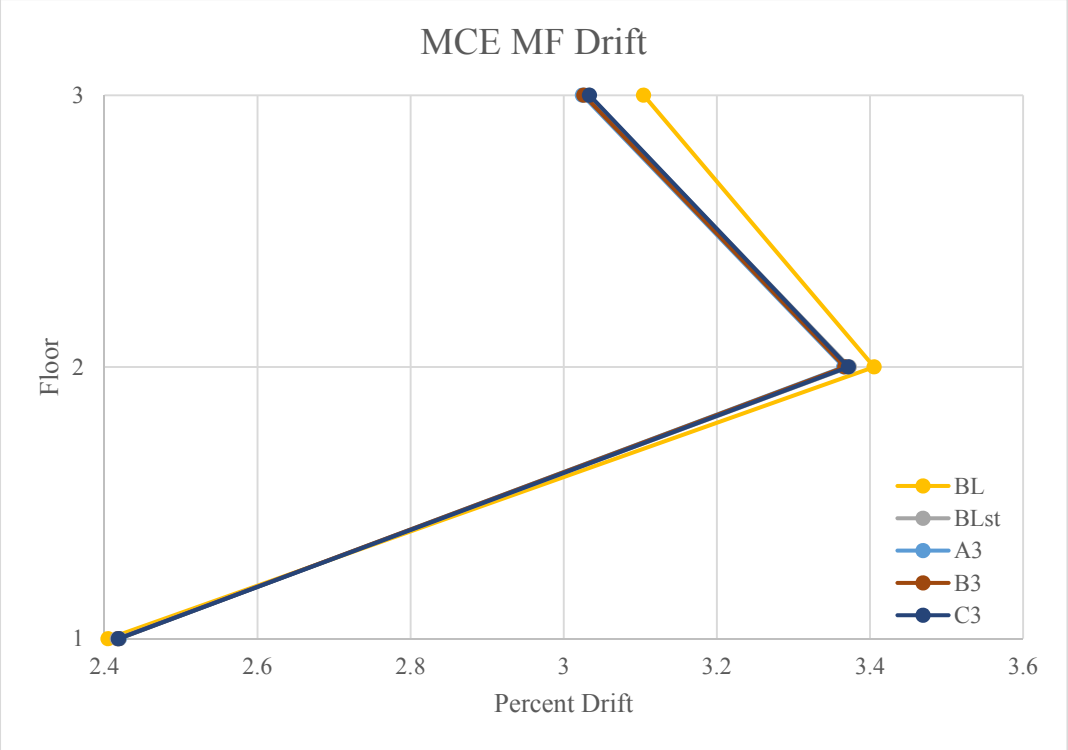

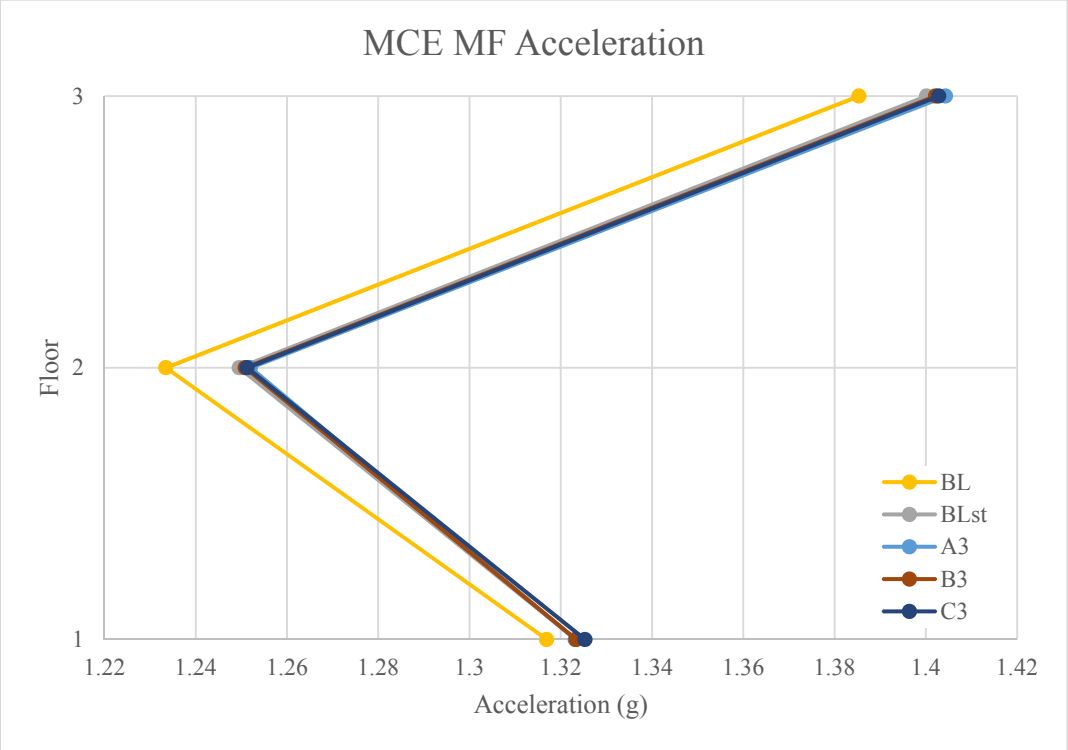

Figure A-11. Three Story MCE MF Average Maximum Global Response (3 kip Slip Force)

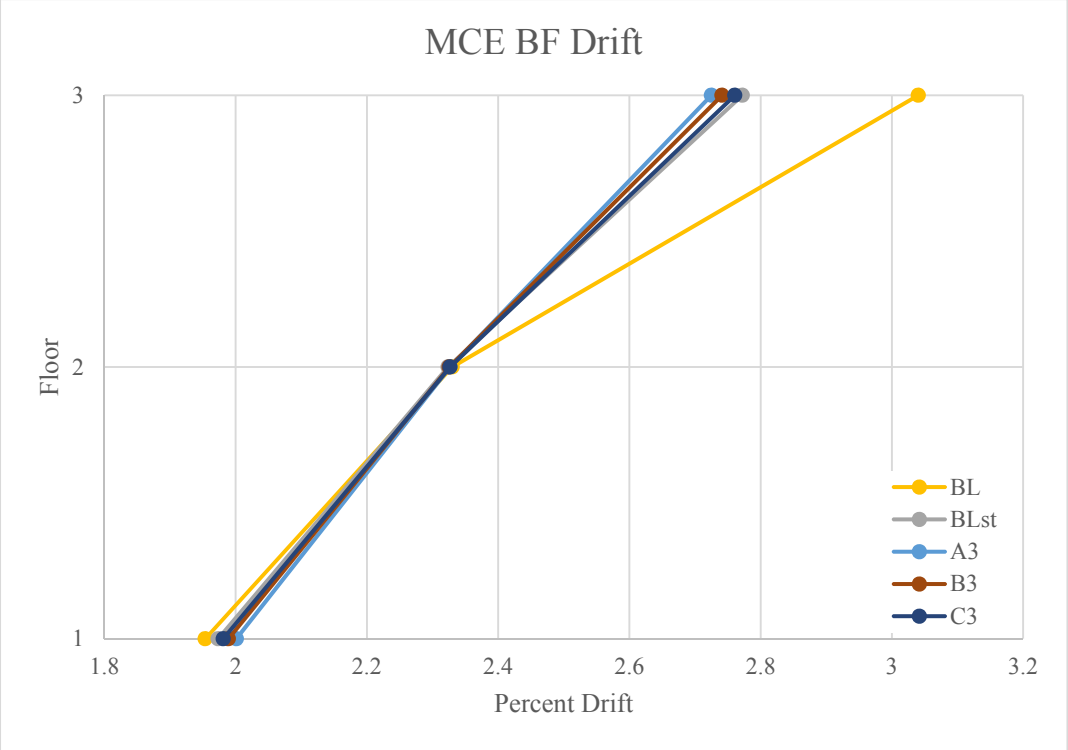

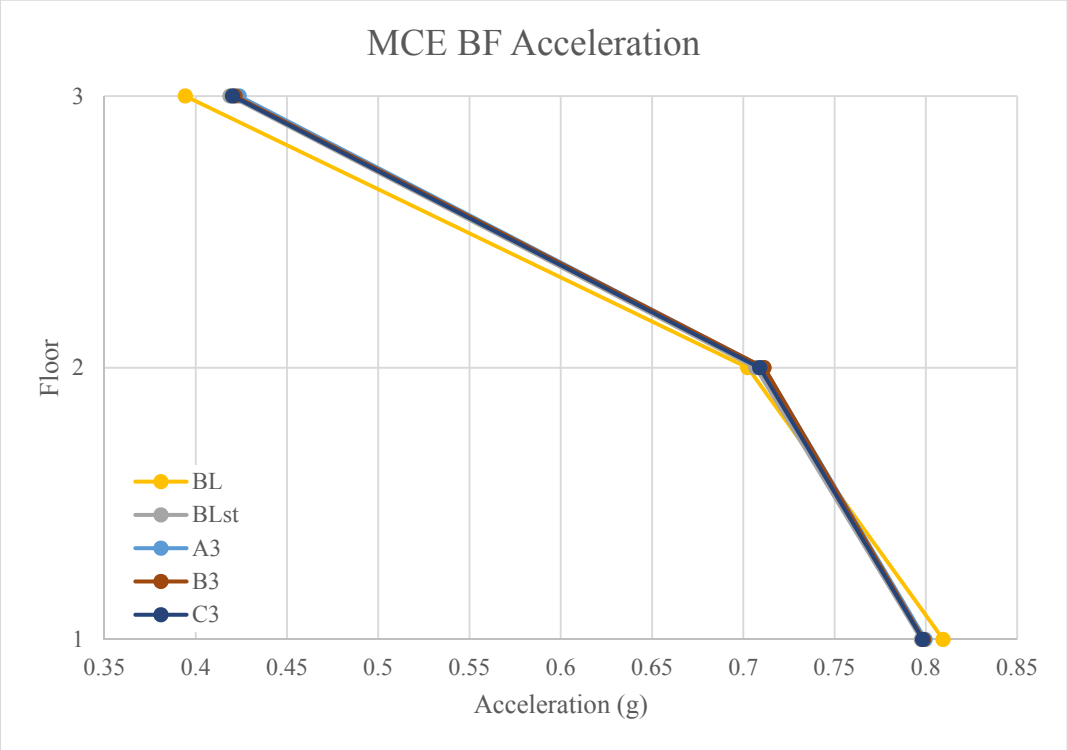

Figure A-12. Three Story MCE BF Average Maximum Global Response (3 kip Slip Force)

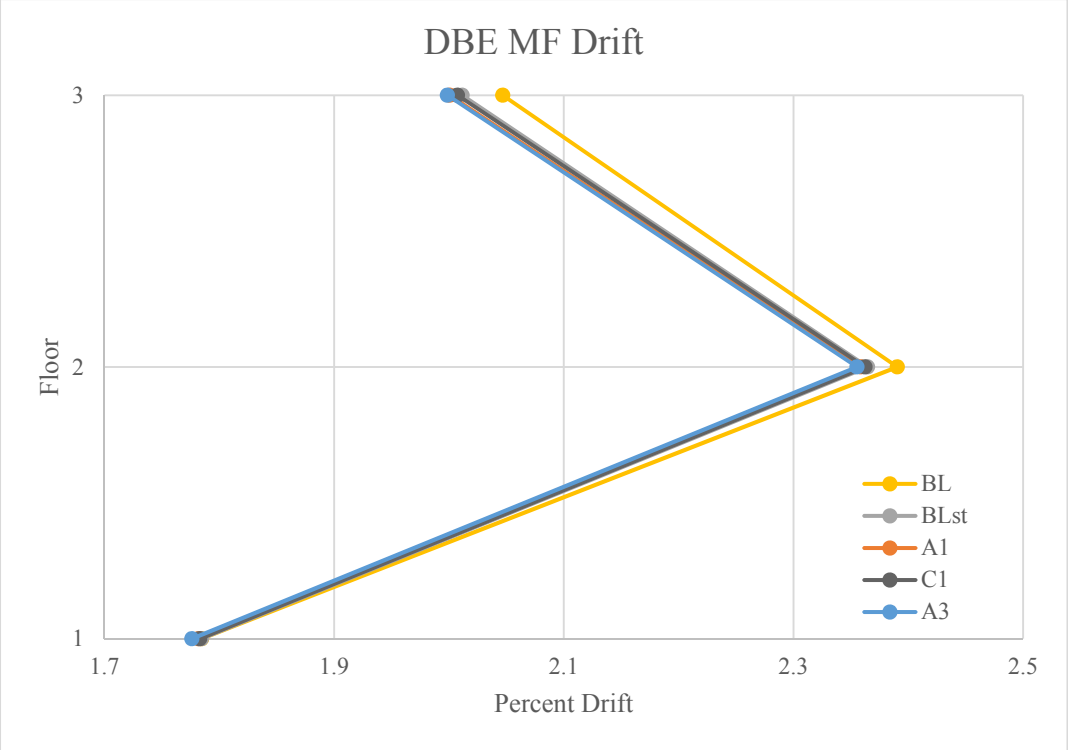

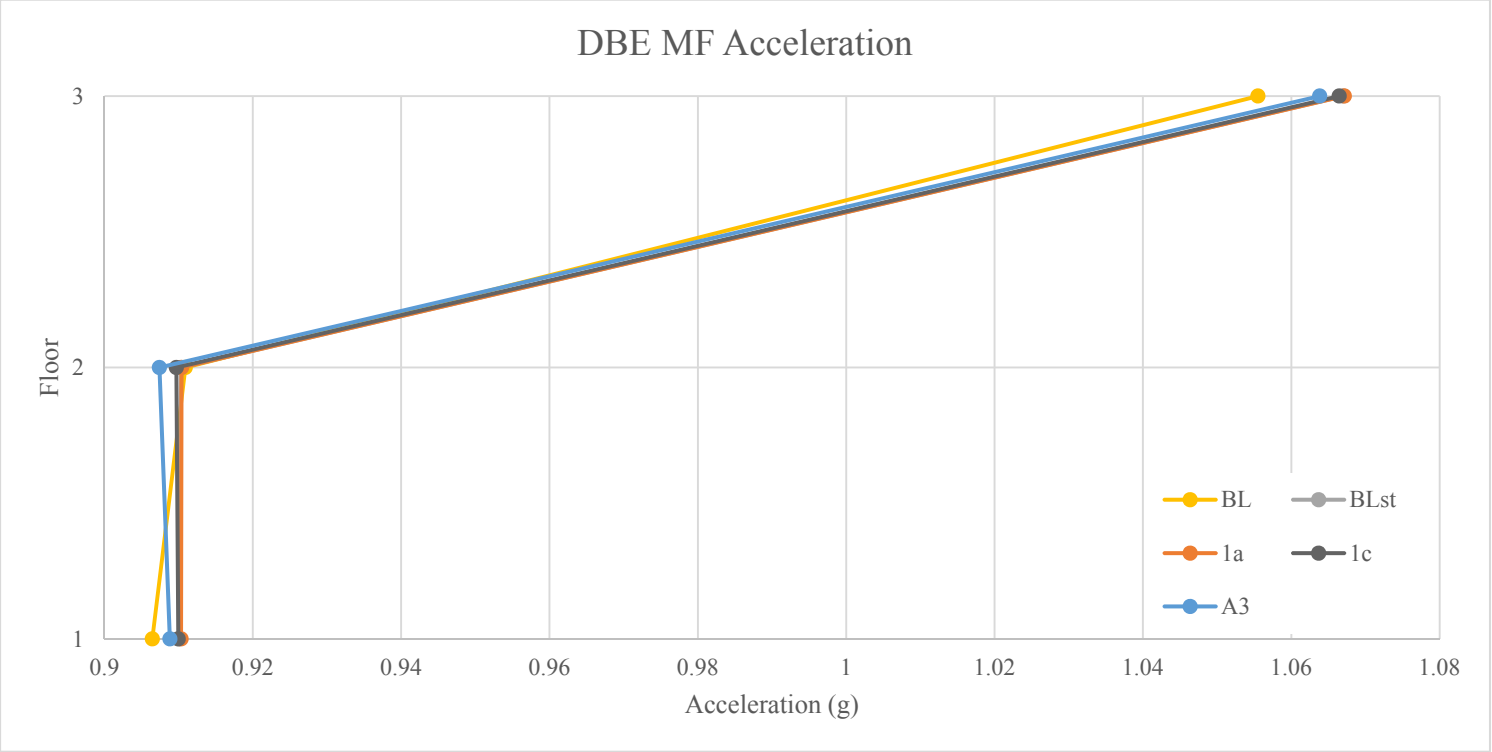

Figure A-13. Three Story DBE MF Average Maximum Global Response

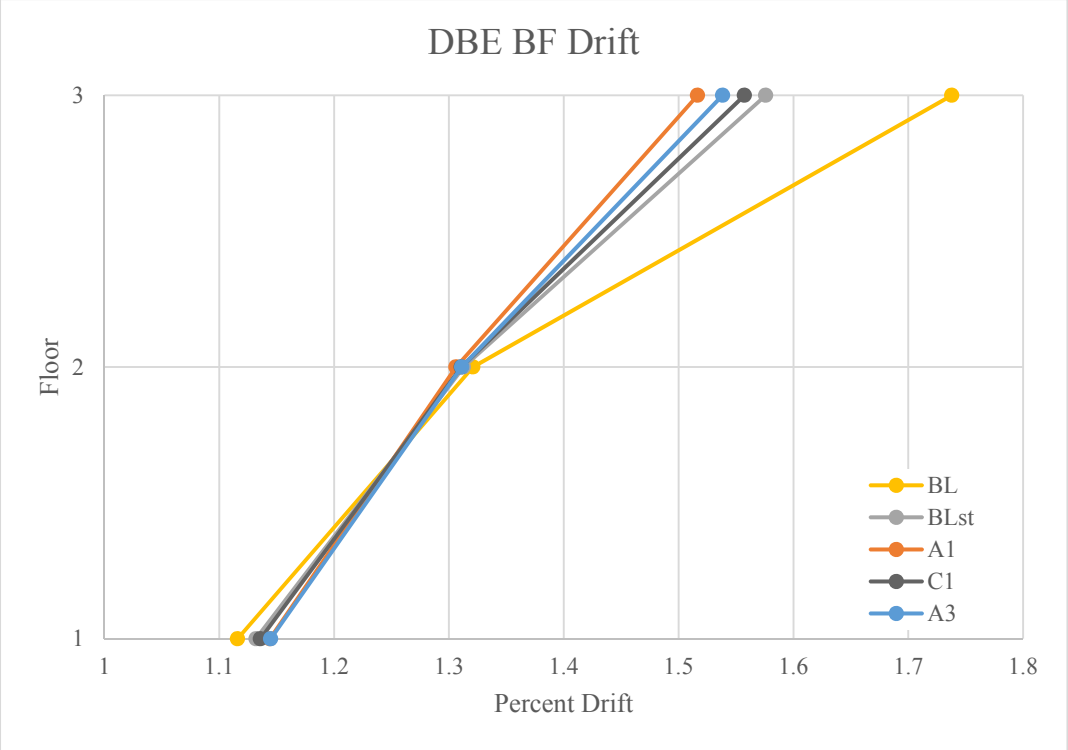

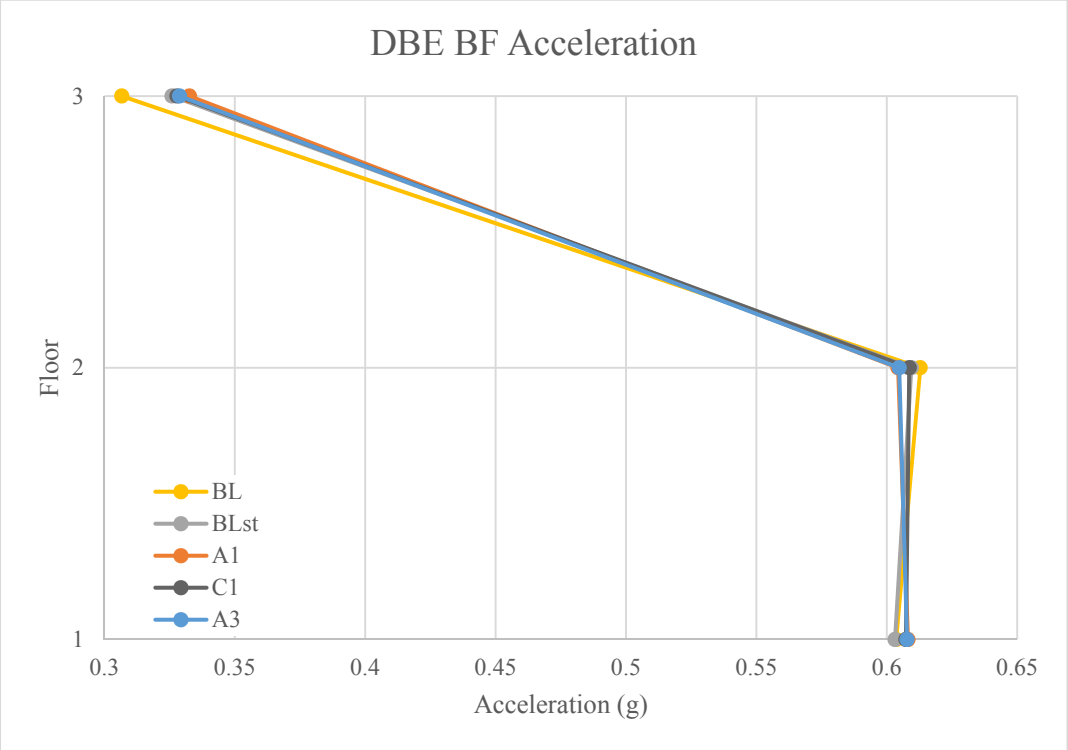

Figure A-14. Three Story DBE BF Average Maximum Global Response

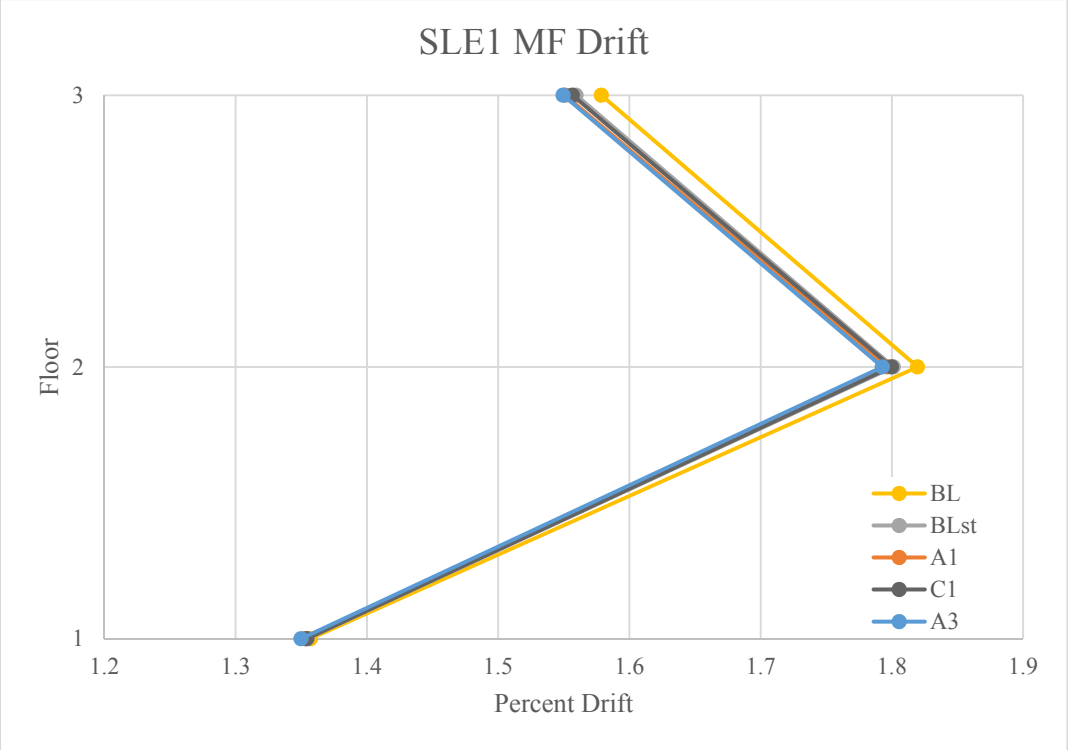

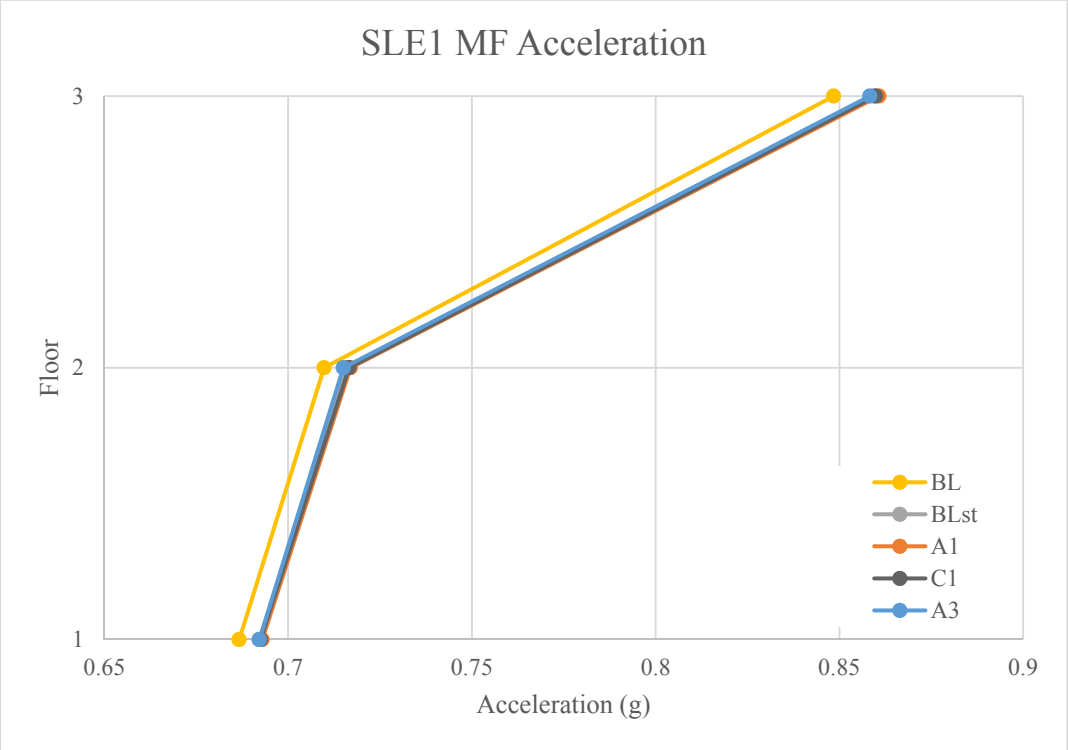

Figure A-15. Three Story SLE1 MF Average Maximum Global Response

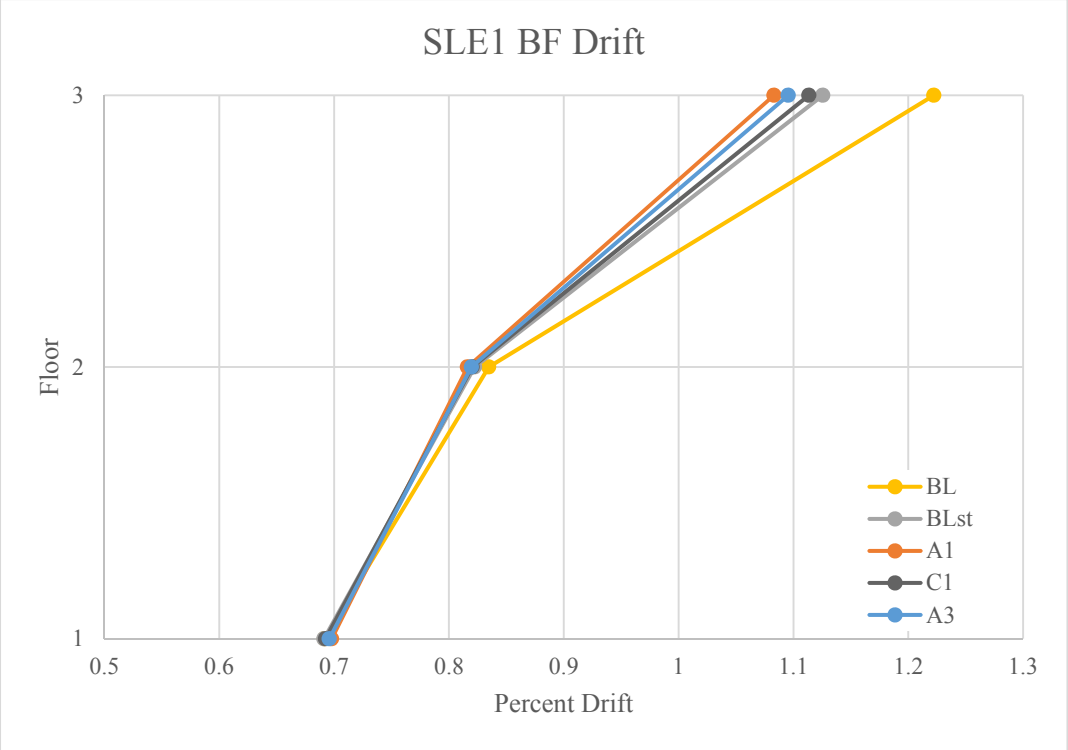

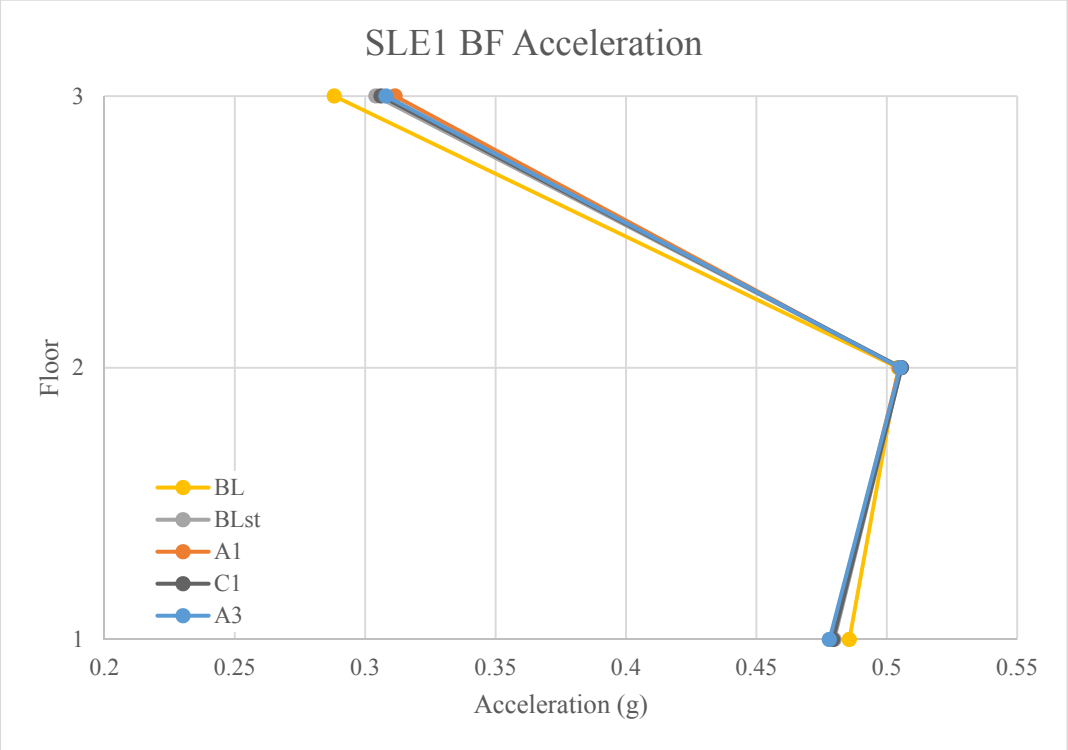

Figure A-16. Three Story SLE1 BF Average Maximum Global Response

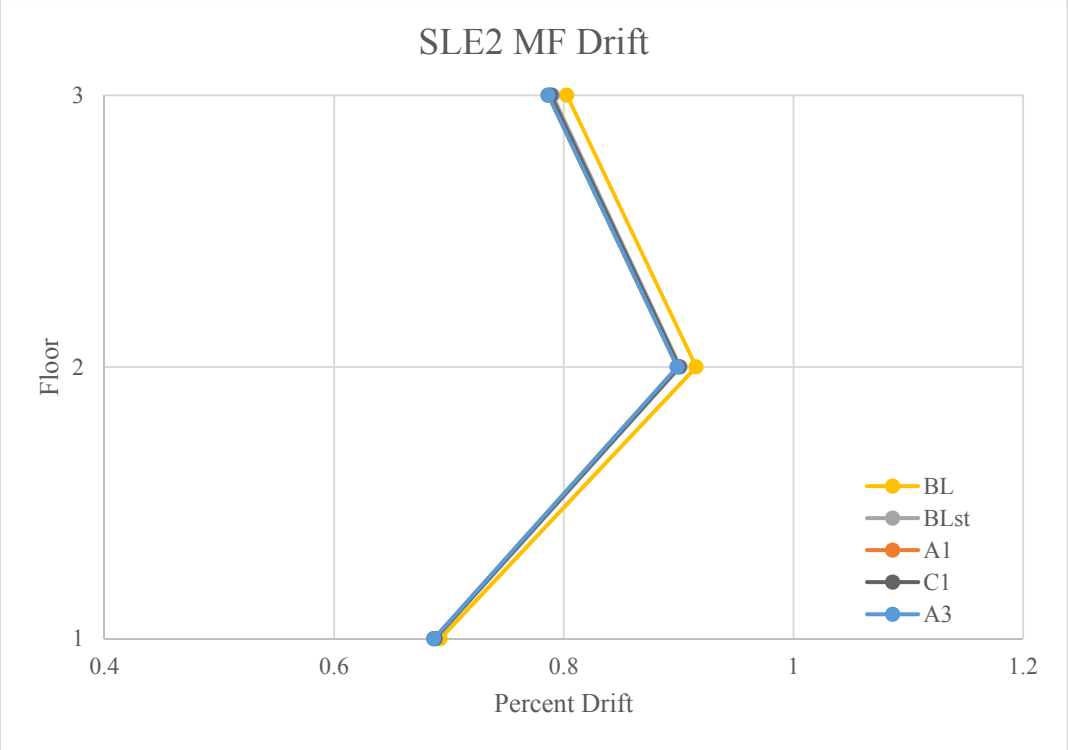

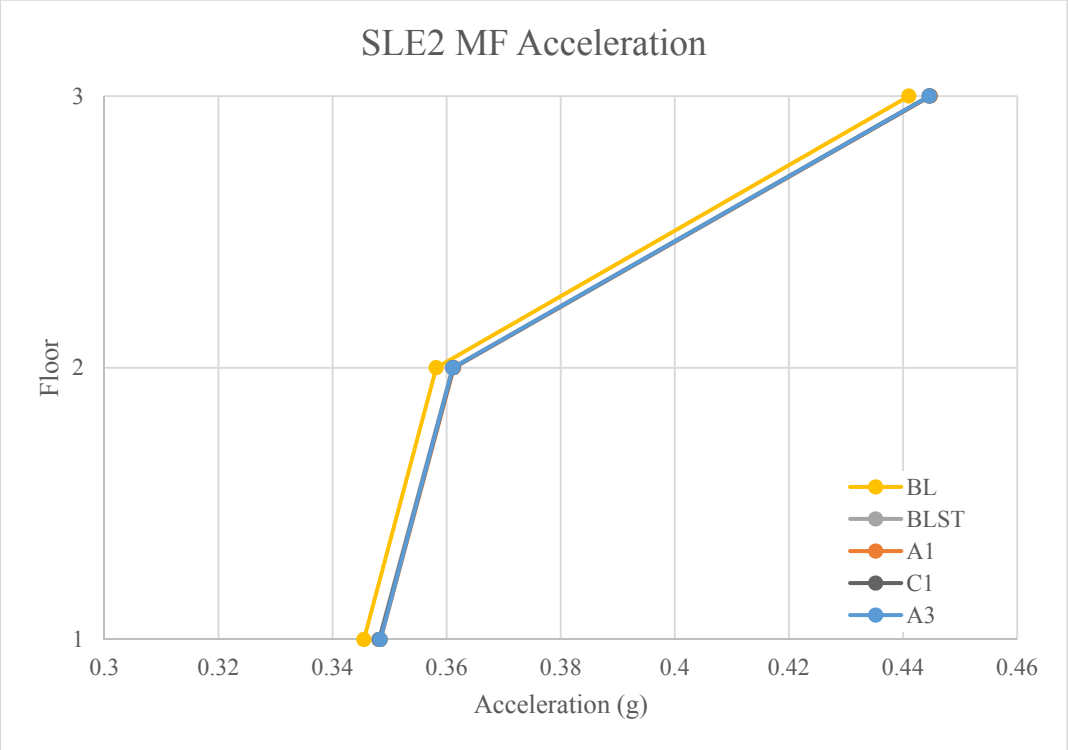

Figure A-17. Three Story SLE2 MF Average Maximum Global Response

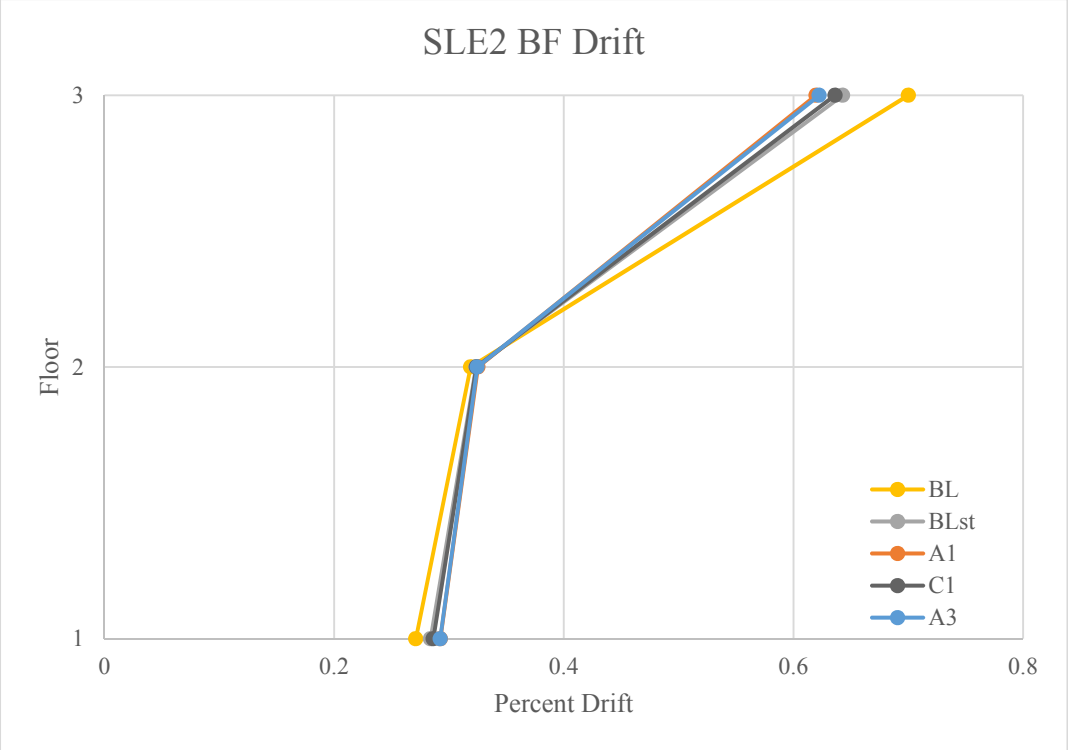

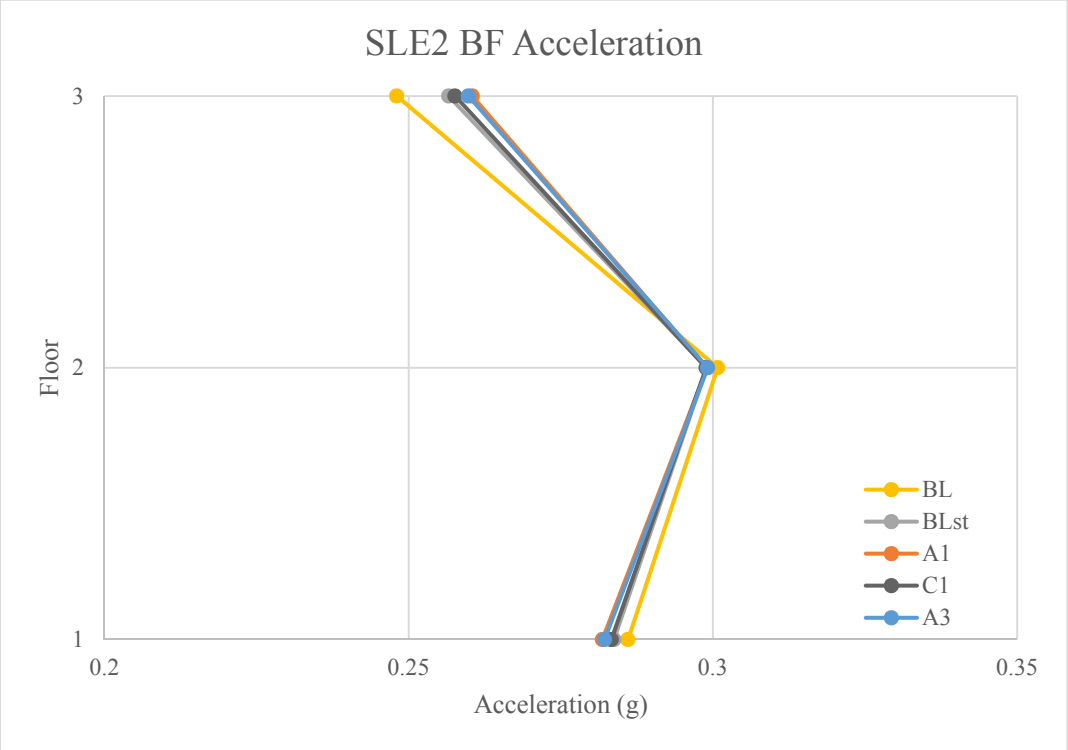

Figure A-18. Three Story SLE2 BF Average Maximum Global Response

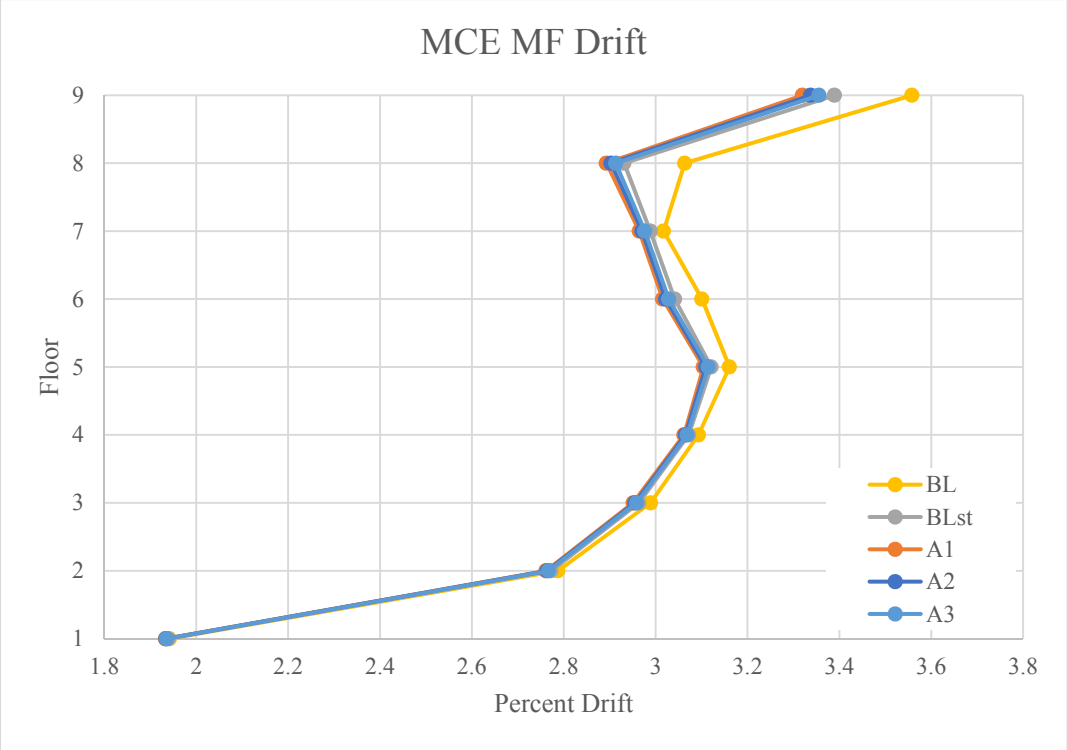

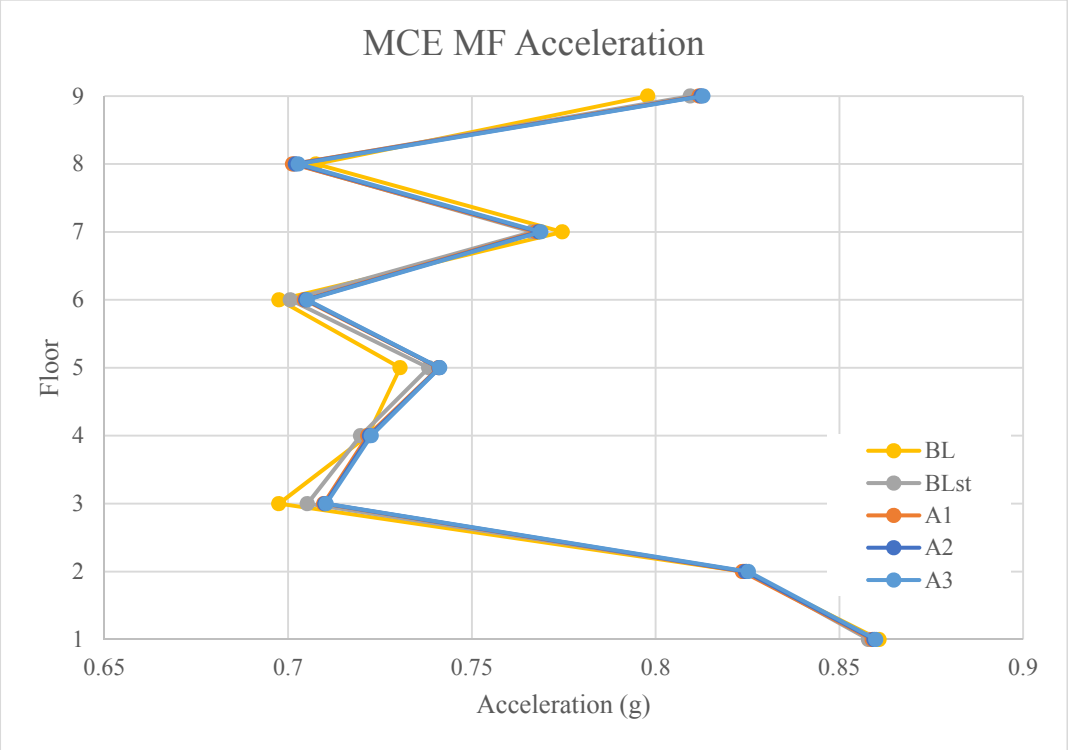

Figure A-19. Nine Story MCE MF Average Maximum Global Response (A Layout)

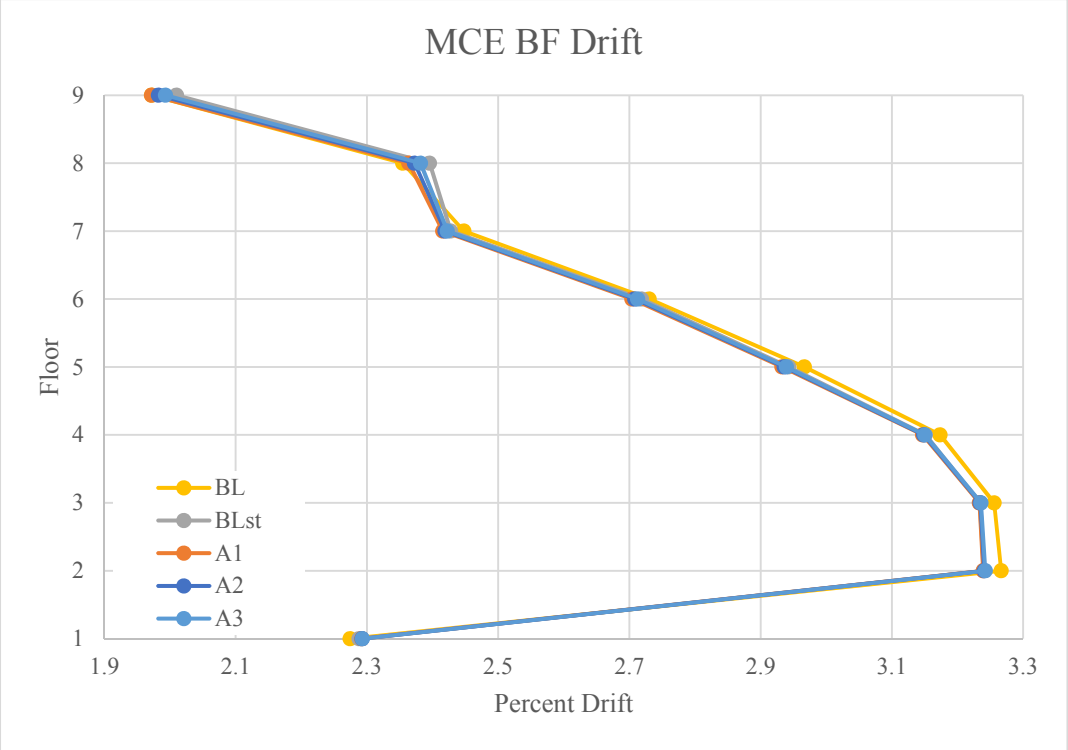

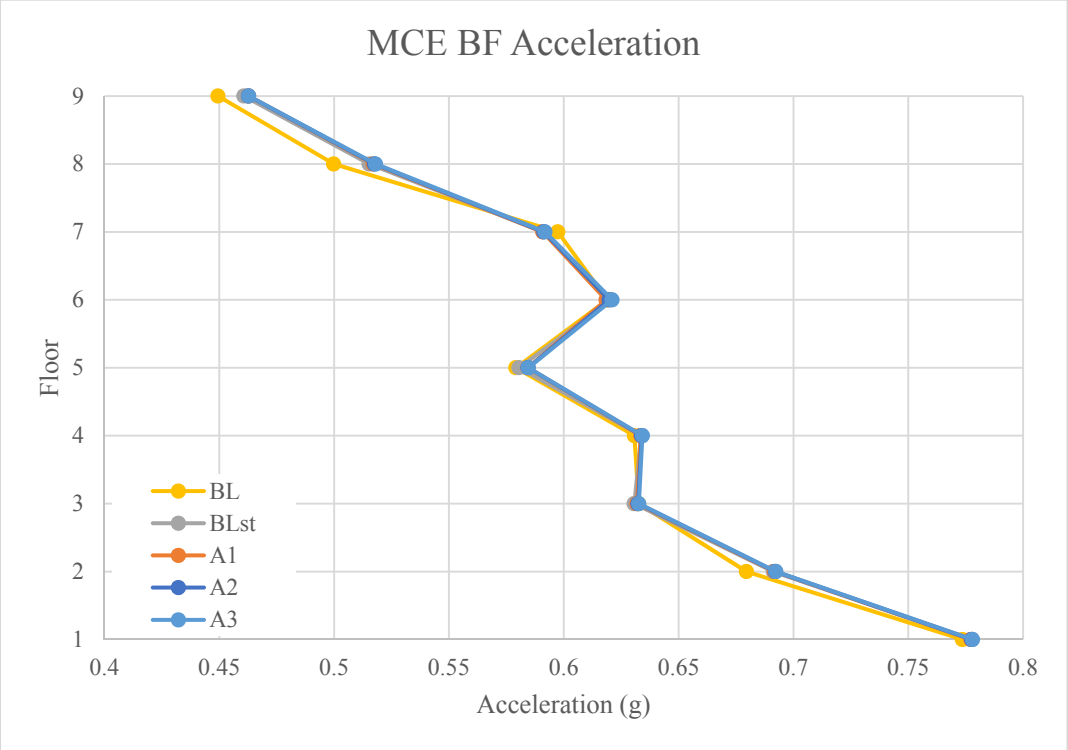

Figure A-20. Nine Story MCE BF Average Maximum Global Response (A Layout)

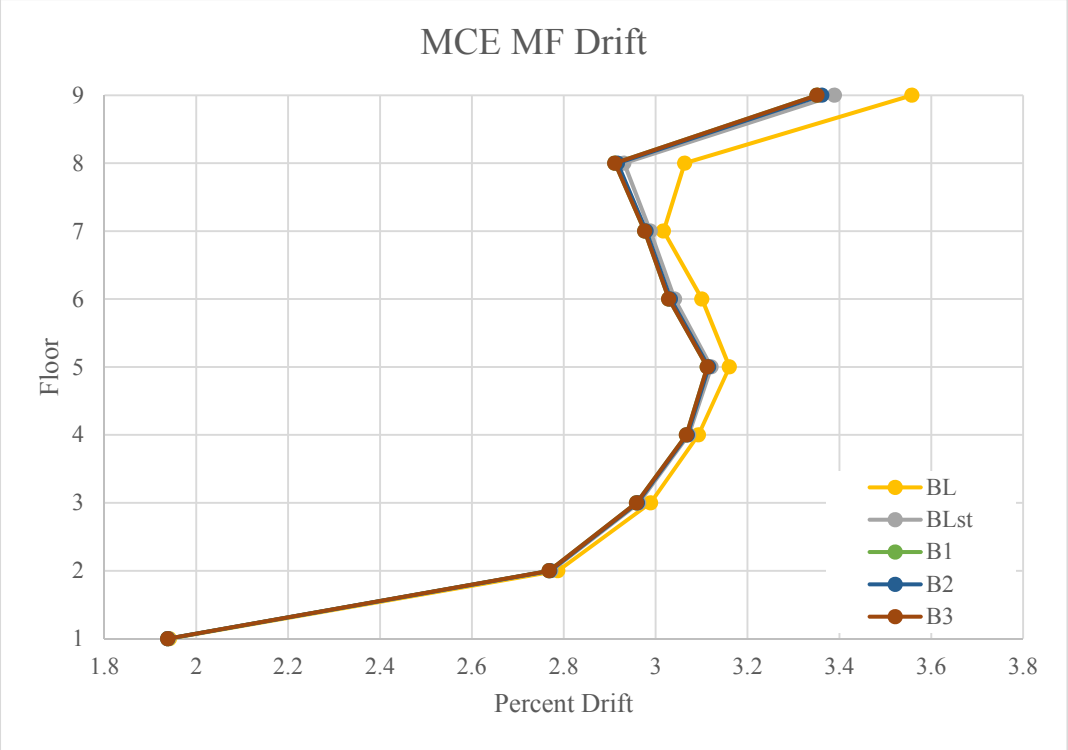

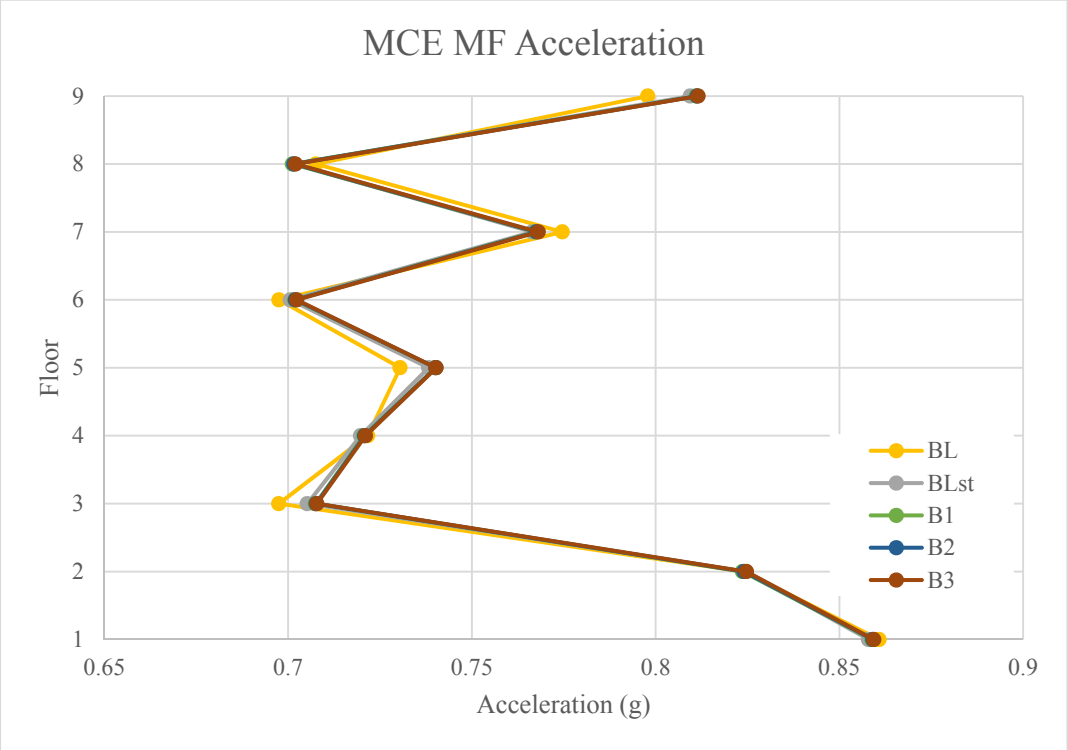

Figure A-21. Nine Story MCE MF Average Maximum Global Response (B Layout)

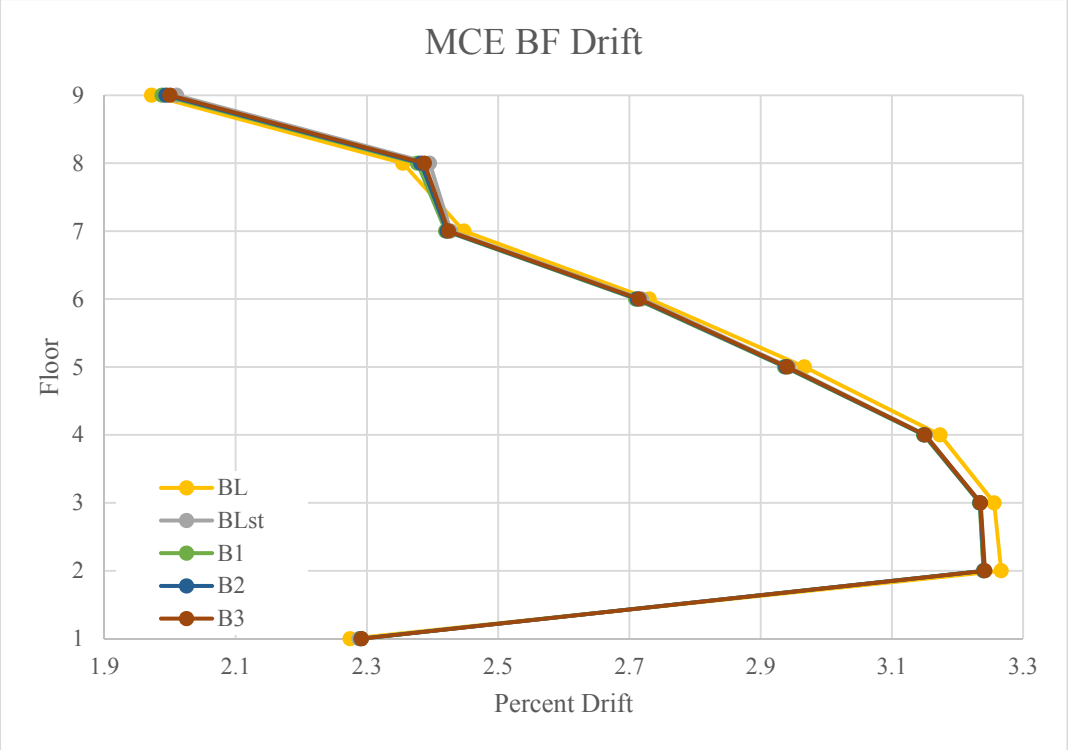

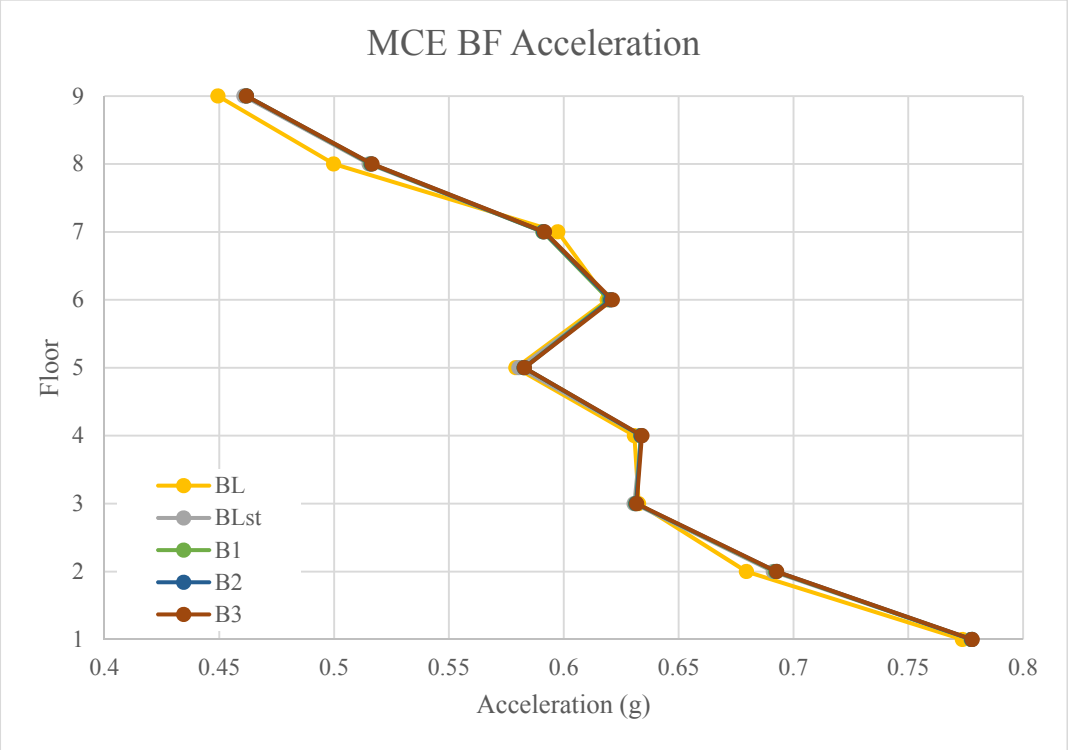

Figure A-22. Nine Story MCE BF Average Maximum Global Response (B Layout)

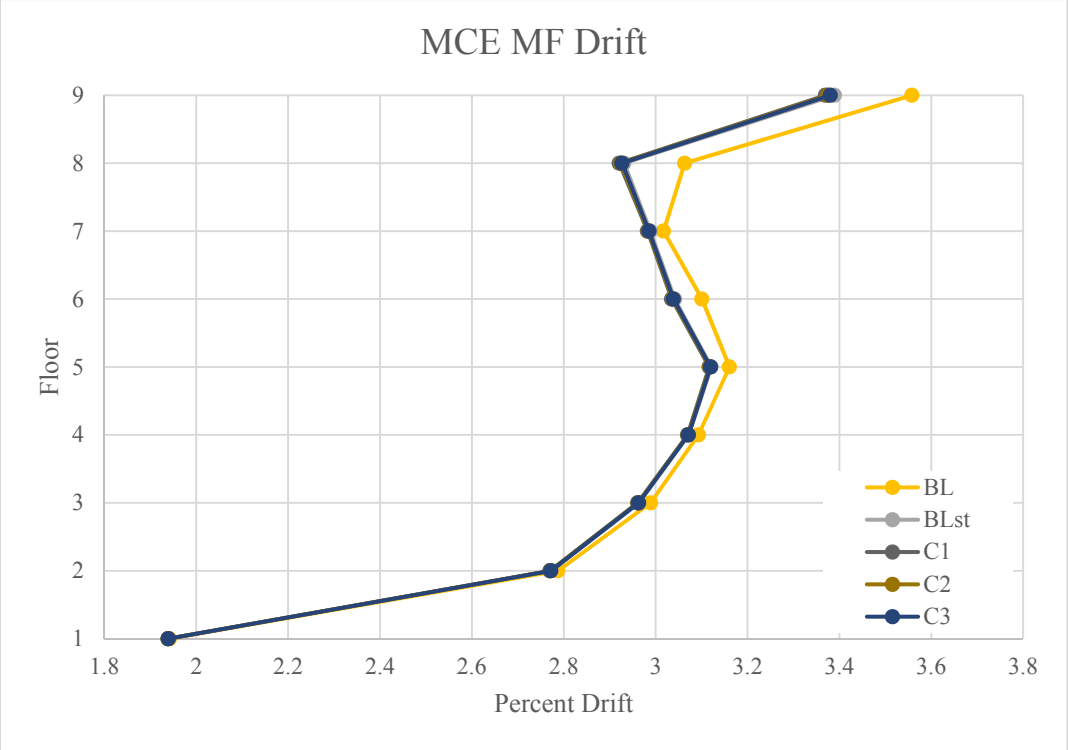

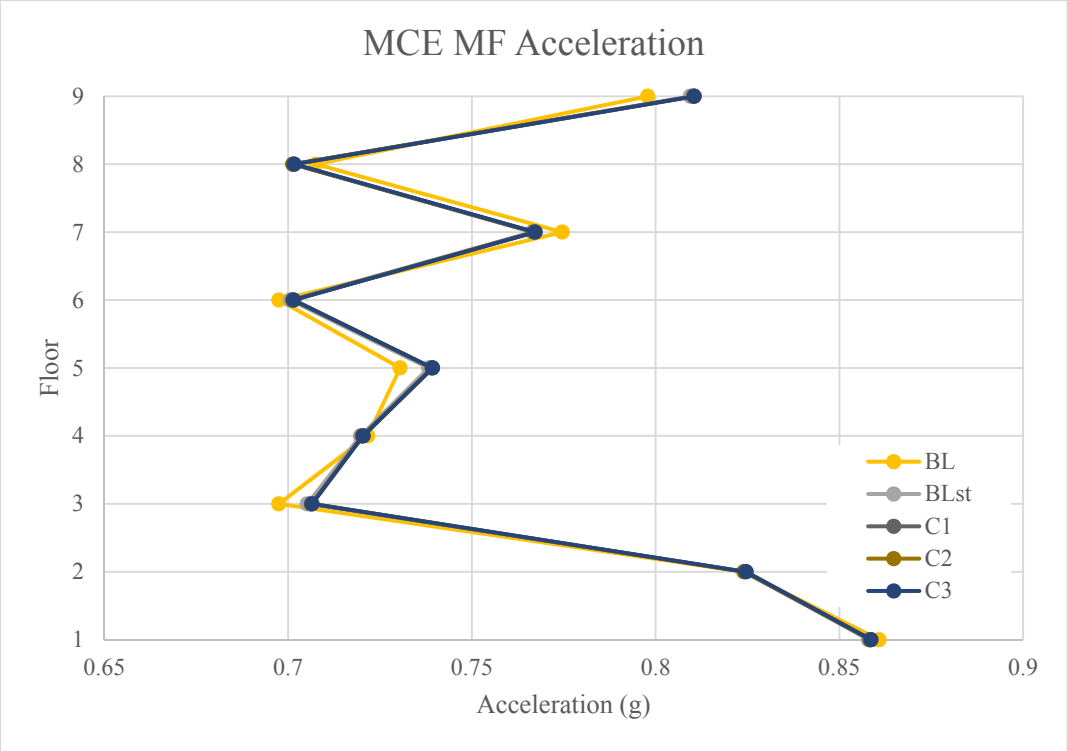

Figure A-23. Nine Story MCE MF Average Maximum Global Response (C Layout)

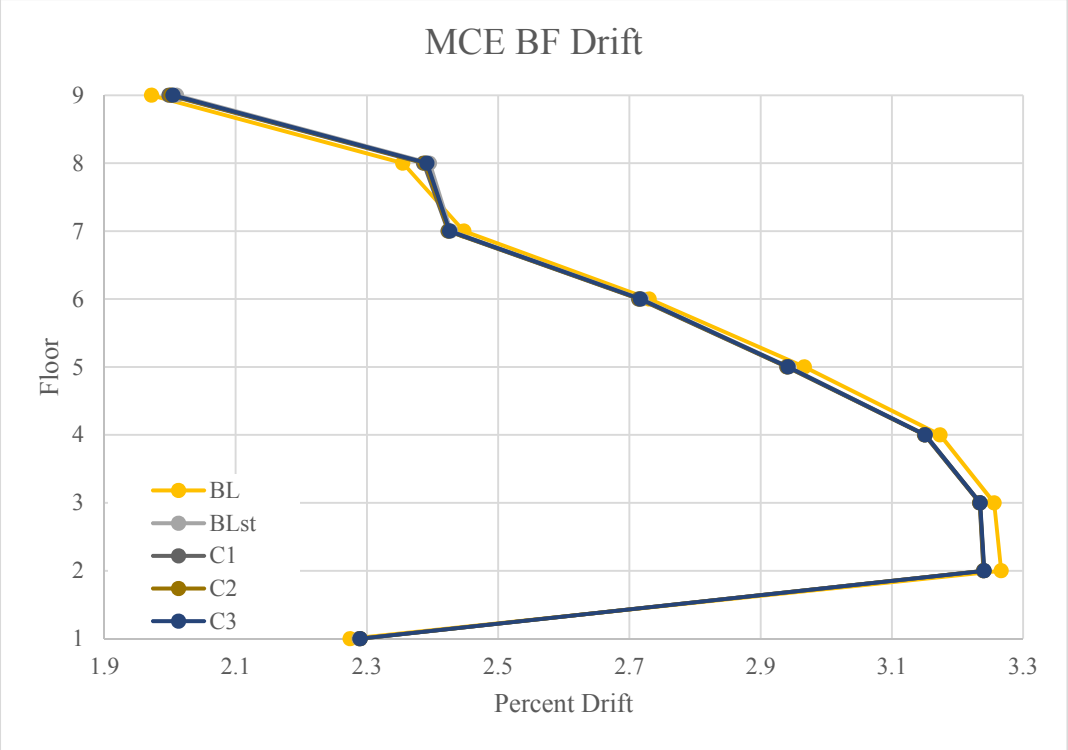

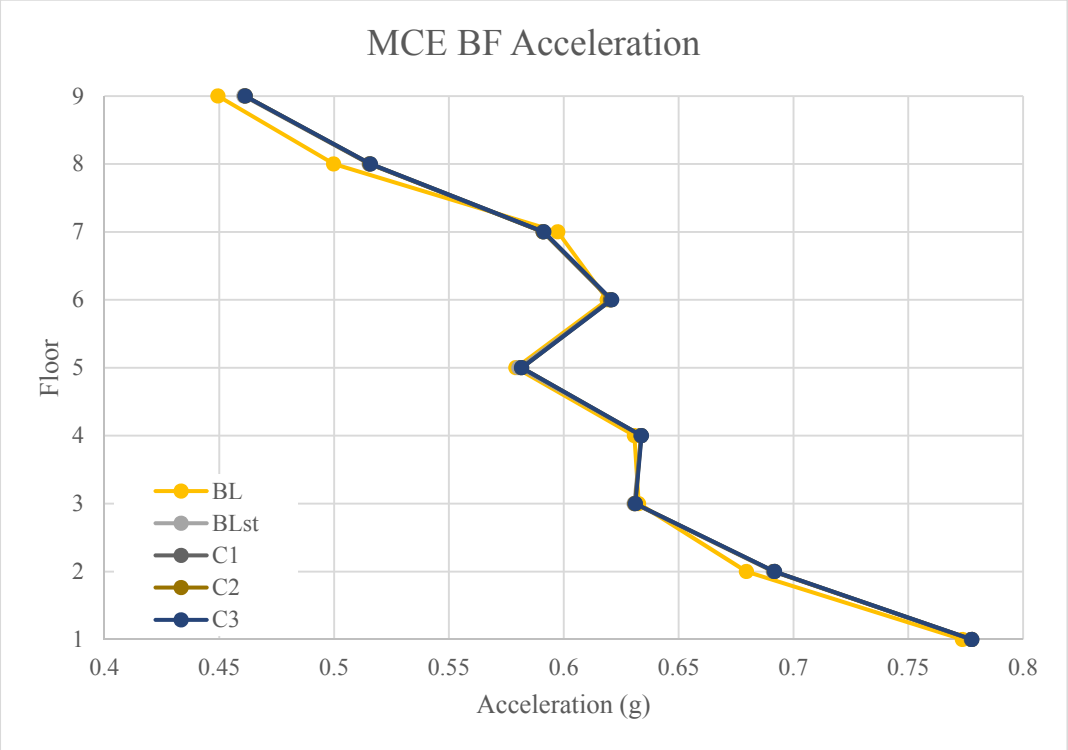

Figure A-24. Nine Story MCE BF Average Maximum Global Response (C Layout)

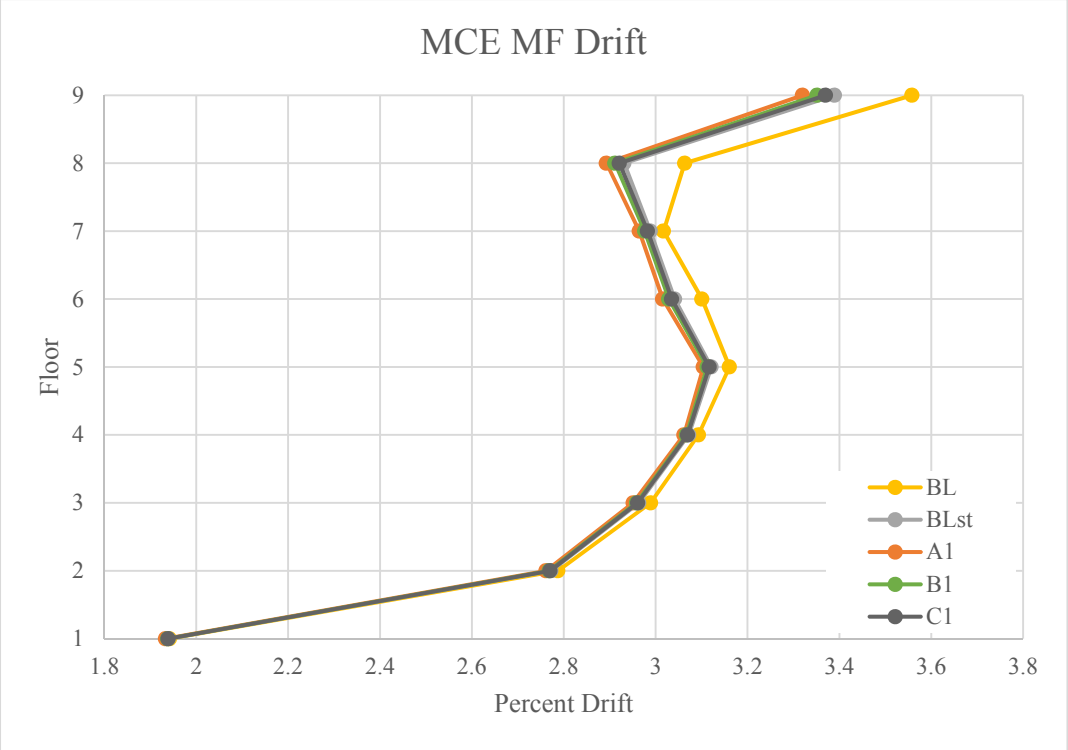

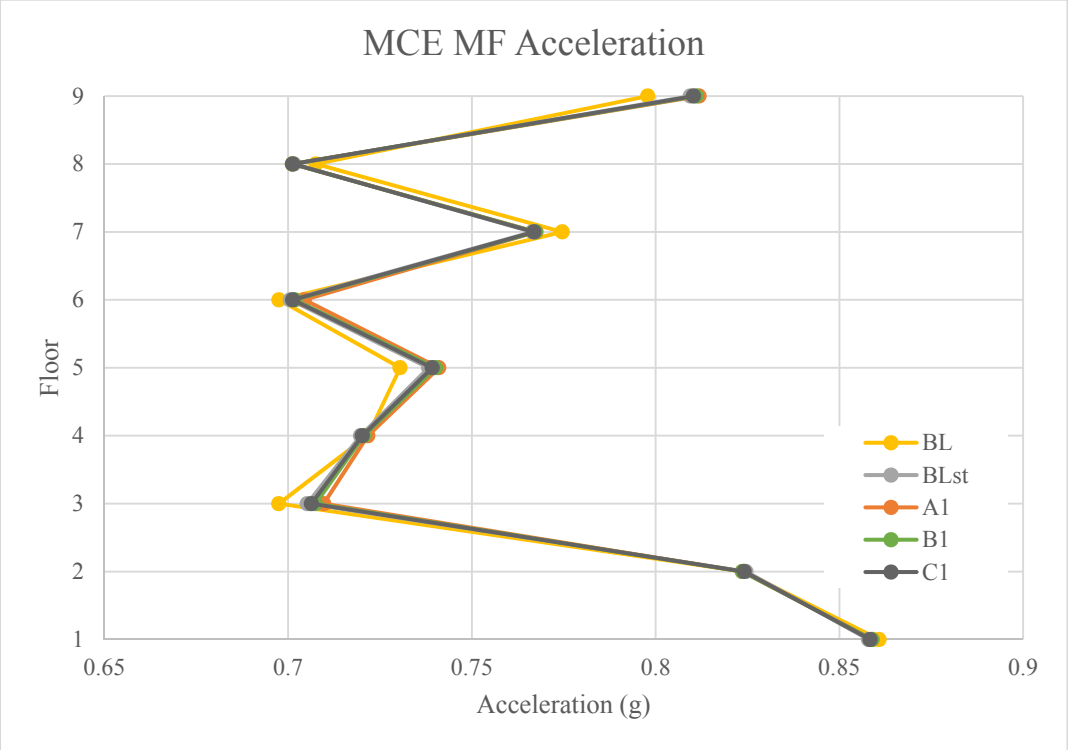

Figure A-25. Nine Story MCE MF Average Maximum Global Response (7 kip Slip Force)

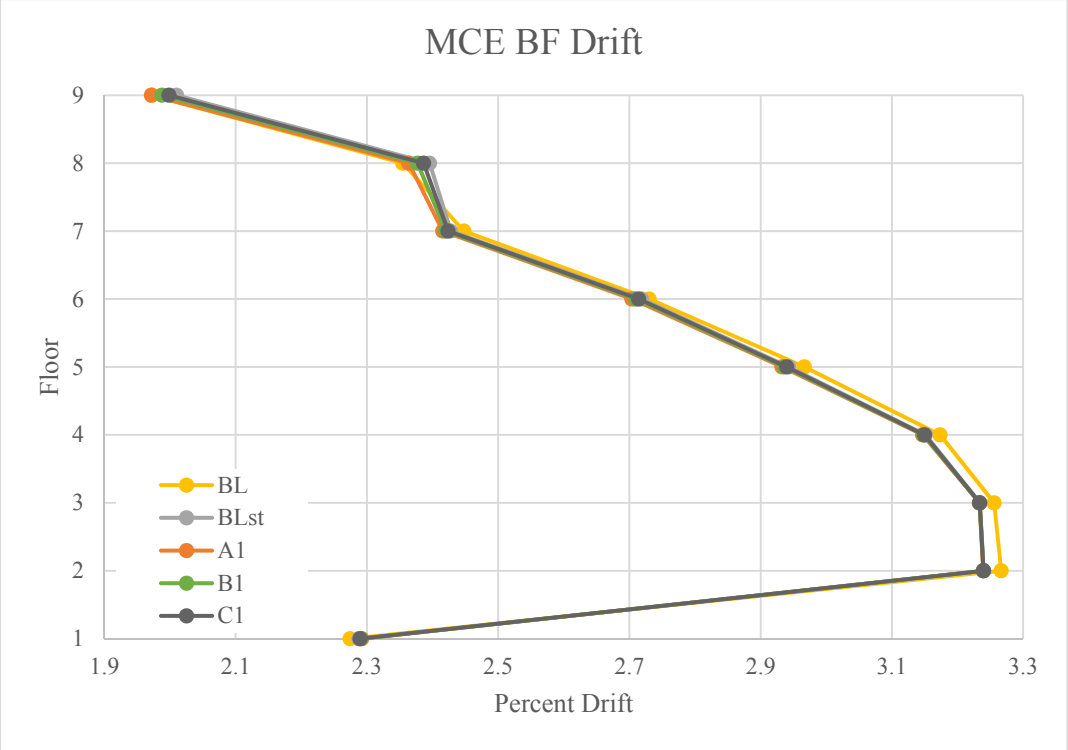

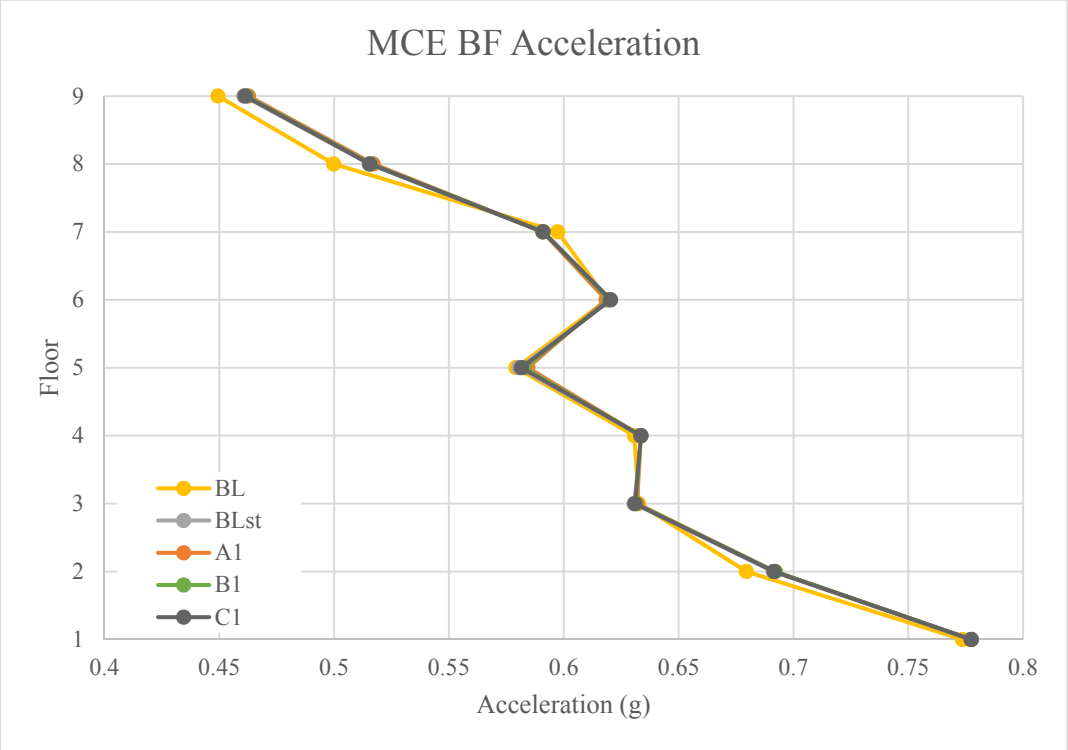

Figure A-26. Nine Story MCE BF Average Maximum Global Response (7 kip Slip Force)

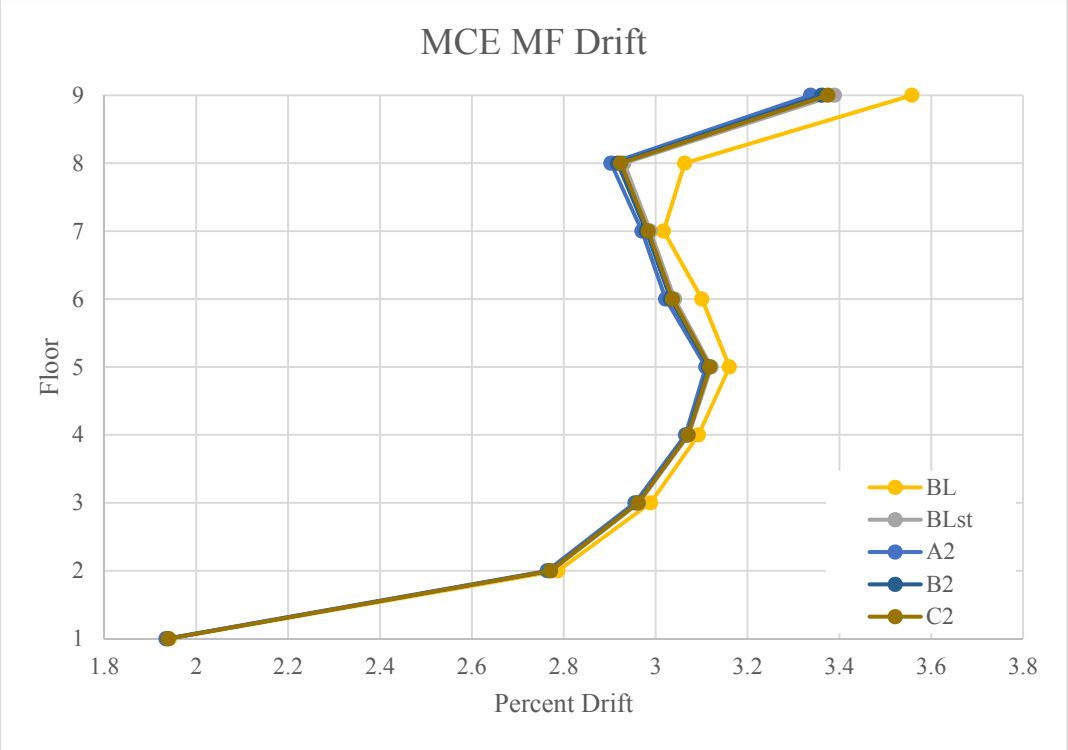

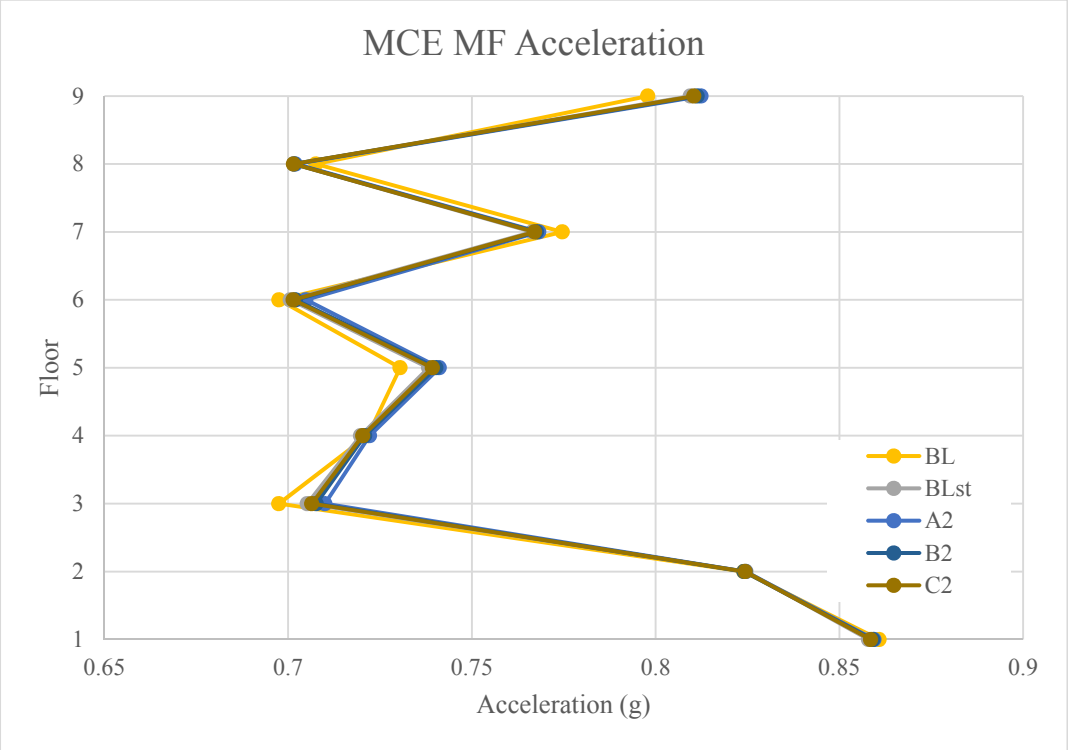

Figure A-27. Nine Story MCE MF Average Maximum Global Response (5 kip Slip Force)

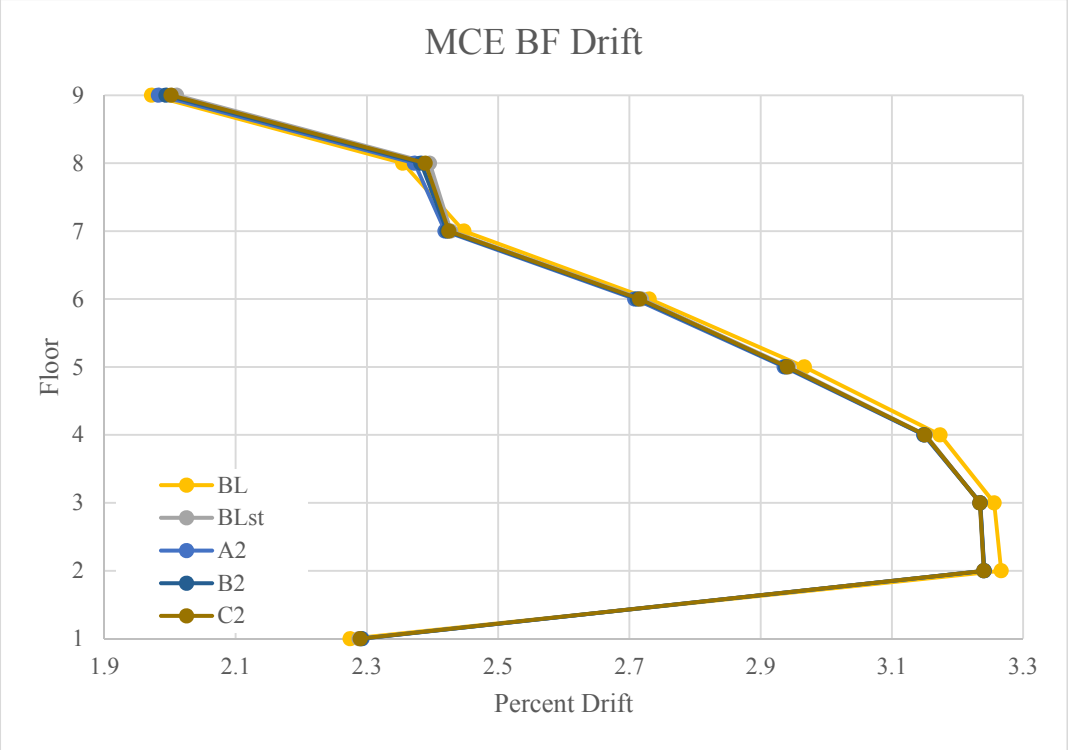

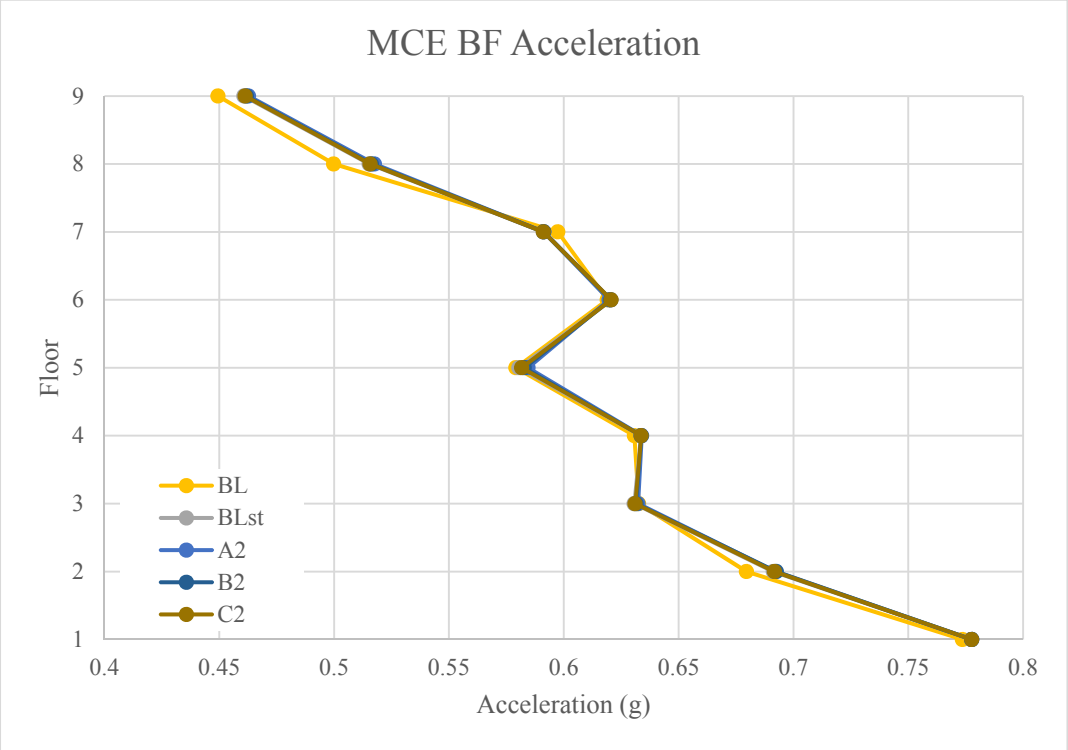

Figure A-28. Nine Story MCE BF Average Maximum Global Response (5 kip Slip Force)

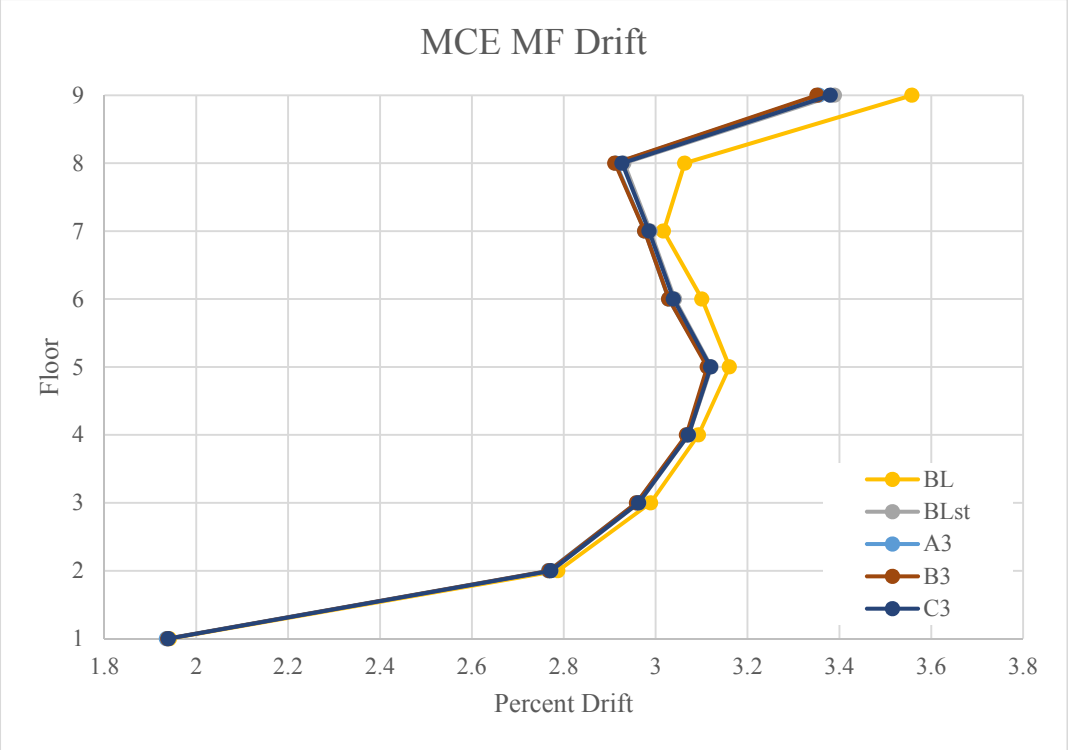

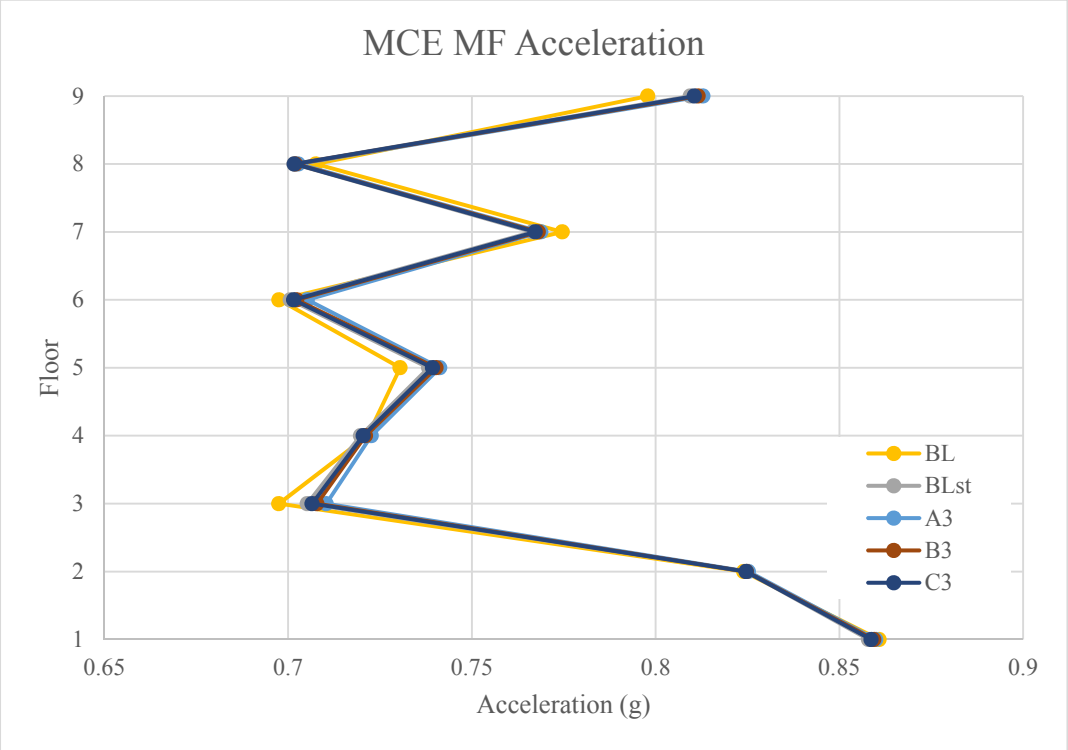

Figure A-29. Nine Story MCE MF Average Maximum Global Response (3 kip Slip Force)

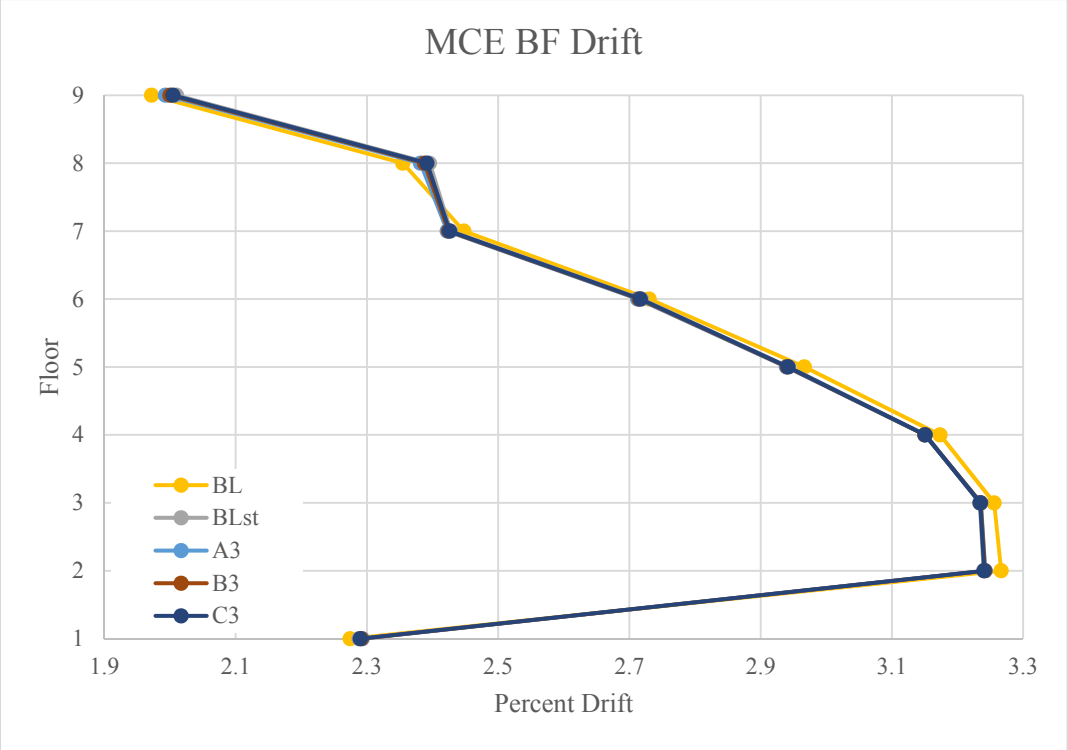

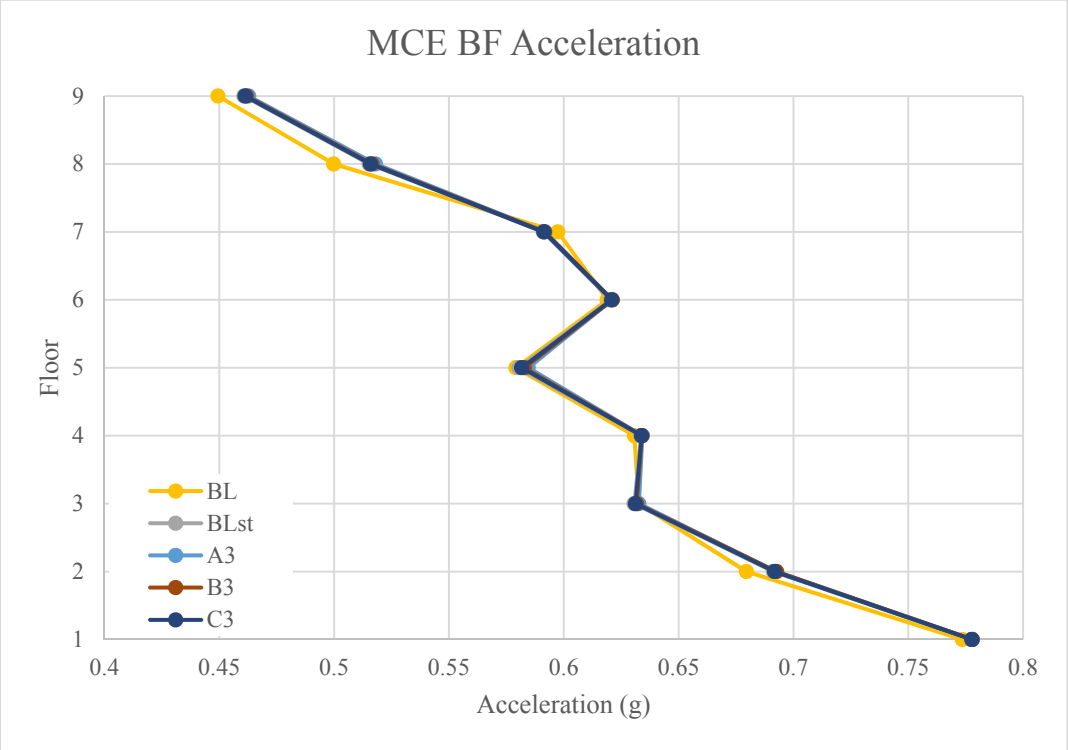

Figure A-30. Nine Story MCE BF Average Maximum Global Response (3 kip Slip Force)

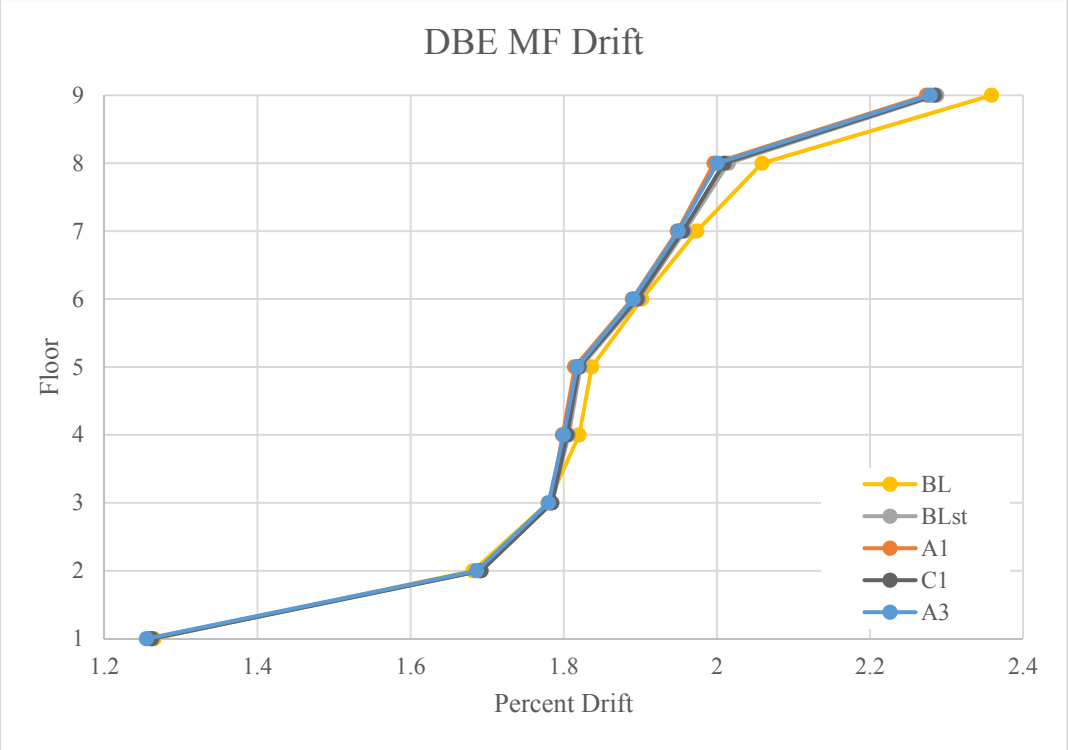

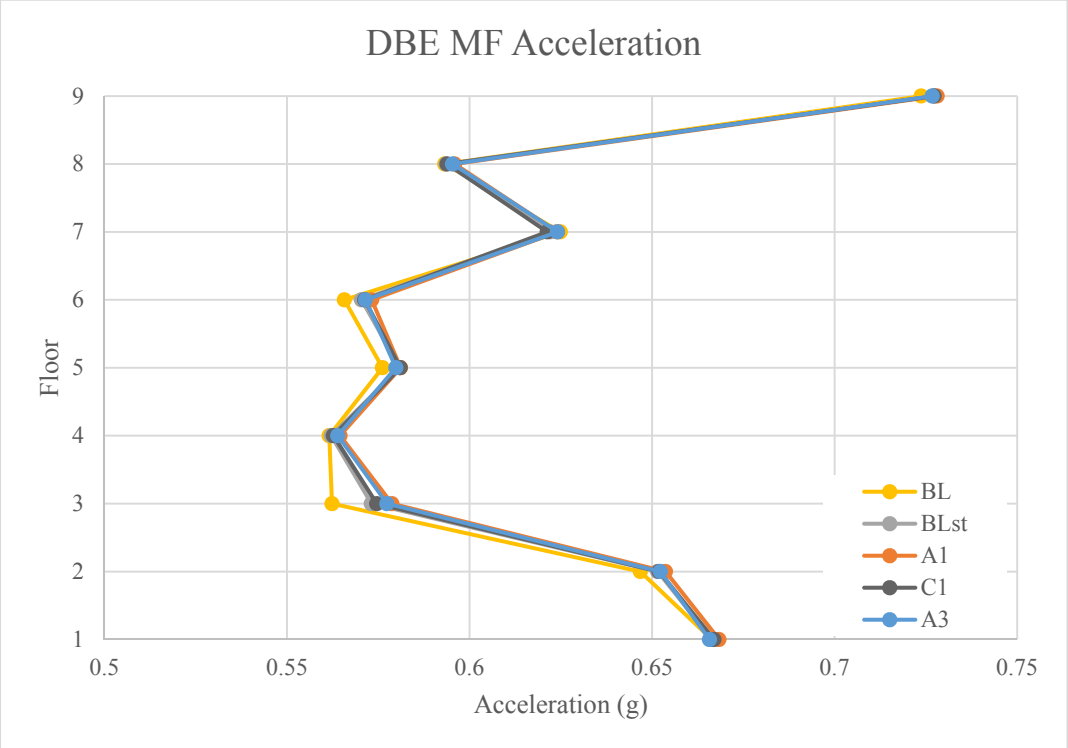

Figure A-31. Nine Story DBE MF Average Maximum Global Response

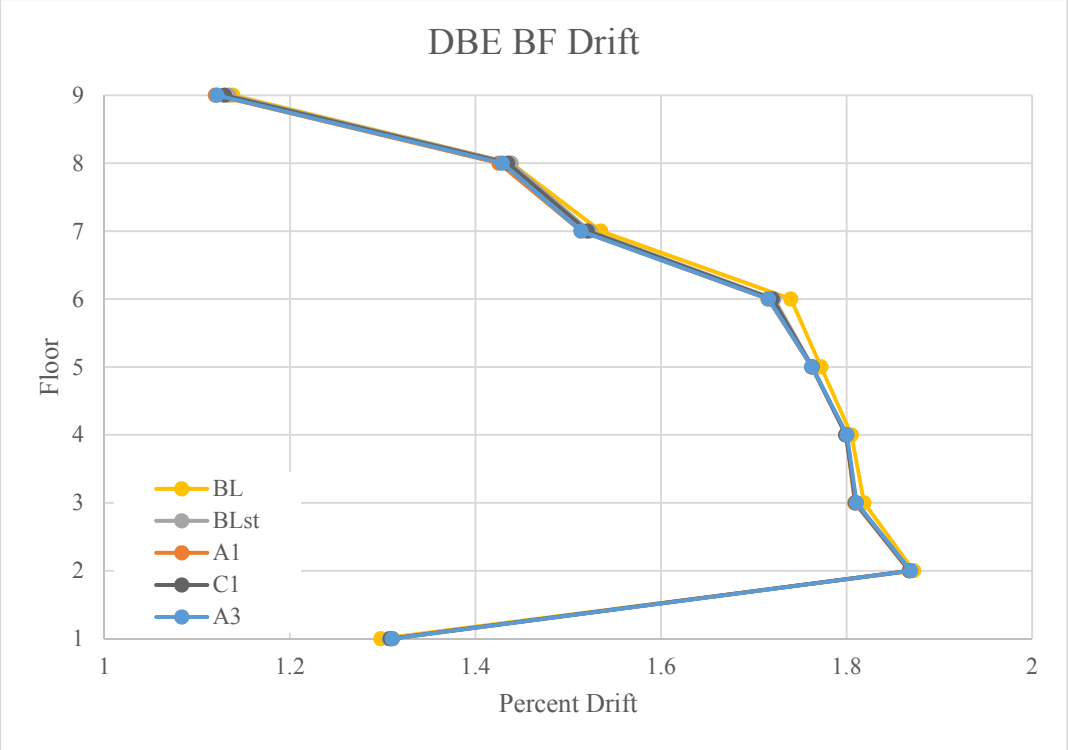

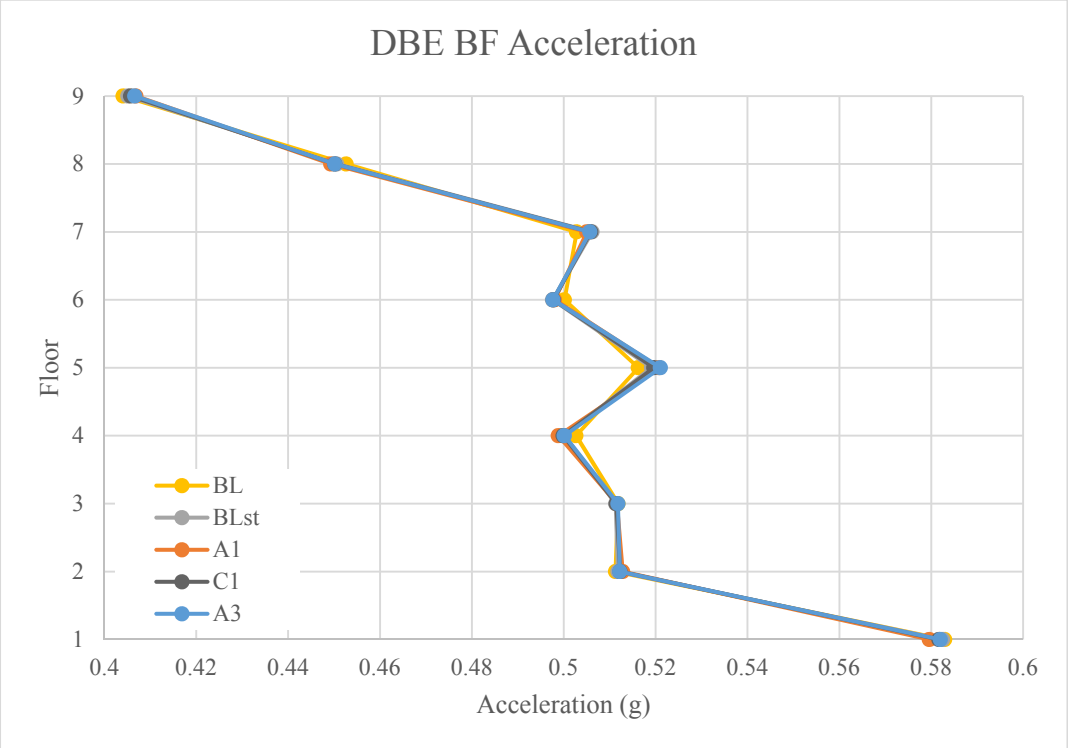

Figure A-32. Nine Story DBE BF Average Maximum Global Response

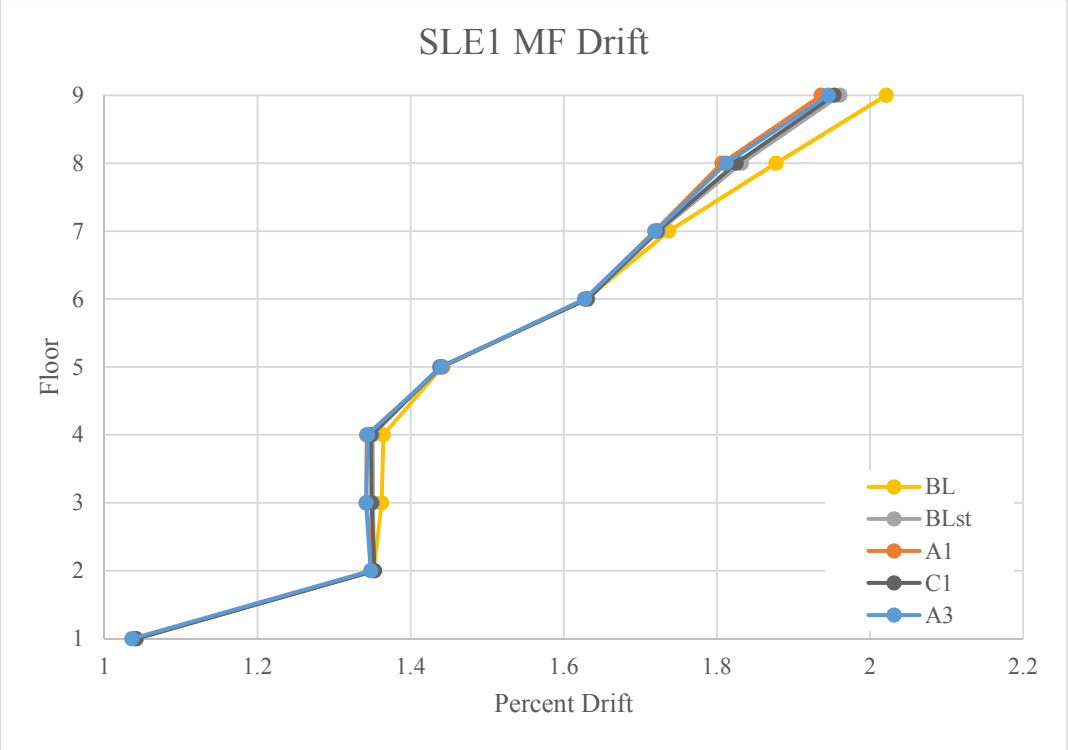

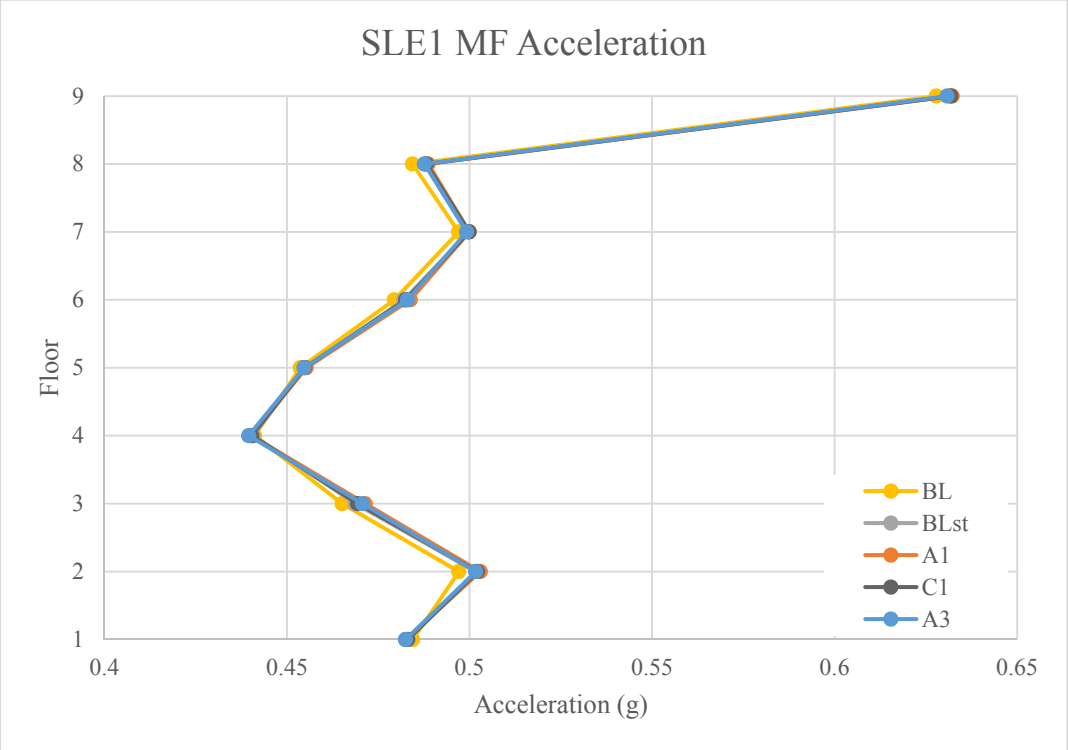

Figure A-33. Nine Story SLE1 MF Average Maximum Global Response

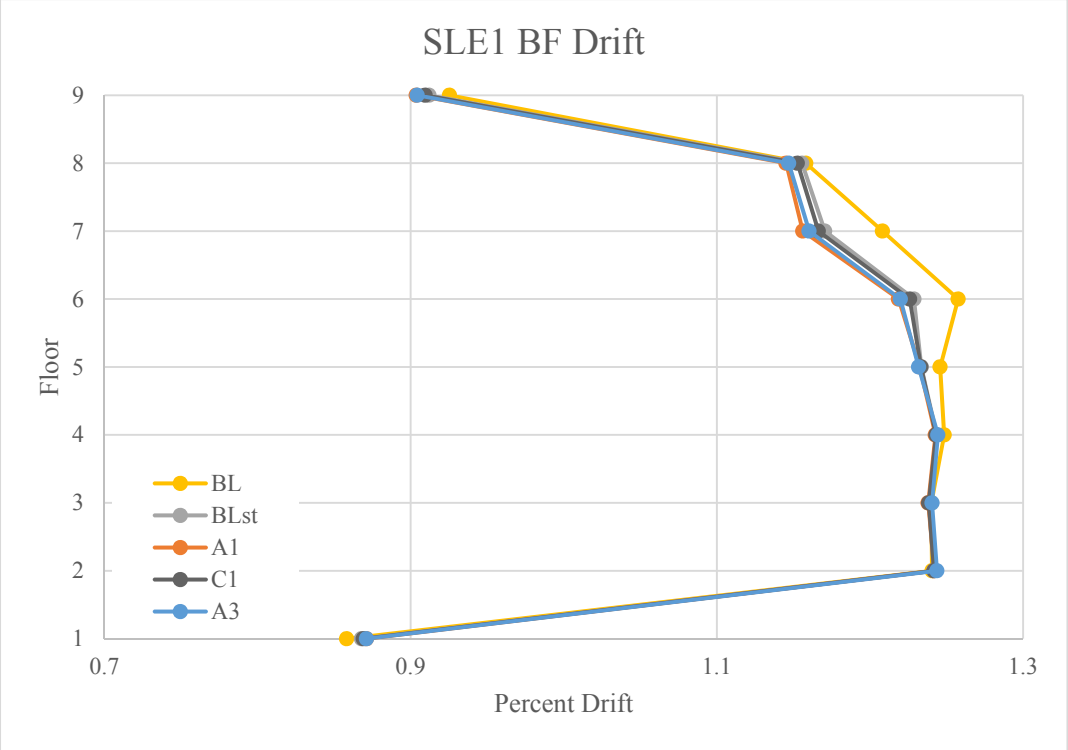

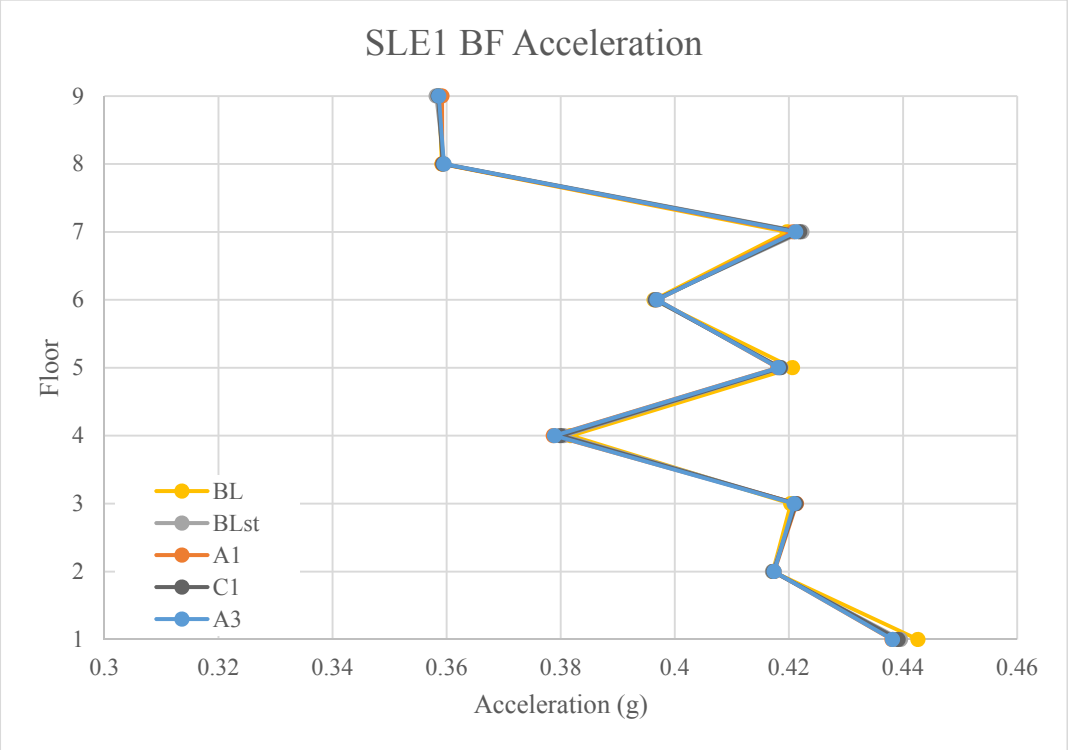

Figure A-34. Nine Story SLE1 BF Average Maximum Global Response

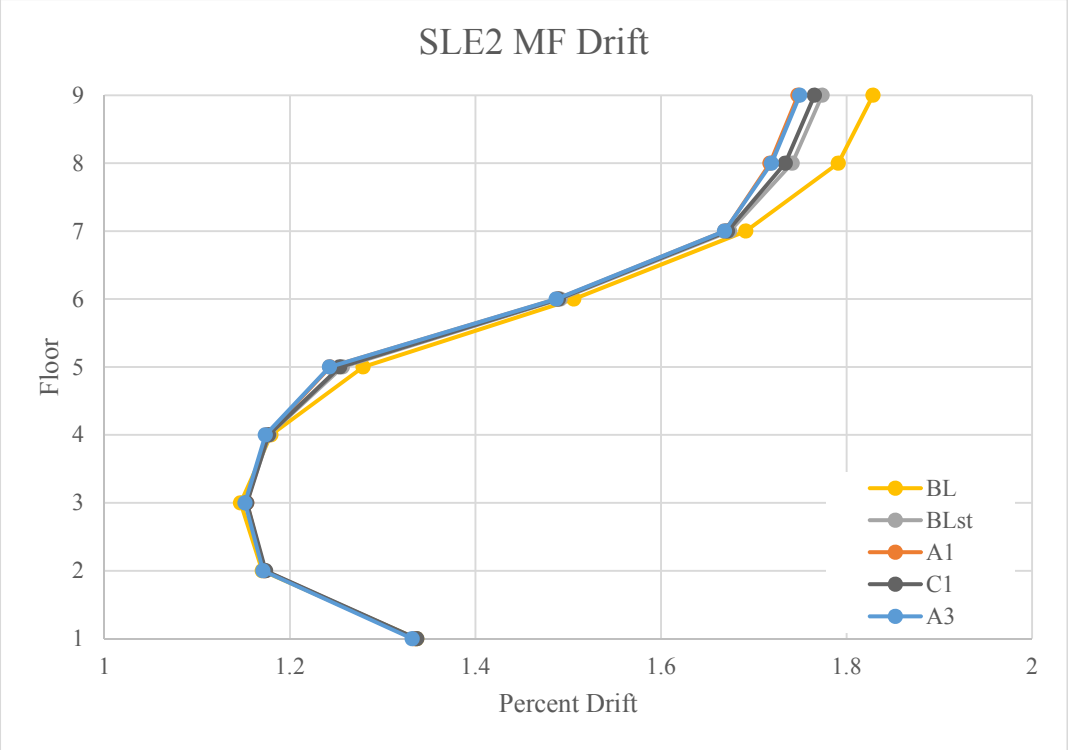

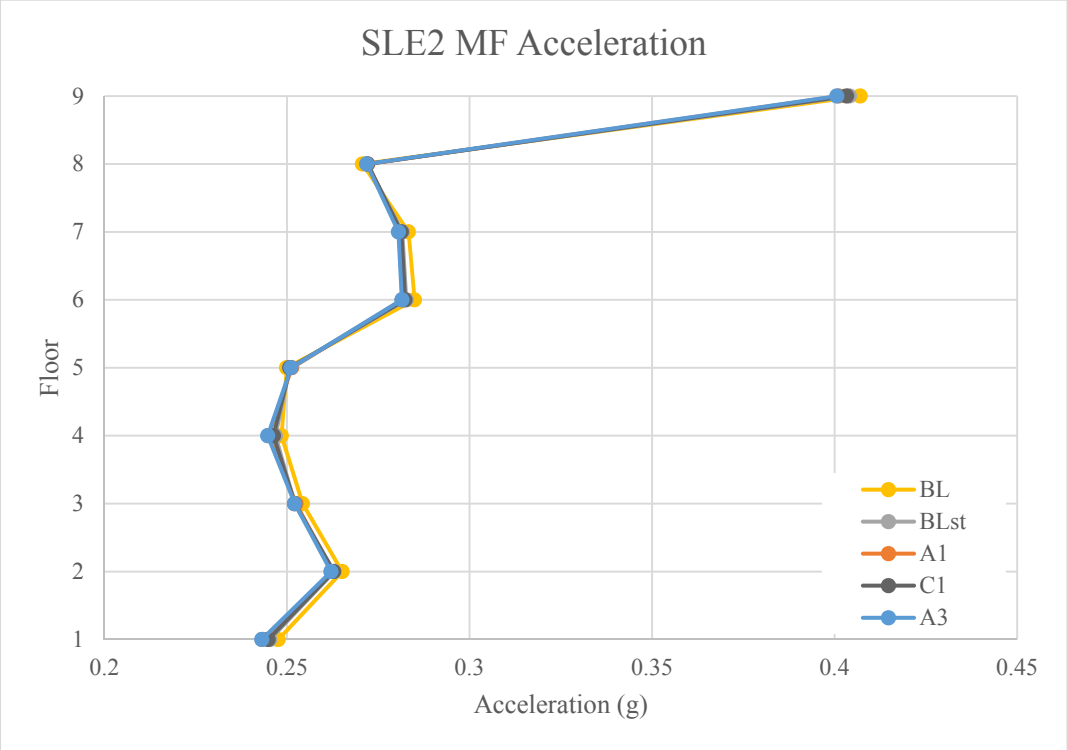

Figure A-35. Nine Story SLE2 MF Average Maximum Global Response

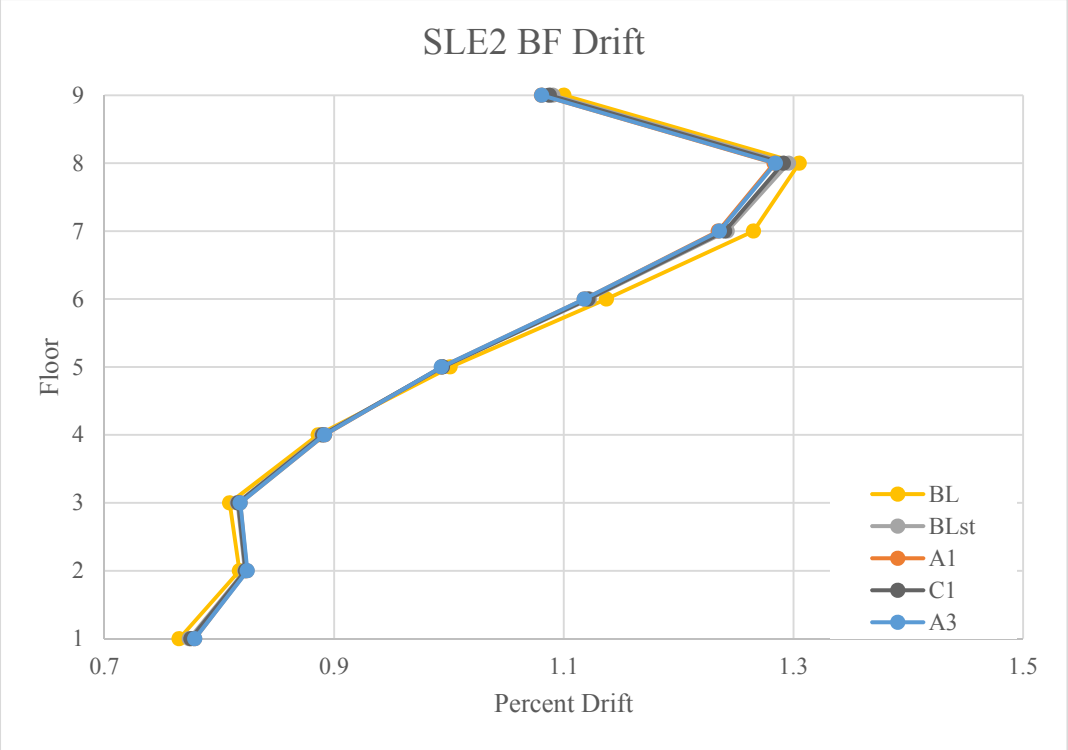

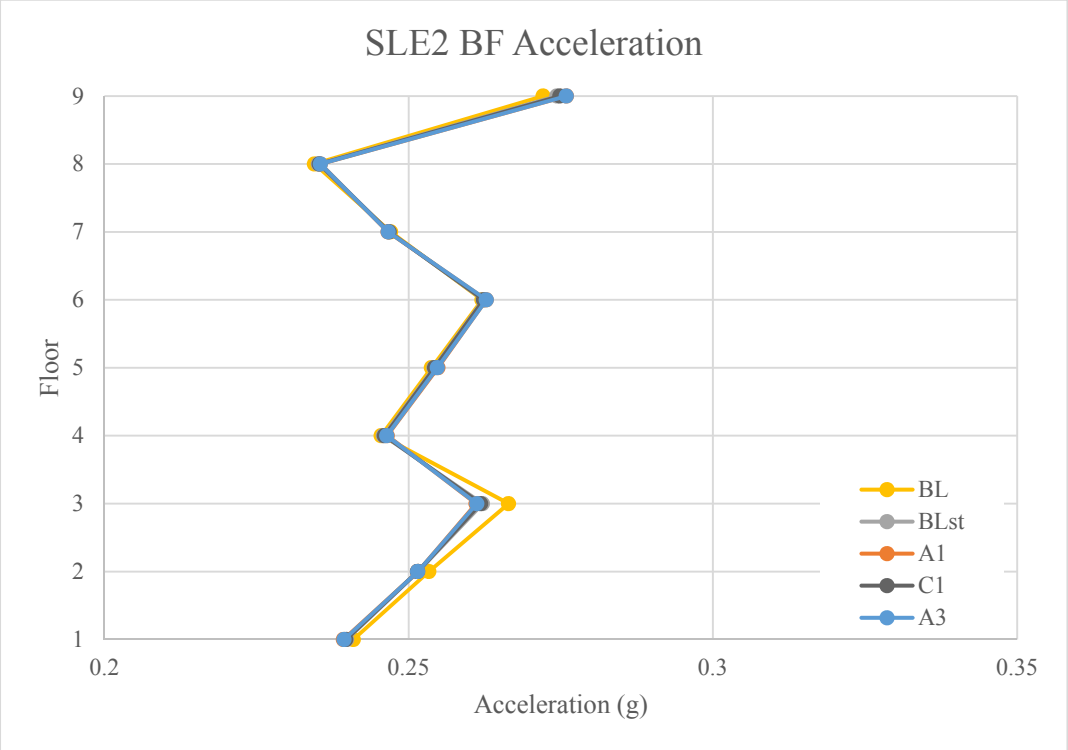

Figure A-36. Nine Story SLE2 BF Average Maximum Global Response

Table A-1. Three Story MCE MF Average Maximum Element Response

		MF Hinge Plastic Rotation (rad)	ST Moment (kip*in)	ST Rotation (rad)	FD Disp Ratio	Story Drift (% Drift)	Story Accl (g)
Floor 3	BL	0.0320	N/A	N/A	N/A	3.10	1.385
	BLst	0.0275	209	0.0270	N/A	3.03	1.400
	A1	0.0266	201	0.0260	1.41	3.02	1.404
	A2	0.0270	203	0.0262	2.00	3.02	1.404
	A3	0.0272	205	0.0264	3.37	3.02	1.404
	B1	0.0267	208	0.0269	1.41	3.03	1.401
	B2	0.0270	208	0.0269	2.01	3.03	1.402
	B3	0.0273	208	0.0269	3.38	3.03	1.402
	C1	0.0269	212	0.0273	1.39	3.03	1.401
	C2	0.0272	211	0.0272	1.99	3.03	1.403
	C3	0.0274	210	0.0272	3.37	3.03	1.403
Floor 2	BL	0.0424	N/A	N/A	N/A	3.41	1.233
	BLst	0.0388	240	0.0314	N/A	3.37	1.250
	A1	0.0380	235	0.0306	1.69	3.36	1.252
	A2	0.0384	236	0.0308	2.40	3.36	1.252
	A3	0.0385	238	0.0310	4.02	3.37	1.252
	B1	0.0381	240	0.0313	1.70	3.37	1.250
	B2	0.0384	240	0.0313	2.40	3.37	1.251
	B3	0.0386	240	0.0313	4.02	3.37	1.251
	C1	0.0383	243	0.0317	1.67	3.37	1.251
	C2	0.0385	242	0.0316	2.38	3.37	1.251
	C3	0.0387	241	0.0315	4.01	3.37	1.251
Floor 1	BL	0.0343	N/A	N/A	N/A	2.40	1.317
	BLst	0.0330	214	0.0276	N/A	2.42	1.323
	A1	0.0327	208	0.0269	1.42	2.42	1.321
	A2	0.0328	210	0.0271	2.01	2.42	1.323
	A3	0.0329	211	0.0273	3.38	2.42	1.323
	B1	0.0327	214	0.0276	1.42	2.42	1.321
	B2	0.0328	214	0.0276	2.01	2.42	1.323
	B3	0.0329	213	0.0276	3.38	2.42	1.323
	C1	0.0328	217	0.0281	1.40	2.42	1.324
	C2	0.0329	216	0.0279	1.99	2.42	1.325
	C3	0.0329	215	0.0278	3.36	2.42	1.325

Table A-2. Three Story MCE BF Average Maximum Element Response

		BRB Force Ratio	BRB Disp Ratio	ST Moment (kip*in)	ST Rotation (rad)	FD Disp Ratio	Story Drift (% Drift)	Story Accl (g)
Floor 3	BL	1.61	17.6	N/A	N/A	N/A	3.04	0.394
	BLst	1.56	16.1	295	0.0292	N/A	2.77	0.419
	A1	1.54	15.6	281	0.0277	2.34	2.68	0.423
	A2	1.54	15.7	284	0.0280	3.32	2.70	0.424
	A3	1.55	15.8	288	0.0284	5.60	2.73	0.424
	B1	1.55	15.8	290	0.0287	1.83	2.72	0.421
	B2	1.55	15.8	291	0.0288	2.65	2.73	0.421
	B3	1.55	15.9	292	0.0289	4.54	2.74	0.422
	C1	1.55	15.9	293	0.0290	1.86	2.74	0.420
	C2	1.55	16.0	293	0.0291	2.68	2.75	0.420
	C3	1.55	16.0	294	0.0291	4.58	2.76	0.420
Floor 2	BL	1.50	13.1	N/A	N/A	N/A	2.33	0.702
	BLst	1.49	13.1	253	0.0245	N/A	2.32	0.707
	A1	1.49	13.1	244	0.0237	1.97	2.32	0.709
	A2	1.49	13.1	245	0.0237	2.77	2.32	0.710
	A3	1.49	13.1	247	0.0240	4.65	2.33	0.711
	B1	1.49	13.1	250	0.0243	1.95	2.32	0.711
	B2	1.49	13.1	250	0.0242	2.76	2.32	0.711
	B3	1.49	13.1	251	0.0243	4.66	2.33	0.711
	C1	1.49	13.1	252	0.0244	1.96	2.32	0.708
	C2	1.49	13.1	252	0.0244	2.79	2.33	0.709
	C3	1.49	13.1	252	0.0245	4.69	2.33	0.709
Floor 1	BL	1.42	11.2	N/A	N/A	N/A	1.95	0.810
	BLst	1.42	11.3	269	0.0261	N/A	1.97	0.798
	A1	1.43	11.4	268	0.0259	2.22	2.00	0.797
	A2	1.43	11.4	268	0.0260	3.12	2.00	0.799
	A3	1.42	11.3	268	0.0260	5.20	2.00	0.800
	B1	1.42	11.4	271	0.0263	1.45	1.99	0.798
	B2	1.42	11.4	271	0.0262	2.07	1.99	0.798
	B3	1.42	11.3	270	0.0261	3.53	1.99	0.799
	C1	1.42	11.3	271	0.0262	1.44	1.98	0.797
	C2	1.42	11.3	270	0.0262	2.08	1.98	0.798
	C3	1.42	11.3	270	0.0261	3.54	1.98	0.798

Table A-3. Three Story SLE1 MF Average Maximum Element Response

		MF Hinge Plastic Rotation (rad)	ST Moment (kip*in)	ST Rotation (rad)	FD Disp Ratio	Story Drift (% Drift)	Story Accl (g)
Floor 3	BL	0	N/A	N/A	N/A	1.58	0.848
	BLst	0	97.6	0.0138	N/A	1.56	0.859
	A1	0	101	0.0131	0.71	1.55	0.861
	C1	0	108	0.0140	0.69	1.56	0.860
	A3	0	103	0.0133	1.69	1.55	0.858
Floor 2	BL	0.0069	N/A	N/A	N/A	1.82	0.710
	BLst	0.0061	117	0.0165	N/A	1.80	0.716
	A1	0.0059	123	0.0158	0.87	1.80	0.717
	C1	0.0060	130	0.0167	0.86	1.80	0.717
	A3	0.0058	125	0.0161	2.09	1.79	0.715
Floor 1	BL	0.0090	N/A	N/A	N/A	1.36	0.687
	BLst	0.0081	108	0.0152	N/A	1.35	0.692
	A1	0.0077	113	0.0146	0.77	1.35	0.693
	C1	0.0080	120	0.0155	0.75	1.35	0.693
	A3	0.0076	115	0.0148	1.83	1.35	0.692

Table A-4. Three Story SLE1 BF Average Maximum Element Response

		BRB Force Ratio	BRB Disp Ratio	ST Moment (kip*in)	ST Rotation (rad)	FD Disp Ratio	Story Drift (% Drift)	Story Accl (g)
Floor 3	BL	1.24	7.07	N/A	N/A	N/A	1.22	0.288
	BLst	1.22	6.52	119	0.0126	N/A	1.13	0.304
	A1	1.21	6.29	120	0.0116	0.98	1.08	0.311
	C1	1.21	6.45	129	0.0125	0.74	1.11	0.306
	A3	1.21	6.37	124	0.0120	2.37	1.10	0.308
Floor 2	BL	1.16	4.85	N/A	N/A	N/A	0.83	0.504
	BLst	1.16	4.78	91.1	0.0096	N/A	0.82	0.506
	A1	1.16	4.75	95.8	0.0093	0.76	0.82	0.505
	C1	1.16	4.77	100	0.0097	0.73	0.82	0.506
	A3	1.16	4.77	97.0	0.0094	1.81	0.82	0.505
Floor 1	BL	1.14	4.18	N/A	N/A	N/A	0.69	0.486
	BLst	1.14	4.18	85.0	0.0090	N/A	0.69	0.480
	A1	1.14	4.22	90.6	0.0088	0.75	0.70	0.479
	C1	1.14	4.19	93.4	0.0090	0.48	0.69	0.479
	A3	1.14	4.21	91.6	0.0089	2.37	0.70	0.478

Table A-5. Nine Story MCE MF Average Maximum Element Response

		MF Hinge Platic Rotation (rad)	ST Moment (kip*in)	ST Rotation (rad)	FD Disp Ratio	Story Drift (% Drift)	Story Accl (g)
Floor 9	BL	0.0323	N/A	N/A	N/A	3.56	0.798
	BLst	0.0306	250	0.0323	N/A	3.39	0.809
	A1	0.0302	239	0.0308	1.67	3.32	0.812
	A2	0.0302	242	0.0312	2.37	3.34	0.812
	A3	0.0303	245	0.0316	4.00	3.36	0.813
	B1	0.0304	251	0.0324	1.62	3.35	0.811
	B2	0.0304	251	0.0324	2.31	3.36	0.811
	B3	0.0305	250	0.0323	3.91	3.37	0.812
	C1	0.0305	252	0.0326	1.63	3.37	0.810
	C2	0.0305	252	0.0325	2.32	3.38	0.810
	C3	0.0305	251	0.0324	3.92	3.38	0.811
Floor 8	BL	0.0255	N/A	N/A	N/A	3.06	0.708
	BLst	0.0243	248	0.0321	N/A	2.93	0.702
	A1	0.0239	239	0.0309	1.85	2.89	0.701
	A2	0.0239	242	0.0312	2.62	2.90	0.702
	A3	0.0239	244	0.0316	4.41	2.91	0.703
	B1	0.0241	249	0.0322	1.82	2.91	0.701
	B2	0.0241	249	0.0322	2.59	2.92	0.702
	B3	0.0241	249	0.0321	4.37	2.92	0.702
	C1	0.0242	251	0.0324	1.83	2.92	0.701
	C2	0.0242	250	0.0323	2.60	2.92	0.701
	C3	0.0242	249	0.0322	4.38	2.93	0.702
Floor 7	BL	0.0257	N/A	N/A	N/A	3.02	0.775
	BLst	0.0245	226	0.0292	N/A	2.99	0.766
	A1	0.0239	220	0.0285	1.86	2.96	0.767
	A2	0.024	222	0.0287	2.63	2.97	0.768
	A3	0.0241	224	0.0289	4.43	2.98	0.769
	B1	0.0241	225	0.0291	1.69	2.98	0.767
	B2	0.0242	225	0.0291	2.39	2.98	0.768
	B3	0.0243	225	0.0291	4.03	2.98	0.768
	C1	0.0243	228	0.0294	1.69	2.98	0.767
	C2	0.0244	227	0.0293	2.40	2.98	0.767
	C3	0.0244	227	0.0293	4.04	2.99	0.767
Floor 6	BL	0.0353	N/A	N/A	N/A	3.10	0.698
	BLst	0.0341	230	0.0297	N/A	3.04	0.701
	A1	0.0335	225	0.0291	1.89	3.02	0.704
	A2	0.0336	227	0.0293	2.66	3.02	0.705
	A3	0.0337	228	0.0295	4.47	3.03	0.705
	B1	0.0338	230	0.0298	1.72	3.03	0.702
	B2	0.0339	230	0.0297	2.44	3.03	0.702
	B3	0.0339	230	0.0297	4.11	3.04	0.702
	C1	0.0339	232	0.0299	1.72	3.04	0.701

	C2	0.034	231	0.0299	2.44	3.04	0.701
	C3	0.034	231	0.0298	4.11	3.04	0.702
Floor 5	**BL**	0.0333	N/A	N/A	N/A	3.16	0.730
	BLst	0.0324	233	0.0306	N/A	3.12	0.738
	A1	0.032	228	0.0299	1.93	3.10	0.741
	A2	0.0321	230	0.0301	2.72	3.11	0.741
	A3	0.0322	231	0.0304	4.57	3.11	0.741
	B1	0.0322	235	0.0309	1.79	3.11	0.740
	B2	0.0323	234	0.0308	2.52	3.12	0.740
	B3	0.0323	233	0.0307	4.24	3.12	0.740
	C1	0.0323	236	0.0311	1.79	3.12	0.739
	C2	0.0323	235	0.0310	2.53	3.12	0.739
	C3	0.0323	234	0.0309	4.25	3.12	0.739
Floor 4	**BL**	0.0382	N/A	N/A	N/A	3.09	0.722
	BLst	0.0373	227	0.0305	N/A	3.07	0.720
	A1	0.037	224	0.0300	1.93	3.06	0.722
	A2	0.0371	225	0.0302	2.72	3.07	0.722
	A3	0.0371	226	0.0304	4.56	3.07	0.723
	B1	0.0372	230	0.0310	1.78	3.07	0.721
	B2	0.0372	229	0.0308	2.52	3.07	0.721
	B3	0.0372	228	0.0307	4.23	3.07	0.721
	C1	0.0373	231	0.0311	1.79	3.07	0.720
	C2	0.0373	230	0.0309	2.52	3.07	0.720
	C3	0.0373	229	0.0308	4.23	3.07	0.720
Floor 3	**BL**	0.0152	N/A	N/A	N/A	2.99	0.697
	BLst	0.0148	219	0.0296	N/A	2.96	0.705
	A1	0.0147	216	0.0291	1.86	2.95	0.710
	A2	0.0147	217	0.0293	2.62	2.95	0.710
	A3	0.0147	218	0.0295	4.39	2.96	0.710
	B1	0.0148	222	0.0300	1.73	2.96	0.707
	B2	0.0148	221	0.0299	2.44	2.96	0.708
	B3	0.0148	220	0.0298	4.10	2.96	0.708
	C1	0.0148	222	0.0301	1.73	2.96	0.706
	C2	0.0148	222	0.0300	2.44	2.96	0.706
	C3	0.0148	221	0.0299	4.10	2.96	0.707
Floor 2	**BL**	0.0126	N/A	N/A	N/A	2.79	0.824
	BLst	0.0124	218	0.0289	N/A	2.77	0.825
	A1	0.0123	215	0.0284	1.81	2.76	0.824
	A2	0.0123	216	0.0286	2.55	2.76	0.824
	A3	0.0123	217	0.0288	4.28	2.77	0.825
	B1	0.0124	221	0.0293	1.70	2.77	0.824
	B2	0.0124	220	0.0292	2.40	2.77	0.824
	B3	0.0124	219	0.0291	4.04	2.77	0.825
	C1	0.0124	222	0.0294	1.70	2.77	0.824
	C2	0.0124	221	0.0293	2.41	2.77	0.824

	C3	0.0124	220	0.0292	4.04	2.77	0.825
Floor 1	**BL**	0.0082	N/A	N/A	N/A	1.94	0.861
	BLst	0.0081	181	0.0234	N/A	1.94	0.858
	A1	0.0080	178	0.0229	1.44	1.93	0.859
	A2	0.0080	179	0.0231	2.03	1.93	0.859
	A3	0.0080	180	0.0233	3.41	1.94	0.860
	B1	0.0080	185	0.0238	1.34	1.94	0.859
	B2	0.0080	184	0.0237	1.89	1.94	0.859
	B3	0.0080	183	0.0236	3.17	1.94	0.859
	C1	0.0080	185	0.0240	1.34	1.94	0.858
	C2	0.0080	185	0.0238	1.89	1.94	0.859
	C3	0.0080	184	0.0237	3.17	1.94	0.859

Table A-6. Nine Story SLE1 MF Average Maximum Element Response

		MF Hinge Plastic Rotation (rad)	ST Moment (kip*in)	ST Rotation (rad)	FD Disp Ratio	Story Drift (% Drift)	Story Accl (g)
Floor 9	**BL**	0.0092	N/A	N/A	N/A	2.02	0.628
	BLst	0.0085	143	0.0184	N/A	1.96	0.632
	A1	0.0084	136	0.0175	0.94	1.94	0.632
	C1	0.0085	145	0.0188	0.91	1.95	0.632
	A3	0.0085	139	0.0179	2.26	1.95	0.631
Floor 8	**BL**	0.0071	N/A	N/A	N/A	1.88	0.484
	BLst	0.0069	150	0.0194	N/A	1.83	0.488
	A1	0.0067	145	0.0187	1.12	1.81	0.489
	C1	0.0068	153	0.0197	1.09	1.83	0.488
	A3	0.0068	147	0.0190	2.67	1.81	0.488
Floor 7	**BL**	0.0098	N/A	N/A	N/A	1.74	0.497
	BLst	0.0096	139	0.0180	N/A	1.72	0.500
	A1	0.0094	135	0.0175	1.13	1.72	0.500
	C1	0.0095	140	0.0181	1.02	1.72	0.500
	A3	0.0096	137	0.0178	2.69	1.72	0.499
Floor 6	**BL**	0.0100	N/A	N/A	N/A	1.63	0.479
	BLst	0.0098	132	0.0170	N/A	1.63	0.482
	A1	0.0099	128	0.0166	1.07	1.63	0.484
	C1	0.0098	133	0.0172	0.97	1.63	0.483
	A3	0.0100	130	0.0168	2.55	1.63	0.483
Floor 5	**BL**	0.0018	N/A	N/A	N/A	1.44	0.454
	BLst	0.0024	118	0.0153	N/A	1.44	0.455
	A1	0.0027	115	0.0149	0.96	1.44	0.455
	C1	0.0025	121	0.0156	0.87	1.44	0.455
	A3	0.0027	117	0.0151	2.28	1.44	0.455
Floor 4	**BL**	0.0031	N/A	N/A	N/A	1.36	0.441
	BLst	0.0025	105	0.0136	N/A	1.35	0.441

	A1	0.0024	102	0.0132	0.85	1.34	0.440
	C1	0.0024	107	0.0139	0.77	1.35	0.440
	A3	0.0023	104	0.0134	2.03	1.34	0.440
Floor 3	**BL**	0.000	N/A	N/A	N/A	1.36	0.465
	BLst	0.000	103	0.0133	N/A	1.35	0.469
	A1	0.000	100	0.0129	0.83	1.34	0.471
	C1	0.000	105	0.0136	0.76	1.35	0.469
	A3	0.000	101	0.0131	1.98	1.34	0.471
Floor 2	**BL**	0.000	N/A	N/A	N/A	1.35	0.497
	BLst	0.000	106	0.0136	N/A	1.35	0.502
	A1	0.000	103	0.0133	0.86	1.35	0.503
	C1	0.000	109	0.0140	0.80	1.35	0.502
	A3	0.000	104	0.0134	2.03	1.35	0.502
Floor 1	**BL**	0.000	N/A	N/A	N/A	1.04	0.484
	BLst	0.000	93.9	0.0121	N/A	1.04	0.483
	A1	0.000	91.3	0.0118	0.74	1.04	0.483
	C1	0.000	96.8	0.0125	0.69	1.04	0.483
	A3	0.000	92.2	0.0119	1.76	1.04	0.483

Table A-7. Nine Story MCE BF Average Maximum Element Response

		BRB Force Ratio	**BRB Disp Ratio**	**ST Moment (kip*in)**	**ST Rotation (rad)**	**FD Disp Ratio**	**Story Drift (% Drift)**	**Story Accl (g)**
Floor 9	**BL**	1.67	11.0	N/A	N/A	N/A	1.95	0.450
	BLst	1.68	11.4	173	0.0168	N/A	2.01	0.450
	A1	1.67	11.1	167	0.0162	0.87	1.97	0.463
	A2	1.67	11.1	169	0.0163	1.23	1.98	0.463
	A3	1.68	11.2	170	0.0165	2.06	1.99	0.463
	B1	1.68	11.2	171	0.0166	0.69	1.99	0.462
	B2	1.68	11.2	172	0.0166	0.99	1.99	0.462
	B3	1.68	11.3	172	0.0167	1.68	2.00	0.462
	C1	1.68	11.3	172	0.0167	0.69	2.00	0.461
	C2	1.68	11.3	172	0.0167	0.99	2.00	0.461
	C3	1.68	11.3	172	0.0167	1.68	2.00	0.461
Floor 8	**BL**	1.39	12.7	N/A	N/A	N/A	2.32	0.500
	BLst	1.41	13.2	214	0.0208	N/A	2.40	0.500
	A1	1.40	13.0	207	0.0201	1.21	2.36	0.517
	A2	1.40	13.1	209	0.0202	1.72	2.37	0.518
	A3	1.41	13.1	210	0.0204	2.87	2.38	0.518
	B1	1.41	13.1	211	0.0204	1.13	2.38	0.516
	B2	1.41	13.1	211	0.0205	1.60	2.38	0.516
	B3	1.41	13.2	212	0.0205	2.70	2.39	0.517
	C1	1.41	13.1	212	0.0205	1.13	2.39	0.516
	C2	1.41	13.2	212	0.0206	1.61	2.39	0.516

	C3	1.41	13.2	212	0.0206	2.71	2.39	0.516
Floor 7	**BL**	1.40	13.2	N/A	N/A	N/A	2.45	0.597
	BLst	1.40	13.1	255	0.0247	N/A	2.43	0.597
	A1	1.40	13.1	249	0.0241	1.43	2.42	0.591
	A2	1.40	13.1	250	0.0242	2.02	2.42	0.591
	A3	1.40	13.1	251	0.0243	3.37	2.42	0.592
	B1	1.40	13.1	252	0.0244	1.38	2.42	0.591
	B2	1.40	13.1	252	0.0244	1.94	2.42	0.591
	B3	1.40	13.1	252	0.0244	3.25	2.42	0.592
	C1	1.40	13.1	252	0.0245	1.38	2.42	0.591
	C2	1.40	13.1	252	0.0244	1.95	2.43	0.591
	C3	1.40	13.1	252	0.0244	3.25	2.43	0.591
Floor 6	**BL**	1.45	14.5	N/A	N/A	N/A	2.73	0.619
	BLst	1.45	14.4	271	0.0262	N/A	2.72	0.619
	A1	1.44	14.4	265	0.0256	1.54	2.70	0.618
	A2	1.44	14.4	266	0.0257	2.16	2.71	0.620
	A3	1.44	14.4	267	0.0258	3.61	2.71	0.621
	B1	1.44	14.4	268	0.0259	1.49	2.71	0.620
	B2	1.44	14.4	268	0.0259	2.10	2.71	0.621
	B3	1.45	14.4	268	0.0260	3.51	2.71	0.621
	C1	1.45	14.4	268	0.0260	1.49	2.71	0.620
	C2	1.45	14.4	268	0.0260	2.10	2.72	0.621
	C3	1.45	14.4	268	0.0260	3.52	2.72	0.621
Floor 5	**BL**	1.49	16.2	N/A	N/A	N/A	2.97	0.579
	BLst	1.48	16.1	300	0.0290	N/A	2.94	0.579
	A1	1.48	16.0	294	0.0284	1.70	2.93	0.584
	A2	1.48	16.0	294	0.0285	2.39	2.94	0.584
	A3	1.48	16.0	295	0.0286	3.99	2.94	0.585
	B1	1.48	16.0	296	0.0287	1.65	2.94	0.583
	B2	1.48	16.0	296	0.0287	2.33	2.94	0.583
	B3	1.48	16.0	296	0.0287	3.90	2.94	0.583
	C1	1.48	16.0	297	0.0288	1.66	2.94	0.582
	C2	1.48	16.0	297	0.0288	2.34	2.94	0.582
	C3	1.48	16.1	297	0.0287	3.90	2.94	0.582
Floor 4	**BL**	1.54	17.3	N/A	N/A	N/A	3.17	0.631
	BLst	1.54	17.1	325	0.0315	N/A	3.15	0.631
	A1	1.53	17.1	319	0.0309	1.85	3.15	0.634
	A2	1.53	17.1	320	0.0310	2.60	3.15	0.634
	A3	1.54	17.1	320	0.0310	4.33	3.15	0.634
	B1	1.53	17.1	322	0.0312	1.80	3.15	0.634
	B2	1.54	17.1	322	0.0312	2.54	3.15	0.634
	B3	1.54	17.1	321	0.0311	4.25	3.15	0.634
	C1	1.54	17.1	322	0.0312	1.81	3.15	0.634
	C2	1.54	17.1	322	0.0312	2.54	3.15	0.634
	C3	1.54	17.1	322	0.0312	4.25	3.15	0.634

Floor 3	BL	1.57	18.5	N/A	N/A	N/A	3.26	0.633
	BLst	1.56	18.3	344	0.0335	N/A	3.23	0.633
	A1	1.56	18.3	340	0.0329	1.96	3.23	0.632
	A2	1.56	18.3	341	0.0330	2.76	3.23	0.632
	A3	1.56	18.3	341	0.0330	4.60	3.24	0.633
	B1	1.56	18.3	342	0.0332	1.91	3.23	0.631
	B2	1.56	18.3	342	0.0332	2.68	3.23	0.631
	B3	1.56	18.3	342	0.0331	4.47	3.24	0.632
	C1	1.56	18.3	343	0.0332	1.91	3.23	0.631
	C2	1.56	18.3	342	0.0332	2.68	3.23	0.631
	C3	1.56	18.3	342	0.0331	4.47	3.23	0.631
Floor 2	BL	1.57	18.3	N/A	N/A	N/A	3.27	0.680
	BLst	1.57	18.1	349	0.0339	N/A	3.24	0.680
	A1	1.57	18.1	347	0.0336	2.02	3.24	0.692
	A2	1.57	18.1	348	0.0337	2.84	3.24	0.692
	A3	1.57	18.1	348	0.0338	4.73	3.24	0.692
	B1	1.57	18.1	349	0.0338	2.02	3.24	0.692
	B2	1.57	18.1	349	0.0338	2.84	3.24	0.693
	B3	1.57	18.1	349	0.0338	4.73	3.24	0.693
	C1	1.57	18.1	350	0.0339	2.02	3.24	0.692
	C2	1.57	18.1	350	0.0339	2.84	3.24	0.692
	C3	1.57	18.1	350	0.0339	4.73	3.24	0.692
Floor 1	BL	1.42	15.9	N/A	N/A	N/A	2.27	0.774
	BLst	1.42	16.0	351	0.0341	N/A	2.29	0.774
	A1	1.42	16.0	347	0.0336	2.01	2.29	0.777
	A2	1.42	16.0	347	0.0337	2.83	2.29	0.778
	A3	1.42	16.0	347	0.0337	4.70	2.29	0.778
	B1	1.42	16.0	349	0.0338	1.67	2.29	0.777
	B2	1.42	16.0	348	0.0338	2.35	2.29	0.778
	B3	1.42	16.0	348	0.0338	3.92	2.29	0.778
	C1	1.42	16.0	348	0.0338	1.67	2.29	0.778
	C2	1.42	16.0	348	0.0338	2.35	2.29	0.778
	C3	1.42	16.0	348	0.0338	3.92	2.29	0.778

Table A-8. Nine Story SLE1 BF Average Maximum Element Response

		BRB Force Ratio	BRB Disp Ratio	ST Moment (kip*in)	ST Rotation (rad)	FD Disp Ratio	Story Drift (% Drift)	Story Accl (g)
Floor 9	BL	1.27	4.53	N/A	N/A	N/A	0.93	0.359
	BLst	1.27	4.58	78.0	0.0076	N/A	0.91	0.358
	A1	1.26	4.56	76.2	0.0074	0.40	0.90	0.359

	C1	1.27	4.57	78.0	0.0076	0.31	0.91	0.359
	A3	1.26	4.55	76.3	0.0074	0.92	0.90	0.359
Floor 8	**BL**	1.17	5.76	N/A	N/A	N/A	1.16	0.359
	BLst	1.17	5.79	102	0.0099	N/A	1.16	0.360
	A1	1.17	5.74	100	0.0097	0.59	1.15	0.359
	C1	1.17	5.77	102	0.0098	0.54	1.15	0.359
	A3	1.17	5.75	100	0.0097	1.37	1.15	0.360
Floor 7	**BL**	1.16	5.74	N/A	N/A	N/A	1.21	0.420
	BLst	1.16	5.55	123	0.0119	N/A	1.17	0.422
	A1	1.15	5.47	120	0.0116	0.69	1.16	0.421
	C1	1.16	5.53	122	0.0118	0.66	1.17	0.422
	A3	1.15	5.49	121	0.0117	1.62	1.16	0.421
Floor 6	**BL**	1.17	6.03	N/A	N/A	N/A	1.26	0.396
	BLst	1.16	5.89	126	0.0122	N/A	1.23	0.397
	A1	1.16	5.84	122	0.0118	0.71	1.22	0.397
	C1	1.16	5.88	125	0.0121	0.68	1.23	0.397
	A3	1.16	5.85	123	0.0119	1.66	1.22	0.397
Floor 5	**BL**	1.17	6.25	N/A	N/A	N/A	1.25	0.421
	BLst	1.17	6.19	133	0.0129	N/A	1.23	0.419
	A1	1.17	6.18	130	0.0126	0.75	1.23	0.418
	C1	1.17	6.19	132	0.0128	0.72	1.23	0.419
	A3	1.17	6.17	130	0.0126	1.75	1.23	0.418
Floor 4	**BL**	1.17	6.16	N/A	N/A	N/A	1.25	0.382
	BLst	1.17	6.14	131	0.0127	N/A	1.24	0.381
	A1	1.17	6.14	129	0.0125	0.74	1.24	0.379
	C1	1.17	6.14	131	0.0127	0.72	1.24	0.380
	A3	1.17	6.15	129	0.0125	1.74	1.24	0.379
Floor 3	**BL**	1.18	6.59	N/A	N/A	N/A	1.24	0.420
	BLst	1.18	6.58	133	0.0129	N/A	1.24	0.421
	A1	1.18	6.58	131	0.0127	0.76	1.24	0.421
	C1	1.18	6.58	133	0.0129	0.73	1.24	0.421
	A3	1.18	6.60	132	0.0128	1.77	1.24	0.421
Floor 2	**BL**	1.19	6.58	N/A	N/A	N/A	1.24	0.417
	BLst	1.19	6.58	134	0.0129	N/A	1.24	0.417
	A1	1.19	6.58	132	0.0128	0.77	1.24	0.417
	C1	1.19	6.58	134	0.0130	0.77	1.24	0.417
	A3	1.19	6.59	133	0.0129	1.80	1.24	0.417
Floor 1	**BL**	1.15	6.05	N/A	N/A	N/A	0.86	0.443
	BLst	1.15	6.11	134	0.0130	N/A	0.87	0.440
	A1	1.15	6.14	132	0.0127	0.76	0.87	0.438
	C1	1.15	6.12	133	0.0129	0.63	0.87	0.439
	A3	1.15	6.14	132	0.0128	1.79	0.87	0.438